Elaboration of novel enzymatic immobilization matrices, based on Metal-Organic Frameworks for the catalytic degradation of environmental pollutants

Effrosyni Gkaniatsou

université PARIS-SACLAY

NNT : 2019SACLV005

Thèse de doctorat

UNIVERSITÉ DE VERSAILLES ST-QUENTIN-EN-YVELINES

université PARIS-SACLAY

Elaboration of novel enzymatic immobilization matrices, based on Metal-Organic Frameworks for the catalytic degradation of environmental pollutants

Thèse de doctorat de l'Université Paris-Saclay
préparée à Université de Versailles Saint-Quentin-en-Yvelines

École doctorale n°573 Interfaces : Approches interdisciplinaires, Fondements, Applications et Innovation
Spécialité de doctorat : Chimie

Thèse présentée et soutenue à Versailles, le 25 Janvier 2019, par

Effrosyni Gkaniatsou

Composition du Jury :

Darren BRADSHAW Associate Professor, University of Southampton	Rapporteur
Claude JOLIVALT Professeur, Université Pierre et Marie Curie	Rapporteur
Marco DATURI Professeur, Université de Caen Normandie	Examinateur
Thibaud CORADIN Directeur de Recherche CNRS, Université Pierre et Marie Curie	Président du Jury
Pierre MIALANE Professeur, Université de Versailles Saint-Quentin-en-Yvelines	Examinateur
Nathalie STEUNOU Professeur, Université de Versailles Saint-Quentin-en-Yvelines	Directeur de thèse
Rémy RICOUX Ingénieur de Recherche CNRS, Université Paris-Sud	Co-Directeur de thèse
Clémence SICARD Maître de conférences, Université de Versailles Saint-Quentin-en-Yvelines	Encadrant de thèse
Jean-Pierre MAHY Professeur, Université Paris-Sud	Invité
Christian SERRE Directeur de Recherche CNRS, Ecole Normale Supérieure, Ecole Supérieure de Physique et de Chimie Industrielles de Paris	Invité

Acknowledgments

First, I would also like to express my appreciation to all the members of the committee, Prof. Darren Bradshaw, Prof. Claude Jolivalt, Prof. Marco Daturi, Dr. Thibaud Coradin and Prof. Pierre Mialane for accepting to participate in my PhD defense. I shall thank once more the two reviewers, Prof. Claude Jolivalt and Prof. Darren Bradshaw for their time and work in evaluating the manuscript.

I would like to thank Prof. Emmanuel Cadot, the director of the group Molécules, Interactions et Matériaux (MIM) for having me in his group.

I also acknowledge the LabEx CHARMMMAT for the financial support of this work.

I would like to express my sincere gratitude to all my supervisors (I have many!), Prof. Nathalie Steunou, Dr. Rémy Ricoux, Dr. Clémence Sicard, Prof. Jean-Pierre Mahy and Dr. Christian Serre. As with all multidisciplinary projects, it has not always been easy to combine the world of materials science with that of enzymes. However, with a good spirit of collaboration and of course some inevitable compromises (!), I believe we have done a great job these three years. I thank you all very much for your ideas, hard work, for your support and for giving me the chance and the tools to discover so many aspects of chemistry.

I'll try to switch to French now, brace yourselves…!

Nathalie, je souhaite te remercier sincèrement pour ta contribution à ce projet. Merci pour ton aide, pour nos nombreuses discussions enrichissantes (et surtout tout ce qui est oxydes et sol-gel !!!), ta vue critique sur mes résultats. Merci pour tes efforts constants à améliorer mon travail et pour toutes tes corrections et conseils sur la rédaction des articles et du manuscrit ! Merci beaucoup de m'avoir fait confiance pendant ces trois ans de thèse, mais aussi pour ton soutien !

Rémy, merci beaucoup de m'avoir guidé dans le monde de la MP8 ! mais aussi de ta patience de m'expliquer des aspects probablement très évidents (mécanismes des enzymes, cofacteurs, cinétiques de réactions !). Merci de m'avoir donné une grande autonomie et de m'avoir fait confiance pour mes travaux de thèse. Je te remercie également de ta bonne humeur, tous les bons moments avec des blagues et aussi de ta volonté de me faire connaitre la ville d'Orsay !!!

Jean-Pierre, je te remercie de m'avoir accueilli à ton équipe. Merci pour toutes les discussions passionnantes et fructueuses, même si on n'était pas toujours d'accord parce que j'étais plutôt fan des matériaux ! je te remercie chaleureusement pour ton implication au projet, ton aide à la rédaction des articles, mais aussi pour la correction de ma thèse. De plus, un grand merci pour ton hospitalité et gentillesse de partager ton bureau avec moi ! C'était un plaisir !

Christian, tout d'abord je te remercie de m'avoir accueilli à ton ancienne équipe « Solides Poreux » a l'ILV pendant mon stage Erasmus et de m'avoir donné la chance de connaitre le monde des MOFs ! Merci beaucoup pour tes conseils et pour toutes nos discussions

enrichissantes pendant différentes réunions. C'était une grande opportunité de travailler avec toi !

Clémence ! je t'ai laissée pour la fin simplement pour souligner l'importance ! Comme tu sais très bien, notre rencontre a été inattendue !!! je n'aurai pu jamais imaginé ces premiers jours à l'ILV, la chance que j'aurai eue de travailler avec toi. Tu es une personne spéciale, rare, hybride je dirais (:P) qui combine à la fois le professionnalisme, la rigueur scientifique, la gentillesse et l'amitié. C'était vraiment un très grand plaisir de te rencontrer, travailler avec toi, faire la fête avec toi !!! Je te remercie pour toutes tes idées originales et magnifiques qui ont donné ces super résultats, ta motivation et tes efforts constants à valoriser ce travail. Je te remercie également pour le temps que tu as consacré à rédiger/corriger des articles et mon manuscrit !!! Un énorme merci pour ton bon moral, ta pensée positive continue, ta patience et ton soutien pendant mes différentes crises !

Je remercie chaleureusement Dr. Thibauld Coradin (Sorbonne Université) d'avoir accepté de participer à mon « comité de suivi de thèse ». Merci beaucoup pour tous vos conseils.

Il est aussi important de remercier toutes les personnes qui ont attribué énormément à l'étude et à la compréhension de ce travail.

Je souhaite remercier Dr. Josefine Schnee et Prof. Marco Daturi (Université de Caen Normandie) pour notre collaboration sur le système BSA@MIL-53(Al)-FA et leurs études d'infrarouge *in-situ*. Merci beaucoup pour votre travail et votre motivation sur le projet !

Merci également à Dr. Charlotte Martineau-Corcos pour les mesures RMN du solide sur les composés BSA@MIL-53(Al)-FA. Merci pour ta disponibilité et ta volonté.

Je remercie aussi Flavien Bourdreux pour toutes les analyses ICP et pour sa patience avec mes blancs et standards contaminés… Mais j'ai appris à la fin !

Merci aussi à Dr. Ingrid Stenger (GEMaC) pour les mesures de spectroscopie Raman sur les composites MP8@MIL-101(Cr)-X et BSA@MIL-53(Al)-FA. Merci pour ta disponibilité et ta volonté.

Je remercie chaleureusement Dr. Jean-Marc Greneche (Le Mans Université) pour les analyses Mössbauer sur les échantillons MIL-101(Cr/Fe). Merci beaucoup pour votre travail et votre motivation de m'expliquer la spectrométrie Mössbauer !

Merci beaucoup à Prof. Nicolas Menguy (Sorbonne Université) pour les images TEM sur les échantillons BSA@MIL-53(Al). Merci pour ton temps, ton travail et ta motivation à m'aider exploiter mes particules assez (très) moches….!

I would also like to thank the group of Prof. Hermenegildo García (Universitat Politècnica de València), Dr. Mónica Jiménez-Marques, Cristina Vallés, Dr. Andrea Santiago, Prof. Mercedes Álvaro and Prof. Sergio Navalón for the nice and fruitful collaboration on the catalytic properties of MIL-(Cr/Fe) materials. ¡Muchas gracias!

Un grand merci aux Dr. Oliver Dalstein et Dr. Marco Faustini (Sorbonne Université) de m'avoir inclus à leur super travail sur les capteurs photoniques à base de MIL-101(Cr) !!!

Very special thanks to all the students that have worked alongside with me, on this project (from newest to oldest!): Amy (Aimee) Irvine, Stellina Giannopoulou, Samanta Salas, Linda Benahmed, Chrysoula Kartsiouka and Narjes Ayoub. From the beginning till the end, it has been a girls' project and without your contribution, I could never have achieved all these results! Thanks a lot for all your hard work!!! My best wishes for the future!

Orsay Ville !

Un grand merci à tous les membres du Laboratoire de Chimie Bioorganique et Bioinorganique (LCBB) à Orsay et plus spécialement à Kalani Kariyawasam Bowithanthri, Yoan Chevalier, Dr. Wadih Ghattas et Dr. Frédéric Avenier. Je vous remercie tous de m'avoir fait sentir toujours la bienvenue à votre labo et bureau !!! Merci beaucoup pour votre aide et patience pendant mes journées à Orsay. Kalani, un spécial merci pour ta gentillesse, ta compagnie et pour toutes nos discussions. Et bien sûr, pour tes superbes gâteaux. :D Kalani et Yoan, bon courage pour la fin de la thèse !!!

Et je bouge à Versailles !

Pendant mon séjour à l'ILV, la grande équipe SOPO a été dissociée et je me suis retrouvée avec un petit groupe des amis plutôt que des collègues : Kevin Dedecker (un belge bizarre), Dr. Virgile Trannoy (un vrai parisien) et Dr. Sara Rojas (une espagnole assassine de souris). Trois énormes labos seulement pour nous quatre, on a bien fait la fiesta !!! C'était une vraie folie avec des échantillons abandonnés (je balance pas… !), de la musique bien forte, des rongeurs démembrés, des histoires folles et tout cela avec une bonne dose de kebab et de bière (belge bien sûr) ! C'est important de noter qu'en même temps on bossait à fond !! (:P). C'était un grand plaisir des vous rencontrer, partager tous ces moments avec vous et devenir votre amie ! je n'oublie pas le non-chimiste de notre groupe, Paco avec ses blagues et ses barbecues ! Hasta luego chica y chicos !!! Et petit chat !!! même si ce n'était pas toujours évident (!), on peut maintenant dire qu'on a réussi ! oui……on a presque fini !!!!!!!!!!!!!!!!!

Merci à tous les postdocs, thésards et stagiaires de l'équipe MIM et plus spécialement ceux du RDC (!) : Marvin, Somia, Lucie, Nastya, Elena, Stellina, Romain (x2), Van, Aimee, Sean, Fa. Merci pour la superbe ambiance au labo, pour toutes nos discussions, plutôt bizarres… (commencées par Kevin, Somia ou Lucie ! et oui c'est la vérité… !!!), pour tous les bons moments qu'on a eus -presque toujours accompagnés par des quantités importantes de nourriture… Un grand merci à Marvin qui m'a beaucoup aidé pendant mon stage à l'ILV, quand j'étais hyper perdue et je ne comprenais rien ! Merci pour ta patience et ta gentillesse ! Merci aussi pour votre solidarité à mes pauses cigarettes ! (ce n'est pas sympa de fumer toute seule !). Un grand merci pour votre soutien et votre patience pendant cette période horrible de la rédaction… :P je sais que ma tête n'était pas très sympa ces derniers mois ! C'était un grand plaisir de travailler avec vous ! (et non ce n'est pas fini, je reste encore un peu !!!)

Also, thanks to our POM-making guys in our lab, Anton and Dr. Clément! Thanks for all the fun working moments and for decorating the lab with beautiful crystals! (P.S. I recently found molybdenum in some of my samples, I think we need to clean again :P).

Merci également à tous les membres permanents de l'équipe MIM et en restant toujours sur mon étage : Dr. Anne Valée, Dr. Nathalie Guiliou, Dr. Carine Livage et Dr. Isabelle Gerard. Un spécial merci à Dr. Carine Livage pour les plusieurs mesures SEM sur mes échantillons !

Je souhaite également remercier tous les anciens postdocs, thésards et stagiaires de l'ancien groupe SOPO a l'ILV : Saad, Hala, Teresa, Monica, Qi, Paul R., Elsa, Tania, Maame, Rhizlaine, Georges, Mazheva, Chrysoula, Eleni, Cameron, Monik, Ana, Xabier, Xavi, Tanay, Tere (et tous ceux que j'ai oublié par erreur !). Un spécial merci à Paul Fabri qui a toujours maintenu l'humour au labo bien élevé et qui nous a accompagné avec ses blagues aux soirées, après nous avoir quittés pour Brucker…! Merci à tous pour les bons moments et la très bonne ambiance au labo !

Un grand merci à Dr. Thomas Devic (Université de Nantes et ancien membre de l'équipe SOPO) pour sa gentillesse et sa volonté de m'aider avec mes divers problèmes MOFs, même si on ne travaillait pas sur des projets communs !

Et enfin l'IMAP !

Je souhaite remercier chaleureusement Dr. Farid Nouar et Dr. Antoine Tissot ! Farid, merci beaucoup pour ton aide et tes conseils, pour les mesures SEM, mais aussi pour nos diverses discussions et pour ta compagnie ! Antoine, également merci beaucoup pour ta gentillesse, ton temps et ta volonté de mesurer tous mes capillaires, mes BET, mes ATG… et pour tous tes conseils ! C'est un vrai plaisir de vous rencontrer et travailler avec vous ! (J'espère que vous venez avec nous faire la fête après la thèse !)

A very special thanks to the very special postdoc Dr. Sujing Wang, whom I had the pleasure to meet (and smoke with) since my first day at the lab! Sujing, many thanks for all the happy times we've shared, with or without alcohol! I want to thank you for all your useful advice and discussions concerning MOF synthesis, along with all the PXRD measurements that you ran for me in Paris (but you took Marcel from us)!!! But most importantly, for always trying to make me feel better! And now that the PhD is over, we can start drinking again!

Un merci à l'autre postdoc spécial de l'IMAP Dr. Florian Moreau ! Florian merci beaucoup pour ta compagnie et pour tous les bons moments aux terrasses de Paris.

Many thanks to the PhD students of the IMAP group, Mégane, Angelica, Ioanna, Lin, Nicolas and Shan for always making me feel welcome during my days in Paris. It was a pleasure to meet you and also to party with you! Mégane, Angelica bon courage pour la fin!

Un énorme merci à Alexandre pour son soutien constant pendant mon séjour en France. Ce n'était pas facile (spécialement au début et à la fin !). Merci de ta motivation, merci de ta

patience (surtout pour tout ce qui est présentation orale !) et enfin merci d'être toujours là pour moi !!!

A very very big thank you to my family, who has supported me during my years abroad. Thank you for always been there for me and for motivating and pushing me to continue when I doubt myself!!! Μαμά, μπαμπά, Θεοδώρα και προφανώς παππού, γιαγιά σας ευχαριστώ όλους πάρα πολύ για την στήριξή σας και την αγάπη σας!!! Merci beaucoup !!!

Enfin, un merci à ma chatte Coco qu'elle m'a accompagnée ces quatre ans en France, contre sa volonté ! (Les apparts parisiens sont trop petits…)

Table of Contents

General Introduction

General Introduction

The use of enzymes for synthetic applications (*e.g.* production of pharmaceuticals and fine chemical, degradation of pollutants, *etc.*) has been a major goal for decades, owing to their unique characteristics.[1] Enzymes are extremely selective and efficient natural catalysts (biocatalysts) that transform their substrate with high turn-over numbers under mild operating conditions (ambient temperature, atmospheric pressure and in aqueous solution).[1] These characteristics could eventually simplify catalytic operations and render them more-cost effective and ecocompatible.[1] The benefits gained from the use of enzymes do not however depict their current use in biocatalytic applications, which covers only a small percentage of the overall enzyme market. This difference derives from multiples reasons.[2] Enzymes -under their natural soluble form- cannot be easily removed from reaction mixtures, hence demanding expensive and time-consuming separation steps to separate the products from the biocatalysts. Furthermore, due to their solubility, the recycling of enzymes and in certain cases that of required co-factors (*e.g.* NAD, NADH) is not possible, thereby increasing the total cost of biocatalysis. The fragile nature of enzymes is another limiting factor for their application.[2] The use of organic solvents and/or high temperatures is sometimes necessary for industrial processes, which however may deactivate or even totally denaturate enzymes. Deactivation of enzymes can also be caused by by-products formed during the catalytic reaction. These barriers on the practical use of enzymes can be addressed through their immobilization on solid supports. An immobilized enzyme can be more easily recovered from the reaction mixture (*e.g. via* filtration, centrifugation...) and reused multiple times. Moreover, the solid matrix can provide a protective and stabilizing environment for enzymes, thus enabling their use under denaturating conditions.[2]

The immobilization matrix must preserve maximal enzymatic activity, *i.e.* maximal loading and minimal leaching, while not hindering the diffusion of reactants/products to and from the enzyme's active site. The field of enzyme immobilization has been under investigation for decades,[3] which allowed the development of four main types of immobilization that are surface adsorption, covalent binding, pore inclusion and entrapment.[4–6] The two first cases concern the immobilization of enzymes at the external surface of materials either *via* weak reversible interactions (van der Waals, electrostatic, hydrophobic/hydrophilic…) or *via* the formation of irreversible covalent bonds. The major limitation of these two methods is the need to control the orientation of the enzyme's active site that must be exposed on the external surface of the particles in order to remain accessible to reactants. Moreover, the enzyme is not protected from the external conditions and may easily be denatured. For the pore inclusion and the entrapment methods, the enzymes are confined into either the internal surface of a porous solid matrix or in the inter-particle porosity of the matrix, respectively. The important difference between pore inclusion and entrapment is that in the first case, the

enzymes are encapsulated inside the cavities of a pre-formed matrix, while in the latter case the immobilization takes place simultaneously with the synthesis of the support around the enzyme. Enzymes are generally protected against denaturing conditions by using these approaches, since the host matrices can create a three-dimensional stabilizing microenvironment for them through specific host–guest interactions and confinement effects. However, the diffusion of reactants to the biomolecules depends on the remaining porosity of the matrices and thus the mass-transfer efficiency of analytes may be strongly limited in some cases. The choice of the immobilization strategy strongly depends on the enzyme/host matrix couple and on the biocatalytic process.

This work focused on the use of heme enzymes (containing an Fe(III)-protoporphyrin IX or heme cofactor) and more specifically on the mini-enzyme, microperoxidase 8 (MP8).[8] While heme enzymes are generally divided into two classes, peroxidases and mono-oxygenases with two distinct catalytic functions,[9] MP8 combines both activities. *Via* the peroxidase-like function, MP8 catalyzes the oxidation of substrates (phenols, sulfur compounds, synthetic dyes…) in the presence of H_2O_2, rendering them less toxic and/or more easily biodegradable.[10] *Via* the mono-oxygenase-like function (typically that of Cytochrome P450s), it catalyzes the hydroxylation of phenols and O- N- dealkylation reactions in the presence of H_2O_2.[10] Despite its remarkable activity, MP8 presents several limitations in solution that prevent its extensive use. It can be easily and irreversibly deactivated in the presence of its co-substrate, H_2O_2. A loss of activity can also occur under acidic conditions, while its tendency to aggregate in aqueous solutions, at concentrations ≥ 2µM also decreases MP8's catalytic activity.[11–13] Moreover, similarly to the majority of enzymes, MP8 in its soluble form cannot be recycled. Finally, due to its simple structure and the lack of a specific catalytic pocket, MP8 shows a poor selectivity towards substrates.[14] The challenge of this project was thus to effectively immobilize MP8 into a solid support, in order to protect it under harsh conditions, allow its recyclability and enhance the efficiency and selectivity of its catalytic activity. To fulfill these objectives, the pore inclusion and the entrapment methods appeared to be the most appropriate as a three-dimensional confinement should allow the protection and stabilization of MP8 by creating a favourable microenvironment.

The solid supports that have been mostly studied for the pore inclusion of enzymes are mesoporous (alumino)silica[15] and clays minerals.[16] While such materials have robust structures and/or well-established biocompatibility, they may suffer from enzyme leaching due to their low affinity for biological molecules, which is not always high enough to stabilize enzymes within their structure. Subsequently, their functionalization or association with organic moieties (*e.g.* biopolymers, cross-linking agents…) is often required to increase the interactions between the enzymes and the host material.[7] The entrapment method requires synthetic conditions that will not degrade the biological activity (*i.e.* aqueous media, low temperature, no toxic by-product....) and has been mainly reported with biopolymers,[17] for compatibility reasons, and inorganic matrices (silica, alumina).[18] While the polymeric matrices may suffer from low stability (swelling, low mechanical properties), inorganic matrices have

led to relatively stable and protecting systems but the diffusion of reactants may be slow. The design of hybrid matrices through the association of different materials may be indispensable to build-up an effective support that combines organic and inorganic characteristics.[7] Moreover, the majority of these materials has a non-ordered porosity with large size distributions. An improved control of the porosity and the presence of large cavities are required to ensure a homogeneous distribution of the enzymes and promote the diffusion of substrates.

Taking into account the aforementioned drawbacks of the commonly used solid supports, Metal-Organic Frameworks (MOFs) were introduced in this work as a promising alternative to enzyme immobilization. MOFs are crystalline, highly porous, hybrid materials that are obtained by the self-assembly of inorganic and organic building blocks, giving rise to porous networks. MOFs can exhibit high internal surface areas (> 6000 m^2/g), with monodispersed and tunable micro or mesoporosity. These characteristics along with the almost unlimited chemical and structural possibilities have rendered MOFs attractive candidates for numerous applications (gas storage/separation, catalysis, drug delivery *etc.*).[19–21] The use of MOFs as host matrices for enzymes has emerged recently, most notably *via* the cage inclusion and the entrapment approaches.[22–24] The first reports were promising, showing minimal leaching and preservation of the enzymatic activity in non-natural environments.[25] These results were attributed to the hybrid nature of MOFs that stabilized the enzymes through specific interactions and to the protective microenvironment provided by the MOF framework.[22–24] Based on these first studies, the use of MOFs for the immobilization of MP8 (and other enzymes) was targeted as a possible strategy to overcome its limitations (stability, selectivity *etc.*).

The manuscript is divided into four main chapters:

The first chapter is a bibliographic survey concerning enzyme immobilization for biocatalytic applications, with a special focus on MOF materials. The interest of enzymes in biocatalysis is briefly presented. It then focuses on microperoxidase 8, its structural characteristics and catalytic properties, along with its limitations in solution. A detailed analysis of the different immobilization techniques, of the most commonly used solid matrices and of the characteristics of such materials is presented. Finally, this chapter deals with Metal-Organic Frameworks (structural properties, synthesis and main applications) and their use as host matrices for the immobilization of enzymes. It is presented in the format of a mini-review that was published in 2017, and then some recent works are highlighted.

The second chapter is focused on the use of mesoporous MOFs for the inclusion of the mini-enzyme MP8. Among the synthetized MOF structures, only the ultra-stable MIL-101(Cr) was finally selected for the cage inclusion of MP8. This immobilization of MP8 in MIL-101(Cr) and the study of its catalytic properties are presented in a format of an article, recently published.

The third chapter is devoted to the functionalization of MIL-101(Cr) and the influence of this functionalization on the encapsulation and the catalytic activity of MP8. The first part covers

the ligand functionalization of MIL-101(Cr) by two different groups (-NH_2 and -SO_3H). The functionalized MOFs were used for the inclusion of MP8. The impact of the functional groups on the enzyme loading and on its catalytic activity towards the sulfoxidation of thioanisole derivatives was evaluated. This work is presented in a format of an article that will be submitted in a near future. The second part of this chapter deals with the functionalization of the metal cluster of MIL-101(Cr) with Fe(III), in order to obtain a stable structure with a catalytic activity (Lewis acid catalysis). The attempts to obtain the mixed-metal MIL-101(Cr/Fe) will be discussed, along with the chemical stability study of this MOF.

The last chapter of the manuscript focuses on the entrapment of enzymes during the *in-situ* synthesis of the MOF material. The first part will present the efforts made to obtain MIL-53(Al)-FA under conditions that are compatible with the presence of enzymes (water as a solvent, room temperature). The synthetic conditions were then transferred for the immobilization a model protein (BSA). The extensive study of the structural characteristics of the bio-hybrid material will be discussed. The second part will focus on an alternative approach for the immobilization of enzymes by shaping hybrid MOF/alginate beads. Finally, some very preliminary results on the encapsulation of the enzyme Horseradish peroxidase and its catalytic activity will be presented, along with a preliminary study on the use of MIL-100(Fe) for the entrapment of BSA.

Finally, the conclusions and perspectives of the project are presented, along with the annexes giving supplementary information on the work.

References

(1) DiCosimo, R.; McAuliffe, J.; Poulose, A. J.; Bohlmann, G. Industrial Use of Immobilized Enzymes. *Chemical Society Reviews* **2013**, *42* (15), 6437. https://doi.org/10.1039/c3cs35506c.

(2) Secundo, F. Conformational Changes of Enzymes upon Immobilisation. *Chemical Society Reviews* **2013**, *42* (15), 6250. https://doi.org/10.1039/c3cs35495d.

(3) *Enzyme Assays: High-Throughput Screening, Genetic Selection and Fingerprinting*; Reymond, J.-L., Ed.; Wiley-VCH: Weinheim, 2006.

(4) Sheldon, R. A.; van Pelt, S. Enzyme Immobilisation in Biocatalysis: Why, What and How. *Chem. Soc. Rev.* **2013**, *42* (15), 6223–6235. https://doi.org/10.1039/C3CS60075K.

(5) Sheldon, R. A. Enzyme Immobilization: The Quest for Optimum Performance. *Advanced Synthesis & Catalysis* **2007**, *349* (8–9), 1289–1307. https://doi.org/10.1002/adsc.200700082.

(6) Dwevedi, A. Basics of Enzyme Immobilization. In *Enzyme Immobilization*; Springer International Publishing: Cham, 2016; pp 21–44. https://doi.org/10.1007/978-3-319-41418-8_2.

(7) Zdarta, J.; Meyer, A.; Jesionowski, T.; Pinelo, M. A General Overview of Support Materials for Enzyme Immobilization: Characteristics, Properties, Practical Utility. *Catalysts* **2018**, *8* (2), 92. https://doi.org/10.3390/catal8020092.

(8) Aron, J.; Baldwin, D. A.; Marques, H. M.; Pratt, J. M.; Adams, P. A. Hemes and Hemoproteins: 1: Preparation and Analysis of the Heme-Containing Octapeptide (Microperoxidase-8) and Identification of the Monomeric Form in Aqueous Solution. *Journal of Inorganic Biochemistry* **1986**, *27* (4), 227–243. https://doi.org/10.1016/0162-0134(86)80064-2.

(9) Poulos, T. L. Heme Enzyme Structure and Function. *Chemical Reviews* **2014**, *114* (7), 3919–3962. https://doi.org/10.1021/cr400415k.

(10) Ricoux, R.; Korri-Youssoufi, H.; Mahy, J. P. Microperoxidase 8 as a Powerful Tool for Biological Applications. *Journal of Biological Sciences* **2005**, *5* (1), 44–49.

(11) Valderrama, B.; Ayala, M.; Vazquez-Duhalt, R. Suicide Inactivation of Peroxidases and the Challenge of Engineering More Robust Enzymes. *Chemistry & biology* **2002**, *9* (5), 555–565.

(12) Adediran, S. A.; Lambeir, A.-M. Kinetics of the Reaction of Compound II of Horseradish Peroxidase with Hydrogen Peroxide to Form Compound III. *European Journal of Biochemistry* **1989**, *186* (3), 571–576. https://doi.org/10.1111/j.1432-1033.1989.tb15246.x.

(13) Wariishi, H.; Akileswaran, L.; Gold, M. H. Manganese Peroxidase from the Basidiomycete Phanerochaete Chrysosporium: Spectral Characterization of the Oxidized States and the Catalytic Cycle. *Biochemistry* **1988**, *27* (14), 5365–5370. https://doi.org/10.1021/bi00414a061.

(14) Dallacosta, C.; Monzani, E.; Casella, L. Reactivity Study on Microperoxidase-8. *JBIC Journal of Biological Inorganic Chemistry* **2003**, *8* (7), 770–776. https://doi.org/10.1007/s00775-003-0478-z.

(15) Hartmann, M.; Kostrov, X. Immobilization of Enzymes on Porous Silicas – Benefits and Challenges. *Chemical Society Reviews* **2013**, *42* (15), 6277. https://doi.org/10.1039/c3cs60021a.

(16) Mousty, C.; Prevot, V. Hybrid and Biohybrid Layered Double Hydroxides for Electrochemical Analysis. *Analytical and Bioanalytic Chemistry* **2013**, *405*, 3513–3523. https://doi.org/10.1007/s00216-013-6797-1.

(17) Ruiz-Hitzky, E.; Darder, M.; Aranda, P. Functional Biopolymer Nanocomposites Based on Layered Solids. *Journal of Materials Chemistry* **2005**, *15* (35–36), 3650. https://doi.org/10.1039/b505640n.

(18) Avnir, D.; Coradin, T.; Lev, O.; Livage, J. Recent Bio-Applications of Sol–Gel Materials. *J. Mater. Chem.* **2006**, *16* (11), 1013–1030. https://doi.org/10.1039/B512706H.

(19) Zhou, H.-C.; Long, J. R.; Yaghi, O. M. Introduction to Metal–Organic Frameworks. *Chemical Reviews* **2012**, *112* (2), 673–674. https://doi.org/10.1021/cr300014x.

(20) Zhou, H.-C. "Joe"; Kitagawa, S. Metal–Organic Frameworks (MOFs). *Chem. Soc. Rev.* **2014**, *43* (16), 5415–5418. https://doi.org/10.1039/C4CS90059F.

(21) Maurin, G.; Serre, C.; Cooper, A.; Férey, G. The New Age of MOFs and of Their Porous-Related Solids. *Chemical Society Reviews* **2017**, *46* (11), 3104–3107. https://doi.org/10.1039/C7CS90049J.

(22) Gkaniatsou, E.; Sicard, C.; Ricoux, R.; Mahy, J.-P.; Steunou, N.; Serre, C. Metal–Organic Frameworks: A Novel Host Platform for Enzymatic Catalysis and Detection. *Materials Horizons* **2017**, *4* (1), 55–63. https://doi.org/10.1039/C6MH00312E.

(23) Lian, X.; Fang, Y.; Joseph, E.; Wang, Q.; Li, J.; Banerjee, S.; Lollar, C.; Wang, X.; Zhou, H.-C. Enzyme–MOF (Metal–Organic Framework) Composites. *Chemical Society Reviews* **2017**, *46* (11), 3386–3401. https://doi.org/10.1039/C7CS00058H.

(24) Doonan, C.; Riccò, R.; Liang, K.; Bradshaw, D.; Falcaro, P. Metal–Organic Frameworks at the Biointerface: Synthetic Strategies and Applications. *Accounts of Chemical Research* **2017**, *50* (6), 1423–1432. https://doi.org/10.1021/acs.accounts.7b00090.

(25) Lykourinou, V.; Chen, Y.; Wang, X.-S.; Meng, L.; Hoang, T.; Ming, L.-J.; Musselman, R. L.; Ma, S. Immobilization of MP-11 into a Mesoporous Metal–Organic Framework, MP-11@mesoMOF: A New Platform for Enzymatic Catalysis. *Journal of the American Chemical Society* **2011**, *133* (27), 10382–10385. https://doi.org/10.1021/ja2038003.

Chapter 1

Enzyme Immobilization

Table of Contents

Introduction

The aim of this work was to investigate the possible use of Metal-Organic Frameworks as enzymatic immobilization matrices. This chapter will thus first cover the interest of enzymes in catalytic processes and highlight the importance of immobilizing them. In a first part, the mini enzyme chosen for immobilization, microperoxidase-8 (MP8) will be presented. The catalytic performances of MP8 along with its limitation in solution will be analyzed to show the reasons why we selected this specific enzyme for this work. The second part of the chapter will deal with the different immobilization techniques that have been reported, using a large variety of solid matrices, and will depict the benefits and limitations of such techniques. The impact of immobilization on the structural conformation of enzymes and their catalytic activities will be discussed. The key parameters that influence the catalytic activities (either in a positive or in a negative way) will be covered. In a third part, typical examples of solid supports used for enzyme immobilization along with their characteristics will be presented. Finally, the last section will be devoted to Metal-Organic frameworks. Their structural properties and synthesis will be detailed as well as their main applications. Some examples of their use for the purposes of immobilization will be provided, along with perspectives for their future use.

A. About enzymes

This section will present enzymes and the benefits gained from their use in bio-catalysis. Some examples of enzymatic processes, used in industry will be provided. Then, the section will focus on heme enzymes and in particular on microperoxidase 8 (MP8), a mini enzyme that combines two catalytic functions (peroxidase- and Cytochrome P450-like activities). The characteristics of MP8 as well as its limitations will be presented.

Biocatalytic applications exhibit many advantages as enzymes are often selective with a high turn-over numbers. They derive from natural sources and require mild operational conditions (ambient temperature, atmospheric pressure and aqueous solution) that simplify catalytic operations and lower their cost. The benefits gained with the use of enzymes, coupled with the advances in biotechnology (tailored-made enzymes, synthesis and purification on a large scale) enabled their use for industrial applications, at a lower cost than before. However, in some cases the need to include co-factors (*e.g.* NAD, NADH) in bio-catalytic processes increases the total cost. The word market of industrial enzymes reached around $4.5-5 billion in 2015, with hydrolases (*e.g.* proteases, amylases, cellulases *etc.*) being the most commonly used enzymes.[1] Some selected examples of commercially used enzymes are presented in Table 1-1.[2,3]

Table 1-1: Some enzymes used in industrial applications. Adapted from[3]

Industry	Enzyme class	Application
Detergent	Protease	Protein stain removal
	Amylase	Starch stain removal
	Lipase	Lipid stain removal
	Cellulase	Cleaning, color clarification
Starch and fuel	Glucose Isomerase	Glucose to fructose conversion
	Xylanase	Viscosity reduction (fuel/starch)
	Cyclodextrin-glycosyltranderase	Cyclodextrin production
	Amylase	Saccharification
Food	Protease	Milk clotting, flavor
	Lipase	Cheese flavor
	Lactase	Lactose removal (milk)
	Pectin methyl esterase	Firming fruit-based products
Baking	Amylase	Bread softness and volume
	Glucose oxidase	Dough strengthening
	Phospholipase	Dough stability and conditioning
	Protease	Biscuits, cookies
Textile	Cellulase	Cotton softening
	Amylase	De-sizing
	Laccase	Bleaching
	Peroxidase	Excess dye removal
Pulp and paper	Protease	Biofilm removal
	Xylase	Bleach boosting
	Cellulase	De-inking
	Amylase	De-inking, drainage improvement
Organic synthesis	Lipase	Chiral alcohols and amides
	Acylase	Semisynthetic penicillin
	Nitrilae	Enandiopure carboxylic acids
Personal care	Amyloglucosidase	Antimicrobial
	Glucose oxidase	Bleaching, antimicrobial
	Peroxidase	Antimicrobial

Enzymes for biocatalytic applications represent only a small amount of the overall enzyme market, which valued around $ 230 million, in 2015 (Figure 1-1).[1] The soluble forms of enzymes used in most applications do not allow their removal from the reaction mixtures and require time-consuming and expensive separation steps to isolate the pure products (e.g in the production of fine chemicals). Moreover, soluble forms do not allow a repetitive use, which increases the overall cost of the procedure. While the progress in enzyme engineering can allow the design of robust enzymes that will not be degraded in non-standard conditions (organic solvents, high temperatures *etc.*), the issue of their recovery still remains.[4] This drawback can be effectively addressed by the immobilization of enzymes in solid supports. The immobilization provides an easier handling of enzymes, when compared to their soluble forms (shaping of the biocatalyst). Moreover, it enables their separation from the products, thus eliminating enzyme contamination, and their recycling and reuse, resulting in a more

cost-effective process. Finally, the solid support used for the immobilization may provide stabilization and protection of the enzymes, under non-natural environments (high temperatures, organic solvents, denaturating factors, extreme pH).

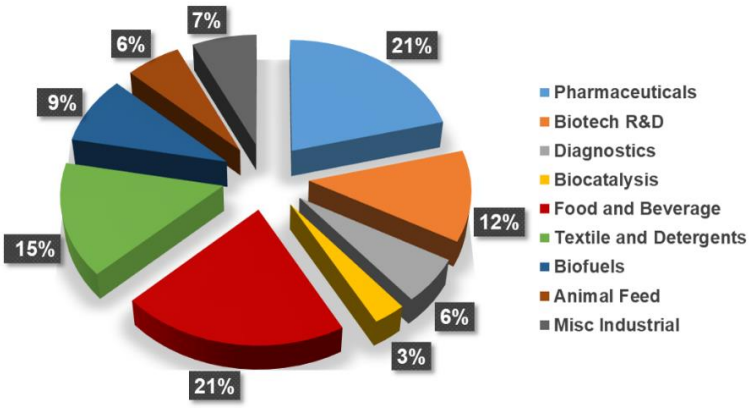

Figure 1-1: Global enzyme market by sector. Adapted from[1]

The current amount of immobilized enzymes used in real industrial applications constitutes a very small part of the total enzyme market.[1] On the contrary, the research devoted to enzyme immobilization (immobilization methods, development of new supports) is constantly increasing over the years. This difference between research and application is related to the specific requirements of industrial processes. As the immobilization procedure adds extra costs, the target is to develop new applications or offer other benefits compared to the soluble enzyme form that would compensate the added cost of immobilization.[1] Table 1-2 shows some industrials processes in which immobilized enzymes are used.

Table 1-2: Some industrial applications using immobilized enzymes. Adapted from[1]

Enzyme	Immobilization process	Application
Glucose isomerase	Cross-linked (cell)/ immobilized/covalently bonded	High fructose corn syrup from corn syrup
Nitrile hydratase	Cross-linked (cell)	Acrylamide from acrylonitrile
Lipase	Immobilized	Trans-esterification of food oils
Lactase	Immobilized	Lactose hydrolysis, galacto-oligosaccharides synthesis
Lipase	Immobilized	Biodiesel from triglycerides
Penicillin G acylase	Covalently bonded	Antibiotic modifications
Aspartase	Cross-linked (cell)/ immobilized	L-aspartic acid from fumaric acid
Thermolysin	Immobilized	Aspartame synthesis
Lipase	Immobilized/covalently bonded	Chiral resolution of alcohols and amines
Immobilized = surface adsorption or pore inclusion or entrapment		

In the following part of this section, a description of heme enzymes will be given and more specifically of microperoxidase 8 (MP8), along with its catalytic activities and applications.

Heme enzymes

Metalloporphyrins are broadly distributed in nature and among them, iron(III) protoporphyrin IX or heme (Figure 1-2) is the most common one. The main functions of heme enzymes in living cells are electron and oxygen transport and they thus constitute a subclass of oxido-reductases. This section will only focus on oxidation reactions, which were used for the purposes of this work. Two classes of heme enzymes with an oxidative activity will be presented, peroxidases that use peroxides (typically H_2O_2) to oxidize substrates (for example horseradish peroxidase, HRP) and mono-oxygenases that use O_2 to oxygenate substrates (for example Cytochrome P450s).[5]

This work focused on the use of a mini-enzyme, microperoxidase 8 (MP8) as it is an effective biocatalyst, combining both types of activities (peroxidase-like and Cytochrome P450-like). The following section will describe the structural characteristics of MP8 and its catalytic functions.

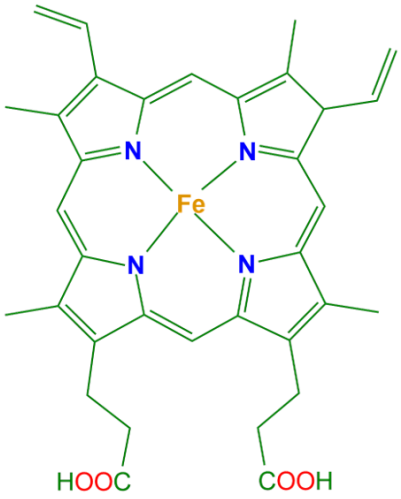

Figure 1-2: Molecular structure of iron protoporphyrin IX (heme).

Microperoxidase 8

Microperoxidases (MPs) are heme-containing peptides obtained by the proteolytic digestion of Cytochrome c (Cyt c). Seven different MPs have been isolated and consist of an iron protoporphyrin IX linked to a peptide, comprising a variable number of amino acids, that derives from Cytochrome c; MP5 (residues 13-14/17-18) MP6 (residues 14-19), MP7 (residues 14-20), MP8 (residues 14-21), MP9 (residues 14-22), MP10 (residues 13-22) and MP11 (residues 11-21).[6] This section will be exclusively focused on MP8.

1. MP8 structure

Until today, no crystal structure of MP8 has been reported. The structural description of MP8 was provided by various spectroscopic studies (mass, NMR, Raman) and dynamic simulations.

MP8, along with MP11, are the most studied peroxidase systems, as their small size facilitates mechanistic studies, allowing the easier characterization of intermediate species in solution.[6] It has been shown that the polypeptide chain retains a similar conformation to that of the amino acid residues of the parent Cytochrome c protein. The chain is covalently linked to the porphyrin moiety *via* two thioether bonds between Cys14 and Cys17 and the vinyl substituents of two pyrrole rings (Figure 1-3).[7] The peptide chain is shielding the proximal face of the porphyrin, whereas the distal face is completely exposed to the solvent. At neutral pH, a nitrogen atom of the imidazole side chain of His18 is coordinated to the iron(III) on the proximal face of the heme whereas on the distal face, the sixth axial position of the iron(III) is occupied by a water molecule. The loosely bound water molecule can be easily replaced by a variety of ligands (*e.g.* imidazole, cyanide, thioethers and primary amines). This ability of MP8 to bind different ligands has been used as a powerful tool to assess the accessibility of the Fe(III) center in MP8 complexes with different species (*e.g.* antibodies), as the coordination results in different absorbing species that can be monitored by UV-vis spectroscopy.[8] The bound H_2O molecule can be replaced by an oxygen donor (*e.g.* H_2O_2), which leads to the formation of highly oxidized intermediates (Compound I and II)[5] and to peroxidase-like and Cytochrome P450-like catalytic reactions.[9]

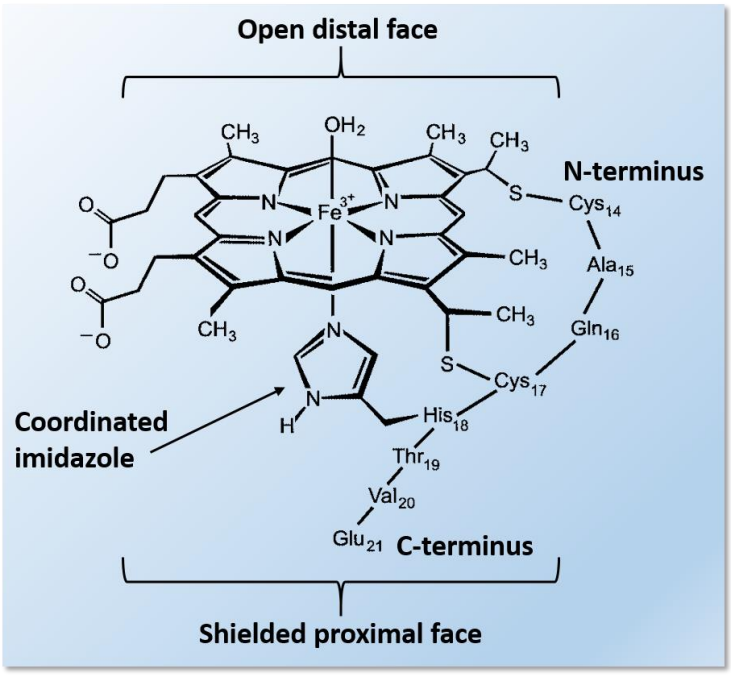

Figure 1-3: Molecular structure of microperoxidase 8. The amino acid residues numbering derives from the parent Cytochrome c from horse heart. Adapted from[9]

The coordination of His18 is crucial for the catalytic function of MP8 and is pH dependent, as seen in Figure 1-4. At low pH, the imidazole of His18 is protonated, which results in a loss of activity. The coordination to the Fe(III) occurs at pH= 4.4. In the same pH range the deprotonation of the heme propionates also occurs.[6,10]

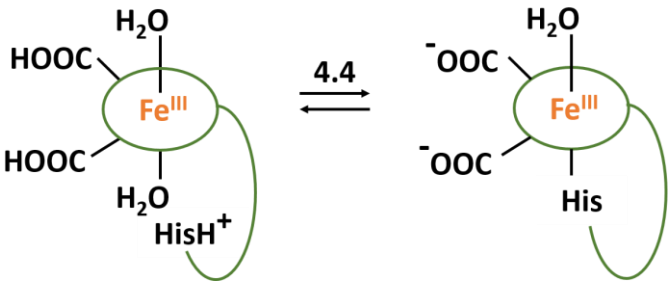

Figure 1-4: Dependence of His18 coordination as a function of pH in MP8 molecule. Adapted from[10]

2. Peroxidase cycle

The catalytic mechanism of peroxidase-like reactions of MP8 is similar to that of common peroxidase enzymes. The first step of the catalytic cycle is the formation of Compound I. In the case of heme peroxidases such as Horseradish peroxidase (HRP) and Cytochrome c peroxidase (CCP), this mechanism is facilitated by a "push-pull" effect, arising from the proximal and distal amino acid residues surrounding the heme.[5,11,12] While many studies have investigated the nature of intermediates in the catalytic cycle of MP8 with H_2O_2, [13–15] the lack of a known crystal structure of MP8 hinders the exact determination of the formed intermediates. Nonetheless, most reports suggest a similar mechanism to that of common peroxidases.[13] Figure 1-5 shows the mechanism of Compound I formation in presence of H_2O_2, for CCP that has been extensively studies thanks to the determination of its crystal structure. Moreover, this mechanism highlights the importance of the proximal and distal amino acids in peroxidases. CCP (as MP8 and most peroxidases) has a proximal Histidine (His) ligand coordinated through the N atom of the imidazole ring to the Fe(III) center. The aspartate residue (Asp) on the proximal side forms a hydrogen bond with the proximal His, which increases the electron density on the imidazole ring and thereby facilitates the heterolytic cleavage of the O–O bond (push effect).[5,16] Meanwhile, the His of the distal pocket acts as a base, withdrawing the proton linked to O_1 atom of H_2O_2. The formed distal histidinium can then transfer its proton to O_2 atom of the coordinated hydroperoxide ion, to facilitate the cleavage (pull effect) of the O-O bond that leads to the formation of the Fe^{IV}=O $CCP^{+\cdot}$ (Compound I). While CCP forms a Trp radical in Compound I, other peroxidases like HRP and MP8 form a porphyrin π cation radical.[5]

As already seen from its structure (Figure 1-3), MP8 has no catalytic pocket, with amino acids assisting the activation of H_2O_2 except the coordinated His18, thus its catalytic efficiency is relatively weaker compared to classic peroxidases. Moreover, the lack of catalytic pocket minimizes the selectivity of MP8.[17]

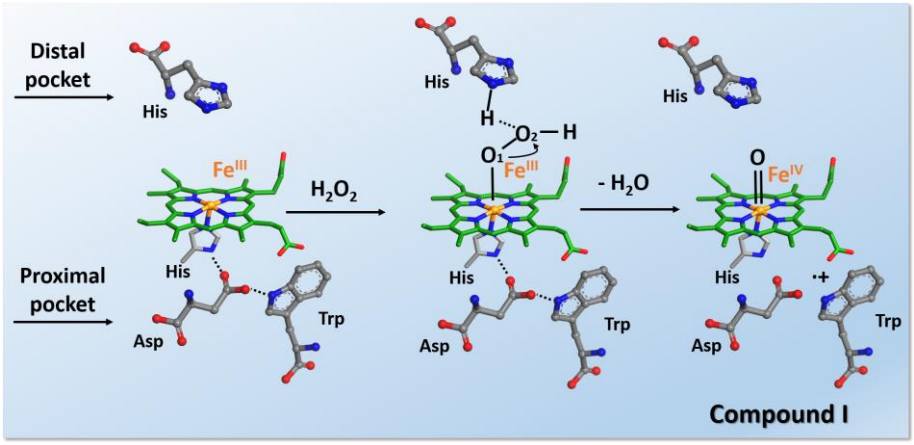

Figure 1-5: Heterolytic cleavage of H_2O_2, assisted by the distal and proximal aminoacids of Cytochrome c peroxidase and formation of Compound I (Fe atoms in orange, N atoms in blue, O atoms in red, H atoms in white and carbon atoms in grey expect carbon atoms of protoporphyrin IX, which are shown in green).Adapted from[5]

After the formation of Compound I, the next step of the peroxidase-like cycle of MP8 concerns the oxidation of a substrate molecule (SH). A first substrate molecule (SH) transfers one electron to Compound I that is reduced into the Fe^{IV} oxo species (Compound II), while the substrate is oxidized ($S^{\cdot}$). (Figure 1-6). Finally, one-electron oxidation of a second substrate molecule leads to the reduction of Fe^{IV} (Compound II) into Fe^{III} (ground state).

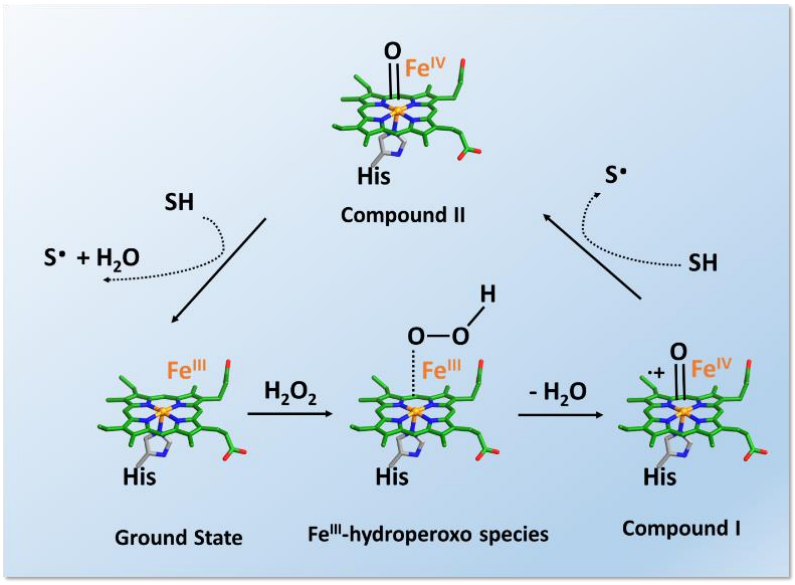

Figure 1-6: Catalytic cycle of MP8 and heme peroxidases (Fe atoms in orange, N atoms in blue, O atoms in red and carbon atoms in grey expect carbon atoms of protoporphyrin IX, which are shown in green). Adapted from[5]

Peroxidase-like reactions

The main examples of this type of activity were reported with typical peroxidase substrates like 2,2'-azino-bis(3-ethylbenzothiazoline-6-sulphonic acid) (ABTS) and 2-methoxyphenol.[18,19] MP8 was also shown to catalyze the nitration of phenolic compounds of biological interest in the presence of H_2O_2 and nitrite.[20] The S-oxidation of sulfides to sulfoxides by MP8 has also been reported, which however resulted in racemic mixtures, due to the lack of catalytic pocket. The mechanism was found to be a two-step oxygen transfer, involving a substrate

derived radical cation intermediate.[21] Moreover, MP8 (like all peroxidases) is known to enzymatically transform industrial pollutants in less toxic and more easily biodegradable products, such as phenols/halogenated phenols,[22] sulfur compounds[21] and synthetic dyes.[23,24]

3. Cytochrome P450 cycle

MP8 has a double catalytic function and beyond peroxidase-like reactions, it can also catalyze cytochrome P450-like reactions, leading to the formation of monooxyganated products.[5] However, instead of O_2 (original oxygen source of Cyt P450)[25] MP8 uses H_2O_2. The first steps of the Cyt P450-like catalytic cycle of MP8 are identical to the peroxidase-like mechanism, described above.[26] The distal water molecule bound to the sixth axial position of the Fe(III) is easily exchanged with H_2O_2, leading to the formation of oxidized intermediate Compound I.[9] The reaction proceeds with Compound I abstracting a hydrogen atom from the substrate (SH) molecule, which forms Compound II and a carbon radical ($S^{\cdot}$).[26,27] The so-called oxygen rebound of Compound II to the one-electron oxidized substrate molecule ($S^{\cdot}$) results in the formation of a monooxyganated product (SOH), while MP8 returns to its ground state (Figure 1-7).[26,27] It is important to note that monooxyganated products can also result through the peroxidase-like mechanism of MP8. In that case, two substrate molecules are oxidized ($S^{\cdot}$) by Compounds I & II (see Figure 1-6 above), and the incorporation of the oxygen to the oxidized substrates is *via* molecular oxygen or water molecules and not *via* H_2O_2.[26–28] The important difference between these two mechanisms is that with the former only monooxyganated products are formed, while with the latter a mixture with dimerized and polymerized products also occur through radical recombination of the oxidized substrates ($S^{\cdot}$).[26–28]

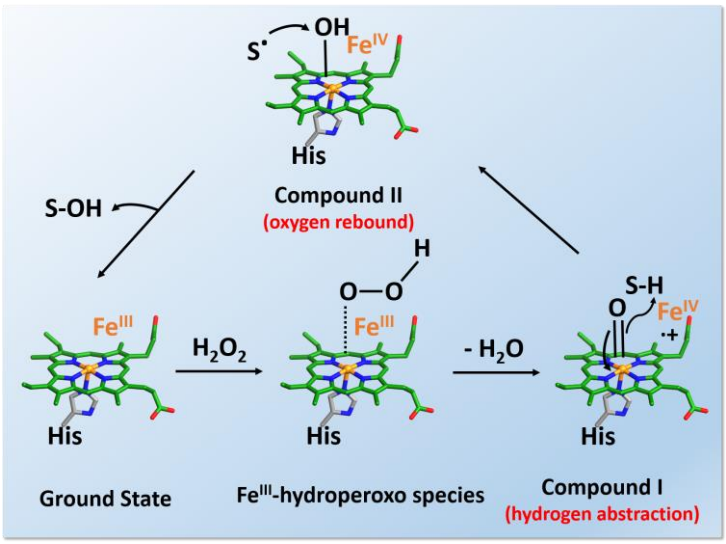

Figure 1-7: Oxygen rebound mechanism of aliphatic hydroxylation catalyzed by MP8. (Fe atoms in orange, N atoms in blue, O atoms in red and carbon atoms in grey expect carbon atoms of protoporphyrin IX, which are shown in green). Adapted from[25]

Cytochrome P450-like reactions

MP8 was shown to catalyze the para-hydroxylation of aniline and phenol derivatives in the presence of H_2O_2. The mechanism of the reaction was proven to be fully P450-like, through

an one-electron oxidation of the substrate by Compound I to give Compound II and a substrate radical that gave rise to the 4-aminophenol.[26] MP8 can also catalyze O- and N-dealkylation reactions.[27] The mechanism can be either peroxidase-like or Cytochrome P450-like. In the peroxidase-like mechanism, many polymeric products were identified and the mechanism was based on radical intermediates. However, when the peroxidase-like mechanism was blocked, the formation of polymeric products was strongly prevented, whereas the dealkylation reactions were not affected.[27] Similar results were also observed during the aromatic monooxygenation of hydrocarbons (*e.g.* benzene, naphthalene and anthracene).[28]

4. Challenges in the use of MP8

Despite the plethora of chemical reactions that MP8 catalyzes, its use in many applications is limited due to its apparent instability in solution. Three main parameters cause the loss of activity of MP8. First, MP8 (like all peroxidases) is deactivated in the presence of its natural substrate H_2O_2. This auto-oxidation is severely destructive for the heme group (heme bleaching) and irreversible. Despite structural variations between different peroxidases, a common deactivation mechanism has been proposed.[16] As seen in Figure 1-8, in the absence of substrate or in the presence of high concentrations of H_2O_2, H_2O_2 reacts with Compound II and generates superoxide radicals that convert Compound II into a highly reactive peroxy-iron(III) porphyrin free radical (Compound III), which is not part of the peroxidase cycle.[29–31] After the formation of Compound III, different decomposition pathways can occur. As the hydroperoxyl radicals are close to the heme group, one possibility is the oxidation of the porphyrin ring. This oxidation results in the cleavage of the carbon bonds that connect the pyrrole rings, leading to the destruction of the porphyrin ring and the formation of an open-chain tetra-pyrrole structure (biliverdin). This pathway can be confirmed by the detection of free Fe(III) in solution (heme bleaching). The destruction of the porphyrin ring has been observed in many peroxidases (hemoglobin, myoglobin, HRP, MP11, MP8 *etc.*)[32–34] The addition of substrate in excess can in some cases eliminate the deactivation of peroxidases, as the substrate would compete with H_2O_2 for binding in MP8.[29,35]

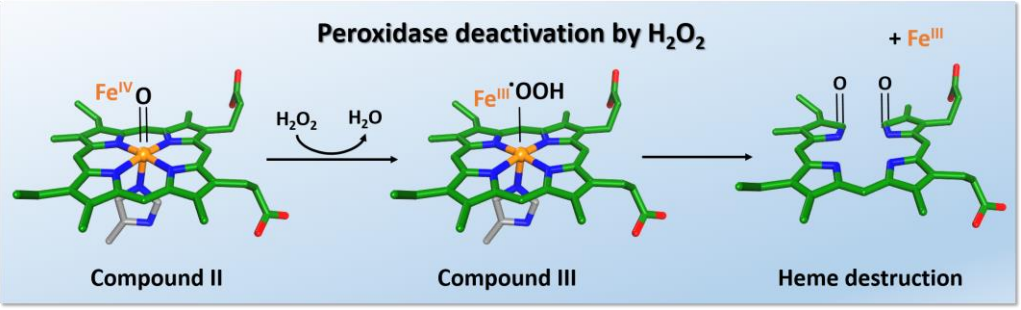

Figure 1-8: Schematic illustration of the deactivation pathway of peroxidases in excess of H_2O_2.[29] The CO groups in the deactivated molecule are shown perpendicular to the heme for reasons of clarity of the schematic illustration. In reality, they are on the same plane with the heme.

Secondly, the catalytic function of MP8 depends strongly on the coordination of His18 to the Fe(III) (push effect) and this coordination depends on the pH conditions. Therefore, under acidic conditions, in which His18 is protonated, the catalytic function of MP8 is almost

negligible, limiting its use under neutral or alkaline conditions. Finally, the use of MP8 is also hampered by its tendency to aggregate in aqueous alkaline solutions, even at low concentrations (~2 μM). Two main mechanisms are involved in the aggregation: (i) a concentration-dependent intermolecular coordination, where the N-terminal amino group of Cys14 is coordinated to the sixth axial position of Fe(III) of another MP8 molecule, thus preventing the coordination of substrates,[6] (ii) π-stacking between the more exposed distal faces of two or more MP8 molecules.[36] The intermolecular coordination can be limited by the acetylation of the amino groups of MP8. Finally, another important disadvantage of MP8 is its relatively low selectivity, due to the lack of a specific catalytic pocket.

B. About immobilization

Types of Immobilization

The immobilization of enzymes is not a new concept; significant efforts have been devoted to the design of effective solid supports for enzymes since at least the second half of last century.[37] The different types of immobilization used so far can be divided into five general categories (Figure 1-9):[2,38,39]

1. Surface Adsorption

The surface adsorption of enzymes on a solid support is achieved *via* van der Waals, electrostatic, hydrophobic interactions and/or hydrogen bonding. The supports used for this technique can be either porous or non-porous, inorganic, organic or carbon 2D or 3D materials. Some typical examples of such supports are oxides (alumina, silica), activated carbons, clays and zeolites. Key parameters for this immobilization are parameters that will drive the interactions between the enzyme and the substrate such as the pH of the mixture, the ionic strength and the relative concentrations of the enzymes and of the support. It is a mild and facile procedure, without constrains regarding the size of the enzymes but requires thorough optimization in order to prevent desorption (leaching) of the enzyme from the supports, as it is only immobilized by weak interactions. Often the cross-linking of the immobilized enzymes with glutaraldehyde is employed to minimize leaching. The orientation of the enzyme's active center must also be controlled to remain accessible to substrates. Moreover, the operating conditions need to be carefully tuned, considering that the support will offer minimal protection to the enzymes.[2,38,39]

2. Covalent Binding

In order to enhance the interactions of the enzyme molecules and the solid supports, covalent binding can be applied, that results to the irreversible binding of the enzyme molecules at the surface of the supports. The attachment of enzymes can occur directly on reactive groups present in the support (hydroxyl, amino, carboxyl groups) or by functionalizing the support with various spacer arms containing such reactive groups. The strong covalent bonds can prevent the leaching of the enzymes from the support and in some cases, provide stabilization

of the enzymes under harsh conditions (temperature, organic solvents *etc.*). However, the reduced mobility of the enzymes can also lead to severe conformational changes and decrease the catalytic activity or even completely denaturate the immobilized enzymes. Moreover, similar to the surface adsorption the exposed enzymes are not protected by the solid matrix and can be easily deactivated (*e.g.* inhibitors, proteolytic enzymes *etc.*), while the control of the orientation of the enzyme's active center is also required.[2,38,39]

3. Pore Inclusion

An alternative to the surface exposed enzymes is the inclusion of enzymes inside the cavities of porous matrices, *via* physical adsorption. An organic, inorganic or hybrid material with a three dimensional arrangement of its structure is generally used for this technique (*e.g.* mesoporous silica, porous carbons, layered double hydroxides, *etc.*). The main advantage of the pore inclusion is that the immobilized enzymes are confined inside the pores and can be possibly protected under harsh operational conditions. A minimal leaching can be also expected if the relative size of the pores and the enzyme match. On the other hand, some limitations of the procedure are the constraints regarding the size of enzymes and the mass transfer efficiency of reactants.[2,38,39]

4. Entrapment

In this category, the immobilization of enzymes takes place simultaneously with the synthesis of the solid support, yielding the entrapment of enzymes inside the support. Since the synthesis of the matrices is taking place in the presence of the enzyme molecules, the choice of the materials should be done carefully, taking into consideration that the synthetic conditions must be compatible with the enzyme's stability (hence, aqueous solutions and ambient temperatures). Typical materials used for entrapment are biopolymers (*e.g.* alginate, chitosan) and sol-gel silica. The facility (one-step procedure) and the mildness of the synthetic conditions render it a cost-effective and sustainable immobilization process. Similarly to the cage inclusion, the 3D confinement of enzymes assists in their protection, due to a favored local microenvironment and provides mechanical constrains for enzyme unfolding. At the same time, the relative low chemical and mechanical stability of certain supports (*e.g.* swelling of biopolymers) can result in severe leaching of the immobilized species. The slower diffusion of reactants through the support can be another drawback that impacts the catalytic activity of the entrapped enzymes.[2,38,39] Alternatively, entrapment of enzymes can also be achieved *via* a coprecipitation method by mixing enzymes molecules and preformed particles in solution (*e.g.* metal oxides, metallic particles…). This process results in the entrapment of enzymes inside the interparticle spaces, eliminating leaching issues that are often present in the surface adsorption.[40] While, this approach may result to efficient bio-hybrid materials, there is no control over the formed microstructure and the porosity of the material and may lead to important diffusion issues.

The combination of several immobilization strategies (*e.g.* surface adsorption and cross-linking) can be used to combine their advantages.

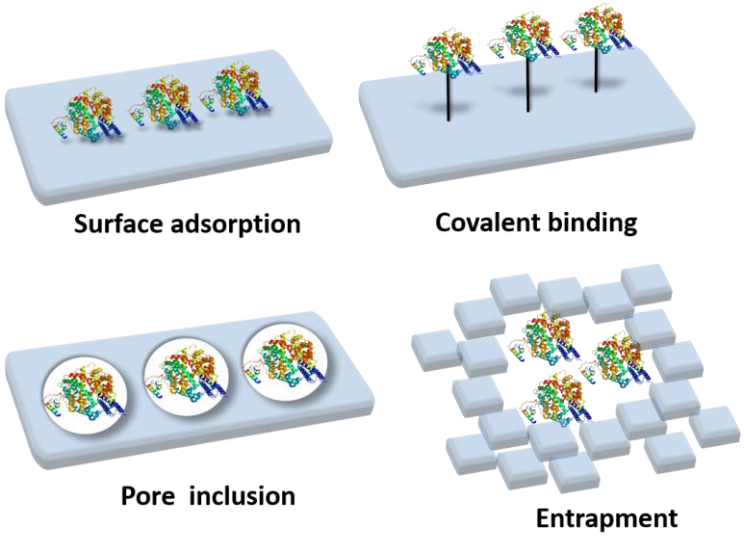

Figure 1-9: Different strategies employed in the immobilization of enzymes.

Different immobilization methods and solid supports are still being developed and the number of publications concerning immobilized enzymes is increasing every year.[41] However, it is not always clear whether the advantages gained by the immobilization result in a more effective and sustainable biocatalyst with respect to its soluble form. On one hand, immobilization provides all the benefits of heterogeneous catalysts (reuse over multiple cycles, separation of biocatalyst from product stream, enhanced stability of biocatalysts, co-immobilization with other enzymes *etc.*). On the other hand, the design of a biocatalyst with high performances requires a careful tuning of the microstructural interfacial properties of the material.

Parameters influencing the activity of immobilized enzymes

The following section will analyze the parameters influencing the catalytic efficiency of immobilized enzymes, and how they can be tuned to result biocatalysts with enhanced activity. As the number of reports concerning enzyme immobilization is vast, a few examples were selected.

1. Conformational and dynamic changes of immobilized enzymes

The conformational changes of immobilized enzymes is one of the main reasons for their activity loss.[1,4] Alteration of their native conformation mostly occurs due to interactions between the immobilized enzyme and the support and strongly depends on the nature of both components. In general, rigid enzymes (*e.g.* HRP) do not undergo as much conformation changes as flexible enzymes (*e.g. Candida Antarctica* lipase), which are more susceptible to interactions with the surface of the matrix.[42]

Enzyme-support interactions

While multiple covalent binding is more likely to cause conformational changes, weaker interactions (polar, hydrophobic/hydrophilic interactions) can also be responsible for several conformational changes, depending on the amino acid composition of the enzyme. Generally, in the quaternary structure of enzymes, hydrophobic amino acids (like phenylalanine, tyrosine

etc.) tend to be orientated towards the core of the protein, whereas acidic and basic amino acids (capable of forming hydrogen bonds) are mainly located at the surface, in order to maximize interactions with the native hydrophilic environments.[4]

- Polar interactions with the support

Conformational changes can result from the variation of the enzyme's charge state in the bulk solvent and at the surface of the support. It is well established that the local pH and ionic strength of the solution near the surface and/or present in the pores of a solid support differ from the bulk solution away from the solid.[43] Consequently, the local pH and ionic strength might not be optimal for the immobilized enzymes, causing alteration in the protonated state of amino acids and the enzyme's hydration shell and thus resulting into severe conformational changes. Moreover, the charged amino acids at the surface of the enzymes can interact electrostatically with charged groups present in the support. The attraction or repulsion can lead to distortion of the enzyme or influence its orientation to the support in a way that its active site is oriented towards the surface, becoming inaccessible to reactants. For example, Hamlin *et al.*, demonstrated that β-galactosidase showed reduced activity when immobilized onto an anionic polyelectrolyte surface, due to the conformational changes, which was not the case when a cationic support was used.[44] A different study showed that the charge density of the matrix could also affect the activity of immobilized enzymes.[45] More precisely, α-chymotrypsin was immobilized inside the mesopores of silica SBA-15 and aluminum doped SBA-15 (SBA = Santa Barbara Amorphous). The presence of Brønsted acid sites in Al-SBA-15 resulted in the protonation of the enzyme's carboxyl groups and to hydrogen bonding of the N-H groups of the enzyme with the negative charges of the support. The modified ionization state of the enzyme and the strong interactions with the support, led to a decreased enzymatic activity, compared to the pure SBA-15.[45] By carefully monitoring the charges of the solid surface (*i.e.* with ζ-potential), the micro-environmental pH (of the surface and or the pores) can be tailored depending on the nature of the selected enzymes.[4,43]

- Hydrophobic/hydrophilic interactions

Even though the surface of enzymes is mostly hydrophilic, some hydrophobic residues can also be exposed at their surface. Those hydrophobic amino acids can interact with hydrophobic surfaces, changing their structure. This was, for example, demonstrated in the case of trypsin immobilization on silica (hydrophilic) and polystyrene (hydrophobic) surfaces.[46] Trypsin showed stronger affinity for the hydrophobic surface, but almost no activity was detected after immobilization due to the structural changes in the secondary and tertiary structures of the enzyme. Moreover, hydrophobic supports have been shown to reduce enzymatic activity as they cause the unfolding of the hydrophobic core toward the surface in order to minimize the energy of the system.[4] It should also be noted however that certain enzymes such as lipases have demonstrated enhanced activities after immobilization on hydrophobic supports.[47]

Dynamics of immobilized enzymes

Another important factor that can affect the activity of enzymes is their decreased mobility after immobilization. Some enzymes like lipases require fine movements in order to perform their catalytic function.[4] In the case of surface bound enzymes, a way to solve the decrease in mobility is the attachment of the enzyme *via* a spacer arm to the surface of the support, allowing a higher dynamic motion for interactions with the substrates.[48] Nevertheless, in some cases the loss of flexibility can have positive effects on the catalytic activity. The immobilized enzymes can be stabilized in a way that no conformational changes can occur under harsh operational conditions. On the contrary, enzymes in solution are expected to lose their activity due to severe conformational changes (Figure 1-10).[49] This is typically observed when enzymes are covalently attached to rigid supports.[50] A similar rigidity occurs for enzymes confined inside rigid, porous supports (*via* entrapment or cage inclusion) that would hinder their unfolding, resulting to more thermostable and tolerant to denaturants enzymes.[51]

Enzyme Loading

The amount of immobilized enzymes can influence the overall activity since it affects the conformation of enzymes and the diffusion of substrates. Very low enzyme loadings can result to reduced enzymatic activities, due to the maximized contact between enzyme molecules and the surface of the support that causes conformational changes. Similarly, very high enzyme loadings can also lead to reduced activities due to mass-transfer limitations that arise from the formation of multilayers or aggregates of enzymes.[42]

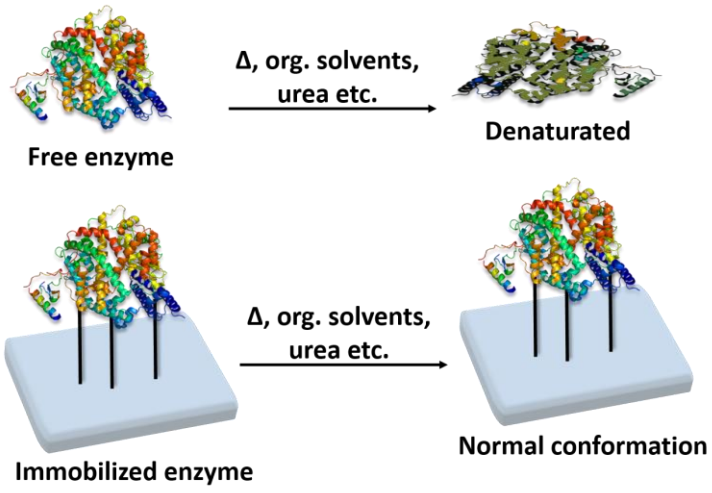

Figure 1-10: Rigidification of immobilized enzyme eliminates conformational changes under harsh operation conditions.

2. Diffusional barriers

An important parameter that can influence the activity of immobilized enzymes is the mass transport limitations and concerns both the diffusion of reactants into the active center of enzymes and the diffusion of the products from the solid support. In the surface immobilization, diffusion limitations arise mostly from the orientation of the enzymes' active

site (if the active center is orientated towards the support surface) and/or the enzyme protein loading (*e.g.* neighboring enzyme molecules blocking the access to the active site).[52] In the pore inclusion immobilization, the morphology of the pores is in very close relation with diffusion limitations. Systems with one-dimensional porosity (1D channels) are more likely to show reduced diffusion of reactants since the enzymes immobilized at the center of porous channels are more difficult to reach, resulting in a reduced activity. An interconnected porosity would limit diffusion issues, if the reactants can easily pass from one meso-channel to the other. Ideally, 3D interconnected porous systems that consist of meso-cages not fully occupied by enzymes are prone to isolate the enzymes from each other, while allowing the diffusion of analytes from all directions. In certain cases, the diffusional issues can however result in enhanced catalytic activities.[50] For instance, when high concentrations of substrates result in the inhibition of enzymes, the slower diffusion can give improved activities. For example, in the case of immobilized peroxidases a limited diffusion of the co-substrate, H_2O_2 can protect them from deactivation (heme destruction or enzyme oxidation).[50]

3. Diffusion of water

The chemical nature of the solid support as well as the diffusion phenomena can play a crucial role in enzymatic reactions, especially in those performed in organic solvents. The enzymatic activity depends strongly on the distribution of free water molecules around the enzymes, as water molecules contribute to their quaternary structure. The large majority of enzymes requires water in order to function and in dehydrated environments they lose most of their activity.[53] The use of highly porous and hydrophilic supports can be applied to ensure high water circulation around the immobilized enzymes. In that way, even when hydrophobic media are required for a specific catalytic reaction, the water molecules adsorbed on the external surface of the support will change their distribution and will be mostly oriented inside the pores, thus providing a sufficient hydrated environment for the immobilized enzymes.[53,54]

Immobilized enzyme systems are more complex compared to their soluble forms as the nature of solid supports and the physical/chemical interactions between enzymes and host matrices can modify their properties. Therefore, the solid support should not be considered as just a vessel to facilitate the use of enzymes, but also as a powerful tool to potentially optimize the properties of immobilized enzymes.

Improved enzymatic activity via immobilization

Even though many parameters can result in a decreased activity after immobilization, numerous examples in the literature report improved activity and selectivity of immobilized enzymes. These improved performances are generally attributed to a stabilization and protective effect of the solid supports, as it will be discussed below.[50]

1. Preventing enzyme aggregation

The aggregation enzymes in the reaction media may occur from different parameters such as the use of anhydrous solvents (in which many enzymes are insoluble), high enzyme

concentrations, pH conditions close to the isoelectric point of enzymes… *etc.* The aggregation results in reduced activities[50,55] but can be minimized through immobilization, *e.g.* by covalent binding, which provides a certain separation, or by pore entrapment, on the condition that each enzyme molecule is isolated inside the pores and has no contact with other enzymes. By eliminating the possibility of aggregation, immobilized enzymes can be used in higher concentrations, in the presence of anhydrous solvents.

2. Preventing inhibitors effect

The activity of enzymes can be affected by the presence of high concentrations of substrates, products/by-products of the catalytic process or inhibitors that can bind to the active site and reduce or even totally cancel the enzymatic activity.[56] In some cases, the immobilization can reduce the effect of those inhibitors and therefore increase the activity of the immobilized enzyme, compared to the enzyme in solution.[57] A possible way to eliminate the inhibition *via* immobilization is the steric exclusion of the inhibitors, as it was demonstrated for example with caldolysin that was covalently attached to Sepharose 4B (Figure 1-11).[58] The covalent binding of the enzyme to the matrix hindered the access of inhibitors to the active site, without significantly affect the catalytic activity.[58]

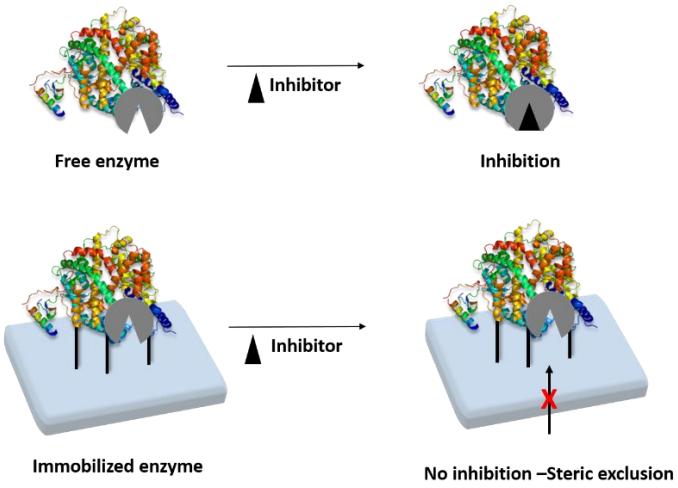

Figure 1-11: Elimination of enzyme inhibition *via* immobilization. Adapted from[50]

3. Increased activity under harsh conditions

Despite the favorable catalytic properties of enzymes, they are relatively unstable with a very narrow range of optimum operational conditions. Their immobilization inside porous supports or in certain cases, *via* covalent binding can enhance their stability under harsh operational conditions. An important parameter that influences the catalytic activity of enzymes is the pH. When immobilized in porous supports (*via* pore inclusion or entrapment), the microenvironment around the immobilized enzyme can differ from the bulk solution and provide smoother pH conditions (Figure 1-12). This was demonstrated in the case of alkaline phosphatase entrapped in silica matrices.[59] The study showed that even if the optimum pH of the enzyme was 9, it remained active when entrapped in silica even at extreme acidic

conditions (pH 0.9). This was attributed to the low number of solvent molecules (H_2O, H_3O^+) that surrounded the entrapped enzyme inside the pore, compared to the bulk solution. The impact of the few hydronium ions that were required to reach the equilibrium of pH inside the pores was therefore almost negligible (minimal denaturation). In that way, the entrapped enzyme was not severely protonated. The same results were obtained in the case of the acid phosphatase (optimum pH 4.5) which maintained its activity at pH 13.[59] The immobilization of enzymes may also allow their protection from denaturating factors. For example, in presence of high concentration of detergents, enzymes may lose their activity due to inhibition or conformational changes, while when immobilized in a porous matrix, they can be partially protected inside the pores, due to steric exclusion.[57] Similar effects can take place in the presence of proteolytic enzymes (*e.g.* pepsin that cleaves the amino acid chains). If the proteolytic enzyme is larger than the pores, it cannot interact with the immobilized enzymes, the activity of which will thus be unchanged.

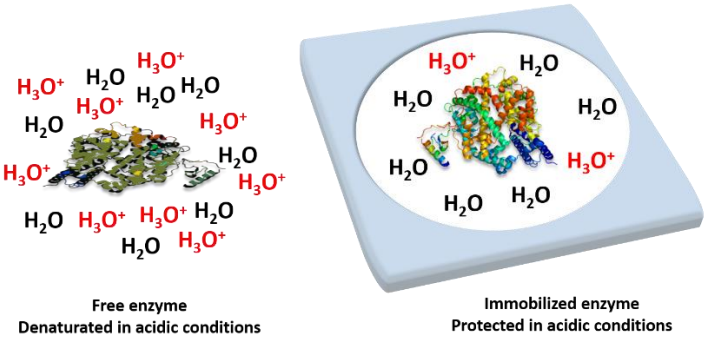

Figure 1-12: Increased activity of immobilized enzyme under acid conditions, thanks to a specific microenvironment inside the pore of the support.

One may notice that most of the discussed parameters may either have a negative or a positive influence on the catalytic activity of enzymes. Consequently, no general rule can be defined for a successful immobilization, as the line between activation/deactivation is very thin. Moreover, no immobilization process is universal and the system should be adapted each time depending the selected enzyme and the envisioned application. Thus, a careful balance needs to be found in order to turn the disadvantages of immobilization into advantages and obtain more stable and active immobilized bio-catalysts. Nevertheless, some general observations can be given. The covalent binding can be considered as an effective technique for simple systems, in which relatively robust enzymes are securely immobilized and the principal focus of the immobilization is recycling. On the contrary, surface adsorption, without any further stabilization (*e.g.* crosslinking with glutaraldehyde), is not always sufficient to retain the enzymes and prevent leaching. For more unstable enzymes, where higher control of their environment is needed (fragility, polymerization, low selectivity…), a 3D encapsulation would be preferred. Effects like steric exclusion, protective microenvironment and controlled diffusion of reactants can be achieved almost exclusively with such encapsulation systems. Considering the limitations of MP8, its 3D confinement inside a porous matrix seems an appropriate way to tackle its drawbacks and design an enhance biocatalyst.

C. Types of solid matrices used in immobilization

In this section, we will describe the most commonly reported immobilization matrices, highlighting their advantages and drawbacks. The materials will be presented based on their chemical composition (organic, inorganic…). A special emphasis toward encapsulation materials will be given, with an attention on their porosity as this method is the most adequate for the immobilization of MP8. Most materials show disordered porous networks, with wide pore distributions (*e.g.* polymers, sol-gel materials…), while others have, inherent ordered porous structures (*e.g.* clay minerals, zeolites, metal-organic frameworks…). In certain cases, the use of surfactants or templates is applied for the formation of ordered porous structures (*e.g.* mesoporous silica). IUPAC has classified porous materials based on the pore diameter into three categories: microporous materials (ø < 2 nm), mesoporous materials (2 nm≤ ø ≤ 50 nm) and macroporous materials (ø > 50 nm) (Figure 1-13). Typical examples of microporous materials are zeolites. Metal-Organic Frameworks (MOFs) fall into the same category, although some mesoporous MOFs also exist. Larger pore diameters are found in mesoporous (organo)silica materials and mesoporous carbons, whereas templated silica gels can also have pores in the range of the macropores, along with carbon foams, hydrogels (polymeric or inorganic) *etc.*[60]

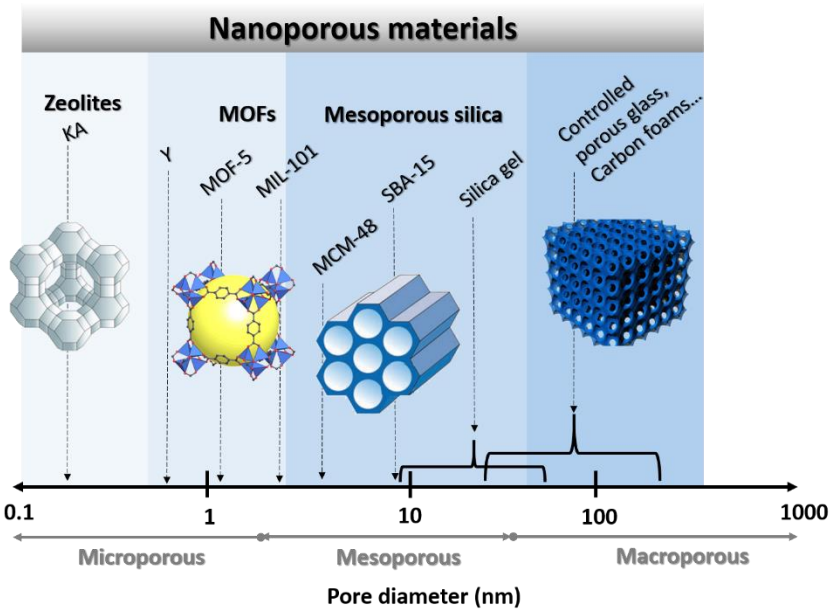

Figure 1-13: Classification of porous materials depending on their pore size. Adapted from[60]

Organic/carbon materials

1. Polymers

Polymers (synthetic and biopolymers) have been widely used as solid supports. An important advantage of polymers is their easy shaping (beads, membranes, fibers *etc.*), which is very convenient for biocatalytic applications. However, they are amorphous or semi-crystalline in nature with large pore distributions, which may not favor a homogeneous immobilization of

enzymes and renders the characterization of the materials and the localization of enzymes rather complicated.

In the case of synthetic polymers, the nature and the amount of the starting monomers determine their characteristics (solubility, porosity, stability and mechanical properties) and thus monomers can be selected based on the specific requirements of a given enzyme molecule.[61] Certain polymers require relatively low-cost synthetic procedures and have stable structures.[62] The enzyme immobilization on polymeric matrices involves usually surface adsorption (van der Waals and hydrophobic interactions). *Candida antartica* lipase B adsorbed on macroporous acrylic resin is an example of commercially available (Novozym 435) enzyme/polymer system.[38] An advantage of polymeric systems is that they can be functionalized (*e.g.* carbonyl. carboxyl, hydroxyl, amine groups *etc.*),[53] in order to provide attachment sites for the covalent binding of enzymes and to minimize the leaching usually observed for physically adsorbed enzymes.[63,64] However, it should be noted that the functionalization of polymers can be a complicated, time-consuming and costly process.[61]

Biopolymers have similar characteristics with synthetic polymers, but also possess other benefits, like natural origin, biocompatibility, biodegradability and good affinity to proteins that render them suitable enzyme supports. A large variety of materials have been extensively studied as immobilization matrices with the most common being chitosan,[65–68] alginate, cellulose[69–71] and proteins like albumin[61] and gelatin.[72–75] Biopolymers can interact with enzymes through electrostatic and van der Waals interactions,[65] as well as through covalent bonds after the functionalization of the biopolymer.[71] Regardless the advantages of biopolymers, their exclusive use is limited due to their low mechanical stability and swelling that leads to sever leaching.[74,75] Moreover, the entrapment of enzymes in hydrogels can cause important diffusion issues.[76] Often, biopolymers are combined with other more robust materials (*e.g.* silica), in order to design stable and biocompatible enzymatic matrices (see following parts). This section will focus on alginate as it was used for the purposes of this work.

Alginates is a class of polyanionic copolymers that derive mainly from brown sea algae.[77] They are linear polysaccharides that consist of α-L-glucuronic acid (G) and β-D-mannuronic acid (M) residues, connected together by β-1-4 linkages (Figure 1-14). Three distinct regions are present in alginates; MM and GG sequences that are intercalated with regions of alternating MG sequences.[78] The key advantage of alginates is their ability to form 3D cross-linked networks (hydrogels) in the presence of divalent or multivalent cations. As it can be seen from Figure 1-14, the soluble sodium salt of alginate readily forms hydrogels with high water contents (> 95 %) upon metal exchange with Ca^{2+}. In the so-called “egg-box” form, each Ca^{2+} is coordinated to the carboxyl and hydroxyl groups of four G-monomers that derive from two different chains of the biopolymer.[77,79–81] Thanks to their compatibility and gelation properties under mild conditions, alginate hydrogels have been among the most studied biopolymers for the immobilization of enzymes and whole cells, as well as for pharmaceutical applications (drug delivery, tissue regeneration *etc.*).[81,82] Alginates are usually studied under the form of beads/capsules but other forms are also possible (films, sponges, fibers) depending on the cross-linking process.[61] The shaping of alginate is also possible without gelation, for example

by ice templating processes that result in alginate foams.[83] Enzymes entrapped in alginate beads have shown enhanced stability under extreme pH conditions and temperatures, although severe leaching was observed in many cases. [61,76,84] Such drawbacks can be limited by combining alginate with other materials and enhance its stability.[85]

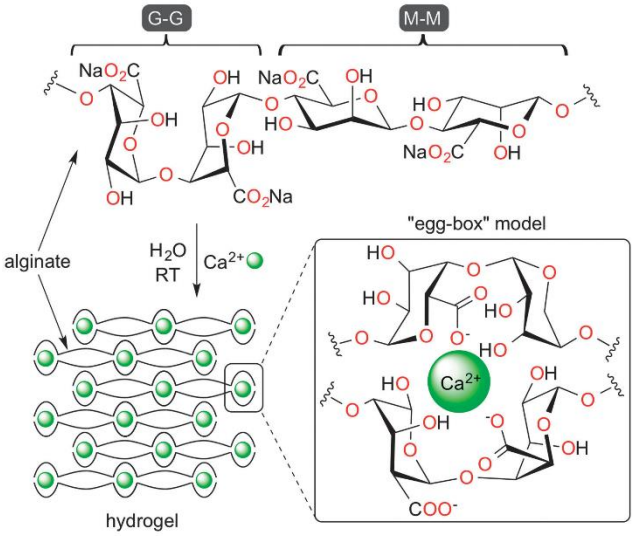

Figure 1-14: Structure of GG and MM segments of sodium alginate and cross-linking process in the presence of Ca^{2+}.[80]

2. Carbon Materials

Carbon-based materials like activated carbons, carbon foams[86] and more recently carbon nanotubes (CNTs),[87] graphene[88] and graphene oxide (GO)[89] have attracted much attention for enzyme immobilization. Carbon materials exhibit high, chemical and mechanical properties, and some of them show good thermal stability. Moreover, they can also enhance electron transfer between substrates and immobilized redox enzymes and this is why most enzyme/carbon systems are tested for bio-electrochemical sensing applications and biofuel cells.[61] The enzyme immobilization in most carbon-based materials is performed *via* surface adsorption and covalent binding, after functionalization. The enzymes are thus, exposed at the surface and not protected by the solid support. In few cases, this drawback has been addressed by the combination of multiple carbon materials (*e.g.* activated carbon and CNTs or CNTs and GO) that resulted in complex systems, with enhanced protection of the enzyme molecules (Figure 1-15).[87,89] However, those approaches may be rather complicated, costly and not easily adaptable for different systems. In the case of porous materials, like activated carbons or carbon foams, the cage inclusion can also be used, which allows a better control of the enzymes' environment. Nonetheless, the large pore size distributions may result in poor homogeneity of the enzyme's distribution and/or to the aggregation of the enzymes in large mesopores of macropores. Alternatively, ordered mesoporous carbons (OMCs) have also been extensively studied for enzymatic immobilization, which are usually synthesized with carbon sources in the presence of silica templates.[90] More recently, some few examples of Covalent Organic Frameworks (COFs) used for the immobilization of enzymes in their mesopores have also been reported.[91,92]

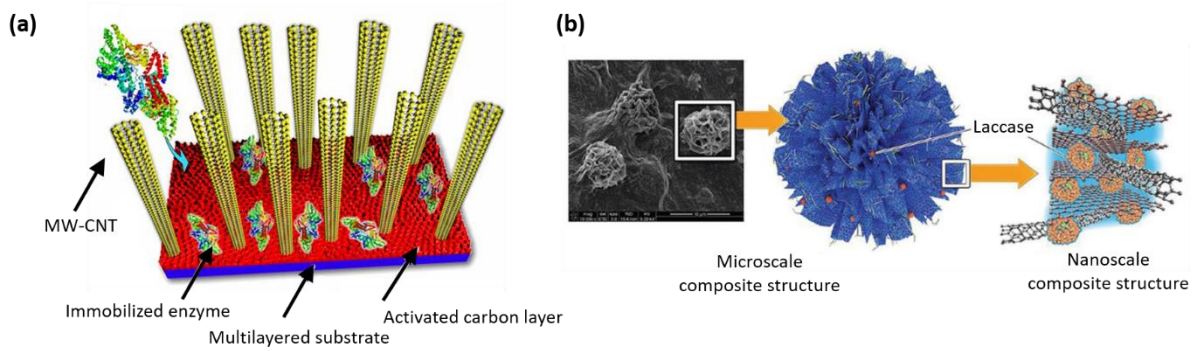

Figure 1-15: (a) Catalase and HRP immobilization *via* covalent binding on carbon film, decorated with multiwall CNTs;[87] (b) Laccase immobilized in a 3D flower-like structure *via* the self-assembly of graphene oxide, CNTs and copper phosphate.[89]

Inorganic Materials

1. Inorganic Oxides

Several inorganic oxides have been used for immobilization purposes. Their robustness (mechanical, chemical and thermal stability), as well as their microbial resistance compared to most organic materials and their biocompatibility have rendered oxides like silica (SiO_2), titania (TiO_2) and alumina (Al_2O_3) important supports for enzymes and other biomolecules.[61] Several enzymes have been immobilized at the surface of inorganic oxides *via* physical adsorption or covalent binding (depending on the nature of the surface).[61,93,94] However, the large advantage of such materials is the possibility to synthesize them under mild conditions at room temperature *via* the sol-gel process, which can be compatible with the enzyme molecules. The typical sol–gel process involves the hydrolysis of metal alkoxide precursors under acidic conditions, followed by the condensation and poly-condensation of the hydroxylated units, leading to the formation of amorphous porous gels.[95] However, while this process is performed in mild condition, the formation of alcohol during the hydrolysis of metal alkoxides and the acidic pH can denaturate enzymes. Several biocompatible routes have been developed to adapt the sol-gel process in the presence of enzymes and biomolecules (*e.g.* addition of biomolecules after alcohol evaporation, use of sodium silicate, use of biocompatible alcohols…).[96] The pore diameters depend strongly on the synthetic and drying conditions of the gels, but they have generally sub-micrometer dimensions.[95] When the enzymes are mixed with the alkoxide precursors, they end-up entrapped inside the metal-oxo polymer matrix, while remaining accessible to external reagents.[97] The following section will focus extensively in the use of silica gel for the immobilization/entrapment of enzymes, as it represents the most studied inorganic oxide for such applications. Nevertheless, titania and alumina gels have also been used for the entrapment of enzymes, resulting in stable enzymes under denaturating conditions, with long-operational performances.[98,99]

Sol-gel silica

Sol-gel silica materials have attracted enormous attention since the early 1900's for the purposes of enzyme immobilization and other biological molecules, like antibodies, DNA,

phospholipids and even whole cells (Figure 1-16).[96,100,101] It has been demonstrated in many studies that the entrapment of enzymes in the sol-gel rigid matrix provides a protective environment, which does not allow their unfolding and denaturation under extreme conditions (non-physiological pH, high temperatures, organic solvents).[59,102–105] Braun *et al.* reported one of the pioneer works on sol-gel immobilized enzymes, in which alkaline phosphatase (ALP) was immobilized in a sol-gel silica glass.[102] The entrapped ALP maintained only 30 % of its activity compared to the free enzyme, but the enhanced stability at elevated temperatures (70 °C) and the high stability over storage at room temperature (2 months) were encouraging results that led to the thorough exploration of sol-gel immobilization matrices.

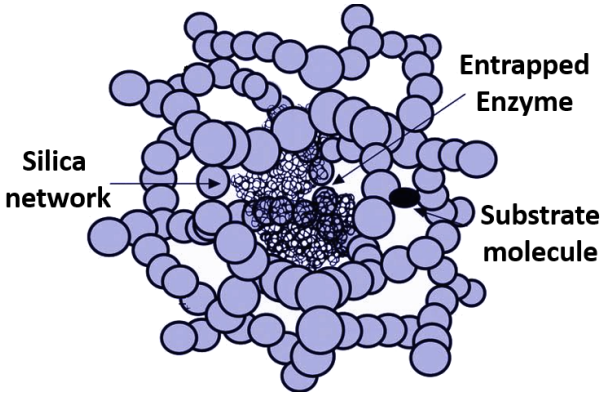

Figure 1-16: Enzyme entrapment in silica gel matrix, which remains accessible to reactants (*e.g.* substrate molecules), *via* the porous network. Adapted from[97]

Silica is composed of SiO_4 tetrahedra with shared vertices. Its structure is an infinite lattice of Si-O-Si siloxane bridges, whereas on its surface silanol groups (Si-OH) are also present due to hydration of silica and/or due to incomplete condensation.[93] The silanol groups have an acidic character, rendering silica surfaces negatively charged in a wide range of pH that can interact with enzyme molecules *via* electrostatic interactions. However, the lack of functional groups in the silica matrix can in certain cases result in the leaching of the enzymes in the solution. This drawback has been addressed by the synthesis of hybrid organic-inorganic sol-gel silica, using either mixtures of organic molecules with the alkoxides or organosilanes.[106,107]

While the entrapment of enzymes in silica gels is an extensively used and effective procedure, in certain cases a more fine control of the porosity is required, with narrow pore distributions and spatial compartmentation of the enzymes. For such cases, the use of ordered mesoporous silica materials can be applied.

Mesoporous Silica

Mesoporous silica materials represent a very important category of porous solids used for enzyme immobilization, thanks to their high surface areas, specific pore volumes and their narrow pore distributions.[108,109] They are generally prepared by the polymerization of silica alkoxide precursors in the presence of surfactants (and triblock copolymers) that act as templating agents. Upon thermal treatment at elevated temperature (~ 500 °C), the templating micelles are removed leaving large mesopores. Even though, mesoporous silica

materials are amorphous, their porosity presents a long-range order, due to the templating mesoscopic organization. Depending on the surfactants used and the synthetic conditions, materials of different pore diameters and surface areas (up to 1500 m^2/g) can be obtained.[110]

The first report on ordered mesoporous silica was made in the early 1900's, with the family of M41S materials, like the hexagonal (MCM-41), the cubic (MCM-48) and the lamellar (MCM-50) forms (MCM = Mobil Composition of Matter) (Figure 1-17).[111,112] These materials possess regular arrays of pores up to 4 nm in diameter, with narrow pore distributions. Even though, the possibility of using these materials for enzyme immobilization was explored, they were mainly used for catalytic applications. The field of enzyme immobilization, using such materials, expanded importantly with the development of extra-large mesoporous silica, like SBA-15[113,114] (SBA = Santa Barbara Amorphous) with pore size up to 8-10 nm that can serve for the cage inclusion of enzymes.

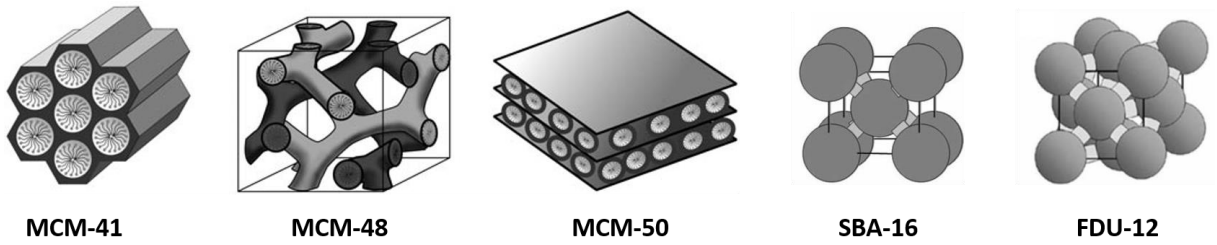

Figure 1-17: Structures of some typical mesoporous silica materials. MCM-41 (2D hexagonal), MCM-48 (cubic) and MCM-50 (lamellar) and the mesoporous cage-like silica, SBA-16 (body-centered cubic) and FDU-12 (face-centered cubic).Adapted from[115,116]

Some of the most studied mesoporous silica for enzyme immobilization are shown in Table 1-3. MCM-41 and SBA-15 have 3D hexagonal structures and exhibit the same 1D porous system (with different pore diameters), whereas FDU-5 (FDU= Fudan University) has a 3D cubic structure, with a bicontinuous, gyroidal pore system. Finally, SBA-16 and FDU-12 have 3D structures with 3D cage-like pores, which are connected together *via* microporous channels. Despite the large pore volume of the cages, the size of the channels can sometimes be a limiting parameter for the immobilization of enzymes.[116,117]

Table 1-3: Some ordered mesoporous silicas used for enzyme immobilization. Adapted from[117]

Mesoporous silica	Pore diameter (nm)	Structure
MCM-41	2-5	Hexagonal array of 1-D channels
SBA-15	5-10	Hexagonal array of 1-D channels
FDU-5	5-8	Bicontinuous gyroidal structure
SBA-16	min. 1-6; max. 4-9	Body-centered arrangement of cages
FDU-12	min. 4-9; max. 10-12	Face-centered arrangement of cages

As discussed for the sol-gel silica, many efforts have been made to incorporate organic groups to mesoporous silica materials and obtain hybrid networks that would provide specific interactions with enzyme molecules and other biomolecules.[115,117–119] However, the incorporation of organic moieties can sometimes result in decreased pore volumes or even to

total pore blockage, depending on the size of the organic groups, as well as to disordered pore systems with relatively wide distributions.[115] Alternatively the cross-linking of enzymes (*e.g.* glutaraldehyde) can also stabilize their immobilization and prevent leaching.

While, inorganic oxides provide many advantages for the immobilization of enzymes, like biocompatibility, stability and the possibility to synthesize them in mild conditions compatible with enzymes, their amorphous nature, along with the wide pore size distributions do not always allow a fine tuning of the immobilization. Moreover, their inorganic nature is sometimes insufficient for the stabilization of enzymes and their functionalization with organic moieties is indispensable to prevent leaching. Finally, concerning the mesoporous silica materials, they represent an effective alternative, when more controlled porous systems are required, but their functionalization is also indispensable.

2. Clay minerals

Clay minerals are two-dimensional lamellar inorganic solids and are generally divided into cationic clays and layered double hydroxides (LDHs) or anionic clays.[120] Cationic clays derive from natural sources and are aluminium or magnesium phyllosilicates, build up from one or two tetrahedral sheets, sandwiching one octahedral metal oxide or hydroxide sheet. In the tetrahedral sheets the dominant cation is Si^{4+}, whereas in the octahedral sheets the cation is usually Al^{3+} or Mg^{2+}. The isomorphic substitutions within the octahedral and/or the tetrahedral sheets lead to negative charges of the layers, which are compensated by interlayer cations.[121] LDHs are synthetic clays with a layered structure, composed of positive layers $[M_{1-x}^{2+}M_x^{3+}(OH)_2]^{x+}$, which are separated by intercalated anions and water molecules $[A_{x/n}\cdot nH_2O]^{x-}$ (Figure 1-18). A variety of chemical composition exists, like MgAl-LDHs, ZnCr-LDHs, NiAl-LDHs, ZnAl-LDHs *etc.*[122] Clay minerals have been extensively used for the development of amperometric (bio)sensors, due to their thermal and chemical stability, their well-defined layered structure, their ion-exchange properties and their low cost.[123] Cationic clays have the ability to swell and adsorb enzymes molecules between their layers. The adsorption of enzyme molecules in LDHs can be performed either by a delamination-restacking process that results in the entrapment of enzymes between the LDHs sheets or by a coprecipitation method in the presence of enzymes.[122] Usually clay minerals suffer from leaching issues that can be addressed *via* covalent binding to reinforce the relatively weak interactions (electrostatic and van der Waals) of such inorganic matrices with enzymes.[121] Alternatively, cross-linking with glutaraldehyde or composites with biopolymers (*e.g.* chitosan and alginate)[120] have also been used to stabilize the enzymes in the matrices, but they may lead to diffusion issues.

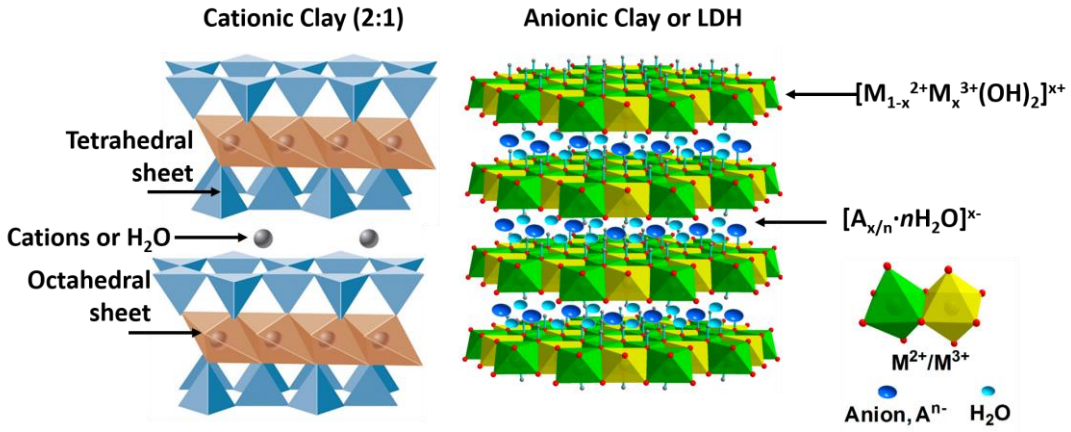

Figure 1-18: Left: Structure of a cationic clay (2:1) in which cations and water molecules separate the negatively charged layers; Right: Structure of an anionic clay or LDH in which anions and water molecules separate the positively charged layers. Adapted from[124]

3. Zeolites

Zeolites are natural or synthetic, crystalline, hydrated aliminosilicates. They are composed of TO_4 tetrahedra (T= Al^{3+} or Si^{4+}) that are corner-linked to each other by sharing all of the four oxygen atoms. The infinite extension of the tetrahedra gives a 3D microporous network. The diameters of the micropores are between 3 and 10 Å and depend on the number of the TO_4 tetrahedra (Figure 1-19).[125] The micropores are occupied by counter ions (mostly Na^+, K^+, Mg^{2+}, Ca^{2+}), which can easily be exchanged with other cations depending on the selected application.[126] Zeolites have been mostly studied and used for gas adsorption/separation thanks to their molecular sieving properties[127] and as catalysts (oil reefing, petrochemical processes *etc.*)[128] However, some examples for enzyme immobilization have also been reported.[129]

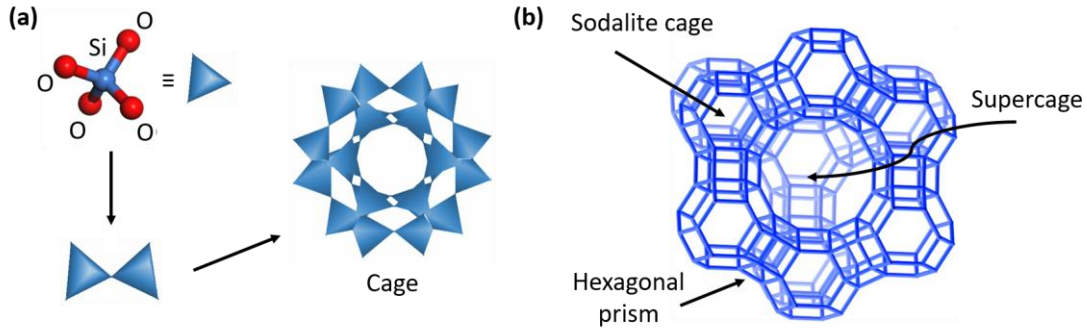

Figure 1-19: (a) Schematic representation of a zeolite assembly, where corner-sharing TO_4 tetrahedra (T= Al^{3+} or Si^{4+}) form the secondary building unit (SBU)of the 3D network; (b) Zeolite framework with faujazite topology, in which sodalite cages and hexagonal prims form a supercage.

The microporosity of zeolites does not allow their use for the pore inclusion strategy, as their sizes are smaller than that of enzymes. Different approaches have been proposed in order to create meso/macroporosity in zeolites. Silica spheres have been used as templating agents to create 3D interconnected macroporous zeolite membranes.[130] Alternatively, a partial desilication with alkaline solutions (partial dissolution of the structure by removal of Si atoms)

can be applied to generate non-periodic mesoporous cavities.[131] However, these approaches can be relatively complex and thus zeolites are not extensively used as enzymatic immobilization matrices.

Evaluating the materials already studied for the immobilization of enzymes, it is impossible to select just one (or even a group of them) as an ideal candidate for immobilization. Nonetheless, depending on the targeted application, different characteristics of solid supports are required. For biocatalytic applications, which is the purpose of this study, the key issues that need to be addressed *via* immobilization are the stabilization and protection of enzymes under denaturation conditions, the minimization of leaching and the enhanced diffusion of substrates. Thus, an "ideal" support should provide specific interactions with enzymes, while been relatively mechanically and chemically robust to prevent leaching. The presence of ordered-porous networks, compatible with the size of enzymes may ensure their protection from non-natural operation conditions, allow a homogeneous immobilization and promote the diffusion of substrates. Based on these requirements some general conclusions can be drawn for the commonly studied matrices.

Organic materials possess the advantages of specific interactions with the biomolecules and some of them are biocompatible. At the same time, they can suffer from swelling, causing enzyme leaching and they also have low mechanical properties. On the other hand, inorganic materials are more robust, but they do not show high affinity to biological molecules. Their organic-functionalization is often necessary either to provide specific interactions and/or to improve the compatibility between the material and the enzyme. Thus, the association of different materials is necessary to provide a hybrid material that combines inorganic-organic characteristics. Furthermore, with the exception of mesoporous silica, most of the materials have poorly controlled porosity, with high size distribution or microporosity, which is incompatible with the size of enzymes. In the next section, the case of the porous hybrid materials named Metal-Organic Frameworks (or MOFs) as potential immobilization matrices will be discussed. MOFs possess hierarchical micro- or mesoporosity that can be exploited for the immobilization of enzymes. Even though, as we will see, MOFs can answer some of the problems mentioned previously (hybrid nature, ordered crystalline structure, hierarchal porosity…), their exploitation as immobilization matrices is in its infancy, compared to traditional supports and lots of questions need to be addressed in the next years. However, the first scientific results seem promising and perhaps the field of enzyme immobilization can take advantage of those materials for industrial applications in the future.

D. Metal-Organic Frameworks

Metal-Organic Frameworks (MOFs) is a class of crystalline, porous, hybrid materials. The assembly of inorganic and organic building blocks gives rise to infinite 3D porous networks (Figure 1-20). Their unique characteristics: high porosity (up to 90 % free volume), high internal surface areas (> 6000 m^2/g) and almost unlimited chemical and structural tunability have rendered MOFs attractive candidates for a vast number of applications (gas

storage/separation, catalysis, drug delivery *etc.*).[132–134] The research on MOF materials began in the late 80's with a first example reported by R. Robson[135] and expanded in the 90's, with multiple groups (S. Kitagawa, O. M. Yaghi and G. Férey) reporting new MOF structures.[136–138] Some of the first well-known MOFs are MOF-5, HKUST-1 (HKUST= Hong-Kong University of Science and Technology), the series of flexible MOFs, MIL-53 and MIL-88 (*i.e.* pores volume increases or decreases upon external stimuli) and the stable mesoporous MOFs, MIL-100 and MIL-101, (MIL= Matériaux Institut Lavoisier).[138–142]

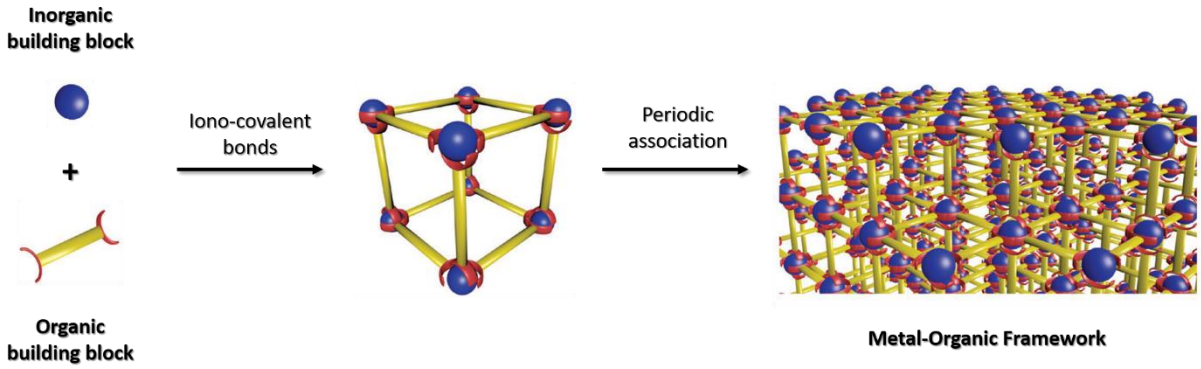

Figure 1-20: Schematic illustration of the construction of Metal-Organic Frameworks. Inorganic and organic building units are associated *via* strong iono-covalent bonds to form elementary units. To periodic association of these units gives rise to infinite 3D frameworks. Adapted from[143]

1. Building blocks of MOFs

The inorganic building block is formed by various elements such as 3p metals (Al^{3+}, Ga^{3+}, In^{3+}), transition metals (Zn^{2+}, Cu^{2+}, Fe^{3+}, Cr^{3+}, Ti^{4+}, Zr^{4+}…), alkaline earths, or also lanthanides and actinides.[144–146] The inorganic blocks can either be single metal atoms, like in the case of ZIF-8 (ZIF = Zeolitic Imidazole Framework), metal clusters or metal chains, known as SBUs (Secondary Building Units). Depending on the nature of the metal cation and its reactivity in solution, different SBUs can be formed in the presence of polydentate organic ligands (Figure 1-21). Some SBUs can also be isolated as molecular complexes (e.g CuO_5 dimer,[147] μ_3-oxo trimers[148] and $Zr_6O_4(OH)_4$ hexamers),[149] whereas others are formed only in the presence of ligands during the MOF synthesis (*e.g.* 1D chains of trans-connected $AlO_4(OH)_2$ octahedra).[150–152] The geometry of the SBUs (along with the synthetic conditions) govern the structural characteristics of the MOF framework.[153] In general, high valence cations (M^{3+} or M^{4+}) result in more stable (chemically and thermally) structures compared to divalent cations, thanks to the stronger metal-oxygen bonds.[144] The organic building blocks can be different di-, tri- or poly-dentate ligands as carboxylic acids, N-donor ligands (*e.g.* imidazole and pyridine), sulfonates and phosphonates (Figure 1-22). A combination of different ligands (with different lengths and functional groups) is also possible. Aromatic carboxylic acids are generally preferred for the synthesis of highly porous and robust structures, as they form strong iono-covalent bonds with metal ions (M-O-C), resulting robust SBUs and MOF structures. Moreover, the ionic nature of such ligands results generally in neutral frameworks, obviating the need

for charge compensating counter-ions in the pores and thus diminishing the risk of framework collapsing after the evacuation/exchange of the counterions.[151]

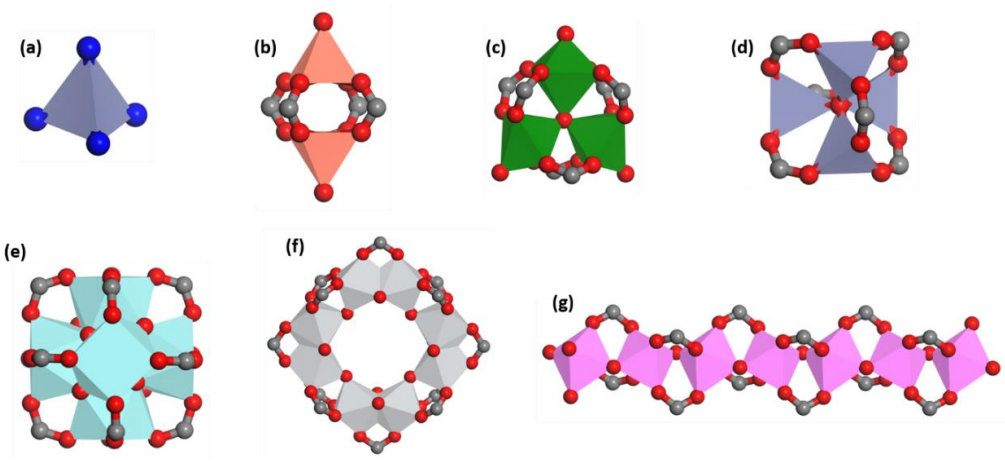

Figure 1-21: Examples of SBUs than can be found in MOF structures. (a) Zn^{2+} ion of ZIF-8, connected with four N atoms of the ligands; (b) CuO_5 dimer of HKUST-1 (or IR-MOF-1); (c) μ_3-oxo trimer of MIL-100/101(Cr,Fe,Al); (d) ZnO_4 tetramer of MOF-5; (e) $Zr_6O_4(OH)_4$ of UiO-66; (f) TiO_5OH octamer of MIL-125 and (g) 1D $AlO_4(OH)_2$ chain of MIL-53 (C atoms in grey, O atoms in red, N atoms in blue).

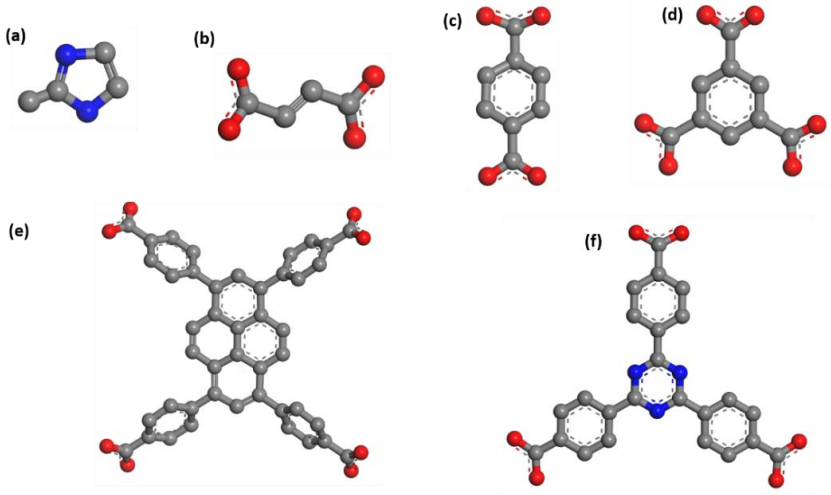

Figure 1-22: Examples of ligands commonly used for the synthesis of MOFs. (a) 2-methylimidazole; (b) fumaric acid; (c) terephthalic acid; (d) trimesic acid; (e) 1,3,6,8-tetrakis(p-benzoic-acid)pyrene (H_4TBAPy) and (f) 4,4',4''-s-triazine-2,4,6-triyl-tri-benzoate (TATB). C atoms (grey), O atoms (red), N atoms (blue), H atoms are omitted for clarity and dotted lines represent aromatic or partial double bonds.

2. Synthesis

The large majority of the reported MOF structures has been obtained by (hydro)-solvothermal syntheses. Solvothermal reactions consist in heating the starting reactants (organic ligand and metal source) in closed vessels, under autogenous pressure above the boiling point of the selected solvent (or water in case of hydrothermal reactions). These conditions favor the dissolution of generally insoluble aromatic ligands and promote the reactivity of inert ions (*e.g.* Cr^{3+}).[154] Some MOFs obtained by (hydro)-solvothermal reactions are MIL-100/101, MIL-53, PCN-333/777, UiO-66, *etc.* (PCN = Porous Coordination Networks, UiO = Universitetet i Oslo). A special sub-class of (hydro)-solvothermal reactions includes those performed under

microwave irradiation (microwave-assisted (hydro)-solvothermal synthesis). The use of microwaves (mw) permits high heating rates and homogeneous heating throughout the sample, which results in the acceleration of the nucleation/crystallization process and possibly the formation of monodispersed, nanoscaled materials. The first example of such synthesis was MIL-100(Cr), which was synthesized in only 4 h, under mw at 220 °C, compared to the conventional hydrothermal synthesis that requires 96 h.[141,155] Since then, the use of mw-synthesis has attracted enormous attention and its extensive use and optimization has resulted in the formation of nanoMOFs (particle size in the nanoscale) in very short reaction times (nanoMIL-101(Cr): 50 nm in 5 min; nanoMIL-101(Fe)-NH_2: 173 nm in 5 min; nanoMIL-100(Fe): 60 nm in 30 min…).[156,157] Reactions at ambient pressure at various temperatures (RT ≤ T ≤ solvent boiling point), such as room temperature or reflux syntheses have also been used for MOF synthesis. Ambient pressure syntheses allow a better control of the reaction conditions and the study of product formation (*via* kinetic studies with aliquots of the reaction) Moreover, such syntheses are more suited for large-scale productions, especially when non-toxic solvents are used. Typical examples of MOFs synthesized under ambient pressure are MOF-5, HKUST-1, ZIF-8 *etc.*, Even though, the number of MOFs synthesized under such conditions are limited compared to the vast number of solvothermally obtained structures, extensive efforts have been made in the last years to optimize the synthetic conditions and pass from (hydro)-solvothermal reactions to more sustainable syntheses.[158] Finally other synthetic methods, such as electrochemical, mechanochemical and sonochemical methods, have also been applied for MOFs, but to a lesser extent.[154] A key point after the synthesis of MOFs is the evacuation of the solvent molecules and the impurities (*e.g.* unreacted ligand molecules) contained in the pores and obtain highly porous materials.

3. Structural characteristics of some M^{3+}-polycarboxylate MOFs

As mentioned above, depending on the chosen metal cation and organic linker, different structures can be obtained. Depending on the synthetic conditions, the same building blocks (inorganic and organic) can lead to MOFs with different topologies that are called "MOF polymorphs". The formation of different polymorphs in respect to the synthetic conditions is a key to understand the driving forces of the synthesis. Another possibility is to obtain similar topologies but with different organic ligands (having the same symmetry). In that case, the term "isostructural MOFs" is employed. It is a very powerful tool to modulate the physicochemical properties (hydrophobic/hydrophilic balance, stability, flexibility…) and the pore size of MOFs. In this section, these two cases will be discussed for M^{3+}-polycarboxylate MOFs, which are the main MOFs studied in the next chapters due to their high chemical stability.

In general, when water in used as solvent, the synthesis of most M^{3+} cation MOFs is performed under slightly acidic conditions to avoid the competing formation of metal oxides/hydroxides, which are predominant in a large range of pH as seen from the Pourbaix diagrams of Cr, Fe and Al in water (Figure 1-23). However, the acidic conditions hinder the solubilization of the organic ligands due to the protonation of the carboxylate group. This obstacle is in most cases

addressed by the use of hydrothermal conditions that allow the increase of temperature above 100 °C, promoting thus the solubilization of the ligands. Typical example are the hydrothermal synthesis of MIL-69(Al) [159] at 210 °C and MIL-101(Cr)[142] at 220 °C. Alternatively, the use of organic solvents allows the solubilization of the ligands and limits the formation of oxides. The use of additives as inhibitors like HF, HCl or monocarboxylic acids can also contribute to the formation of highly crystalline MOF structures.[144]

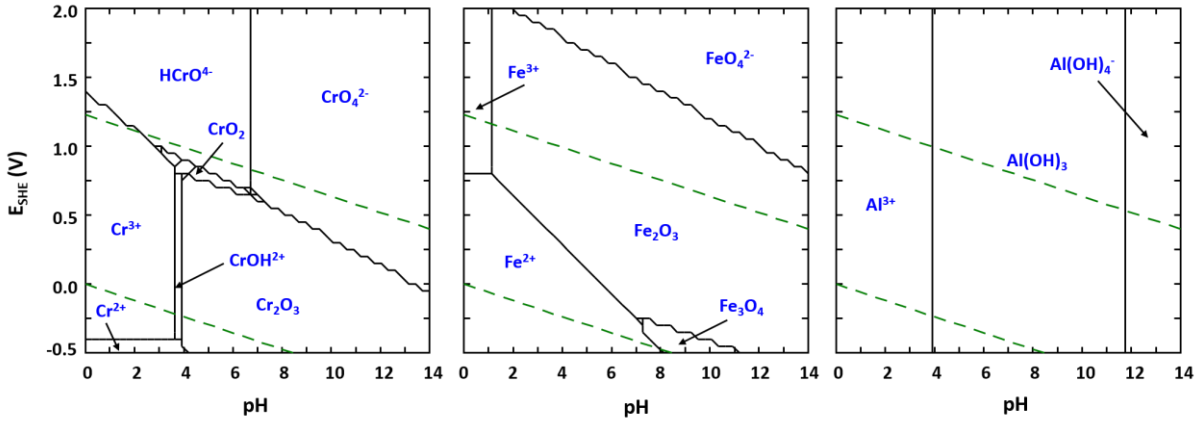

Figure 1-23: Pourbaix diagrams of chromium (left), iron (middle) and aluminum (right) calculated for [M^{3+}] = 0.001 M, at 25 °C, using the Hydra/Medousa software. Green dashed lines represent the redox couples O_2/H_2O and H_2O/H_2.

MOF polymorphs

Among the possible SBUs of M^{3+} cations (Al, Sc, V, Cr, Fe…) formed with polycarboxylate ligands, two SBUs are mostly predominant: the 1D chain build up from μ_2-hydroxo corner-sharing octahedra and the μ_3-oxo trimer of MO_6 octahedra (Figure 1-22 c and g).[144]

When the 1D chain SBU is combined with linear dicarboxylate ligands, two polymorphs are mostly formed, MIL-68 and MIL-53 with the M(OH)(BDC) formula (BDC= benzene dicarboxylic acid, *i.e.* terephthalic acid).[139,160,161] Both MOFs have 3D structures and 1D micropores (or channels), which are either triangular or hexagonal-shaped (MIL-68) or diamond-shaped (MIL-53) (Figure 1-24). The main difference between these two polymorphs is that MIL-68 has a rigid structure, whereas MIL-53 is a flexible MOF (*i.e.* expansion or contraction of the framework, resulting in different unit cell volumes). The flexibility of the framework depends on multiple stimuli like temperature, guest molecules and (mechanical) pressure.[162,163] MIL-53 is generally easier to obtain under various conditions, whereas the synthesis of MIL-68 is favored when organic solvents such as DMF (Dimethylformamide) are used, possibly due to a templating effect that stabilizes the triangle-shaped 1D channels.[144,164]

The combination of terephthalic acid with the trimeric SBU (μ_3-oxo trimer of M(III) octahedra) results in two polymorphs, MIL-88B (or MOF-235) and MIL-101 with formula $M_3O(BTC)_3X(H_2O)_2{\cdot}nH_2O$ (X= F^-, OH^-… depending the synthetic/treatment conditions) (Figure 1-25). The structure of MIL-88B consists of triangle-based hybrid bipyramid, in which each corner is occupied by a trimeric SBU. The combination of the bipyramids with the terephthalic

acid forms two types of micropores, one along the axis of the bipyramids and the other one perpendicular to this axis. MIL-88B has an acs topology (acs = aligned, corner sharing) and a flexible structure, which depends on the solvent used.[144,150,163]

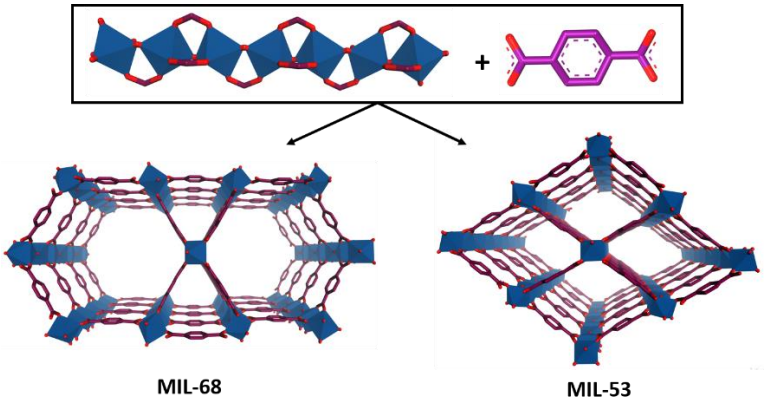

Figure 1-24: Two MOF polymorphs, starting from 1D chain SBU and terephthalic acid: MIL-68, a rigid MOF and MIL-53, a flexible MOF.

MIL-101 is build-up by supertetrahedra, formed by the self-assembly of the trimeric SBU (at the corners) and terephthalic acid (on the edges). The supertetrahedra are connected together to result in a mesoporous structure with an augmented zeolitic MTN-type topology (MTN = Mobil Thirty-Nine). Two different 3D pores (or cages) are present in the structure; a large cage of 34 Å in diameter with microporous pentagonal (12 Å in diagonal) and hexagonal (12 × 16 Å in diagonal) windows and a small cage of 29 Å in diameter with microporous pentagonal windows (12 Å in diagonal) (Figure 1-26). The cages of MIL-101 are interconnected, rendering accessible all the internal surface of the material. The synthesis of MIL-101(Cr) was a milestone in the field of MOFs, as at the time it was one of the few stable mesoporous MOFs reported, with a surface area of ~5900 m^2/g (the mesoporous MIL-100 had been reported one year earlier).[142] Analogues of MIL-101 based on Fe, Al, V have also been reported, however they show less stable structures, possibly due to the higher reactivity of their cations compared to that of Cr(III).[165–167] A detailed discussion on the porosity/stability of MOFs is given below.

Depending on the synthetic conditions used, it is possible to obtain a mixture of these different structures (*e.g.* MIL-53/MIL-88B/MIL-101), as the starting precursors are the same (MIL-68 is mostly favored in organic solutions). The reaction time, temperature, nature of the solvent and the concentration of the reactants selected will favor the formation of one structure over the other. In general, MIL-53 is more thermodynamically stable than MIL-88B and MIL-101 and thus, longer reaction times can induce its formation, whereas higher temperatures and shorter reaction times may induce the formation of the kinetic phases, MIL-88B and MIL-101 (when the same metal cation is employed).[144]

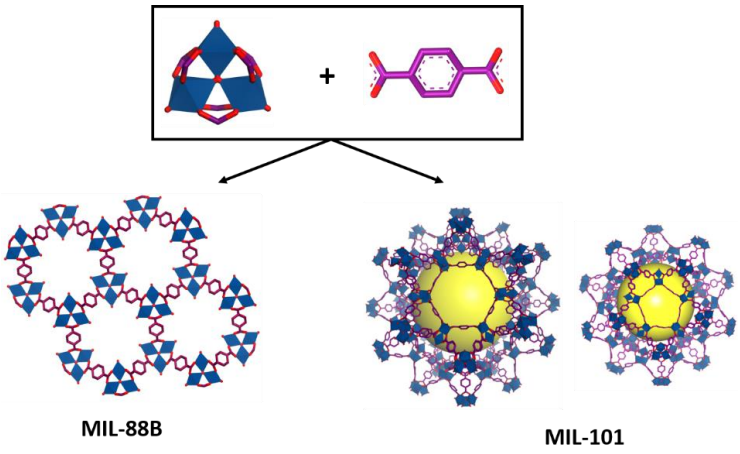

Figure 1-25: Two MOF polymorphs, starting from μ_3-oxo trimer and terephthalic acid: MIL-88B, a flexible microporous MOF and MIL-101 a rigid mesoporous MOF. Yellow spheres represent the pore volume.

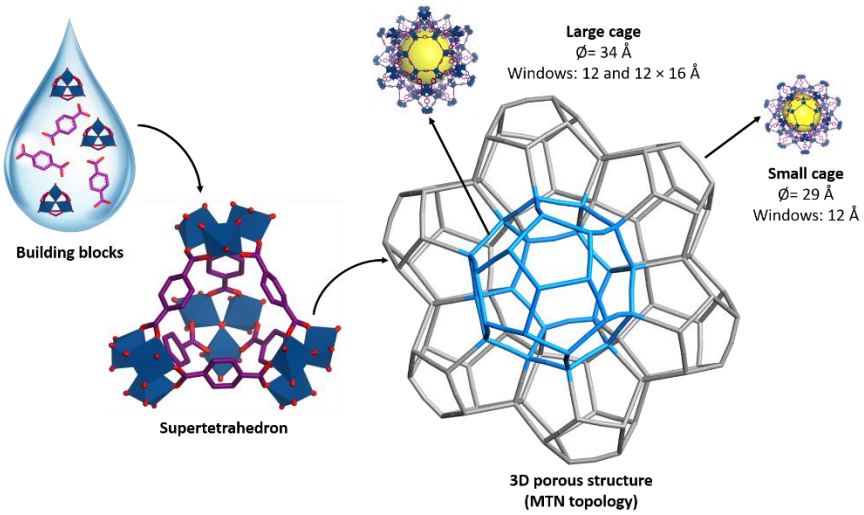

Figure 1-26: Schematic illustration of the construction of MIL-101. In solution, the building blocks are self-assembled to give supertetrahedra, which are further connected together to result in the 3D porous structure with a MTN topology. MIL-101 has two different mesoporous interconnected cages.

Isostructural MOFs

The combination of a specific SBU with different ligands of the same connectivity results in the formation of MOFs with similar structures, but different characteristics that are governed by the nature of the chosen ligand. Typical examples of such MOFs comprise the series of isostructural MIL-53(Al) that have been obtained by replacing the terephthalic acid with linear dicarboxylates (Figure 1-27). MIL-53 has a flexible structure, which is also described as breathing effect.[168,169] In the case of MIL-53(Al), the as-synthesized solid shows 1D rhombic channels of 2.6 × 13.6 Å free aperture (cell volume 1383 Å^3) and is described as the narrow pore configuration. The thermal treatment of this MOF (~ 272 °C) (or other stimuli, solvent exchange, pressure) results in the increase of the channel whose dimensions reach 8.8 × 8.5 Å free aperture and in a larger cell volume of 1383 Å^3 (large pore configuration).[152] When terephthalic acid is replaced by 2,6-naphthalenedicarboxylic acid, the isostructural MIL-69(Al) is obtained with 1D channels of 2.7 × 19.4 Å.[159] This structure has a lower flexibility than MIL-

53(Al) as the strong π-π interactions between the ligands do not allow the pore opening after dehydration.[152] An other isostructure that will be discussed here is the MIL-53(Al)-FA (FA = fumaric acid) or Basolite A520.[170] The combination of fumaric acid with 1D Al-chains gives a non-flexible structure due to the rigidity of the ligand with 1D microporous channels of 5.7 × 6.0 Å.[171] Basolite A520 is one of the six MOFs that are currently commercialized by BASF and Sigma-Aldrich and is used commercially as a sorbent for the storage and delivery of natural gas to automotive applications (large scale production: 3600 kg $m^{-3}day^{-1}$).[172] Even though Basolite A520 appeared in the patent literature since 2007,[173] the poor crystallinity of this MOF did not allow the resolution of its structure before 2015, when Alvarez *et al.* reported an optimized synthesis with higher crystallinity that allowed the structure resolution by a combination of PXRD, solid-state NMR, molecular simulation and IR spectroscopy.[171] The advantages of MIL-53(Al)-FA that promoted its commercialization were its water-based synthesis with low-cost and non-toxic reactants (Al-sulfate and fumaric acid), the high-yield production (98 mol %) and the relatively large surface area of the material (1080-1300 m^2/g).[172] Moreover, Basolite A520 shows excellent water-stability, with a uniform hydrophilicity of the internal surface area.[173] Other isostructural MIL-53(Al) MOFs also exist, like DUT-5 (DUT= Dresden University of Technology) with 4,4'-biphenyldicarboxylic acid, CAU-13 (CAU = Christian-Albrechts-Universität) with 1, 4-cyclohexanedicarboxylic acid and Al(OH)(1,4-ndc) (ndc = naphthalenedicarboxylate) with 1, 4-naphthalenedicarboxylic acid, but they will not be discussed further.[174–176]

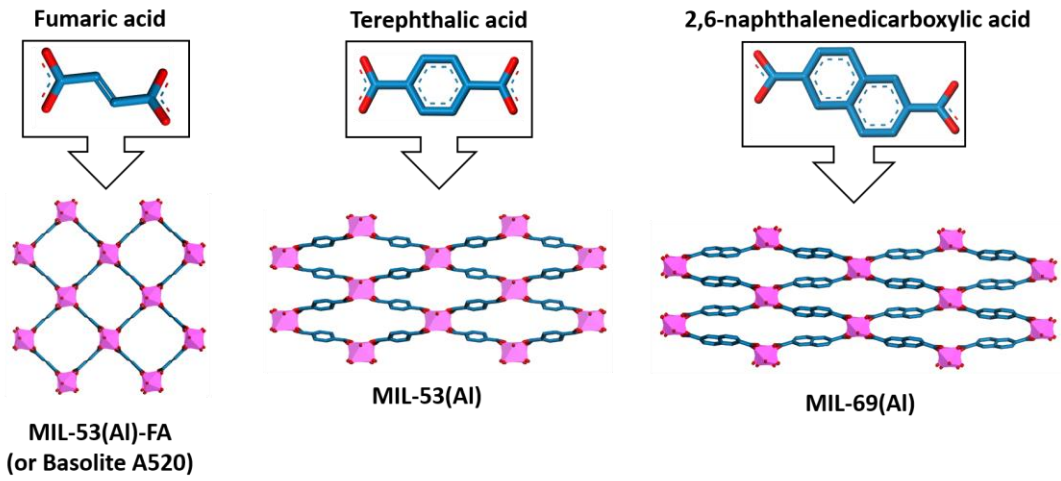

Figure 1-27: Some isostructural MOFs obtained by the combination of 1D Al-chains with linear dicarboxylate ligands. MIL-53(Al)-FA with fumaric acid; MIL-53(Al) with terephthalic acid; and MIL-69(Al) with 2,6-naphthalenedicarboxylic acid. MIL-53 and MIL-69 are shown in their narrow pore configuration.

4. Open-metal sites and catalytically active MOFs

An interesting characteristic of MOFs is the presence of open-metal sites (OMSs) that are also referred to as coordinatively unsaturated metal sites (CUSs). OMSs are generally produced by the removal of coordinated guest molecules (*via* thermal treatment) from the SBU, which leads to Lewis acid sites (Figure 1-28).[177] The presence of defects (missing ligands, SBUs) in the MOF structures tends to increase the number of OMSs. Such sites in a MOF can be investigated

using spectroscopic techniques such as *in-situ* and operando IR with probe molecules (*e.g.* CO and NO) that are known to coordinate to the OMSs.[178] A large variety of MOFs with OMSs has been studied with the most famous being HKUST-1, MIL-100/MIL-101(Cr,Fe), UiO-66, *etc.* The reactivity of OMSs has been used for different applications such as catalysis, gas or hydrocarbons adsorption and separation.[179,180] Among the catalytic applications, OMSs have been used as mild Lewis acids for the oxidation of various substrates, in the presence the oxidizing agent H_2O_2, because molecular oxygen can generally not be activated by the OMSs under mild reaction conditions. Typical oxidation reactions performed by MOFs with OMSs are the oxidation of sulfides (MIL-101(Cr))[181], oxidation of waste water pollutants (HKUST-10),[182] alcohol oxidation and olefin hydrogenation (Pd-based MOF).[183] However, the presence of reductive metals in the SBU can generate redox pairs, such as Fe^{3+}/Fe^{2+} (upon proper thermal activation) that can form peroxides directly from molecular oxygen.[177] It has also been demonstrated that the catalytic activity of OMSs of MOFs depends on the accessibility of the catalytic site, as well as the nature of the metal ions. For example, several MOFs were tested for Prins condensation reactions and it was shown that highly porous MOFs (MIL-100(Cr,Fe)) showed better activities than microporous MOFs (ZIF-8, MIL-53(Al) and Fe-BTC). The Fe-based MIL-100 showed the highest activity due to the electroactivity of Fe ions.[184]

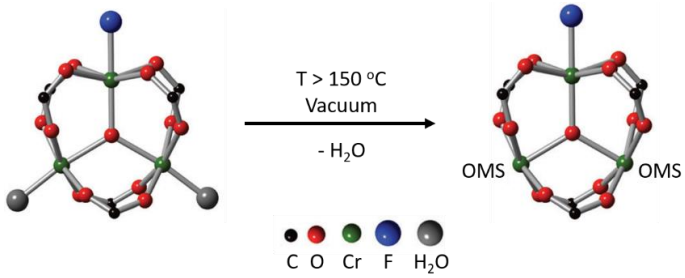

Figure 1-28: Generation of open-metal sites in the trimeric SBU of MIL-101(Cr). Adapted from[177]

Finally, an interesting catalytic property of Fe(III)-based MOFs is their peroxidase-like activity, without the need for thermal activation. Different Fe(III)-phases (MIL-53[185], MIL-100,[186] MIL-88B,[187]MIL-68[188]…) are able to catalytically activate H_2O_2 through electron transfer and produce $HO^{\cdot}$ radicals that are able to oxidize various substrates, through a Fenton mechanisms. This characteristic of Fe(III)-based MOFs is very interesting for the design of cascade systems with immobilized enzymes.

5. Ligand functionalization

The introduction of functional groups on MOFs is of great interest, as it can modify the physicochemical properties of the framework. Such functionalities can provide specific interactions with targeted molecules (gas molecules, drugs, molecular complexes, enzymes *etc.*),[189] modify certain characteristics (*e.g.* stability, breathing behavior)[190,191] and bring new properties (*e.g.* fluorescence, proton conductivity, catalytic properties).[192,193] Thus, an important part of research has been focused on the functionalization of MOFs. Two general approaches are used: the *in-situ* functionalization, by introducing functionalized ligands or a mixture of ligands into the MOF's synthesis[194]; and the post-synthetic functionalization that involves either the chemical introduction of the functional group on the organic ligand or a

partial exchange of the parent ligand with a new functionalized one.[189] In some cases these two approaches can be combined.[190]

The first approach is a direct one-step process, which is always desirable in terms of facility and superior control over the localization of the functional groups. However, as most MOFs are obtained by (hydro)-solvothermal syntheses at high temperatures, some functionalized groups cannot be incorporated since the functional groups usually decompose under such synthetic conditions. Moreover, functionalized ligands can have different solubility and reactivity than their unfunctionalized analogues, thus a synthesis optimization is often required.[166,195] Lammert *et al.* have performed a high-throughput investigation on the synthesis of single- and mixed-ligand MIL-101(Cr) derivatives, in order to obtain thermally and chemically stable functionalized MOFs with high porosities.[194] The tested chromium precursors along with functionalized ligands are shown in Figure 1-29. One of the challenges of this work was to obtain pure MIL-101 phases as a competition with the polymorphs MIL-53 and MIL-88B was observed. Pure functionalized MOFs were obtained in the cases of bromo- and methyl-terephthalic acids, and mixed functionalized MIL-101(Cr) derivatives were also formed (*e.g.* -Br/-NO_2; -Br/-SO_3/H, -SO_3H/-NO_2, -SO_3H/-H *etc.*) Pure MIL-101(Cr)-SO_3H and MIL-101(Cr)-NH_2 could not be isolated using these conditions, however it was demonstrated that a post-synthetic reduction of MIL-101(Cr)-NO_2 could give the pure MIL-101(Cr)-NH_2, as it was previously reported.[196] Pure MIL-101(Cr)-SO_3H can nevertheless be obtained directly using CrO_3 as precursors[197] but, due to the high toxicity of Cr^{6+}, usually post-synthetic modifications of MIL-101(Cr) obtained from Cr^{3+} precursors are preferred.[198]

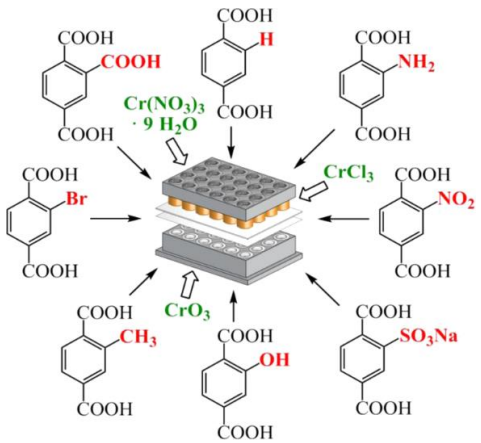

Figure 1-29: Schematic representation of terephthalic acid derivatives and chromium precursors used in the high-throughput screening to obtain single- and mixed-ligand MIL-101(Cr)-X compounds.[194]

Regarding the post-synthetic modification, two main approaches are used (different variations also exist): the post-synthetic modification either by the covalent attachment of a functional groups to the organic ligand or by covalent bonding of a functional group to the OMSs of MOFs (Figure 1-30). Typical examples of the ligand functionalization are the decoration with anhydrides and isocyanates of amine-functionalized Zn^{2+}-MOFs, like IRMOF-3. Some examples of the decoration of SBUs, are the alkylamine- and proline-functionalization of MIL-101(Cr), that resulted in organocatalytic frameworks.[189] We will not focus on the post-

synthetic modification since for simple functionalization (*e.g.* -NH_2, -SO_3H, -COOH *etc.*) the direct approach is preferred, as it will be discussed in chapter 3.

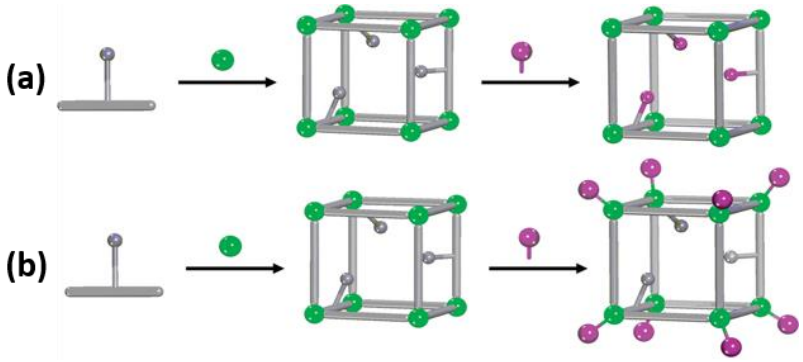

Figure 1-30: Different strategies used in post-synthetic modifications. (a) covalent attachment of a functional group to the ligand and (b) iono-covalent bonding of a functional group to the OMS of a MOF's SBU.[189]

6. Mixed-metal MOFs

Another type of functionalization is the incorporation of different metals in a framework. The different metals can be incorporated either directly or *via* a post-synthetic metal-exchange process.[199] Mixed-metal MOFs show modified properties like gas uptake or fluorescence.[200] For example, the synthesis of mixed MIL-125(Fe/M^{2+}) (M^{2+} = Ni^{2+}, Co^{2+} and Mg^{2+}) resulted in MOFs with much higher sorption properties of CO_2 and CO than the pure Fe-form of MIL-125.[201] A mixed MIL-53(Cr/Fe) also showed enhanced CO_2 uptake with respect to the pure MIL-53(Cr, Fe) phases, by tuning the breathing effect of the structure.[202] In another work, the doping of MIL-78(Y) with different lanthanides (Eu, Tb, Dy), gave high luminescent MOFs with different emissions of red, green and blue respectively.[203] However, one of the most exciting applications of mixed-metal MOFs is in the field of catalysis.[199] Mitchell *et al.* reported the direct synthesis of mixed MIL-100(Sc/M, M = Al, Cr, Fe).[204] It was shown that the activity of mixed-metal MOFs, in the Lewis-acid catalyzed Friedel-Crafts reaction, increased with increasing amounts of Sc. Moreover, as the Fe-based MOFs are known to promote oxidation reactions (described above), the mixed MIL-100(Sc/Fe) was used for a tandem Friedel-Crafts addition and oxidation reaction and was compared with a mixture of pure MIL-100(Sc) and MIL-100(Fe). It was shown that the simple physical mixture of MOFs also catalyzed the sequential reaction, but with a lower conversion (78%) than that obtained with the mixed-metal MOF (95%), suggesting that the combination of the two active sites within the same particle, reduced the average diffusion path, thus enhancing the activity.[204] As we will see in the next chapters the incorporation of Fe into stable MOFs is of great interest for such oxidation reactions.

7. Porosity

The large majority of MOFs are microporous and even though this microporosity is a desired characteristic for many applications demanding molecular sieving properties such as gas separation (H_2/CO_2 and CO_2/N_2),[205] other applications requiring high adsorption capacities are mostly favored when mesoporous materials are used (*e.g.* (bio)-catalysis, drug delivery, gas

storage, heat storage, *etc.*) Consequently, much research has been devoted to the synthesis of large-pore MOFs, since almost the beginning of the MOF's research field.

Extended ligand approach

One typical approach for the increase of the pore size is the use of extended ligands that can replace the shorter parent ligand and result in isostructural topologies with increased pore sizes. Eddaoudi *et al.* used this strategy to replace the terephthalate ligand of MOF-5 (Zn^{2+}-carboxylate MOF) with a series of linear dicarboxylate extended ligands.[206] As seen in Figure 1-31, the pore diameter increases proportionally to the length of the ligand, leading to free volumes up to 91.1 % of the crystal volume (IRMOF-16, IRMOF = Isoreticular MOF). Considering that the parent MOF, MOF-5 is unstable in water or moisture,[207] the extended frameworks showed even more unstable structures (chemically and thermally). This work however, paved the way for the expansion of MOFs' frameworks.

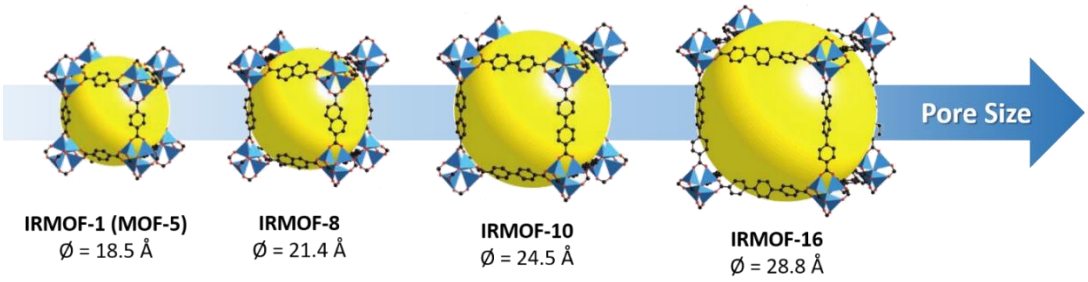

Figure 1-31: Some isostructures of MOF-5 with extended organic ligands and increasing pore sizes. Adapted from[206]

The same approach was used for the expansion of a number of MOF structures such as MOF-74 with channel sizes up to 98 × 85 Å free aperture,[208] MIL-100/ MIL-101 with cage diameters up to 55 and 68 Å,[209] PCN-333 (PCN= Porous Coordination Network) with cage diameters up to 42 and 55 Å *etc.*[210] Details on these extended MOFs are included in the following minireview that we published. While this approach is promising for the synthesis of ultra-large mesoporous MOFs, it shows several limitations such as low chemical stability of the extended frameworks and a risk of obtaining interpenetrated structures. Additionally, the complexity of the organic synthesis that is often required for the production of extended ligands, severely limits their application.

Macropores hollow capsules and etching approach

An alternative approach to create large porosity (usually macroporosity) is the fabrication of hollow capsules of MOFs. This can be achieved when oil/water systems are used for the dispersion of the ligands in oil and the metal precursors in water. MOF capsules are formed at the oil/water interface.[211] Such systems can be formed using either microfluidic approaches (reported for Cu-BTC and MIL-88A)[211,212] or typical oil-in-water (o/w) emulsions (reported for ZIF-8).[213]When enzymes are mixed in the water solution, they can be *in-situ* immobilized.[212] In order to enhance the diffusion pathways, an etching approach[206] (*i.e.* controlled dissociation of the framework) can be applied. More specifically, a recent work demonstrated the

fabrication of ZIF-8 colloidosomes (hollow capsules) by a one-pot o/w emulsion-templating method.[213] The colloidosomes were then treated with an aqueous solution of imidazole (Im), which resulted in the formation of macropores through an etching mechanism that consists in a proton exchange between the imidazole and the more basic 2-methylimidazole (2-MeIm) of the ZIF-8 framework (Figure 1-32). This resulted in the controlled dissociation of the capsule and the formation of diffusional pathways.[213] A different way to create mesoporosity is the acidic etching of stable high valence metal-based MOF containing labile ligands that can easily be hydrolyzed upon acidic treatment, resulting in defects (missing ligands).[214] The defects (or resulted mesopores) can be controlled by adjusting the initial amount of labile ligands incorporated in the framework. This was demonstrated for the microporous Zr-based MOF, PCN-160, which contains the labile to hydrolysis ligand, 4-carboxybenzylidene-4-aminobenzate. Upon treatment with acetic acid, the ligand dissociates into 4-amino benzoic acid and 4-formylbenzoic acid, resulting in the removal of the metal cluster connected with the hydrolyzed ligands. Using this approach, the porosity of PCN-160 was increased from 1.5 nm to 18 nm.[214]

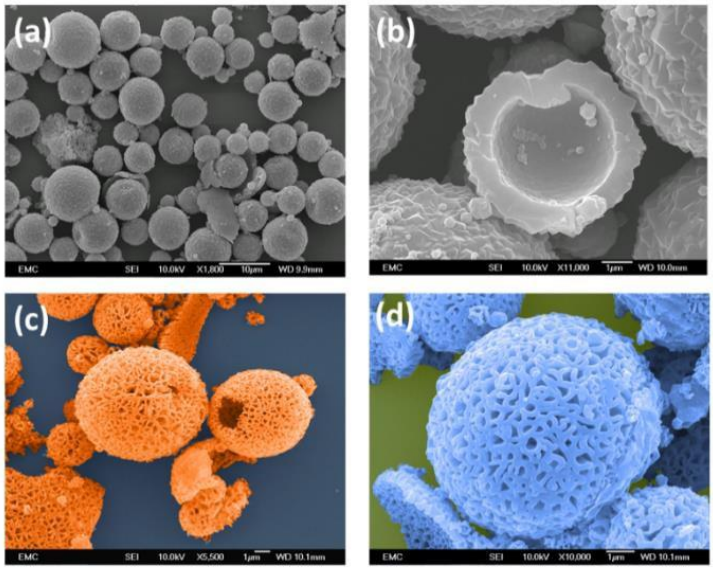

Figure 1-32: SEM images of ZIF-8 colloidosomes formed by a dodecane-water emulsion template (scale bars, 10 µm for (a) and 1 µm for (b); (c) and (d) colored SEM images highlighting the hierarchical hollow structures of the etched colloidosomes by imidazole (scale bars 1 µm for both).[213]

Other methods to obtain ultra-large mesoporosity or macroporosity consist in templating approaches with the use of surfactants and block-copolymers (similar to mesoporous silica templating approaches).[215–217] Alternatively, metal oxides have also been used as templates and sacrificial metal sources for the MOF formation to result in highly ordered macroporous MOFs.[218] As these approaches are far from the scope of this work, they will not be discussed.

8. Stability

Depending on the selected application, stability in different conditions is required. For example, chemical (water, vapor) and thermal stability are required for gas

storage/separation and catalysis, whereas for bio-catalysis or bio-detection water stability and stability under various pH conditions are more important than thermal stability. The following section deals with the characteristics of MOFs that govern their thermal and chemical stability.

Thermal stability

The thermal stability of a MOF strongly depends on the nature of both the SBU and the organic ligand and vary globally from 150 °C to 500 °C. Compared to the materials described before (inorganic oxides, zeolites, carbon materials *etc.*), the presence of the organic ligands in MOFs represents a limiting factor for their thermal stability. However, for applications like bio-catalysis, that is the focus of this work, the thermal stability of MOFs is more than adequate. Different parameters can influence the thermal stability. For example, when comparing the nature of the metal cation in MIL-53, (Al, Cr or Fe) it seems that the increasing strength of the metal-ligand bond (Fe-O: 1.95 Å, Cr-O: 1.93 Å and Al-O: 1.87 Å) results in more thermally stable MOFs.[144,219,220] The nature of the SBU also influences the stability as MOFs with infinite SBUs show increased stabilities compared to those having molecular SBUs. For example, MIL-101(Cr) (trimeric SBU) decomposes at ~230 °C, whereas MIL-53(Cr) (infinite chain decomposes at ~330 °C.[144]

Chemical stability

The chemical stability of MOFs depends on multiple parameters, like the charge and coordination number of the metal cation along with its redox properties, the pK_a of the complexing groups of the ligand, the hydrophobicity and the porosity of the frameworks *etc.*[221] The different parameters that influence the overall water stability of a framework can be divided into thermodynamic and kinetic factors.

Thermodynamic factors:

The chemically weak point of MOFs stands in the iono-covalent metal-ligand bonds in presence of water. This iono-covalent bond that involves the electrophilic metal center and the nucleophilic ligand can be prone to hydrolysis, depending on the reaction conditions and the nature of the metal and ligand.[221] Acidic conditions can accelerate the hydrolysis, leading to protonated ligands, while basic conditions can lead to the formation of oxides and hydroxides.[220] Low et *al.*, performed an extensive study on the hydrothermal stability of several MOFs, which was monitored by PXRD and calculated the activation energy of ligand displacement by a water molecule (Figure 1-33). Some general observations are discussed below.[222]

Concerning MOFs with divalent cations like Zn^{2+}, the use of ionic, N-containing ligands often yields to more chemically stable MOFs like ZIFs and ZMOFs (Zeolite-like MOFs) than those with carboxylic acids.[220] Their stability has been attributed to the higher pK_a of those ligands (> 10), compared to that of carboxylate ligands (pK_a around 3.5-5.5), explaining the difference in stability of ZIF-8 (Zn^{2+}-imidazolate) compared to MOF-5 (Zn^{2+}-terephthalate).[144]

For MOFs containing the same type of ligand, *e.g.* carboxylic acid, it was shown that the oxidation state of the cation is in direct relation with the chemical stability. Thus, metals with low oxidation states (Cu^{2+}, Zn^{2+}), form less stable structures (MOF-5, HKUST-1), than metal with higher oxidation states (Al^{3+}, Cr^{3+}, Ti^{4+}), which form stable structures (MIL-53, MIL-101…).[144,222]

Another parameter influencing the chemical stability of MOFs is the redox properties of the metal. Frameworks containing metal species that are not easily reduced tend to be more stable. For example, the V^{4+}-based MIL-53, which can be partially reduced to V^{3+} showed the lowest stability compared to the Cr^{3+} and Al^{3+} analogues.[219]

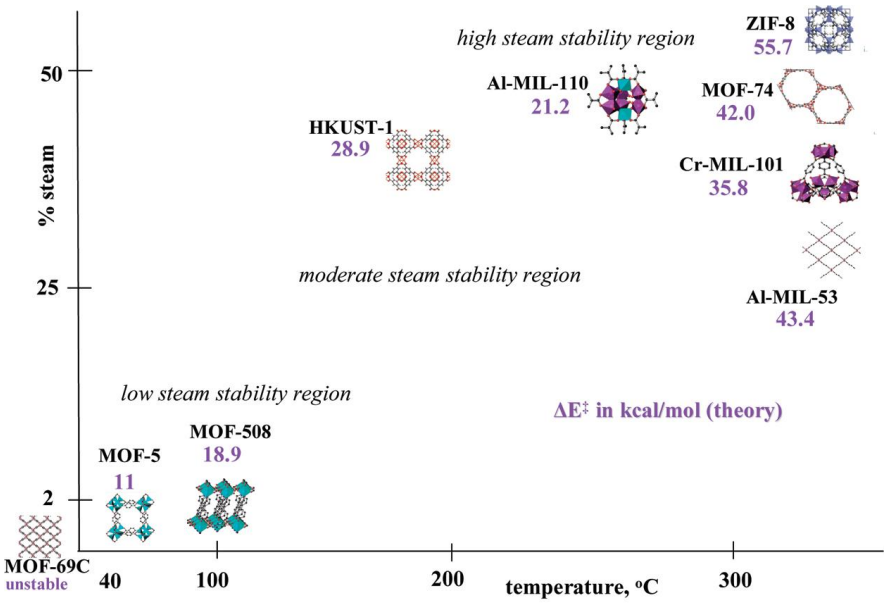

Figure 1-33: Hydrothermal stability of several MOFs, as a function of temperature and water vapor, monitored by PXRD. The calculated energy of activation (ΔE) for ligand displacement is shown in magenta. Adapted from[222]

Kinetic Factors:

An important factor that governs the kinetic stability of MOFs is the water exchange rate for a metal cation, which depends on the ionic radius and charge of the metal ion, along with the electronic configuration of the d-orbitals (for transition metal ions).[223] Figure 1-34 shows the exchange rate constants (kH_2O) of different metal ions. Cations with $kH_2O < 10^{-1}$ are kinetically inert, while those with $kH_2O > 10^{-1}$ are kinetically labile. In general, the transition metal ions of the first row of the periodic table are more labile compared to those of the second and third row, with the exception of Cr^{3+}. The electron configuration Cr^{3+} ([Ar] d^3) stabilizes the octahedral environment and render it very chemically inert ($k_{H2O} = 10^{-6}$ s^{-1}),[224] thus octahedral Cr SBUs are very stable. On the contrary, Fe^{3+} ([Ar] d^5) is highly labile to substitution ($k_{H2O} = 10^2$ s^{-1}). The Al^{3+} cation shows a medium inertness ($k_{H2O} = 1$ s^{-1}) that is attributed to its small ionic radius (0.53 Å) and consequently to the polarization of the coordinated water molecules.[223] The water exchange rate constants of the cations can possibly explain the

difference in the water stability of MIL-101(Cr) > MIL-101(Al) > MIL-101(Fe) and MIL-53(Cr) >MIL-53(Al).[219]

Other parameters that can result to enhanced kinetic stability is the hydrophobicity of the framework and steric effects, arising from the small pore opening that can hinder the adsorption of water molecules.[220]

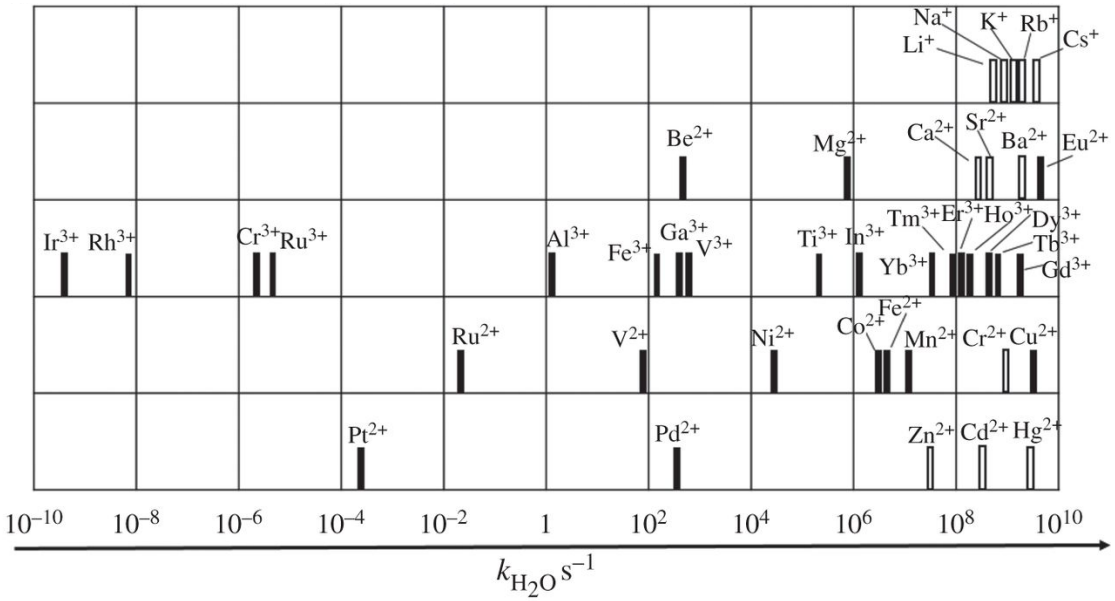

Figure 1-34: Water exchange rate constants (k_{H2O}) in the first coordination sphere of $[M(H_2O)^n]^{m+}$. Black bars represent determined values and white bars calculated ones. Adapted from[223]

Thanks to the combination of unique characteristics (crystallinity, high surface areas, hierarchical porosity, easy functionalization, catalytic properties *etc.*) MOFs have been proposed for a large number of applications. One of the most important applications concern gas separation and storage.[205,225] Some MOFs like Basolite A520 and C300 are already produced industrially by BASF and used for CH_4 storage.[172] In the same category are the works studying the removal of toxic gases and VOC's using MOFs.[226,227] Catalytic and biomedical applications also represent a very important part of the MOFs' research, with works been reported almost from the beginning of the field.[228–230] However, the combination of MOFs with other species (polymers, oxides, nanoparticles, POMs, carbon materials etc)[158,231] to form optimized composites has paved the way for the application of MOFs in new fields (electronics, proton-conduction *etc.*)[232,233] The use of MOFs as matrices for enzyme immobilization is also one of the emerging applications, which appeared only in the last few years.[234] The following section will describe the advances in that field.

E. MOFs as matrices for enzyme immobilization

Metal-Organic Frameworks: a novel host platform for enzymatic catalysis and detection

Introduction and contributions

The following section is a useful survey concerning the design of MOFs as host matrices of enzymes. In a first part, the work will be presented in the format of mini-review that was published in Material Horizons (RSC publications) in 2017, with the following title: “Metal-Organic frameworks: a new host platform for enzymatic catalysis and detection”. In a second part, the main developments since the mini-review publication will be highlighted.

The mini-review briefly describes the properties of MOFs used for such applications and the expected advantages compared to more traditional supports, like polymers and silica materials. The different strategies applied for the immobilization of enzymes were presented and a detailed state of the art of the field was given. Afterward, the review focused on some specific examples that demonstrate the usefulness of MOFs for such applications (in catalysis and sensing) and the advantages gained from using hybrid, highly porous and ordered materials. Finally, the limitations on the current MOF field along with the perspectives for the preparation of more effective and enhanced enzyme-MOFs composites were critically highlighted.

The bibliographic research for this work was performed by myself and Dr. Clémence Sicard along with the writing of the manuscript. Prof. Nathalie Steunou was strongly implicated on the writing and the revision of this work. Dr. Christian Serre, Prof. Jean-Pierre Mahy and Dr. Rémy Ricoux were strongly implicated on the revision of the manuscript and for further fruitful discussions.

Materials Horizons

MINIREVIEW

Metal–organic frameworks: a novel host platform for enzymatic catalysis and detection

Effrosyni Gkaniatsou,[a] Clémence Sicard,*[a] Rémy Ricoux,[b] Jean-Pierre Mahy,[b] Nathalie Steunou*[a] and Christian Serre[ac]

Cite this: *Mater. Horiz.*, 2017, 4, 55

Received 17th August 2016,
Accepted 22nd November 2016

DOI: 10.1039/c6mh00312e

www.rsc.li/materials-horizons

The use of metal–organic frameworks (MOFs) as immobilization matrices for enzymes as a platform for emerging applications is reported. In addition to an overview of strategies developed to prepare enzyme–MOF biocomposites, the features that render MOFs interesting matrices for bio-immobilization are highlighted along with their potential benefits beyond a solid-state support in the design of innovative biocomposites.

1. Introduction

Metal–organic frameworks (MOFs) or porous coordination polymers (PCPs) are an attractive class of porous crystalline hybrid solids, built from almost endless combinations of inorganic nodes and organic linkers with complexing groups (carboxylates, azolates, phosphonates…). Chemical and structural features are easily tunable, resulting in a vast array of micro- or meso-porous solids displaying regular porosity (typically S_{BET} within the 100–6000 $m^2\ g^{-1}$ range). These tailored porous materials show great promise for numerous applications such as gas storage, separation, catalysis, sensing, biomedicine, among others.[1–3]

A new range of potential applications has recently emerged using MOFs as immobilization matrices for biomolecules, most notably enzymes. Enzymes are well known as being efficient and selective catalysts, ubiquitous in a wide range of areas from chemical synthesis to drug delivery. However, their use often requires immobilization on a solid support for ease of separation and recovery (improving cost-effectiveness), and may enhance enzyme activity.[4,5] The immobilization method must retain maximal enzyme activity while not hindering the diffusion of analytes to and from the enzyme active site. To date, no method has been developed that entirely fulfills these requirements, therefore tailored solutions are needed for each unique enzyme–support-application.[6] The development of novel immobilization matrices that can stabilize enzymes under a wide range of operating conditions remains of key interest for enzymatic applications.

As a result of the fascinating physico-chemical properties of MOFs (*e.g.* large and tuneable pore size, pore shape, pore volume, and polar/apolar balance), they are perfectly suited to create a stabilizing microenvironment for enzymes through specific host–guest interactions and/or confinement effect, as already observed with other organic molecules.[7] Since the first report in 2006,[8] the number of studies dealing with enzyme–MOF composites per year has increased exponentially and various combination approaches have now been developed.

In this review, we describe the current methods for enzyme immobilization in MOF materials and provide examples of enzyme–MOF bioreactors and biosensors. The main objective of this review is to outline key features of MOFs that improve the overall performance of biocomposites, as well as highlight the numerous remaining challenges. An extensive list of enzyme–MOF biocomposites reported to date is provided in Table 1, and more detailed descriptions of these materials can be found in recently published reviews.[9–12]

2. Strategies for enzyme immobilization with MOFs

Enzyme–MOF biocomposites are designed to retain active enzymes with maximal loading and minimal leaching, and are typically produced either by surface adsorption, covalent binding, cage inclusion or *in situ* synthesis (Fig. 1). While the first three methods involve a similar immobilization process to

[a] *Institut Lavoisier de Versailles, UMR CNRS 8180, Université de Versailles St Quentin en Yvelines, Université Paris Saclay, 45 avenue des Etats-Unis, 78035 Versailles Cedex, France. E-mail: clemence.sicard@uvsq.fr, nathalie.steunou@uvsq.fr; Fax: +33-1-39-25-44-52; Tel: +33-1-39-25-43-71, +33-1-39-25-43-73*

[b] *Laboratoire de Chimie Bioorganique et Bioinorganique, Institut de Chimie Moléculaire et des Matériaux d'Orsay, UMR 8182, Université Paris Sud, Université Paris Saclay, rue du doyen Georges Poitou, 91405 Orsay, France*

[c] *Institut des Matériaux Poreux de Paris, FRE CNRS 2000, Ecole Normale Supérieure, Ecole Supérieure de Physique et de Chimie Industrielles de Paris, Paris Research University, Paris, France*

Table 1 Summary of the enzyme–MOF biocomposites reported

Method	Enzyme	MOF	Application/remarks	Ref.
Adsorption	Lipase	UiO-66(Zr), carbonized MIL-53(Al)	Bioreactor (warfarin synthesis)	52
Adsorption	Lipase	HKUST-1	Bioreactor (esterification)	53
Adsorption	Laccase	MMU (Zr-MOF)	Bioreactor (proof of concept)	54
Adsorption	Trypsin	HKUST-1	Bioreactor (magnetic separation)	40
Adsorption	Glucose dehydrogenase	ZIF-70, ZIF-7, ZIF-8, ZIF-67, ZIF-68	Electrochemical biosensing of glucose	20
Adsorption (chitosan film)	Tyrosinase	Cu-MOF Cu(bdc)(ted)$_{0.5}$	Electrochemical biosensing of bisphenol	41
Adsorption (chitosan film)	Tyrosinase	Cu-MOF Cu(bdc)(ted)$_{0.5}$	Electrochemical biosensing of bisphenol	55
Indirect adsorption	Trypsin–NDC	UiO-66 (Zr), CYCU-4(Al)	Bioreactor (proteolysis)	21
Indirect adsorption	Trypsin–FTIC	CYCU-4(Al), MIL-101(Cr)	Bioreactor (proteolysis)	56
Glutaraldehyde cross-linking[a]	Beta-glucosidase	MIL-53(Al)-NH_3	Prove interest of method	57
Glutaraldehyde cross-linking[a]	Glucose oxidase	MIL-100(Fe), MIL-100(Cr, Al), MIL-127(Fe)	Electrochemical biosensing of glucose	45
Glutaraldehyde cross-linking[a]	Laccase	MIL-100(Fe)	Oxygen reduction reaction	47
Glutaraldehyde cross-linking[a]	Hydrolase	UiO-66-NH_2	Bioreactor (enantiopure octanediol)	58
Covalent binding (EDC/NHS)	Hemoglobin	MIL-125(Ti)-NH_2	Oxygen binding (proof of concept)	48
Covalent binding (EDC/NHS)	Trypsin	ZIF-8 monolith	Bioreactor (proteolysis)	59
Covalent binding (DCC)	Trypsin	MIL-88B(Cr)-NH_2 MIL-88B(Cr), MIL-101(Cr)	Bioreactor (proteolysis)	22
Covalent binding (DCC/EDC)	EGFP, Lipase	IRMOF-3	Bioreactor (transesterification)	60
Cage inclusion	Vitamin B_{12}, GFP, myoglobin	IRMOF-74-Y	Proof of concept	28
Cage inclusion	Microperoxidase 11	Tb-TATB	Bioreactor (proof of concept)	26
Cage inclusion	HRP, Cyt *c*, microperoxidase 11	PCN-333(Al)	Bioreactor (proof of concept)	29
Cage inclusion	Cytochrome *c*	Tb-TATB	Mechanism comprehension	27
Cage inclusion	Microperoxidase 11	Tb-TATB	Mechanism comprehension	38
Cage inclusion	Myoglobin	Tb-TATB	Bioreactor (size selectivity)	42
Cage inclusion	Vitamin B_{12}, Cyt *c*, myoglobin, horseradish peroxidase	POST-66(Y)	Bioreactor (proof of concept)	31
In situ synthesis (with polyvinylpyrrolidone)	Cytochrome *c* horseradish peroxidase, lipase	ZIF-8, ZIF-10	Biosensor for organic peroxides	32
In situ synthesis	Bovine serum albumin, OVA, lipase, hemoglobin, lysozyme, insulin, HRP, trypsin, urease…	ZIF-8, HKUST-1, Eu/Tb-BDC, MIL-88A	Bioreactor (proof of concept), controlled release	33
In situ synthesis	Catalase	ZIF-90	Bioreactor (size sheltering)	61
In situ synthesis (microcapsule)	Enhanced green fluoresecent protein, lipase, beta-galactosidase	ZIF-8	Bioreactor (size selectivity, magnetic separation)	37
In situ synthesis (micelles)	Horseradish peroxidase	ZIF-8	Bioreactor (proof of concept)	62
In situ synthesis (capsules)	Glucose oxidase	ZIF-8	Electrochemical biosensing of glucose	63
In situ synthesis	Bovine serum albumin	ZIF-8	Patterning, fingerprint detection	64
In situ synthesis (PVP)	Glucose oxidase	ZIF-8	Colorimetric biosensing of glucose	65
In situ synthesis	Glucose oxidase	ZIF-8 (+ polydopamine)	Bioreactor (proof of concept)	66
In situ synthesis	Glucose oxidase + HRP	ZIF-8	Multi-enzyme systems	34
In situ synthesis	Dehydrogenase, HRP, AchE	MIL-88A(Fe) hollow sphere	Bioreactor (proof of concept)	36
In situ synthesis	Urease	ZIF-8	Comparison of 2 strategies	35

[a] Cross-linking corresponds to the reticulation of the protein, whereas covalent binding corresponds to a chemical bonding between the enzyme and the support material.

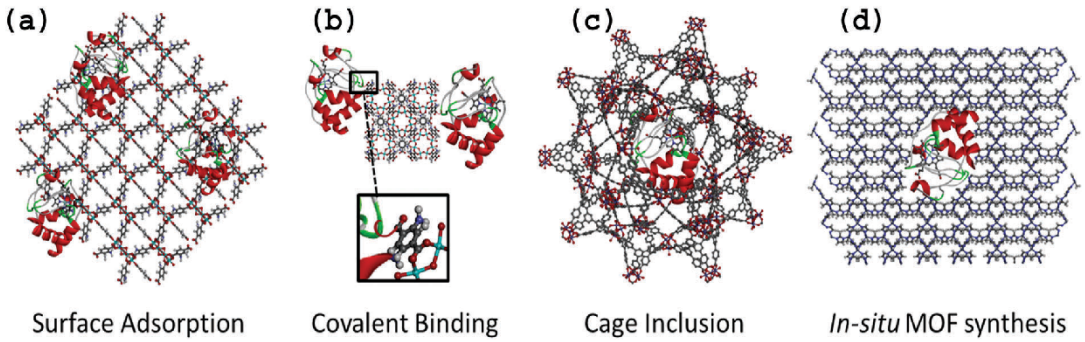

Fig. 1 Schematic representation of the different immobilization methods for cytochrome c (water molecules were omitted for clarity): (a) surface adsorption on MIL-125-NH_2 (view along 010 direction); (b) covalent binding on MIL-125-NH_2 (view along 001 direction); (c) cage inclusion in a cage of MIL-100-Fe-BTB (BTB = 1,3,5-Tris(4-carboxyphenyl)benzene) (view on the 5 member ring window); (d) *in situ* MOF synthesis with ZIF-8 (view along 110 direction).

that reported for other porous or dense solid-state support material (*e.g.* biopolymers, layered double hydroxides, oxides, mesoporous oxides),[4,5,13,14] *in situ* synthesis is specific to MOF materials due to the possible use of gentle synthesis conditions that prevent enzyme degradation.

It is noteworthy to mention the remarkable approach proposed by Sontz *et al.*,[15] in which a modified protein (Ferritin) was used as the MOF metallic building block with preserved bioactivity. However, this work will not be discussed further since the methodology is relatively complex and beyond the scope of the present review.

Surface adsorption

Surface adsorption is commonly used for the preparation of bioelectrodes relying on the physical adsorption of enzymes onto the material *via* van der Waals forces and hydrophobic and electrostatic interactions (Fig. 1a). Due to possible leaching of proteins, this method can be coupled to a reticulation step of the protein by using cross-linking agents such as glutaraldehyde.[4,16,17] As previously reported for other supports, surface adsorption offers the advantage of entrapping a large and precisely known amount of enzyme at the surface of a material, and therefore is particularly well suited for classical electrodes (Pt, glassy carbon, ITO…) as well as for interdigitated microelectrodes.[18,19] By mixing a solution of pre-formed MOF with enzyme, Ma *et al.* studied the surface adsorption of glucose dehydrogenase (GDH) and methylene green (MG) on a series of ZIFs (Zeolitic Imidazole Frameworks) with various surface areas and functional groups.[20] They evaluated their GDH adsorption capacities and showed that ZIF-68 [Zn(benzimidazole)(nitroimidazole)] and ZIF-70 [Zn(imidazole)$_{1.13}$(nitroimidazole)$_{0.87}$] led to the highest adsorbed amount of GDH. This was attributed to their large external surface area as well as to their strong hydrophobic character. By FT-IR spectroscopy, the presence of donor–acceptor and hydrogen bonding interactions between GDH and ZIF-70 was observed, showing that GDH adsorption on ZIF-70 was not only due to physical interactions, but also to chemical interactions. This example is a good illustration of the importance of the hybrid nature and tunability of the functional groups of MOFs when used as immobilization matrices.

An alternative strategy exploits the porosity of MOFs using an enzyme covalently attached to a small molecule. The size of the small molecule allows diffusion through the pores of the MOF, while the much larger enzyme remains adsorbed on the outer surface. Liu and co-workers used this technique to immobilize Trypsin (Try), an enzyme commonly used for protein digestion, through covalent coupling with the dye 4-chloro-7-nitrobenzofurazan (NBD).[21] Enzyme loading and distribution could be monitored from the fluorescence properties of the dye, and multipoint anchoring could be achieved by attaching two or more dye molecules per enzyme. The resulting trypsin-based bioreactor demonstrated high efficiency for protein digestion. In another study, the topical UiO-66(Zr) ($Zr_6O_4(OH)_4$[benzenedicarboxylate]$_6$) was used to produce a NBD-Try-UiO-66 material exhibiting high proteolytic activity that is stable over several cycles. The authors compared the performance of NBD-Try-UiO-66(Zr) to either a purely surface adsorbed sample (Try-UiO-66) or a composite prepared with a larger dye, fluorescein isothiocyanate (FITC-Try-UiO-66) for which significant enzyme leaching was observed. Thus, if the dye is carefully chosen to match the window size, this method is a relatively easy way to achieve increased stability.

Covalent binding

The chemical bonding of biomolecules to solid matrices has been extensively studied,[5] so it is not surprising that this method is also used to immobilize enzymes on MOF surfaces. Furthermore, MOF surfaces present a wide array of functional groups (*e.g.* free carboxyl, amino, hydroxyl groups *etc.*) that can be activated for coupling with reactive groups on the surface of the enzyme (Fig. 1b).

A typical example of covalent immobilization is the work of Shih *et al.*, who used the highly stable mesoporous MIL-101(Cr) ($Cr_3O(OH)(H_2O)_2$[benzenedicarboxylate]$_3$) and microporous MIL-88B(Cr) (polymorph of MIL-101(Cr)) and its amino-functionalized analogue MIL-88B-NH_2(Cr) ($Cr_3O(OH)(H_2O)_2$[benzenedicarboxylate-NH_2]$_3$) for the grafting of Try.[22] The goal was to determine how the functionalization and structural properties of MOFs may impact the stabilization of enzyme activity. Due to the harmful effect of Cr on the environment, such materials may not however be considered for any biotechnological application. The MOFs were first activated using dicyclohexyl carbodiimide (DCC), which allowed them to react with the amino groups of Try to form the MOF–Try conjugate. The various Try–MOFs were used for the digestion of Bovine Serum Albumine (BSA), and it was found that Try-MIL-88B-NH_2(Cr) showed an enzymatic activity similar to that of the free Try, whereas activity of Try-MIL-88B(Cr) and Try-MIL-101(Cr) was reduced by almost half. The authors argued that the amino functionalization increased the surface hydrophilicity, which helped the stabilization of the enzyme (or BSA molecules) through the formation of additional hydrogen bonds. This highlights how varying the functionalization of MOFs can be an important tool for improving biocomposite performance. The authors also performed simple physical adsorption of Try onto MIL-88B-NH_2, which resulted in minimal activity, demonstrating that despite a rather complicated approach with multiple steps for activation of functional groups (during which the enzyme can be deactivated), covalently bonding enzyme molecules to MOFs can be helpful to obtain robust biocomposites with minimal leaching.

Cage inclusion

The cage inclusion approach involves the encapsulation of small enzymes inside the cages of mesoporous MOFs by diffusion (Fig. 1c). This method has been extensively used to encapsulate active ingredients, inorganic nanoparticles or molecular complexes within MOF pores.[7,23] In contrast to adsorption, the encapsulation of enzymes may significantly enhance their stabilization, even under harsh conditions or in unnatural environments. The isolation of protein molecules not only prevents their aggregation and thereby deactivation, but also provides a protective environment that limits the influence of denaturation factors (*e.g.* toxic solvents,

strongly acidic or basic media, temperature). Moreover, the confinement of enzymes in 3D microenvironments is known to increase stability and minimize protein unfolding.[24] This entrapment of enzymes also reduces leaching of enzymes from the support, which can be regarded as one of the main shortcomings of numerous other immobilization methods.[25] On the other hand, a dense host matrix may hinder the accessibility to the entrapped biomolecules and thus the mass-transfer efficiency of analytes may be strongly limited.[25] Due to their high porosity, MOFs should be very interesting host matrices although encapsulation is not feasible for large enzymes due to size limitations.

The entrapment approach is simple and rapid, and only requires mixing pre-formed MOF with an enzyme in aqueous solution and stirring at low temperatures (RT-37 °C). Given the typical dimensions of enzymes – even microenzymes – one shall consider here only MOFs with large pores (cages < 4 nm) or ultra-large pores (cages > 4 nm) which are quite rare, compared to the vast number of common microporous MOFs reported in the literature. One of the earliest reports was by Lykourinou *et al.*, based on the mesoporous Tb-TATB MOF (TATB = triazine-1,3,5-tribenzoate), with cage diameters of 3.9 and 4.7 nm, accessible by windows of 1.3 and 1.7 nm diameters, respectively, to immobilize the Microperoxidase-11 (MP-11, 3.3 × 1.7 × 1.1 nm).[26] The resulting composite showed better peroxidase activity and reusability than free MP-11, which tends to aggregate in aqueous solutions thus losing its activity. It is important to note that enzyme encapsulation within MOF cages requires enzyme diffusion through windows that are smaller in size than the cavity itself. The same group demonstrated the possibility of encapsulating cytochrome *c*, a protein that is significantly larger (2.6 × 3.2 × 3.3 nm) than the Tb-MOF windows (1.3 and 1.7 nm).[27] A mechanism similar to translocation process was proposed, where the enzyme undergoes conformational changes while migrating into the MOF cavities. The enzyme conformation within the cages is neither its native, nor its denatured form.[27]

The use of extended ligand is the easiest way to obtain expanded isoreticular structures of already known MOFs as shown in Fig. 2. Deng *et al.* reported the expansion of MOF-74 (M_2(2,5-dioxidoterephthalate, M = Zn^{2+}, Mg^{2+})) by increasing the number of phenyl rings present on the organic spacer. Vitamin B_{12} (2.7 nm), myoglobin (Mb, 2.1 × 3.5 × 4.4 nm) and Green Fluorescent Protein (GFP, 3.4 × 4.5 nm) were encapsulated in various extended IRMOF-74-Y (Y = number of phenyl rings on the ligand).[28] Feng *et al.*[29] developed a series of MOFs that can be described as extended isoreticular forms of the MIL-100 topology, (MIL-100: $M_3O(OH)(H_2O)_2$[benzenetricarboxylate]$_2$, with M = Cr^{3+}, Al^{3+}, Fe^{3+}...) as previously reported by using the BTB ligand[30] (BTB = 1,3,5-tris(4-carboxylphenyl)benzene). PCN-333(Al) ($Al_3O(OH)(H_2O)_2$[TATB]$_2$, TATB = triazine-1,3,5-tribenzoate) exhibits two types of mesoporous cages – smaller cages of 4.2 nm, accessible through pentagonal windows of 2.6 nm, and larger cages of 5.5 nm with two types of windows (*i.e.* pentagonal windows of 2.6 nm and hexagonal windows of 3 nm). It was chosen as a host matrix for horseradish peroxidase (HRP, 4.0 × 4.4 × 6.8 nm), cytochrome *c* (Cyt *c*, 2.6 × 3.2 × 3.3 nm) and MP-11. Immobilized HRP and Cyt *c* showed better

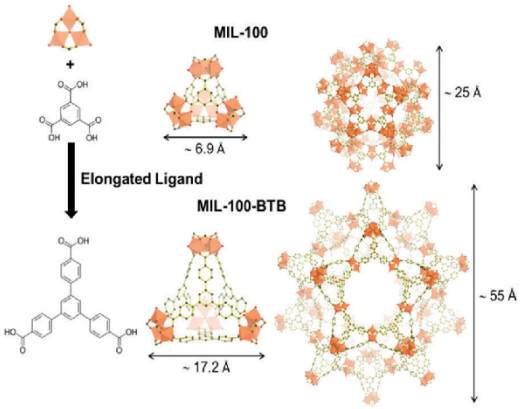

Fig. 2 Schematic representation of the elongated ligand approach to increase the pores size of MIL-100 (top) into MIL-100-BTB (bottom). The assembly of the organic ligand (right) with oxo-centered metal trimers (top left hand corner) is forming the supertetrahedron sub-unit (ST, middle). Small mesoporous cages (left) result from the combination of 20 ST. Dimensions of the ST and cages are included. Iron polyhedra, carbon and oxygen are represented in orange, black and red, respectively (hydrogen atoms are omitted for clarity). Adapted from Horcajada *et al.*[30]

catalytic activity in water media compared to that of the free enzymes. In contrast, MP-11 showed decreased activity after its immobilization, likely because of the presence of several enzyme molecules within a cage that may lead to aggregation. The composites exhibited experimental loadings in agreement with the maximum theoretical capacities and maintained their activity after several catalytic cycles, showing almost no leaching.[29]

Despite recent promising results obtained with mesoporous MOFs based composites, the vast majority of these ultra-large mesoporous MOFs, with the exception of MIL-100/101 series, remain relatively unstable under various conditions (solvents, pH, air *etc.*) for a prolonged period of time. This drastically hampers their practical use as enzyme immobilization matrices under real conditions. Therefore, improvement in the stability of ultra-large mesoporous MOF is needed to fully exploit the potential of this immobilization strategy and produce industrially viable bio-composite materials.

An alternative was recently proposed by Kim *et al.*, who synthesized a microporous MOF, POST-66(Y) ($\{Y_4(H_2O)\}_{\beta3}$[methyl substituted truxene tricarboxylate]$_8(OH)_6(NO_3)_6$), which was then transformed into a micro/mesoporous structure *via* a post-synthetic procedure involving the partial hydrolysis and degradation of the MOF in water.[31] Mesopores ranging from 3 to 20 nm are then formed and coexist with the micropores of the initial MOF structure. In contrast to untreated POST-66(Y), several guest molecules (vitamin B_{12}, Cyt *c*, Mb and HRP) were successfully encapsulated in the post-treated MOF. The catalytic activity of entraped HRP was maintained and the composite showed better stability in organic solvents (*e.g.* DMSO) than free HRP and good recyclability as well. This strategy is a valuable approach for enzyme entrapment in a range of microporous MOFs, whereas the cage inclusion method is restricted to only

ultra-large mesoporous MOFs. However, there are several key limitations such as long-term stability of the water unstable MOF, minimal control over the transformation of the framework, and the lack of reproducibility of mesopore distribution.

In situ MOF synthesis

For the "*in situ* MOF synthesis" approach, nucleation and growth of MOF formation and enzyme immobilization take place simultaneously in a single step. The enzyme and MOF precursors (ligands and metal ions, and eventually additives) are mixed together in solution, resulting in the crystallization of MOF particles with embedded enzymes, either at the particle surface or as a core–shell material (Fig. 1d). Similar to the cage inclusion protocol, this method provides a 3D microenvironment for the enzyme with minimal leaching, but a major advantage of "*in situ* MOF synthesis" is that a greater number of enzymes can be considered since immobilization is not restrained by the size of the pores of the MOF. The major limitation of the "*in situ* MOF synthesis" is that it is restricted to MOFs capable of forming under mild conditions (preferably aqueous solutions and low temperature) to prevent enzyme denaturation. This is why Zeolitic Imidazolate Frameworks (ZIFs), which are known in most cases to form easily under mild biocompatible conditions, have been used. The first example with the "*in situ* MOF synthesis" approach was reported by Lyu *et al.*, who successfully immobilized Cyt *c* in ZIF-8 (Zn[imidazole]$_2$).[32] It is important to note that Cyt *c* was mixed with the polymer polyvinylpyrrolidone (PVP) before being mixed with the ZIF's components in order to protect the enzyme from denaturation and aggregation, and enabling the use of methanol as a solvent. The peroxidase activity of Cyt *c*–ZIF-8 showed a 10-fold increase as compared to the free enzyme.

Liang *et al.*, reported an interesting alternative method for the preparation of bovine serum albumine–ZIF-8 composites using water as the sole solvent and thus removing the need for protective PVP.[33] It is suggested that crystallization of MOF particles is induced by the affinity between MOF molecular precursors and functional groups on the biomolecules *via* intermolecular hydrogen bonding, electrostatic and hydrophobic interactions, leading to local accumulation and thus nucleation and growth of the particles. The authors demonstrated the versatility of this approach through the use of a wide range of biomolecules (ovalbumin, ribonuclease A, human serum albumin, pyrroloquinoline quinone-dependent glucose dehydrogenase, lipase, hemoglobin, lysozyme, insulin, HRP, trypsin, urease and oligonucleotide) and also numerous MOFs, including the metal polycarboxylates HKUST (Cu_3[$(H_2O)_3$benzenetricarboxylate]$_2$), MIL-88A(Fe) (Fe_3O(OH)-$(H_2O)_2$[fumarate]$_3$) and Eu/Tb$_2$[1,4-(benzenedicarboxylate)]$_3$$(H_2O)_4$. The nature of the biomolecule strongly impacted the morphogenesis of the MOF particles, leading to a series of ZIF-8 crystals with varying morphologies. Such observation is consistent with a "biomineralization" or biocrystallization process for the nucleation and growth of MOFs. Enzyme leaching was negligible and the composites were shown to maintain enzymatic activity, even under harsh conditions.

The work of Wu *et al.* was also based on this approach and described a multi-enzymatic system with ZIF-8 particles.[34] Glucose oxidase (GOx) and HRP were mixed with the ZIF-8 precursors at room temperature, to yield the final product GOx&HRP@ZIF-8. The unique aspect of this approach is the possibility to perform enzymatic cascade reactions within the particle. GOx converts glucose into D-glucono-1,5-lactone that further hydrolyses into gluconic acid, generating H_2O_2, which is then used by HRP to oxidise the ABTS substrate. Catalytic tests showed that GOx&HRP@ZIF-8 had higher activity than GOx@ZIF-8 or HRP@ZIF-8, which was attributed to the immediate use by HRP of the H_2O_2 produced by the GOx reaction, confirming thus the importance of confining bi-enzymatic systems in close proximity.

Although these preliminary studies appear promising, they rely on the use of MOFs that can be prepared under simple and biocompatible synthetic conditions. Therefore, unless drastic improvements to synthesis conditions of MOFs are reached in a near future, this immobilization method will be limited to only a few MOF candidates. In addition, many aspects need further investigation and optimization, such as the enzyme spatial localization and dispersion within the MOF particles and the control of MOF coating thickness, which are critical parameters for biocatalytic applications. Enzyme spatial localization within the MOFs has recently been investigated by electron microscopy studies.[31,35] The effect of PVP on the location of enzymes was clearly evidenced, showing the presence of enzymes at the outer surface of MOFs in the presence of PVP or the homogeneous distribution of enzymes in the MOF crystal in the absence of PVP.

An alternative "indirect" *in situ* MOF synthesis approach was proposed by Jeong *et al.* through the synthesis of MIL-88A(Fe) hollow spheres *via* interfacial reaction in-droplet microfluidics.[36] These spheres, with controlled size ranging from 35 to 2000 μm, were prepared by an *in situ* approach in which an aqueous phase containing the metal precursor and poly(vinyl alcohol) (to stabilize droplets) in water, and an organic phase containing the organic linker (fumaric acid) and tributylamine (to deprotonate the ligands) in octanol, were separately introduced into a microfluidic channel. This resulted in the formation of iron chloride microdroplets within a stream of organic solvent containing the fumaric acid that finally yielded the hollow spheres of MIL-88A. The spheres were used as encapsulation matrices for three different enzymes (glycerol dehydroxygenase, HRP and acetylcholinesterase) and results showed the entrapped enzymes maintained activity while having better recyclability than free ones. This method offers the opportunity of solubilizing the ligand in a non-aqueous solvent without enzyme deterioration, which allows a wider range of MOF materials to be synthesized.

In another "indirect" *in situ* MOF synthesis approach reported by Huo *et al.*, MOF particles were also formed *in situ* but around a pre-formed microcapsule.[37] A magnetic MOF bioreactor was prepared, containing *Candida antarctica lipase B* (CALB), using inversed phase Pickering emulsions. First, the emulsion containing CALB (1.5% agarose hydrogel droplets in a continuous paraffin oil phase) was stabilized with UiO-66 nanoparticles, acting also as a surface for further MOF nucleation and growth. Afterwards, a ZIF-8 shell was synthesized *in situ* around the capsule's core in order to stabilize it and to provide size selectivity

toward various substrates. It is worth noting that Fe_3O_4 nanoparticles were also introduced in the initial emulsion to induce magnetic separation of the bioreactor. This method is not as straightforward as the direct *in situ* MOF growth, since several steps are needed, but the pre-stabilization of the enzyme within microdroplets enables the use of synthetic conditions that are not biocompatible (*e.g.* butanol) and the incorporation of additional nanoparticles (Fe_3O_4). It therefore opens up the possibility of designing more complex enzyme–MOF composites.

These indirect *in situ* MOF synthesis methods overcome some of the limitations of direct *in situ synthesis* approaches (higher number of MOF–enzyme couples possible, control of enzymes loading and localization), but these methods are undeniably more complicated to implement experimentally.

3. Discussion

MOFs have recently emerged as an important family of porous hybrid materials owing to their unique structural and functional properties. Among their most attractive features are crystalline structure, high pore volume and highly modular nature, related to a wide choice of possible organic linkers and inorganic building units. This allows modification of the physical environment of the pores, thereby tuning the interactions with guest species. Functionalization of the framework may also strongly affect the chemical stability of the MOF structure under different conditions. As highlighted by the many examples discussed in this review,[20,22] the hybrid nature of MOFs plays a key role in enzyme stabilization. The ability to easily tune the hydrophilic–hydrophobic balance of a MOF using ligands with specific functional groups can improve compatibility of a MOF with a given enzyme. Furthermore, the orientation of the enzyme active site can be modulated through specific interactions between both components, thus increasing catalytic activity of the composite.

Overcoming enzyme leaching and thus improving the performance, stability and reusability of a biocomposite is a key point that appears to be successfully addressed by MOF-based matrices following however model conditions over a few cycles only. Functional groups on organic linkers in the framework can be selected to provide specific interaction sites for the enzyme and thus minimize its leaching and improve its stability in the matrix. This hypothesis was confirmed in the work of Chen *et al.*, where they studied the interactions between MP-11 molecules and Tb-mesoMOF by Raman spectroscopy.[38] The study revealed that MP-11 molecules interact with the framework of Tb-mesoMOF, through π–π interactions between the heme of MP-11 and the conjugated triazine and benzene rings of the linkers. These interactions resulted in the retention of MP-11 molecules within the pores. In contrast, for a mesoporous silica matrix such as MCM-41, a severe leaching of the enzyme was observed as a result of the lack of specific interactions between the biomacromolecules and the silica phase. No comparison to organo-functionalized silica was reported in this work.

The reusability and recyclability of MOF–enzyme based catalysts can be further improved by the introduction of magnetic moieties to allow magnetic separation from reaction mixtures, as previously reported for other multi-components materials.[39] Zhao *et al.* used Fe_3O_4 nanoparticles, treated with polydopamine (PDA), as a magnetic core onto which a MOF shell (HKUST-1: Cu_3[benzenetricarboxylate]$_2$) was grown.[40] The magnetic nano-MOFs were then used for immobilization of Trypsin and exhibited high magnetic responsiveness, allowing easy removal from the reaction mixture. Fe_3O_4 magnetic particles were also used by Huo *et al.*, which resulted in similar recyclability.[37]

Beyond the solid-support matrices

In most previous studies of MOF-based enzymatic immobilization, MOFs have been considered mostly as improved solid matrices without fully considering their intrinsic properties (*e.g.* separation) from a view of potential applications.

Following this concept, Wang *et al.* constructed an electrochemical tyrosinase-based sensor for the detection of bisphenol A (BPA).[41] The presence of CuMOF ([Cu(benzenedicarboxylic)-(triethyelediamine)$_{0.5}$]·2DMF·0.2H_2O) on the bioelectrodes led to improved sensitivity for the detection of BPA, attributed to the high surface area of the MOF that not only helped enzyme immobilization but also BPA adsorption. The authors proposed that the preconcentration of BPA at the electrode surface may be due to π–π stacking interactions between the aromatic ring of BPA and the MOF constitutive organic ligand.

The porous character of MOF-based matrices has also been exploited to gain size selectivity. For example, the peroxidase activity of myoglobin (Mb) encapsulated in Tb-mesoMOF was evaluated by using two substrates, 2,2′-azinobis(3-ethylbenzthiazoline)-6-sulfonate (ABTS) with molecular dimensions: 1.01 × 1.73 nm and 1,2,3-trihydroxybenzene (THB) with molecular dimensions of 0.57 × 0.58 nm.[42] This resulted in size-selective catalytic activity, as the larger substrate (ABTS) could not pass through the remaining pores of the Tb-mesoMOF (0.8 nm) showing almost no conversion. In contrast, for the smaller substrate, THB, the composite demonstrated enhanced catalytic activity compared to the free enzyme. Similar results were reported by Huo *et al.*, using ZIF-8 shell microcapsules for the encapsulation of *Candida antarctica lipase B* (CALB).[37] The biocatalytic activity was evaluated through transesterification reactions using small and large substrates. When small substrates (1-butanol + vinyl acetate) were used, activity was higher than that for the free enzyme, although 100% conversion was reached more slowly (12 h and 48 h for free and encapsulated CALB, respectively) suggesting diffusion limitations of reactants and products through the narrow micropores of the ZIF-8 capsule's shell. When larger substrates were used (3-(4-hydroxyphenyl) propan-1-ol + vinyl laurate), an extremely slow conversion rate was observed reflecting the physical barrier imposed by the microporous MOF.

Expanding this concept further, even more careful combination of properties from both enzyme and MOF should lead to improved biocomposites. For example, the catalytic properties of a wide range of MOFs have been extensively reported over the last years based on the presence of a large number of spatially controlled acid/base sites (Lewis, Brønsted), redox, and/or functionalized organic linkers within their pores.[43,44] One can thus envision a

system for MOF-based immobilization, in which the MOF contributes to the overall catalytic activity of the composite by way of cascade reactions or synergistic effects.

This idea is nicely illustrated by the recent work of Patra *et al.* which exploits the redox nature of MIL-100(Fe) for building enzymatic bioelectrodes that can be used either for glucose sensing or for oxygen reduction reactions (ORR).[45] First, several MIL-100 solids based on various metal(III) cations (Fe, Cr, Al), in addition to the microporous iron(III) tetracarboxylate MIL-127(Fe) ($Fe_3O(OH)_{0.66}Cl_{0.33}(C_{16}N_2O_8H_6)_{1.5}(H_2O)_3{\cdot}nH_2O$), were tested as matrices for the immobilization of glucose oxidase (GOx). The resulting biocomposites based on MIL-100(Fe) exhibited much higher catalytic performance than Cr or Al analogues or the MIL-127(Fe) solid. This was attributed to the strong synergism between GOx and the catalytic/redox properties of Fe^{3+} centers of MIL-100(Fe) that exhibit intrinsic peroxidase-like activity.[46] Recently, MIL-100(Fe) was first exploited as a novel and efficient matrix for the co-immobilization of laccase and ABTS.[47] This particular bioelectrode presents a high electrocatalytic current density of ORR and a reproducible electrochemical response characterized by a high stability over a long period of time (3 weeks). These results represent a significant leap forward in the field of laccase-based bioelectrocatalysts for the design of biofuel cells. Wang *et al.* also proposed a GOx/ZIF-8 system for the electrochemical detection of glucose that incorporates graphene nano-sheets to increase the electron transfer rate at the electrode.[48] Similarly, Hou *et al.* designed a GOx/ZIF-8 system for colorimetric detection of glucose by taking advantage of the peroxidase activity of ZIF-8 to enhance the detection performance of the biosensor.[65]

4. Conclusion and perspectives

MOFs are an emerging class of viable host matrices for enzymes. Robust methods such as surface adsorption, covalent binding, cage inclusion, and new *in situ* synthesis processes have been developed, all of which have shown promising results to immobilize enzymes in a manner that retains biological function with minimal leaching. The examples covered within this review emphasize how the multimodal porosity and hybrid nature of MOFs are certainly key advantages for bio-immobilization and biocatalysis applications. The structural and chemical diversity and functionality of MOFs, combined with their high specific surface area, can produce a wide range of biocatalysts with suitable properties in terms of catalytic activity, stability or recyclability. Recently, MOF–enzyme based bioelectrodes have shown great promise for glucose sensing and ORR due to their high sensitivity, catalytic efficiency, and long-term stability. Biocatalysts reported in the literature clearly reveal that MOFs are appealing host matrices to create stabilizing microenvironments for enzymes through specific host–guest interactions. Immobilization can be achieved through different approaches depending on the specific MOF–enzyme couple and the targeted catalytic process. While surface adsorption, covalent binding, and cage inclusion were classically reported for other enzyme host matrices, the "*in situ* MOF synthesis" methods are more specific to MOF chemistry. Cage inclusion and "*in situ* MOF synthesis" enable 3D encapsulation of enzymes in a microenvironment created either by the porosity of MOFs or by the aggregation of MOFs particles. These methods are particularly attractive for enzymatic devices since they improve long-term stability by preventing leaching and denaturation of entrapped enzymes. However, cage inclusion is restricted to a few enzyme/MOFs couples with appropriate size matching (*i.e.* microenzymes and mesoporous MOFs) while the "*in situ* MOF synthesis" approach is limited to MOFs that have biocompatible synthesis conditions (room temperature, non toxic reactants or solvents).

Independent of the immobilization strategy used, the synthesis and processing of enzyme–MOFs composites suffer from the same issues as those of pure MOFs. Although a huge family of MOFs has already been described in the literature, practical application of these matrices is often hampered by inadequate chemical stability (especially in water), and difficulty of controlling the diameter, morphology, structure and defects of particles. Overcoming these drawbacks is imperative to implementing MOF-based devices in different fields and is also crucial for the scale-up of laboratory syntheses into reliable manufacturing procedures. Moreover, it is worth noting that only a limited number of studies has investigated the long term stability of MOFs based composites under enzymatic operating conditions while a few MOFs in aqueous or buffer solutions (PBS) have demonstrated limited stability.

The design of MOF–enzyme biocomposites is still in its infancy and MOFs have not yet reached the maturity of other immobilization matrices such as oxides or clays. However, research into novel MOFs–enzyme composites is rapidly growing, exploring new compositions and materials processing. Recent progress in the synthesis of multi-component materials by combining MOFs, magnetic particles and/or polymers was reported illustrating the potential for this class of materials in the development of sophisticated and multi-functional devices.

One remaining critical issue for this family of biohybrid materials concerns the chemical and thermodynamic compatibility between enzyme and MOF particle that governs the loading, dispersion and orientation of enzymes in MOF matrices. The performance of biocatalytic and biosensing devices might be driven by the functionality and defects of the framework, and the surface chemistry of MOF particles. Therefore, the characterization and/or modeling of the microstructural properties of MOFs[49–51] is a necessary step towards enhancing the interfacial properties of MOF–enzyme composites and could finally provide a useful guide for the design of optimized bionanocomposites.

Acknowledgements

The authors acknowledge the help of Dr Farid Nouar for the graphical representations and Dr Meghan J. McFadden for correcting the English of the manuscript. The authors also thank the ANR-11-LABEX-0039 for funding.

References

1 S. Kaskel, *The Chemistry of Metal-Organic Frameworks: Synthesis, Characterization, and Applications*, Wiley, Weinheim, 2016.
2 Themed issue, *Chem. Soc. Rev.*, 2014, 43, 5415–6176.

3 Themed issue, *Chem. Rev.*, 2012, 2, 673–1268.
4 Themed issue, *Chem. Soc. Rev.*, 2013, 42, 6211–6568.
5 L. Cao, *Carrier-bound Immobilized Enzymes: Principles, Application and Design*, Wiley, Weinheim, 2006.
6 E. Forsberg, C. Sicard and J. D. Brennan, *Annu. Rev. Anal. Chem.*, 2014, 7, 337–359.
7 P. Horcajada, R. Gref, T. Baati, P. K. Allan, G. Maurin, P. Couvreur, G. Férey, R. E. Morris and C. Serre, *Chem. Rev.*, 2012, **112**, 1232–1268.
8 T. J. Pisklak, M. Macías, D. H. Coutinho, R. S. Huang and K. J. Balkus, *Top. Catal.*, 2006, **38**, 269–278.
9 J. Mehta, N. Bhardwaj, S. K. Bhardwaj, K.-H. Kim and A. Deep, *Coord. Chem. Rev.*, 2016, **322**, 30–40.
10 D. Raja, W.-L. Liu, H.-Y. Huang and C.-H. Lin, *Comments Inorg. Chem.*, 2015, **35**, 332–350.
11 X. Wu, M. Hou and J. Ge, *Catal. Sci. Technol.*, 2015, **5**, 5077–5085.
12 Y. Chen and S. Ma, *Dalton Trans.*, 2016, **45**, 9744–9753.
13 C. Mousty, *Anal. Bioanal. Chem.*, 2010, **396**, 315–325.
14 D. Avnir, T. Coradin, O. Lev and J. Livage, *J. Mater. Chem.*, 2006, **16**, 1013–1030.
15 P. A. Sontz, J. B. Bailey, S. Ahn and F. A. Tezcan, *J. Am. Chem. Soc.*, 2015, **137**, 11598–11601.
16 N. Steunou, C. Mousty, O. Durupthy, C. Roux, G. Laurent, C. Simonnet-Jegat, J. Vigneron, A. Etcheberry, C. Bonhomme, J. Livage and T. Coradin, *J. Mater. Chem.*, 2012, **22**, 15291–15302.
17 S. Datta, L. R. Christena and Y. R. S. Rajaram, *3 Biotech.*, 2013, **3**, 1–9.
18 P. Torres-Salas, A. Monte-Martinez, B. Cutiño-Avila, B. Rodriguez-Colinas, M. Alcalde, A. O. Ballesteros and F. J. Plou, *Adv. Mater.*, 2011, **23**, 5275–5282.
19 D. Brady and J. Jordaan, *Biotechnol. Lett.*, 2009, **31**, 1639–1650.
20 W. Ma, Q. Jiang, P. Yu, L. Yang and L. Mao, *Anal. Chem.*, 2013, **85**, 7550–7557.
21 W.-L. Liu, C.-Y. Wu, C.-Y. Chen, B. Singco, C.-H. Lin and H.-Y. Huang, *Chem. – Eur. J.*, 2014, **20**, 8923–8928.
22 Y.-H. Shih, S.-H. Lo, N.-S. Yang, B. Singco, Y.-J. Cheng, C.-Y. Wu, I.-H. Chang, H.-Y. Huang and C.-H. Lin, *ChemPlusChem*, 2012, **77**, 982–986.
23 J. Juan-Alcañiz, J. Gascon and F. Kapteijn, *J. Mater. Chem.*, 2012, **22**, 10102–10118.
24 (*a*) V. V. Vinogradov and D. Avnir, *RSC Adv.*, 2015, **5**, 10862–10868; (*b*) V. V. Vinogradov and D. Avnir, *J. Mater. Chem. B*, 2014, **2**, 2868–2873; (*c*) D. T. Nguyen, M. Smit, B. Dunn and J. I. Zink, *Chem. Mater.*, 2002, **14**, 4300–4306.
25 (*a*) M. Hartmann and X. Kostrov, *Chem. Soc. Rev.*, 2013, **42**, 6277–6289; (*b*) E. Magner, *Chem. Soc. Rev.*, 2013, **42**, 6211–6222.
26 V. Lykourinou, Y. Chen, X.-S. Wang, L. Meng, T. Hoang, L.-J. Ming, R. L. Musselman and S. Ma, *J. Am. Chem. Soc.*, 2011, **133**, 10382–10385.
27 Y. Chen, V. Lykourinou, C. Vetromile, T. Hoang, L.-J. Ming, R. W. Larsen and S. Ma, *J. Am. Chem. Soc.*, 2012, **134**, 13188–13191.
28 H. Deng, S. Grunder, K. E. Cordova, C. Valente, H. Furukawa, M. Hmadeh, F. Gandara, A. C. Whalley, Z. Liu, S. Asahina, H. Kazumori, M. O'Keefe, O. Terasaki, J. F. Stoddart and O. Yaghi, *Science*, 2012, **336**, 1018–1023.
29 D. Feng, T.-F. Liu, J. Su, M. Bosch, Z. Wei, W. Wan, D. Yuan, Y.-P. Chen, X. Wang, K. Wang, X. Lian, Z.-Y. Gu, J. Park, X. Zou and H.-C. Zhou, *Nat. Commun.*, 2015, **6**, 5979.
30 P. Horcajada, H. Chevreau, D. Heurtaux, F. Benyettou, F. Salles, T. Devic, A. Garcia-Marquez, C. Yu, H. Lavrard, C. L. Dutson, E. Magnier, G. Maurin, E. Elkaim and C. Serre, *Chem. Commun.*, 2014, **50**, 6872–6874.
31 Y. Kim, T. Yang, G. Yun, M. B. Ghasemian, J. Koo, E. Lee, S. J. Cho and K. Kim, *Angew. Chem., Int. Ed.*, 2015, **54**, 13273–13278.
32 F. Lyu, Y. Zhang, R. N. Zare, J. Ge and Z. Liu, *Nano Lett.*, 2014, **14**, 5761–5765.
33 K. Liang, R. Ricco, C. M. Doherty, M. J. Styles, S. Bell, N. Kirby, S. Mudie, D. Haylock, A. J. Hill, C. J. Doonan and P. Falcaro, *Nat. Commun.*, 2015, **6**, 7240.
34 X. Wu, J. Ge, C. Yang, M. Hou and Z. Liu, *Chem. Commun.*, 2015, **51**, 13408–13411.
35 K. Liang, C. J. Coghlan, S. G. Bell, C. Doonan and P. Falcaro, *Chem. Commun.*, 2016, **52**, 473–476.
36 G.-Y. Jeong, R. Ricco, K. Liang, J. Ludwig, J.-O. Kim, P. Falcaro and D.-P. Kim, *Chem. Mater.*, 2015, **27**, 7903–7909.
37 J. Huo, J. Aguilera-Sigalat, S. El-Hankari and D. Bradshaw, *Chem. Sci.*, 2015, **6**, 1938–1943.
38 Y. Chen, S. Han, X. Li, Z. Zhang and S. Ma, *Inorg. Chem.*, 2014, **53**, 10006–10008.
39 P. Falcaro, R. Ricco, A. Yazdi, I. Imaz, S. Furukawa, D. Maspoch, R. Ameloot, J. D. Evans and C. J. Doonan, *Coord. Chem. Rev.*, 2016, **307**, 237–254.
40 M. Zhao, X. Zhang and C. Deng, *Chem. Commun.*, 2015, **51**, 8116–8119.
41 X. Wang, X. Lu, L. Wu and J. Chen, *Biosens. Bioelectron.*, 2015, **65**, 295–301.
42 Y. Chen, V. Lykourinou, T. Hoang, L.-J. Ming and S. Ma, *Inorg. Chem.*, 2012, **51**, 9156–9158.
43 J. Y. Lee, O. K. Farha, J. Roberts, K. A. Scheidt, S. B. T. Nguyen and J. T. Hupp, *Chem. Soc. Rev.*, 2009, **38**, 1450–1459.
44 M. Zhang, Z.-Y. Gu, M. Bosch, Z. Perry and H.-C. Zhou, *Coord. Chem. Rev.*, 2014, **293–294**, 327–356.
45 S. Patra, T. H. Crespo, C. Serre, A. Permyakova, C. Sicard, A. Chaussé, N. Steunou and L. Legrand, *J. Mater. Chem. B*, 2015, **3**, 8983–8992.
46 J.-W. Zhang, H.-T. Zhang, Z.-Y. Du, X. Wang, S.-H. Yu and H.-L. Jiang, *Chem. Commun.*, 2014, **50**, 1092–1094.
47 S. Patra, S. Sene, C. Mousty, C. Serre, A. Chaussé, L. Legrand and N. Steunou, *ACS Appl. Mater. Interfaces*, 2016, **8**, 20012–20022.
48 W. Wang, L. Wang, Y. Huang, Z. Xie and X. Jing, *Chem. – Asian J.*, 2016, **11**, 750–756.
49 H. Zhang, Y. Lv, T. Tan and D. Spoel, *J. Phys. Chem. B*, 2016, **120**, 477–484.
50 R. Semino, N. A. Ramsahye, A. Ghoufi and G. Maurin, *ACS Appl. Mater. Interfaces*, 2016, **8**, 809–819.
51 M. Benzaqui, R. Semino, N. Menguy, F. Carn, T. Kundu, J.-M. Guigner, N. B. McKeown, K. J. Msayib, M. Carta, R. Malpass-Evans, C. Guillouzer, G. Clet, N. A. Ramsahye,

C. Serre, G. Maurin and N. Steunou, *ACS Appl. Mater. Interfaces*, 2016, **8**, 27311–27321.
52 W.-L. Liu, N.-S. Yang, Y.-T. Chen, S. Lirio, C.-Y. Wu, C.-H. Lin and H.-Y. Huang, *Chem. – Eur. J.*, 2015, **21**, 115–119.
53 Y. Cao, Z. Wu, T. Wang, Y. Xiao, Q. Huoa and Y. Liu, *Dalton Trans.*, 2016, **45**, 6998–7003.
54 S. Pang, Y. Wu, X. Zhang, B. Li, J. Ouyang and M. Ding, *Process Biochem.*, 2016, **51**, 229–239.
55 X. Lu, X. Wang, L. Wu, L. Wu, Dhanjai, L. Fu, Y. Gao and J. Chen, *ACS Appl. Mater. Interfaces*, 2016, **8**, 16533–16539.
56 W.-L. Liu, S.-H. Lo, B. Singco, C.-C. Yang, H.-Y. Huang and C.-H. Lin, *J. Mater. Chem. B*, 2013, **1**, 928–932.
57 C. M. Doherty, G. Grenci, R. Riccò, J. I. Mardel, J. Reboul, S. Furukawa, S. Kitagawa, A. J. Hill and P. Falcaro, *Adv. Mater.*, 2013, **25**, 4701–4705.
58 S.-L. Cao, D.-M. Yue, X.-H. Li, T. J. Smith, N. Li, M.-H. Zong, H. Wu, Y.-Z. Ma and W.-Y. Lou, *ACS Sustainable Chem. Eng.*, 2016, **4**, 3586–3595.
59 L. Wen, A. Gao, Y. Cao, F. Svec, T. Tan and Y. Lv, *Macromol. Rapid Commun.*, 2016, **37**, 551–557.
60 S. Jung, Y. Kim, S.-J. Kim, T.-H. Kwon, S. Huh and S. Park, *Chem. Commun.*, 2011, **47**, 2904–2906.
61 F.-K. Shieh, S.-C. Wang, C.-I. Yen, C.-C. Wu, S. Dutta, L.-Y. Chou, J. V. Morabito, P. Hu, M.-H. Hsu, K. C.-W. Wu and C.-K. Tsung, *J. Am. Chem. Soc.*, 2015, **137**, 4276–4279.
62 P. Chulkaivalsucharit, X. Wu and J. Ge, *RSC Adv.*, 2015, **5**, 101293.
63 Y. Wang, C. Hou, Y. Zhang, F. He, M. Liu and X. Li, *J. Mater. Chem. B*, 2016, **4**, 3695–3702.
64 K. Liang, C. Carbonell, M. J. Styles, R. Ricco, J. Cui, J. J. Richardson, D. Maspoch, F. Caruso and P. Falcaro, *Adv. Mater.*, 2015, **27**, 7293–7298.
65 C. Hou, Y. Wang, Q. Ding, L. Jiang, M. Li, W. Zhu, D. Pan, H. Zhu and M. Liu, *Nanoscale*, 2015, 7, 18770–18779.
66 X. Wu, C. Yang, J. Ge and Z. Liu, *Nanoscale*, 2015, 7, 18883–18886.

Some more recent works

Since the publication of the mini-review, some important works in the field of enzymatic immobilization using MOFs have been reported. It was thus essential to discuss them here. This description will be based on the immobilization method used. The cage inclusion and the *in-situ* synthesis methods are more specific to MOFs matrices and provide enhanced protection, compared to the surface adsorption and the covalent binding. Therefore, the majority of works were performed using exclusively these two methods.

1. Advances using the cage inclusion method

As it has been extensively discussed in previous sections, immobilized enzymes often suffer from severe diffusional issues. The work of Li *et al.*, demonstrated the importance of having hierarchical porous systems with free diffusion pathways.[235] A Zr-based MOF, NU-1000 (Northwestern University) was selected for the immobilization of the enzyme cutinase (4.5 × 3.0 × 3.0 nm). NU-1000 has hexagonal channels (Ø = 3.1 nm), as well as triangular channels (Ø = 1.5 nm) that are interconnected. Cutinase could only be encapsulated inside the hexagonal channels, leaving the other channels free for the diffusion of reactants. This system was compared to cutinase immobilized in PCN-600, which only has hexagonal channels of around 3.0 nm in diameter. It was demonstrated that in the NU-1000 93 % of the immobilized enzyme was active, whereas for PCN-600 only 6 % was active. The low activity of the cutinase@PCN-600 was attributed to the blockage of the mesoporous channels by cutinase molecules, where the substrates could not diffuse anymore, whereas for cutinase@NU-1000, the smaller triangular channels, that were not occupied by the enzymes, could be used for substrate diffusion.[235] Similarly, isostructural NU-1000 frameworks, with extended ligands were used for the formation of MOFs with larger pore apertures with diameters from 3.3 to 6.7 nm (same pore system as above).[236] The isostructural series of NU-1000 were used for the immobilization of lactate dehydrogenase (LDH) in the hexagonal channels, while the triangular channels of those MOFs were used for the immobilization of the co-enzymes nicotinamide adenine dinucleotide (NAD and NADH). It was demonstrated that the activity of the immobilized LDH was dependent on the pore windows and channels because of different diffusion rates of the substrates and the co-enzymes (Figure 1-35).[236]

A different study demonstrated the importance of having hierarchical pore systems, in a different way. An isostructural MIL-100 MOF, named PCN-888(Al) with two different cages with diameters of 5.0 and 6.2 nm was used for the encapsulation of glucose oxidase (GOx) and horseradish peroxidase (HRP). GOx (6.0 × 5.2 × 7.7 nm) could only fit in the large cage, whereas HRP (4.0 × 4.4 × 6.8 nm) could be accommodated in both cages.[237] Thus, a stepwise encapsulation (starting from GOx) was important in order to precisely control the distribution of GOx and HRP in the large and the small cage, respectively. An opposite strategy would result in the encapsulation of HRP in both cages, rendering impossible the immobilization of GOx. The bi-enzymatic system was tested for the oxidation of ABTS by HRP, in which the H_2O_2 co-

substrate was produced *in situ* by the catalytic oxidation of glucose by GOx and showed good catalytic efficiency.[237]

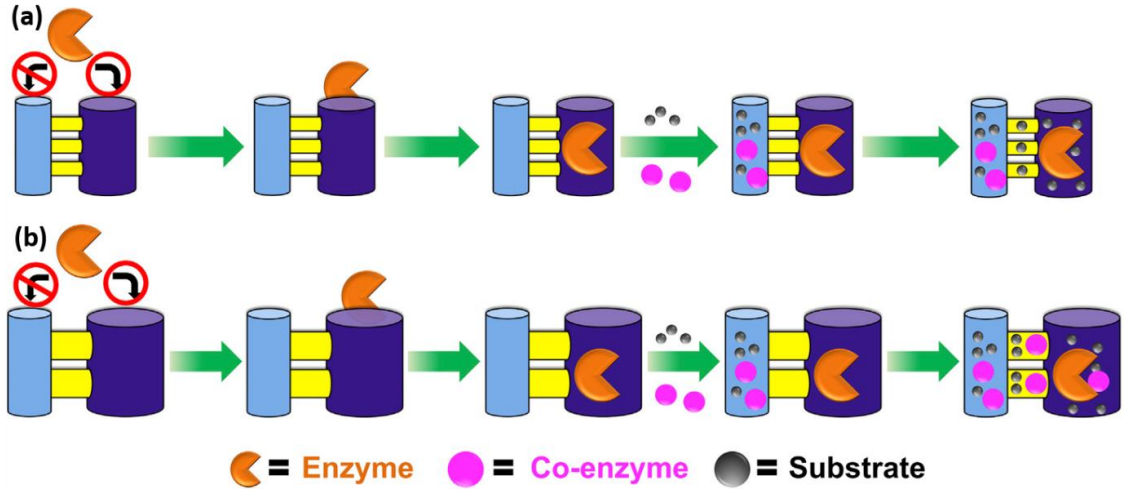

Figure 1-35: Schematic representation of the immobilization of enzymes and co-enzymes in interconnected hierarchical MOFs with different channel apertures. (a) The narrow windows and channels allows the diffusion of co-enzymes and substrates and limit the space for enzyme-co-enzyme recognition; (b) a system with wide windows and channels shows fast diffusion rates for the co-enzymes and the substrates and sufficient space for enzyme-co-enzyme recognition.[236]

Finally, an important parameter was demonstrated in these new studies: the role of the crystal size on the diffusion of the reactants and thus, on the overall activity. NU-1003 (same structure as the series above) was used for the immobilization of the nerve agent hydrolyzing enzyme, organophosphorous acid anhydrolase (OPAA).[238] The immobilization was performed with particles of different sizes (micro- and nano-particles) and it was demonstrated that by nanosizing the MOF carrier (particle size = 300 nm), the catalytic activity of the immobilized OPAA, was improved compared to the OPAA immobilized in larger particles (particle size = 7000 nm) and even compared to the free enzyme. This was attributed to the improved substrate diffusion, due to the small size of the particles. (Figure 1-36).[238] MOF enzymatic nanocarriers have also been used to other studies, related to *in vitro* and *in vivo* applications.[239,240]

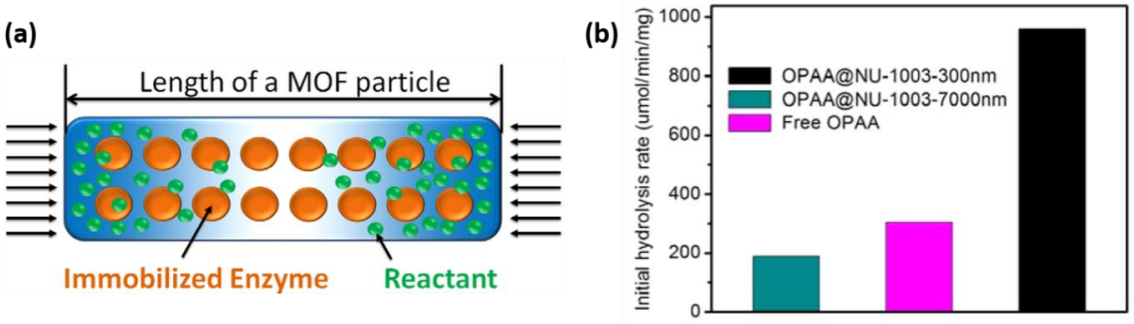

Figure 1-36: (a) Schematic illustration of an enzyme-MOF carrier, with evenly immobilized enzymes and the diffusion of reactants from the solution into the carrier's particle; (b) Initial turnover rate of OPAA@NU-1003 (300 nm), OPAA@NU-1003 (7000 nm) and free OPAA. Adapted from[238]

These new studies provided insights on the cage inclusion strategy and addressed one of the main problems of encapsulated enzymes, the diffusion issues. Thanks to the vast possibilities of chemical structures of MOFs and the ability to tune the particle size, it seems rather likely to minimize such limitation in the future.

2. Advances using the in-situ synthesis method

Regarding the *in-situ* synthesis method, great attention has been given to the use of ZIF-8 since the first report on the so called biomimetic mineralization of this MOF in the presence of enzymes and other biomolecules.[241] Most MOF structures are synthesized under conditions non-compatible for enzymes (high temperatures, pressures, organic solvents *etc.*..). It is thus of high interest to fully exploit a MOF as a host matrix that can be synthesized under mild conditions. Several works have used ZIF-8 for the entrapment of enzymes like Cyt c, HRP, CALB, GOx, which has led to enhanced stability under unnatural environments..[242–245] It was even extended to other biomolecules such as viruses[246] and yeast cells.[247]

However, the original authors of this ZIF-8 based approach have recently reported that this process strongly depends on various parameters (concentration of reactants, relative molar ratios, stirring conditions *etc.*).[248] The variation of those parameters can either form the ZIF-8 phase (sodalite topology), which is the kinetic phase, a different, more thermodynamically favored phase (diamond topology), an amorphous phase or mixtures of them. Moreover, different spatial distributions of biomolecules in the ZIF-8 matrix were observed, depending on the surface chemistry of the biomolecules and their affinity to Zn^{2+} cations. When rhodamine B-tagged BSA (ζ-potential= -13.5 at pH = 9.5), with a high affinity to the Zn-cations was used, the protein was localized in the core and at the exterior of the ZIF-8 particles. However, when fluorescein isothiocyanate-tagged BSA (ζ-potential= -9.4 at pH = 9.5) was used, the protein molecules were predominantly localized at the surface of the ZIF-8 crystal. A further layer (or multiple layers of ZIF-8/BSA) was then applied to ensure the entrapment of the biomolecule (Figure 1-37).[248]

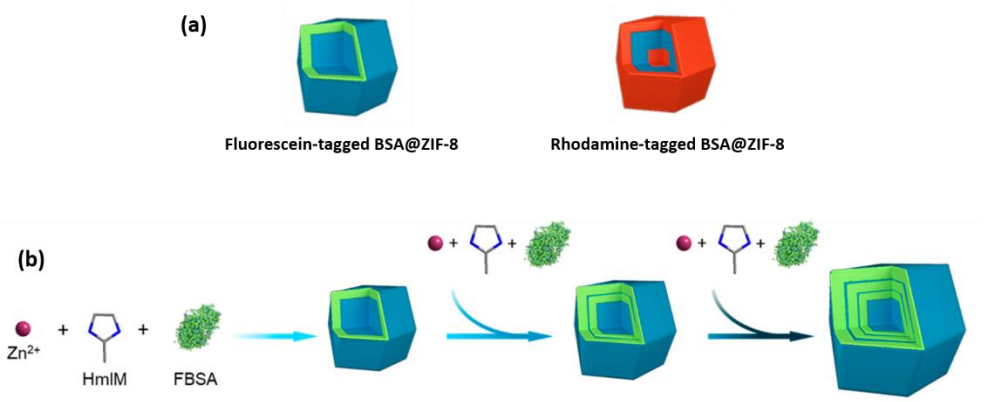

Figure 1-37: Schematic illustrations of (a) different BSA spatial distributions in the ZIF-8 crystal, depending on the surface chemistry of the protein (on the left FTIC-BSA in green, on the right RhoB-BSA in red) and (b) synthetic method of the multiple-core-shell fluorescein-tagged BSA@ZIF-8 composite. Adapted from[248]

A further investigation on the influence of the surface chemistry of the protein on the process was then reported.[249] The chemical modification of the amino acids of the surface of different biomolecules (BSA, pepsin, myoglobin and hemoglobin) was performed either by succinylation, acetylation (lysine residue) or amination (aspartate and glutamate residues). The modified biomolecules along with the non-modified were tested for their ability to induce biomimetic mineralization. It was demonstrated that biomolecules bearing high concentration of acidic residues, which are negatively charged under basic conditions (e.g aspartate and glutamate), induced the formation of ZIF-8. On the contrary, biomolecules having high isoelectric point values (*e.g.* lysine and arginine on their surfaces) and are thus positively charged, did not allow the formation of ZIF-8 (Figure 1-38). Following these results, the authors proceeded to the functionalization of the biomolecules, leading to the modification of the overall surface charge. The biomolecules with ζ-potential values below -30 mV induced the precipitation of ZIF-8 (after succinylation or acetylation), whereas biomolecules with higher ζ-potential values did not (after amination) These results were attributed to the affinity of the overall negatively charged surfaces to the Zn cations.[249]

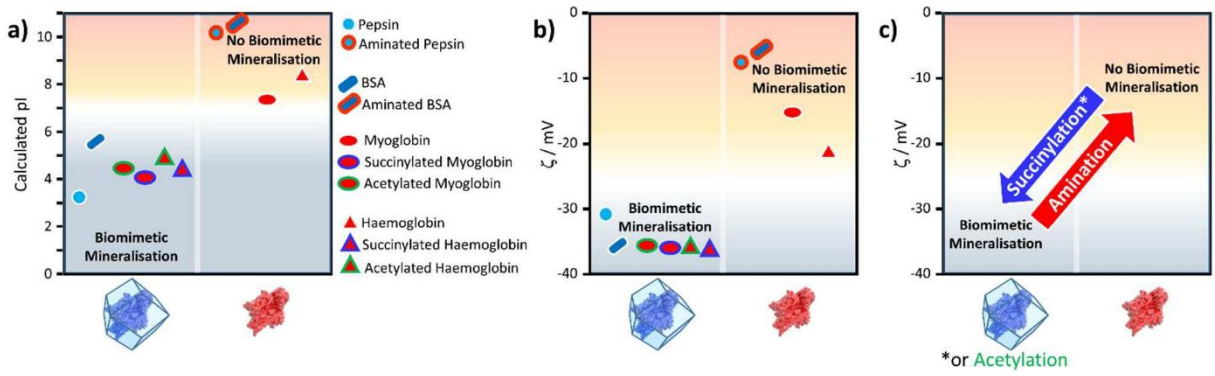

Figure 1-38: Plots (a) of the calculated pI of BSA, pepsin, myoglobin and hemoglobin with or without surface modifications; (b) experimental ζ-potentials for the same biomolecules and (c) the general changes in ζ-potential for the three types of chemical modifications used (succinylation, acetylation and amination).[249]

ZIF-8 has been also used for the simultaneous immobilization of NiPd hollow nanoparticles and GOx for the fabrication of an artificial enzyme system for tandem catalysis.[250] NiPd particles exhibited peroxidase-like activity and consumed the H_2O_2 produced catalytically by the immobilized GOx. This system showed rapid detection of glucose and could be used as an effective colorimetric sensor.[250]

While the ZIF-8 system seems very promising for the entrapment of enzymes in a facile and effective way, a careful control of the synthetic conditions, together with a careful selection of the enzyme must be made in order to obtain the desired system. Moreover, ZIF-8 is a microporous hydrophobic MOF and for bio-catalytic applications, the choice of a more hydrophilic or amphiphilic MOF seems more adequate.

The group of Sanchez-Sanchez has presented a series of works for the preparation of amphiphilic MOFs under mild aqueous conditions, like MIL-100(Fe)[251], Basolite F300 (a semi-amorphous Fe-BTC phase)[252] and MIL-53(Al)-H or -NH_2.[253] MIL-100(Fe) synthesized at room

temperature (RT) had high surface area (1974 m^2/g) and crystallinity, similar to that of the original MOF structure (2028 m^2/g) and could be a very promising candidate for the entrapment of enzymes. Moreover, the peroxidase-like activity of this Fe(III)-MOF could be used for cascade enzymatic reactions.[251] Basolite F300 was used for the immobilization of multiple enzymes (alcohol dehydrogenase, lipase and GOx).[252] The immobilized enzymes showed reduced activities, possibly due to diffusional limitations caused by the poor crystallinity of Basolite F300. MIL-53(Al)-H and -NH_2 systems were used for the immobilization of β-galactosidase. The MOFs showed much higher enzyme loadings and retention than the respective surface immobilized systems and improved catalytic activities.[253]

F. Conclusions

In this chapter, we explored the interest of bio-catalysis and the need for the immobilization of enzymes in order to provide protection under harsh operational conditions and gain the possibility of recycling them.

The first part presented heme enzymes and in particular microperoxidase 8, a small enzyme that combines the activity of both peroxidases and monooxygenases (typically that of Cytochrome P450s). Both catalytic mechanisms were detailed. The peroxidase-like activity enables the oxidation of a wide range of substrates in presence of H_2O_2 (eg organic dyes phenols, organosulfur compounds…), whereas the monoxygenase-like activity allows hydroxylation of phenol derivatives and O- and N- dealkylation reactions. The interest of MP8 for this work beyond its remarkable activity, resides in its limitations in solution. Indeed, MP8 -in its soluble form- is easily deactivated under acidic conditions and in the presence of high concentrations of H_2O_2 (oxidative degradation). An activity loss also derives due to polymerization (< 2 µM). Moreover, the lack of a specific catalytic pocket renders MP8 non-selective. Thus, it is of interest to immobilize MP8 to limit the aforementioned disadvantages and possibly enhance its selectivity by its confinement inside a solid matrix. Additionally, the small size of MP8 renders it a perfect candidate for the immobilization inside the cavities of porous matrices.

In a second part, the methods, benefits and limitations of enzyme immobilization were discussed. Immobilization is performed to stabilize and protect enzymes under denaturation conditions, enables their separation from the reaction mixtures and their recycling, while providing an easier handling compared to their soluble forms (shaping of the biocatalyst). Different immobilization techniques have been reported with various solid matrices and can be classified into four categories: surface adsorption, covalent binding, pore inclusion and entrapment. While being relatively simple techniques, the major limitation of the surface immobilization (either by adsorption or covalent binding) is their incapacity to provide any protection to the enzymes from denaturation factors. Porous matrices are generally more protective due to 3D confinement of enzymes that limits their unfolding and can lead to favorable local micro-environments. The pore inclusion method is limited to systems with a size matching between the enzyme size and the pore size of the host matrix. This is not required for the entrapment method, but in that case, synthetic conditions compatible with the preservation of the enzymatic activity (*i.e.* aqueous media, room temperature) are necessary. Furthermore, the support used may lead to slower diffusion of reactants.

The impact of immobilization on the structural conformation of enzymes and their catalytic activities was then described. Specific interactions between the enzyme and the support (polar, hydrophobic/hydrophilic), the dynamics of immobilized enzymes and the enzyme loading can drastically modify the enzymatic activity. Other important parameters are the mass transfer limitations that concerns the diffusion of reactants to and from the enzyme's active site, along with water diffusion.

Typical examples of solid supports along with their characteristics were then presented. Organic solids (polymers, carbon materials) provide ideal interaction sites for enzyme molecules, but they are not always sufficiently robust to ensure a stable immobilization. On the contrary, inorganic supports (silica, clay minerals, zeolites) are highly stable, but need extra functionalization to ensure interaction sites with enzymes. In many cases, a combination of organic/inorganic materials is needed for an effective immobilization. Furthermore, besides mesoporous silica, most of the aforementioned materials have poorly controlled porosity, with large pore size distributions or microporosity, which is incompatible with the size of enzymes.

Finally, the last section was devoted to a new class of immobilization supports, the Metal-Organic Frameworks. The hybrid, crystalline nature of MOFs along with the uniform porosity, the high surface areas and the easy tunability of their structures make MOFs ideal candidates as enzymatic host matrices. Interesting results have been reported in terms of minimal leaching and preservation of the enzymatic activity in unnatural environments. This is attributed to the confinement of the enzyme within the matrix and to the hybrid nature of MOF that creates stabilizing microenvironments for enzymes through specific host-guest interactions. Also, the porosity of the MOF matrices was used to implement size selectivity to the enzymatic reactions.

The use of MOFs for the immobilization of MP8 seems thus an interesting strategy to overcome its limitations (stability, selectivity…).

G. References

(1) DiCosimo, R.; McAuliffe, J.; Poulose, A. J.; Bohlmann, G. Industrial Use of Immobilized Enzymes. *Chemical Society Reviews* **2013**, *42* (15), 6437. https://doi.org/10.1039/c3cs35506c.

(2) Sheldon, R. A.; van Pelt, S. Enzyme Immobilisation in Biocatalysis: Why, What and How. *Chem. Soc. Rev.* **2013**, *42* (15), 6223–6235. https://doi.org/10.1039/C3CS60075K.

(3) Kirk, O.; Borchert, T. V.; Fuglsang, C. C. Industrial Enzyme Applications. *Current Opinion in Biotechnology* **2002**, *13* (4), 345–351. https://doi.org/10.1016/S0958-1669(02)00328-2.

(4) Secundo, F. Conformational Changes of Enzymes upon Immobilisation. *Chemical Society Reviews* **2013**, *42* (15), 6250. https://doi.org/10.1039/c3cs35495d.

(5) Poulos, T. L. Heme Enzyme Structure and Function. *Chemical Reviews* **2014**, *114* (7), 3919–3962. https://doi.org/10.1021/cr400415k.

(6) Marques, H. M. Insights into Porphyrin Chemistry Provided by the Microperoxidases, the Haempeptides Derived from Cytochrome C. *Dalton Transactions* **2007**, No. 39, 4371. https://doi.org/10.1039/b710940g.

(7) Aron, J.; Baldwin, D. A.; Marques, H. M.; Pratt, J. M.; Adams, P. A. Hemes and Hemoproteins: 1: Preparation and Analysis of the Heme-Containing Octapeptide (Microperoxidase-8) and Identification of the Monomeric Form in Aqueous Solution. *Journal of Inorganic Biochemistry* **1986**, *27* (4), 227–243. https://doi.org/10.1016/0162-0134(86)80064-2.

(8) de Lauzon, S.; Mansuy, D.; Mahy, J.-P. Coordination Chemistry of Iron (III)–Porphyrin–Antibody Complexes. *The FEBS Journal* **2002**, *269* (2), 470–480.

(9) Korri-Youssoufi, H.; Desbenoit, N.; Ricoux, R.; Mahy, J.-P.; Lecomte, S. Elaboration of a New Hydrogen Peroxide Biosensor Using Microperoxidase 8 (MP8) Immobilized on a Polypyrrole Coated Electrode. *Materials Science and Engineering: C* **2008**, *28* (5–6), 855–860. https://doi.org/10.1016/j.msec.2007.10.062.

(10) Marques, H. M.; Baldwin, D. A.; Pratt, J. M. Hemes and Hemoproteins. 3. the Reaction of Microperoxidase-8 with Cyanide: Comparison with Aquocobalamin and Hemoproteins. *Journal of Inorganic Biochemistry* **1987**, *29* (1), 77–91. https://doi.org/10.1016/0162-0134(87)80014-4.

(11) Rodrıguez-Lopez, J. N.; Lowe, D. J.; Hernandez-Ruiz, J.; Hiner, A. N. P.; Garcıa-Canovas, F.; Thorneley, R. N. F. Mechanism of Reaction of Hydrogen Peroxide with Horseradish Peroxidase: Identification of Intermediates in the Catalytic Cycle. 10.

(12) Wang, R.; de Visser, S. P. How Does the Push/Pull Effect of the Axial Ligand Influence the Catalytic Properties of Compound I of Catalase and Cytochrome P450? *Journal of Inorganic Biochemistry* **2007**, *101* (10), 1464–1472. https://doi.org/10.1016/j.jinorgbio.2007.06.022.

(13) Primus, J.-L.; Grunenwald, S.; Hagedoorn, P.-L.; Albrecht-Gary, A.-M.; Mandon, D.; Veeger, C. The Nature of the Intermediates in the Reactions of Fe(III)- and Mn(III)-Microperoxidase-8 with H_2O_2: A Rapid Kinetics Study. *Journal of the American Chemical Society* **2002**, *124* (7), 1214–1221. https://doi.org/10.1021/ja016907u.

(14) Wang, J.-S.; Baek, H. K.; Van Wart, H. E. High-Valent Intermediates in the Reaction of Na-Acetyl Microperoxidase-8 with Hydrogen Peroxide: Models for Compounds 0, I and II of Horseradish Peroxidase. *Biochemical and Biophysical Research Communications* **1991**, *179* (3), 1320–1324.

(15) Low, D. W.; Winkler, J. R.; Gray, H. B. Photoinduced Oxidation of Microperoxidase-8: Generation of Ferryl and Cation-Radical Porphyrins. *Journal of the American Chemical Society* **1996**, *118* (1), 117–120. https://doi.org/10.1021/ja9530477.

(16) *Biocatalysis Based on Heme Peroxidases: Peroxidases as Potential Industrial Biocatalysts*; Díaz Torres, E., Ayala, M., Eds.; Springer-Verlag: New York, 2010.

(17) Dallacosta, C.; Monzani, E.; Casella, L. Reactivity Study on Microperoxidase-8. *JBIC Journal of Biological Inorganic Chemistry* **2003**, *8* (7), 770–776. https://doi.org/10.1007/s00775-003-0478-z.

(18) Adams, P. A. The Peroxidasic Activity of the Haem Octapeptide Microperoxidase-8 (MP-8): The Kinetic Mechanism of the Catalytic Reduction of H,O, by MP-8 Using 2,Z'- Azinobis-(3-Ethylbenzothiazoline-6-Sulphonate) (ABTS) as Reducing Substrate. *J. CHEM. SOC. PERKIN TRANS.* **1990**, 8.

(19) Cunningham, I. D.; Bachelor, J. L.; Pratt, J. M. Kinetic Study of the H2O2 Oxidation of Phenols, Naphthols and Anilines Catalysed by the Haem Octapeptide Microperoxidase-8. *Journal of the Chemical Society, Perkin Transactions 2* **1991**, No. 11, 1839. https://doi.org/10.1039/p29910001839.

(20) Ricoux, R.; Boucher, J.-L.; Mansuy, D.; Mahy, J.-P. Microperoxidase 8 Catalyzed Nitration of Phenol by Nitrogen Dioxide Radicals. *European Journal of Biochemistry* **2001**, *268* (13), 3783–3788.

(21) Ricoux, R.; Lukowska, E.; Pezzotti, F.; Mahy, J.-P. New Activities of a Catalytic Antibody with a Peroxidase Activity: Formation of Fe(II)-RNO Complexes and Stereoselective Oxidation of Sulfides. *European Journal of Biochemistry* **2004**, *271* (7), 1277–1283. https://doi.org/10.1111/j.1432-1033.2004.04032.x.

(22) Longoria, A.; Tinoco, R.; Vázquez-Duhalt, R. Chloroperoxidase-Mediated Transformation of Highly Halogenated Monoaromatic Compounds. *Chemosphere* **2008**, *72* (3), 485–490. https://doi.org/10.1016/j.chemosphere.2008.03.006.

(23) Hamid, M.; Khalil-ur-Rehman. Potential Applications of Peroxidases. *Food Chemistry* **2009**, *115* (4), 1177–1186. https://doi.org/10.1016/j.foodchem.2009.02.035.

(24) Shaffiqu, T. S.; Roy, J. J.; Nair, R. A.; Abraham, T. E. Degradation of Textile Dyes Mediated by Plant Peroxidases. *Applied Biochemistry and Biotechnology* **2002**, *102–103* (1–6), 315–326. https://doi.org/10.1385/ABAB:102-103:1-6:315.

(25) Huang, X.; Groves, J. T. Beyond Ferryl-Mediated Hydroxylation: 40 Years of the Rebound Mechanism and C–H Activation. *JBIC Journal of Biological Inorganic Chemistry* **2017**, *22* (2–3), 185–207. https://doi.org/10.1007/s00775-016-1414-3.

(26) Osman, A. M.; Koerts, J.; Boersma, M. G.; Boeren, S.; Veeger, C.; Rietjens, I. M. C. M. Microperoxidase/H_2O_2-Catalyzed Aromatic Hydroxylation Proceeds by a Cytochrome-*P*-450-Type Oxygen-Transfer Reaction Mechanism. *European Journal of Biochemistry* **1996**, *240* (1), 232–238. https://doi.org/10.1111/j.1432-1033.1996.0232h.x.

(27) Boersma, M. G.; Primus, J.-L.; Koerts, J.; Veeger, C.; Rietjens, I. M. C. M. Heme-(Hydro)Peroxide Mediated O- and N-Dealkylation: A Study with Microperoxidase. *European Journal of Biochemistry* **2000**, *267* (22), 6673–6678. https://doi.org/10.1046/j.1432-1327.2000.01764.x.

(28) Dorovska-Taran, V.; Posthumus, M. A.; Boeren, S.; Boersma, M. G.; Teunis, C. J.; Rietjens, I. M. C. M.; Veeger, C. Oxygen Exchange with Water in Heme-Oxo Intermediates during H2O2-Driven Oxygen Incorporation in Aromatic Hydrocarbons Catalyzed by Microperoxidase-8. *European Journal of Biochemistry* **1998**, *253* (3), 659–668. https://doi.org/10.1046/j.1432-1327.1998.2530659.x.

(29) Valderrama, B.; Ayala, M.; Vazquez-Duhalt, R. Suicide Inactivation of Peroxidases and the Challenge of Engineering More Robust Enzymes. *Chemistry & biology* **2002**, *9* (5), 555–565.

(30) Adediran, S. A.; Lambeir, A.-M. Kinetics of the Reaction of Compound II of Horseradish Peroxidase with Hydrogen Peroxide to Form Compound III. *European Journal of Biochemistry* **1989**, *186* (3), 571–576. https://doi.org/10.1111/j.1432-1033.1989.tb15246.x.

(31) Wariishi, H.; Akileswaran, L.; Gold, M. H. Manganese Peroxidase from the Basidiomycete Phanerochaete Chrysosporium: Spectral Characterization of the Oxidized States and the Catalytic Cycle. *Biochemistry* **1988**, *27* (14), 5365–5370. https://doi.org/10.1021/bi00414a061.

(32) Nagababu, E.; Rifkind, J. M. Heme Degradation during Autoxidation of Oxyhemoglobin. *Biochemical and Biophysical Research Communications* **2000**, *273* (3), 839–845. https://doi.org/10.1006/bbrc.2000.3025.

(33) Spector, A.; Zhou, W.; Ma, W.; Chignell, C. F.; Reszka, K. J. Investigation of the Mechanism of Action of Microperoxidase-11, (MP11), a Potential Anti-Cataract Agent, with Hydrogen Peroxide and Ascorbate. *Experimental Eye Research* **2000**, *71* (2), 183–194. https://doi.org/10.1006/exer.2000.0867.

(34) Nakajima, R.; Yamazaki, I. The Conversion of Horseradish PeroxidaseC to a Verdohemoprotein by a Hydroperoxide Derived Enzymaticallyfrom Indole-3-Acetic Acid and by m-Nitroperoxybenzoic Acid. 6.

(35) Hiner, A. N. P.; Ruiz, J. H.; López, J. N. R.; Cánovas, F. G.; Brisset, N. C.; Smith, A. T.; Arnao, M. B.; Acosta, M. Reactions of the Class II Peroxidases, Lignin Peroxidase and *Arthromyces Ramosus* Peroxidase, with Hydrogen Peroxide: CATALASE-LIKE ACTIVITY, COMPOUND III FORMATION, AND ENZYME INACTIVATION. *Journal of Biological Chemistry* **2002**, *277* (30), 26879–26885. https://doi.org/10.1074/jbc.M200002200.

(36) Caputi, L.; Di Tullio, A.; Di Leandro, L.; De Angelis, F.; Malatesta, F. A New Microperoxidase from Marinobacter Hydrocarbonoclasticus. *Biochimica et Biophysica Acta (BBA) - General Subjects* **2005**, *1725* (1), 71–80. https://doi.org/10.1016/j.bbagen.2005.05.023.

(37) *Enzyme Assays: High-Throughput Screening, Genetic Selection and Fingerprinting*; Reymond, J.-L., Ed.; Wiley-VCH: Weinheim, 2006.

(38) Sheldon, R. A. Enzyme Immobilization: The Quest for Optimum Performance. *Advanced Synthesis & Catalysis* **2007**, *349* (8–9), 1289–1307. https://doi.org/10.1002/adsc.200700082.

(39) Dwevedi, A. Basics of Enzyme Immobilization. In *Enzyme Immobilization*; Springer International Publishing: Cham, 2016; pp 21–44. https://doi.org/10.1007/978-3-319-41418-8_2.

(40) Steunou, N.; Mousty, C.; Durupthy, O.; Roux, C.; Laurent, G.; Simonnet-Jégat, C.; Vigneron, J.; Etcheberry, A.; Bonhomme, C.; Livage, J.; et al. A General Route to Nanostructured M[V3O8] and

Mx[V6O16] (x = 1 and 2) and Their First Evaluation for Building Enzymatic Biosensors. *Journal of Materials Chemistry* **2012**, *22* (30), 15291–15302. https://doi.org/10.1039/c2jm30485f.

(41) Cipolatti, E. P.; Manoel, E. A.; Fernandez-Lafuente, R.; Freire, D. M. G. Support Engineering: Relation between Development of New Supports for Immobilization of Lipases and Their Applications. *Biotechnology Research and Innovation* **2017**, *1* (1), 26–34. https://doi.org/10.1016/j.biori.2017.01.004.

(42) Cruz, J. C.; Pfromm, P. H.; Tomich, J. M.; Rezac, M. E. Conformational Changes and Catalytic Competency of Hydrolases Adsorbing on Fumed Silica Nanoparticles: I. Tertiary Structure. *Colloids and Surfaces B: Biointerfaces* **2010**, *79* (1), 97–104. https://doi.org/10.1016/j.colsurfb.2010.03.036.

(43) Talbert, J. N.; Goddard, J. M. Enzymes on Material Surfaces. *Colloids and Surfaces B: Biointerfaces* **2012**, *93*, 8–19. https://doi.org/10.1016/j.colsurfb.2012.01.003.

(44) Hamlin, R. E.; Dayton, T. L.; Johnson, L. E.; Johal, M. S. A QCM Study of the Immobilization of β-Galactosidase on Polyelectrolyte Surfaces: Effect of the Terminal Polyion on Enzymatic Surface Activity. *Langmuir* **2007**, *23* (8), 4432–4437. https://doi.org/10.1021/la063339t.

(45) Secundo, F.; Roda, G.; Vittorini, M.; Ungureanu, A.; Dragoi, B.; Dumitriu, E. Effect of Chemical Composition of SBA-15 on the Adsorption and Catalytic Activity of α-Chymotrypsin. *Journal of Materials Chemistry* **2011**, *21* (39), 15619. https://doi.org/10.1039/c1jm11475a.

(46) Koutsopoulos, S.; Patzsch, K.; Bosker, W. T. E.; Norde, W. Adsorption of Trypsin on Hydrophilic and Hydrophobic Surfaces. *Langmuir* **2007**, *23* (4), 2000–2006. https://doi.org/10.1021/la062238s.

(47) Manoel, E. A.; dos Santos, J. C. S.; Freire, D. M. G.; Rueda, N.; Fernandez-Lafuente, R. Immobilization of Lipases on Hydrophobic Supports Involves the Open Form of the Enzyme. *Enzyme and Microbial Technology* **2015**, *71*, 53–57. https://doi.org/10.1016/j.enzmictec.2015.02.001.

(48) Rodrigues, R. C.; Berenguer-Murcia, Á.; Fernandez-Lafuente, R. Coupling Chemical Modification and Immobilization to Improve the Catalytic Performance of Enzymes. *Advanced Synthesis & Catalysis* **2011**, *353* (13), 2216–2238. https://doi.org/10.1002/adsc.201100163.

(49) Mateo, C.; Palomo, J. M.; Fernandez-Lorente, G.; Guisan, J. M.; Fernandez-Lafuente, R. Improvement of Enzyme Activity, Stability and Selectivity via Immobilization Techniques. *Enzyme and Microbial Technology* **2007**, *40* (6), 1451–1463. https://doi.org/10.1016/j.enzmictec.2007.01.018.

(50) Rodrigues, R. C.; Ortiz, C.; Berenguer-Murcia, Á.; Torres, R.; Fernández-Lafuente, R. Modifying Enzyme Activity and Selectivity by Immobilization. *Chem. Soc. Rev.* **2013**, *42* (15), 6290–6307. https://doi.org/10.1039/C2CS35231A.

(51) Jin, W.; Brennan, J. D. Properties and Applications of Proteins Encapsulated within Sol–Gel Derived Materials. *Analytica Chimica Acta* **2002**, *461* (1), 1–36. https://doi.org/10.1016/S0003-2670(02)00229-5.

(52) Liese, A.; Hilterhaus, L. Evaluation of Immobilized Enzymes for Industrial Applications. *Chemical Society Reviews* **2013**, *42* (15), 6236. https://doi.org/10.1039/c3cs35511j.

(53) Cantone, S.; Ferrario, V.; Corici, L.; Ebert, C.; Fattor, D.; Spizzo, P.; Gardossi, L. Efficient Immobilisation of Industrial Biocatalysts: Criteria and Constraints for the Selection of Organic Polymeric Carriers and Immobilisation Methods. *Chemical Society Reviews* **2013**, *42* (15), 6262. https://doi.org/10.1039/c3cs35464d.

(54) Basso, A.; De Martin, L.; Ebert, C.; Gardossi, L.; Linda, P. High Isolated Yields in Thermodynamically Controlled Peptide Synthesis in Toluene Catalysed by Thermolysin Adsorbed on Celite R-640. *Chemical Communications* **2000**, No. 6, 467–468. https://doi.org/10.1039/b000797h.

(55) Hudson, E.; Eppler, R.; Clark, D. Biocatalysis in Semi-Aqueous and Nearly Anhydrous Conditions. *Current Opinion in Biotechnology* **2005**, *16* (6), 637–643. https://doi.org/10.1016/j.copbio.2005.10.004.

(56) Ghanbari, F.; Rowland-Yeo, K.; Bloomer, J. C.; Clarke, S. E.; Lennard, M. S.; Tucker, G. T.; Rostami-Hodjegan, A. A Critical Evaluation of the Experimental Design of Studies of Mechanism Based Enzyme Inhibition, with Implications for In Vitro-In Vivo Extrapolation. 20.

(57) Mogensen, J. E.; Sehgal, P.; Otzen, D. E. Activation, Inhibition, and Destabilization of *Thermomyces Lanuginosus* Lipase by Detergents †. *Biochemistry* **2005**, *44* (5), 1719–1730. https://doi.org/10.1021/bi0479757.

(58) Cowan, D. A.; Daniel, R. M.; Morgan, H. W. Some Observations on the Inhibition and Activation of a Thermophilic Protease. *International Journal of Biochemistry* **1987**, *19* (5), 483–486. https://doi.org/10.1016/0020-711X(87)90073-5.

(59) Frenkel-Mullerad, H.; Avnir, D. Sol−Gel Materials as Efficient Enzyme Protectors: Preserving the Activity of Phosphatases under Extreme PH Conditions. *Journal of the American Chemical Society* **2005**, *127* (22), 8077–8081. https://doi.org/10.1021/ja0507719.

(60) Malgras, V.; Ataee-Esfahani, H.; Wang, H.; Jiang, B.; Li, C.; Wu, K. C.-W.; Kim, J. H.; Yamauchi, Y. Nanoarchitectures for Mesoporous Metals. *Advanced Materials* **2016**, *28* (6), 993–1010. https://doi.org/10.1002/adma.201502593.

(61) Zdarta, J.; Meyer, A.; Jesionowski, T.; Pinelo, M. A General Overview of Support Materials for Enzyme Immobilization: Characteristics, Properties, Practical Utility. *Catalysts* **2018**, *8* (2), 92. https://doi.org/10.3390/catal8020092.

(62) Gray, C. J.; Weissenborn, M. J.; Eyers, C. E.; Flitsch, S. L. Enzymatic Reactions on Immobilised Substrates. *Chemical Society Reviews* **2013**, *42* (15), 6378. https://doi.org/10.1039/c3cs60018a.

(63) Ashly, P. C.; Joseph, M. J.; Mohanan, P. V. Activity of Diastase α-Amylase Immobilized on Polyanilines (PANIs). *Food Chemistry* **2011**, *127* (4), 1808–1813. https://doi.org/10.1016/j.foodchem.2011.02.068.

(64) Wang, W.; Zhou, W.; Li, J.; Hao, D.; Su, Z.; Ma, G. Comparison of Covalent and Physical Immobilization of Lipase in Gigaporous Polymeric Microspheres. *Bioprocess and Biosystems Engineering* **2015**, *38* (11), 2107–2115. https://doi.org/10.1007/s00449-015-1450-3.

(65) Krajewska, B. Application of Chitin- and Chitosan-Based Materials for Enzyme Immobilizations: A Review. *Enzyme and Microbial Technology* **2004**, *35* (2–3), 126–139. https://doi.org/10.1016/j.enzmictec.2003.12.013.

(66) Jesionowski, T.; Zdarta, J.; Krajewska, B. Enzyme Immobilization by Adsorption: A Review. *Adsorption* **2014**, *20* (5–6), 801–821. https://doi.org/10.1007/s10450-014-9623-y.

(67) Hsieh, H.-J.; Liu, P.-C.; Liao, W.-J. Immobilization of Invertase via Carbohydrate Moiety on Chitosan to Enhance Its Thermal Stability. *Biotechnology Letters* **2000**, *22* (18), 1459–1464.

(68) El-Ghaffar, M. A. A.; Hashem, M. S. Immobilization of α-Amylase onto Chitosan and Its Amino Acid Condensation Adducts. *Journal of Applied Polymer Science* **2009**, *112* (2), 805–814. https://doi.org/10.1002/app.29292.

(69) O'SULLIVAN, A. C. Cellulose: The Structure Slowly Unravels. 35.

(70) Klemm, D.; Heublein, B.; Fink, H.-P.; Bohn, A. Cellulose: Fascinating Biopolymer and Sustainable Raw Material. *Angewandte Chemie International Edition* **2005**, *44* (22), 3358–3393. https://doi.org/10.1002/anie.200460587.

(71) Turner, M. B.; Spear, S. K.; Holbrey, J. D.; Daly, D. T.; Rogers, R. D. Ionic Liquid-Reconstituted Cellulose Composites as Solid Support Matrices for Biocatalyst Immobilization. *Biomacromolecules* **2005**, *6* (5), 2497–2502. https://doi.org/10.1021/bm050199d.

(72) Steunou, N. Interfacing Gelatin with (Hydr)Oxides and Metal Nanoparticles: Design of Advanced Hybrid Materials for Biomedical Engineering Applications. In *Advanced Materials Interfaces*; Wiley-Scrivener, 2016; pp 277–324.

(73) Samal, S. K.; Dash, M.; Van Vlierberghe, S.; Kaplan, D. L.; Chiellini, E.; van Blitterswijk, C.; Moroni, L.; Dubruel, P. Cationic Polymers and Their Therapeutic Potential. *Chemical Society Reviews* **2012**, *41* (21), 7147. https://doi.org/10.1039/c2cs35094g.

(74) Jaiswal, N.; Prakash, O.; Talat, M.; Hasan, S. H.; Pandey, R. K. α-Amylase Immobilization on Gelatin: Optimization of Process Variables. *Journal of Genetic Engineering and Biotechnology* **2012**, *10* (1), 161–167. https://doi.org/10.1016/j.jgeb.2012.03.003.

(75) Shen, Q.; Yang, R.; Hua, X.; Ye, F.; Zhang, W.; Zhao, W. Gelatin-Templated Biomimetic Calcification for β-Galactosidase Immobilization. *Process Biochemistry* **2011**, *46* (8), 1565–1571. https://doi.org/10.1016/j.procbio.2011.04.010.

(76) Blandino, A.; Macías, M.; Cantero, D. Immobilization of Glucose Oxidase within Calcium Alginate Gel Capsules. *Process Biochemistry* **2001**, *36* (7), 601–606. https://doi.org/10.1016/S0032-9592(00)00240-5.

(77) ErtesvÃ¥g, H. Alginate-Modifying Enzymes: Biological Roles and Biotechnological Uses. *Frontiers in Microbiology* **2015**, *6*. https://doi.org/10.3389/fmicb.2015.00523.

(78) Goh, C. H.; Heng, P. W. S.; Chan, L. W. Alginates as a Useful Natural Polymer for Microencapsulation and Therapeutic Applications. *Carbohydrate Polymers* **2012**, *88* (1), 1–12. https://doi.org/10.1016/j.carbpol.2011.11.012.

(79) GRANT, G. T.; MON, E. R.; REES, S. D. A.; SMITI-I, P. J. C. BIOLOGICAL INTERACTIONS BETWEEN POLYSACCHARtDES AND DIVALENT CATIONS: THE EGG-BOX MODEL. *FEBS LETTERS* 4.

(80) Kühbeck, D.; Mayr, J.; Häring, M.; Hofmann, M.; Quignard, F.; Díaz Díaz, D. Evaluation of the Nitroaldol Reaction in the Presence of Metal Ion-Crosslinked Alginates. *New Journal of Chemistry* **2015**, *39* (3), 2306–2315. https://doi.org/10.1039/C4NJ02178A.

(81) Lee, K. Y.; Mooney, D. J. Alginate: Properties and Biomedical Applications. *Progress in Polymer Science* **2012**, *37* (1), 106–126. https://doi.org/10.1016/j.progpolymsci.2011.06.003.

(82) Willaert, R. Cell Immobilization: Engineering Aspects. In *Encyclopedia of Industrial Biotechnology*; John Wiley & Sons, Inc.: Hoboken, NJ, USA, 2009. https://doi.org/10.1002/9780470054581.eib200.
(83) Christoph, S.; Kwiatoszynski, J.; Coradin, T.; Fernandes, F. M. Cellularized Cellular Solids via Freeze-Casting: Cellularized Cellular Solids via Freeze-Casting. *Macromolecular Bioscience* **2016**, *16* (2), 182–187. https://doi.org/10.1002/mabi.201500319.
(84) Tanriseven, A.; Doğan, Ş. Immobilization of Invertase within Calcium Alginate Gel Capsules. *Process Biochemistry* **2001**, *36* (11), 1081–1083. https://doi.org/10.1016/S0032-9592(01)00146-7.
(85) Lu, L.; Zhao, M.; Wang, Y. Immobilization of Laccase by Alginate–Chitosan Microcapsules and Its Use in Dye Decolorization. *World Journal of Microbiology and Biotechnology* **2007**, *23* (2), 159–166. https://doi.org/10.1007/s11274-006-9205-6.
(86) Wu, S.; Ju, H. X.; Liu, Y. Conductive Mesocellular Silica–Carbon Nanocomposite Foams for Immobilization, Direct Electrochemistry, and Biosensing of Proteins. *Advanced Functional Materials* **2007**, *17* (4), 585–592. https://doi.org/10.1002/adfm.200600491.
(87) Kondyurin, A.; Levchenko, I.; Han, Z.-J.; Yick, S.; Mai-Prochnow, A.; Fang, J.; Ostrikov, K.; Bilek, M. M. M. Hybrid Graphite Film–Carbon Nanotube Platform for Enzyme Immobilization and Protection. *Carbon* **2013**, *65*, 287–295. https://doi.org/10.1016/j.carbon.2013.08.028.
(88) Ramakrishna, T. R. B.; Nalder, T. D.; Yang, W.; Marshall, S. N.; Barrow, C. J. Controlling Enzyme Function through Immobilisation on Graphene, Graphene Derivatives and Other Two Dimensional Nanomaterials. *Journal of Materials Chemistry B* **2018**, *6* (20), 3200–3218. https://doi.org/10.1039/C8TB00313K.
(89) Li, H.; Hou, J.; Duan, L.; Ji, C.; Zhang, Y.; Chen, V. Graphene Oxide-Enzyme Hybrid Nanoflowers for Efficient Water Soluble Dye Removal. *Journal of Hazardous Materials* **2017**, *338*, 93–101. https://doi.org/10.1016/j.jhazmat.2017.05.014.
(90) Zhou, Z.; Hartmann, M. Progress in Enzyme Immobilization in Ordered Mesoporous Materials and Related Applications. *Chemical Society Reviews* **2013**, *42* (9), 3894. https://doi.org/10.1039/c3cs60059a.
(91) Sun, Q.; Fu, C.-W.; Aguila, B.; Perman, J.; Wang, S.; Huang, H.-Y.; Xiao, F.-S.; Ma, S. Pore Environment Control and Enhanced Performance of Enzymes Infiltrated in Covalent Organic Frameworks. *Journal of the American Chemical Society* **2018**, *140* (3), 984–992. https://doi.org/10.1021/jacs.7b10642.
(92) Zhang, S.; Zheng, Y.; An, H.; Aguila, B.; Yang, C.-X.; Dong, Y.; Xie, W.; Cheng, P.; Zhang, Z.; Chen, Y.; et al. Covalent Organic Frameworks with Chirality Enriched by Biomolecules for Efficient Chiral Separation. *Angewandte Chemie International Edition* **2018**. https://doi.org/10.1002/anie.201810571.
(93) Zucca, P.; Sanjust, E. Inorganic Materials as Supports for Covalent Enzyme Immobilization: Methods and Mechanisms. *Molecules* **2014**, *19* (9), 14139–14194. https://doi.org/10.3390/molecules190914139.
(94) Hou, J.; Dong, G.; Ye, Y.; Chen, V. Laccase Immobilization on Titania Nanoparticles and Titania-Functionalized Membranes. *Journal of Membrane Science* **2014**, *452*, 229–240. https://doi.org/10.1016/j.memsci.2013.10.019.
(95) Kandimalla, V. B.; Tripathi, V. S.; Ju, H. Immobilization of Biomolecules in Sol–Gels: Biological and Analytical Applications. *Critical Reviews in Analytical Chemistry* **2006**, *36* (2), 73–106. https://doi.org/10.1080/10408340600713652.
(96) Avnir, D.; Coradin, T.; Lev, O.; Livage, J. Recent Bio-Applications of Sol–Gel Materials. *J. Mater. Chem.* **2006**, *16* (11), 1013–1030. https://doi.org/10.1039/B512706H.
(97) Pierre, A. C. The Sol-Gel Encapsulation of Enzymes. *Biocatalysis and Biotransformation* **2004**, *22* (3), 145–170. https://doi.org/10.1080/10242420412331283314.
(98) Yu; Ju. Preparation of Porous Titania Sol−Gel Matrix for Immobilization of Horseradish Peroxidase by a Vapor Deposition Method. *Analytical Chemistry* **2002**, *74* (14), 3579–3583. https://doi.org/10.1021/ac011290k.
(99) Vinogradov, V. V.; Avnir, D. Exceptional Thermal Stability of Therapeutical Enzymes Entrapped in Alumina Sol–Gel Matrices. *Journal of Materials Chemistry B* **2014**, *2* (19), 2868. https://doi.org/10.1039/c3tb21643h.
(100) Singh, A. K.; Gupta, A.; Mulchandani, A.; Chen, W.; Bhatia, R. B.; Schoeniger, J. S.; Ashley, C. S.; Brinker, C. J. Encapsulation of Enzymes and Cells in Sol-Gel Matrices for Biosensor Applications; Fallahi, M., Swanson, B. I., Eds.; Boston, MA, 1999; p 10. https://doi.org/10.1117/12.372912.
(101) Sicard, C.; Brayner, R.; Margueritat, J.; Hémadi, M.; Couté, A.; Yéprémian, C.; Djediat, C.; Aubard, J.; Fiévet, F.; Livage, J.; et al. Nano-Gold Biosynthesis by Silica-Encapsulated Micro-Algae: A “Living” Bio-Hybrid Material. *Journal of Materials Chemistry* **2010**, *20* (42), 9342. https://doi.org/10.1039/c0jm01735c.

(102) Braun, S.; Rappoprt, S.; Zusman, R.; Avnir, D.; Ottolenghi, M. Biochemically Active Sol-Gel Glasses: The Trapping of Enzymes. *Materials Letters* **1990**, *10* (1), 1–5. https://doi.org/10.1016/0167-577X(90)90002-4.

(103) Nguyen, D. T.; Smit, M.; Dunn, B.; Zink, J. I. Stabilization of Creatine Kinase Encapsulated in Silicate Sol−Gel Materials and Unusual Temperature Effects on Its Activity. *Chemistry of Materials* **2002**, *14* (10), 4300–4306. https://doi.org/10.1021/cm020398t.

(104) Besanger, T. R.; Brennan, J. D. Entrapment of Membrane Proteins in Sol-Gel Derived Silica. *Journal of Sol-Gel Science and Technology* **2006**, *40* (2–3), 209–225. https://doi.org/10.1007/s10971-006-8132-1.

(105) Wang, X.; Ahmed, N.; Alvarez, G.; Tuttolomondo, M.; Helary, C.; Desimone, M.; Coradin, T. Sol-Gel Encapsulation of Biomolecules and Cells for Medicinal Applications. *Current Topics in Medicinal Chemistry* **2015**, *15* (3), 223–244. https://doi.org/10.2174/1568026614666141229112734.

(106) Livage, J.; Coradin, T.; Roux, C. Encapsulation of Biomolecules in Silica Gels. *J. Phys.: Condens. Matter* **2001**, *13*, R673–R691.

(107) Reetz, M. T.; Winter, M.; Tesche, B. Self-Assembly of Tetraalkylammonium Salt-Stabilized Giant Palladium Clusters on Surfaces. *Chemical Communications* **1997**, No. 2, 147–148.

(108) Hartono, S. B.; Qiao, S. Z.; Liu, J.; Jack, K.; Ladewig, B. P.; Hao, Z.; Lu, G. Q. M. Functionalized Mesoporous Silica with Very Large Pores for Cellulase Immobilization. *The Journal of Physical Chemistry C* **2010**, *114* (18), 8353–8362. https://doi.org/10.1021/jp102368s.

(109) Park, M.; Park, S. S.; Selvaraj, M.; Zhao, D.; Ha, C.-S. Hydrophobic Mesoporous Materials for Immobilization of Enzymes. *Microporous and Mesoporous Materials* **2009**, *124* (1–3), 76–83. https://doi.org/10.1016/j.micromeso.2009.04.032.

(110) Hartmann, M. Ordered Mesoporous Materials for Bioadsorption and Biocatalysis. *Chemistry of Materials* **2005**, *17* (18), 4577–4593.

(111) Kresge, C. T.; Leonowicz, M. E.; Roth, W. J.; Vartuli, J. C.; Beck, J. S. Ordered Mesoporous Molecular Sieves Synthesized by a Liquid-Crystal Tmplate Mechanism. *Nature* **1992**, *359*, 710–712. https://doi.org/10.1038/359710a0.

(112) Kresge, C. T.; Vartuli, J. C.; Roth, W. J.; Leonowicz, M. E. The Discovery of ExxonMobil's M41S Family of Mesoporous Molecular Sieves. *Studies in Surface Science and Catalysis* **2004**, *148*, 53–67. https://doi.org/10.1016/S0167-2991(04)80193-9.

(113) Zhao, D. Triblock Copolymer Syntheses of Mesoporous Silica with Periodic 50 to 300 Angstrom Pores. *Science* **1998**, *279* (5350), 548–552. https://doi.org/10.1126/science.279.5350.548.

(114) Zhao, D.; Huo, Q.; Feng, J.; Chmelka, B. F.; Stucky, G. D. Nonionic Triblock and Star Diblock Copolymer and Oligomeric Surfactant Syntheses of Highly Ordered, Hydrothermally Stable, Mesoporous Silica Structures. *Journal of the American Chemical Society* **1998**, *120* (24), 6024–6036. https://doi.org/10.1021/ja974025i.

(115) Hoffmann, F.; Cornelius, M.; Morell, J.; Fröba, M. Silica-Based Mesoporous Organic–Inorganic Hybrid Materials. *Angewandte Chemie International Edition* **2006**, *45* (20), 3216–3251. https://doi.org/10.1002/anie.200503075.

(116) Yue, W.; Zhou, W. Porous Crystals of Cubic Metal Oxides Templated by Cage-Containing Mesoporous Silica. *Journal of Materials Chemistry* **2007**, *17* (47), 4947. https://doi.org/10.1039/b709076e.

(117) Yiu, H. H. P.; Wright, P. A. Enzymes Supported on Ordered Mesoporous Solids: A Special Case of an Inorganic–Organic Hybrid. *Journal of Materials Chemistry* **2005**, *15* (35–36), 3690. https://doi.org/10.1039/b506090g.

(118) Price, P. M.; Clark, J. H.; Macquarrie, D. J. Modified Silicas for Clean Technology. *Journal of the Chemical Society, Dalton Transactions* **2000**, No. 2, 101–110. https://doi.org/10.1039/a905457j.

(119) Balistreri, N.; Gaboriau, D.; Jolivalt, C.; Launay, F. Covalent Immobilization of Glucose Oxidase on Mesocellular Silica Foams: Characterization and Stability towards Temperature and Organic Solvents. *Journal of Molecular Catalysis B: Enzymatic* **2016**, *127*, 26–33. https://doi.org/10.1016/j.molcatb.2016.02.003.

(120) Mousty, C. Biosensing Applications of Clay-Modified Electrodes: A Review. *Analytical and Bioanalytical Chemistry* **2010**, *396* (1), 315–325. https://doi.org/10.1007/s00216-009-3274-y.

(121) An, N.; Zhou, C. H.; Zhuang, X. Y.; Tong, D. S.; Yu, W. H. Immobilization of Enzymes on Clay Minerals for Biocatalysts and Biosensors. *Applied Clay Science* **2015**, *114*, 283–296. https://doi.org/10.1016/j.clay.2015.05.029.

(122) Mousty, C.; Prevot, V. Hybrid and Biohybrid Layered Double Hydroxides for Electrochemical Analysis. *Analytical and Bioanalytic Chemistry* **2013**, *405*, 3513–3523. https://doi.org/10.1007/s00216-013-6797-1.

(123) de Melo, J. V.; Cosnier, S.; Mousty, C.; Martelet, C.; Jaffrezic-Renault, N. Urea Biosensors Based on Immobilization of Urease into Two Oppositely Charged Clays (Laponite and Zn-Al Layered Double Hydroxides). *Analytical Chemistry* **2002**, No. 74, 4037–4043.

(124) Li, T.; Miras, H.; Song, Y.-F. Polyoxometalate (POM)-Layered Double Hydroxides (LDH) Composite Materials: Design and Catalytic Applications. *Catalysts* **2017**, *7* (9), 260. https://doi.org/10.3390/catal7090260.

(125) Smith, J. V. Definition of a Zeolite. *Zeolites* **1984**, *4* (4), 309–310. https://doi.org/10.1016/0144-2449(84)90003-4.

(126) Csicsery, S. M. Shape-Selective Catalysis Inzeolites. *Zeolites* **1984**, *4*, 202–213.

(127) Kusakabe, K.; Kuroda, T.; Murata, A.; Morooka, S. Formation of a Y-Type Zeolite Membrane on a Porous r-Alumina Tube for Gas Separation. 7.

(128) Shi, J.; Wang, Y.; Yang, W.; Tang, Y.; Xie, Z. Recent Advances of Pore System Construction in Zeolite-Catalyzed Chemical Industry Processes. *Chemical Society Reviews* **2015**, *44* (24), 8877–8903. https://doi.org/10.1039/C5CS00626K.

(129) Yu, T.; Zhang, Y.; You, C.; Zhuang, J.; Wang, B.; Liu, B.; Kang, Y.; Tang, Y. Controlled Nanozeolite-Assembled Electrode: Remarkable Enzyme-Immobilization Ability and High Sensitivity as Biosensor. *Chemistry - A European Journal* **2006**, *12* (4), 1137–1143. https://doi.org/10.1002/chem.200500562.

(130) Wang, Y.; Caruso, F. Macroporous Zeolitic Membrane Bioreactors. *Advanced Functional Materials* **2004**, *14* (10), 1012–1018. https://doi.org/10.1002/adfm.200400144.

(131) Mitchell, S.; Pérez-Ramírez, J. Mesoporous Zeolites as Enzyme Carriers: Synthesis, Characterization, and Application in Biocatalysis. *Catalysis Today* **2011**, *168* (1), 28–37. https://doi.org/10.1016/j.cattod.2010.10.058.

(132) Zhou, H.-C.; Long, J. R.; Yaghi, O. M. Introduction to Metal–Organic Frameworks. *Chemical Reviews* **2012**, *112* (2), 673–674. https://doi.org/10.1021/cr300014x.

(133) Zhou, H.-C. "Joe"; Kitagawa, S. Metal–Organic Frameworks (MOFs). *Chem. Soc. Rev.* **2014**, *43* (16), 5415–5418. https://doi.org/10.1039/C4CS90059F.

(134) Maurin, G.; Serre, C.; Cooper, A.; Férey, G. The New Age of MOFs and of Their Porous-Related Solids. *Chemical Society Reviews* **2017**, *46* (11), 3104–3107. https://doi.org/10.1039/C7CS90049J.

(135) Hoskins, B. F.; Robson, R. Infinite Polymeric Frameworks Consisting of Three Dimensionally Linked Rod-like Segments. *Journal of the American Chemical Society* **1989**, *111* (15), 5962–5964. https://doi.org/10.1021/ja00197a079.

(136) Kondo, M.; Yoshitomi, T.; Matsuzaka, H.; Kitagawa, S.; Seki, K. Three-Dimensional Framework with Channeling Cavities for Small Molecules:{[M2(4, 4'-Bpy)3(NO3)4]·xH2O}n(M□ Co, Ni, Zn). *Angewandte Chemie International Edition in English* **1997**, *36* (16), 1725–1727. https://doi.org/10.1002/anie.199717251.

(137) Yaghi, O. M.; Li, G.; Li, H. Selective Binding and Removal of Guests in Microporous Metal-Organic Frameworks. *Nature* **1995**, *378*, 703–706. https://doi.org/10.1038/378703a0.

(138) Serre, C.; Millange, F.; Thouvenot, C.; Noguès, M.; Marsolier, G.; Louër, D.; Férey, G. Very Large Breathing Effect in the First Nanoporous Chromium(III)-Based Solids: MIL-53 or $Cr^{III}(OH)\cdot\{O_2C-C_6H_4-CO_2\}\cdot\{HO_2C-C_6H_4-CO_2H\}_x\cdot H_2O_y$. *Journal of the American Chemical Society* **2002**, *124* (45), 13519–13526. https://doi.org/10.1021/ja0276974.

(139) Serre, C.; Mellot-Draznieks, C.; Surble, S.; Audebrand, N.; Filinchuk, Y.; Ferey, G. Role of Solvent-Host Interactions That Lead to Very Large Swelling of Hybrid Frameworks. *Science* **2007**, *315* (5820), 1828–1831. https://doi.org/10.1126/science.1137975.

(140) Barthelet, K.; Marrot, J.; Riou, D.; Férey, G. A Breathing Hybrid Organic–Inorganic Solid with Very Large Pores and High Magnetic Characteristics. *Angewandte Chemie International Edition* **2002**, *41* (2), 281. https://doi.org/10.1002/1521-3773(20020118)41:2<281::AID-ANIE281>3.0.CO;2-Y.

(141) Férey, G.; Serre, C.; Mellot-Draznieks, C.; Millange, F.; Surblé, S.; Dutour, J.; Margiolaki, I. A Hybrid Solid with Giant Pores Prepared by a Combination of Targeted Chemistry, Simulation, and Powder Diffraction. *Angewandte Chemie International Edition* **2004**, *43* (46), 6296–6301. https://doi.org/10.1002/anie.200460592.

(142) Férey, G.; Mellot-Draznieks, C.; Serre, C.; Millange, F.; Gutour, J.; Surblé, S.; Margiolaki, I. A Chromium Terephthalate-Based Solid with Unusually Large Pore Volumes and Surface Area. *Science* **2005**, *309* (5743), 2040–2042. https://doi.org/10.1126/science.1116275.

(143) Lismont, M.; Dreesen, L.; Wuttke, S. Metal-Organic Framework Nanoparticles in Photodynamic Therapy: Current Status and Perspectives. *Advanced Functional Materials* **2017**, *27* (14), 1606314. https://doi.org/10.1002/adfm.201606314.

(144) Devic, T.; Serre, C. High Valence 3p and Transition Metal Based MOFs. *Chem. Soc. Rev.* **2014**, *43* (16), 6097–6115. https://doi.org/10.1039/C4CS00081A.

(145) Fordham, S.; Wang, X.; Bosch, M.; Zhou, H.-C. Lanthanide Metal-Organic Frameworks: Syntheses, Properties, and Potential Applications. In *Lanthanide Metal-Organic Frameworks*; Cheng, P., Ed.; Springer Berlin Heidelberg: Berlin, Heidelberg, 2014; Vol. 163, pp 1–27. https://doi.org/10.1007/430_2014_162.

(146) Dolgopolova, E. A.; Rice, A. M.; Shustova, N. B. Actinide-Based MOFs: A Middle Ground in Solution and Solid-State Structural Motifs. *Chemical Communications* **2018**, *54* (50), 6472–6483. https://doi.org/10.1039/C7CC09780H.

(147) Shekhah, O.; Wang, H.; Zacher, D.; Fischer, R. A.; Wöll, C. Growth Mechanism of Metal-Organic Frameworks: Insights into the Nucleation by Employing a Step-by-Step Route. *Angewandte Chemie International Edition* **2009**, *48* (27), 5038–5041. https://doi.org/10.1002/anie.200900378.

(148) Surblé, S.; Serre, C.; Mellot-Draznieks, C.; Millange, F.; Férey, G. A New Isoreticular Class of Metal-Organic-Frameworks with the MIL-88 Topology. *Chem. Commun.* **2006**, No. 3, 284–286. https://doi.org/10.1039/B512169H.

(149) DeStefano, M. R.; Islamoglu, T.; Garibay, S. J.; Hupp, J. T.; Farha, O. K. Room Temperature Synthesis of UiO-66 and the Thermal Modulation of Densities of Defect Sites. *Chemistry of Materials* **2017**, *29* (3), 1357–1361. https://doi.org/10.1021/acs.chemmater.6b05115.

(150) Serre, C.; Millange, F.; Surblé, S.; Férey, G. A Route to the Synthesis of Trivalent Transition-Metal Porous Carboxylates with Trimeric Secondary Building Units. *Angewandte Chemie International Edition* **2004**, *43* (46), 6285–6289. https://doi.org/10.1002/anie.200454250.

(151) Eddaoudi, M.; Moler, D. B.; Li, H.; Chen, B.; Reineke, T. M.; O'Keeffe, M.; Yaghi, O. M. Modular Chemistry: Secondary Building Units as a Basis for the Design of Highly Porous and Robust Metal−Organic Carboxylate Frameworks. *Accounts of Chemical Research* **2001**, *34* (4), 319–330. https://doi.org/10.1021/ar000034b.

(152) Loiseau, T.; Volkringer, C.; Haouas, M.; Taulelle, F.; Férey, G. Crystal Chemistry of Aluminium Carboxylates: From Molecular Species towards Porous Infinite Three-Dimensional Networks. *Comptes Rendus Chimie* **2015**, *18* (12), 1350–1369. https://doi.org/10.1016/j.crci.2015.08.006.

(153) Yaghi, O. M.; O'Keeffe, M.; Ockwig, N. W.; Chae, H. K.; Eddaoudi, M.; Kim, J. Reticular Synthesis and the Design of New Materials. *Nature* **2003**, *423* (6941), 705–714. https://doi.org/10.1038/nature01650.

(154) Stock, N.; Biswas, S. Synthesis of Metal-Organic Frameworks (MOFs): Routes to Various MOF Topologies, Morphologies, and Composites. *Chemical Reviews* **2012**, *112* (2), 933–969. https://doi.org/10.1021/cr200304e.

(155) Jhung, S. H.; Lee, J.-H.; Chang, J.-S. Microwave Synthesis of a Nanoporous Material, Chromium Trimase. *Bulletin of the Korean Chemical Society* **2005**, *26* (6), 880–881.

(156) Demessence, A.; Horcajada, P.; Serre, C.; Boissière, C.; Grosso, D.; Sanchez, C.; Férey, G. Elaboration and Properties of Hierarchically Structured Optical Thin Films of MIL-101(Cr). *Chemical Communications* **2009**, No. 46, 7149. https://doi.org/10.1039/b915011k.

(157) Horcajada Patricia; Chalati Tamim; Serre Christian; Gillet Brigitte; Sebrie Catherine; Baati Tarek; Eubank Jarrod F.; Heurtaux Daniela; Clayette Pascal; Kreuz Christine; et al. Porous Metal–Organic-Framework Nanoscale Carriers as a Potential Platform for Drug Delivery and Imaging. *Nature Materials* **2010**, *9* (2), 172–178. https://doi.org/10.1038/nmat2608.

(158) Benzaqui, M.; Pillai, R. S.; Sabetghadam, A.; Benoit, V.; Normand, P.; Marrot, J.; Menguy, N.; Montero, D.; Shepard, W.; Tissot, A.; et al. Revisiting the Aluminum Trimesate-Based MOF (MIL-96): From Structure Determination to the Processing of Mixed Matrix Membranes for CO_2 Capture. *Chemistry of Materials* **2017**, *29* (24), 10326–10338. https://doi.org/10.1021/acs.chemmater.7b03203.

(159) Loiseau, T.; Mellot-Draznieks, C.; Muguerra, H.; Férey, G.; Haouas, M.; Taulelle, F. Hydrothermal Synthesis and Crystal Structure of a New Three-Dimensional Aluminum-Organic Framework MIL-69 with 2,6-Naphthalenedicarboxylate (Ndc), Al(OH)(Ndc)·H2O. *Comptes Rendus Chimie* **2005**, *8* (3–4), 765–772. https://doi.org/10.1016/j.crci.2004.10.011.

(160) Barthelet, K.; Marrot, J.; Férey, G.; Riou, D. $V^{III}(OH)\{O_2C–C_6H_4–CO_2\}.(HO_2C–C_6H_4–CO_2H)x(DMF)_y(H_2O)z$ (or MIL-68), a New Vanadocarboxylate with a Large Pore Hybrid Topology : Reticular Synthesis with Infinite Inorganic Building Blocks? *Chem. Commun.* **2004**, No. 5, 520–521. https://doi.org/10.1039/B312589K.

(161) Volkringer, C.; Meddouri, M.; Loiseau, T.; Guillou, N.; Marrot, J.; Férey, G.; Haouas, M.; Taulelle, F.; Audebrand, N.; Latroche, M. The Kagomé Topology of the Gallium and Indium Metal-Organic Framework Types with a MIL-68 Structure: Synthesis, XRD, Solid-State NMR Characterizations, and Hydrogen Adsorption. *Inorganic Chemistry* **2008**, *47* (24), 11892–11901. https://doi.org/10.1021/ic801624v.

(162) Yot, P. G.; Boudene, Z.; Macia, J.; Granier, D.; Vanduyfhuys, L.; Verstraelen, T.; Van Speybroeck, V.; Devic, T.; Serre, C.; Férey, G.; et al. Metal–Organic Frameworks as Potential Shock Absorbers: The Case of the Highly Flexible MIL-53(Al). *Chem. Commun.* **2014**, *50* (67), 9462–9464. https://doi.org/10.1039/C4CC03853C.

(163) Férey, G.; Serre, C. Large Breathing Effects in Three-Dimensional Porous Hybrid Matter: Facts, Analyses, Rules and Consequences. *Chemical Society Reviews* **2009**, *38* (5), 1380. https://doi.org/10.1039/b804302g.

(164) Fateeva, A.; Horcajada, P.; Devic, T.; Serre, C.; Marrot, J.; Grenèche, J.-M.; Morcrette, M.; Tarascon, J.-M.; Maurin, G.; Férey, G. Synthesis, Structure, Characterization, and Redox Properties of the Porous MIL-68(Fe) Solid. *European Journal of Inorganic Chemistry* **2010**, *2010* (24), 3789–3794. https://doi.org/10.1002/ejic.201000486.

(165) Lupu, D.; Ardelean, O.; Blanita, G.; Borodi, G.; Lazar, M. D.; Biris, A. R.; Ioan, C.; Mihet, M.; Misan, I.; Popeneciu, G. Synthesis and Hydrogen Adsorption Properties of a New Iron Based Porous Metal-Organic Framework. *International Journal of Hydrogen Energy* **2011**, *36* (5), 3586–3592. https://doi.org/10.1016/j.ijhydene.2010.12.043.

(166) Stavitski, E.; Goesten, M.; Juan-Alcañiz, J.; Martinez-Joaristi, A.; Serra-Crespo, P.; Petukhov, A. V.; Gascon, J.; Kapteijn, F. Kinetic Control of Metal-Organic Framework Crystallization Investigated by Time-Resolved In Situ X-Ray Scattering. *Angewandte Chemie International Edition* **2011**, *50* (41), 9624–9628. https://doi.org/10.1002/anie.201101757.

(167) Biswas, S.; Couck, S.; Grzywa, M.; Denayer, J. F. M.; Volkmer, D.; Van Der Voort, P. Vanadium Analogues of Nonfunctionalized and Amino-Functionalized MOFs with MIL-101 Topology - Synthesis, Characterization, and Gas Sorption Properties. *European Journal of Inorganic Chemistry* **2012**, *2012* (15), 2481–2486. https://doi.org/10.1002/ejic.201200106.

(168) Millange, F.; Guillou, N.; Walton, R. I.; Grenèche, J.-M.; Margiolaki, I.; Férey, G. Effect of the Nature of the Metal on the Breathing Steps in MOFs with Dynamic Frameworks. *Chemical Communications* **2008**, No. 39, 4732. https://doi.org/10.1039/b809419e.

(169) Trung, T. K.; Trens, P.; Tanchoux, N.; Bourrelly, S.; Llewellyn, P. L.; Loera-Serna, S.; Serre, C.; Loiseau, T.; Fajula, F.; Férey, G. Hydrocarbon Adsorption in the Flexible Metal Organic Frameworks MIL-53(Al, Cr). *Journal of the American Chemical Society* **2008**, *130* (50), 16926–16932. https://doi.org/10.1021/ja8039579.

(170) Leung, E.; Müller, U.; Trukhan, N.; Mattenheimer, H.; Cox, G.; Blei, S. Process for Preparing Porous Metal-Organic Frameworks Based on Aluminium Fuamrate. *EP Patentanmeldung 10183283.0* **2010**.

(171) Alvarez, E.; Guillou, N.; Martineau, C.; Bueken, B.; Van de Voorde, B.; Le Guillouzer, C.; Fabry, P.; Nouar, F.; Taulelle, F.; de Vos, D.; et al. The Structure of the Aluminum Fumarate Metal-Organic Framework A520. *Angewandte Chemie International Edition* **2015**, *54* (12), 3664–3668. https://doi.org/10.1002/anie.201410459.

(172) Gaab, M.; Trukhan, N.; Maurer, S.; Gummaraju, R.; Müller, U. The Progression of Al-Based Metal-Organic Frameworks – From Academic Research to Industrial Production and Applications. *Microporous and Mesoporous Materials* **2012**, *157*, 131–136. https://doi.org/10.1016/j.micromeso.2011.08.016.

(173) Jeremias, F.; Fröhlich, D.; Janiak, C.; Henninger, S. K. Advancement of Sorption-Based Heat Transformation by a Metal Coating of Highly-Stable, Hydrophilic Aluminium Fumarate MOF. *RSC Adv.* **2014**, *4* (46), 24073–24082. https://doi.org/10.1039/C4RA03794D.

(174) Senkovska, I.; Hoffmann, F.; Fröba, M.; Getzschmann, J.; Böhlmann, W.; Kaskel, S. New Highly Porous Aluminium Based Metal-Organic Frameworks: Al(OH)(Ndc) (Ndc=2,6-Naphthalene Dicarboxylate) and Al(OH)(Bpdc) (Bpdc=4,4'-Biphenyl Dicarboxylate). *Microporous and Mesoporous Materials* **2009**, *122* (1–3), 93–98. https://doi.org/10.1016/j.micromeso.2009.02.020.

(175) Niekiel, F.; Ackermann, M.; Guerrier, P.; Rothkirch, A.; Stock, N. Aluminum-1,4-Cyclohexanedicarboxylates: High-Throughput and Temperature-Dependent in Situ EDXRD Studies. *Inorganic Chemistry* **2013**, *52* (15), 8699–8705. https://doi.org/10.1021/ic400825b.

(176) Comotti, A.; Bracco, S.; Sozzani, P.; Horike, S.; Matsuda, R.; Chen, J.; Takata, M.; Kubota, Y.; Kitagawa, S. Nanochannels of Two Distinct Cross-Sections in a Porous Al-Based Coordination Polymer. *Journal of the American Chemical Society* **2008**, *130* (41), 13664–13672. https://doi.org/10.1021/ja802589u.

(177) Rogge, S. M. J.; Bavykina, A.; Hajek, J.; Garcia, H.; Olivos-Suarez, A. I.; Sepúlveda-Escribano, A.; Vimont, A.; Clet, G.; Bazin, P.; Kapteijn, F.; et al. Metal–Organic and Covalent Organic Frameworks as Single-Site Catalysts. *Chemical Society Reviews* **2017**, *46* (11), 3134–3184. https://doi.org/10.1039/C7CS00033B.

(178) Wuttke, S.; Bazin, P.; Vimont, A.; Serre, C.; Seo, Y.-K.; Hwang, Y. K.; Chang, J.-S.; Férey, G.; Daturi, M. Discovering the Active Sites for C3 Separation in MIL-100(Fe) by Using Operando IR Spectroscopy. *Chemistry - A European Journal* **2012**, *18* (38), 11959–11967. https://doi.org/10.1002/chem.201201006.

(179) Dietzel, P. D. C.; Johnsen, R. E.; Fjellvåg, H.; Bordiga, S.; Groppo, E.; Chavan, S.; Blom, R. Adsorption Properties and Structure of CO2 Adsorbed on Open Coordination Sites of Metal–Organic Framework Ni2(Dhtp) from Gas Adsorption, IR Spectroscopy and X-Ray Diffraction. *Chemical Communications* **2008**, No. 41, 5125. https://doi.org/10.1039/b810574j.

(180) Alaerts, L.; Maes, M.; van der Veen, M. A.; Jacobs, P. A.; De Vos, D. Metal-Organic Frameworks as High-Potential Adsorbents for Liquid-Phase Separations of Olefins, Alkylnaphthalens and Dichlorobenzenes. *Physical Chemistry Chemical Physics* **2009**, *11* (16), 2903–2911. https://doi.org/10.1039/b905015a.

(181) Hwang, Y. K.; Hong, D.-Y.; Chang, J.-S.; Seo, H.; Yoon, M.; Kim, J.; Jhung, S. H.; Serre, C.; Férey, G. Selective Sulfoxidation of Aryl Sulfides by Coordinatively Unsaturated Metal Centers in Chromium Carboxylate MIL-101. *Applied Catalysis A: General* **2009**, *358* (2), 249–253. https://doi.org/10.1016/j.apcata.2009.02.018.

(182) De Rosa, S.; Giordano, G.; Granato, T.; Katovic, A.; Siciliano, A.; Tripicchio, F. Chemical Pretreatment of Olive Oil Mill Wastewater Using a Metal-Organic Framework Catalyst. *Journal of Agricultural and Food Chemistry* **2005**, *53* (21), 8306–8309. https://doi.org/10.1021/jf0512609.

(183) Llabresixamena, F.; Abad, A.; Corma, A.; Garcia, H. MOFs as Catalysts: Activity, Reusability and Shape-Selectivity of a Pd-Containing MOF. *Journal of Catalysis* **2007**, *250* (2), 294–298. https://doi.org/10.1016/j.jcat.2007.06.004.

(184) Opanasenko, M.; Dhakshinamoorthy, A.; Hwang, Y. K.; Chang, J.-S.; Garcia, H.; Čejka, J. Superior Performance of Metal-Organic Frameworks over Zeolites as Solid Acid Catalysts in the Prins Reaction: Green Synthesis of Nopol. *ChemSusChem* **2013**, *6* (5), 865–871. https://doi.org/10.1002/cssc.201300032.

(185) Ai, L.; Li, L.; Zhang, C.; Fu, J.; Jiang, J. MIL-53(Fe): A Metal-Organic Framework with Intrinsic Peroxidase-Like Catalytic Activity for Colorimetric Biosensing. *Chemistry - A European Journal* **2013**, *19* (45), 15105–15108. https://doi.org/10.1002/chem.201303051.

(186) Patra, S.; Hidalgo Crespo, T.; Permyakova, A.; Sicard, C.; Serre, C.; Chaussé, A.; Steunou, N.; Legrand, L. Design of Metal Organic Framework–Enzyme Based Bioelectrodes as a Novel and Highly Sensitive Biosensing Platform. *J. Mater. Chem. B* **2015**, *3* (46), 8983–8992. https://doi.org/10.1039/C5TB01412C.

(187) He, J.; Zhang, Y.; Zhang, X.; Huang, Y. Highly Efficient Fenton and Enzyme-Mimetic Activities of NH2-MIL-88B(Fe) Metal Organic Framework for Methylene Blue Degradation. *Scientific Reports* **2018**, *8* (1). https://doi.org/10.1038/s41598-018-23557-2.

(188) Zhang, J.-W.; Zhang, H.-T.; Du, Z.-Y.; Wang, X.; Yu, S.-H.; Jiang, H.-L. Water-Stable Metal–Organic Frameworks with Intrinsic Peroxidase-like Catalytic Activity as a Colorimetric Biosensing Platform. *Chem. Commun.* **2014**, *50* (9), 1092–1094. https://doi.org/10.1039/C3CC48398C.

(189) Cohen, S. M. Postsynthetic Methods for the Functionalization of Metal–Organic Frameworks. *Chemical Reviews* **2012**, *112* (2), 970–1000. https://doi.org/10.1021/cr200179u.

(190) Rubin, H. N.; Reynolds, M. M. Functionalization of Metal–Organic Frameworks To Achieve Controllable Wettability. *Inorganic Chemistry* **2017**, *56* (9), 5266–5274. https://doi.org/10.1021/acs.inorgchem.7b00373.

(191) Devic, T.; Horcajada, P.; Serre, C.; Salles, F.; Maurin, G.; Moulin, B.; Heurtaux, D.; Clet, G.; Vimont, A.; Grenèche, J.-M.; et al. Functionalization in Flexible Porous Solids: Effects on the Pore Opening and the Host−Guest Interactions. *Journal of the American Chemical Society* **2010**, *132* (3), 1127–1136. https://doi.org/10.1021/ja9092715.

(192) Nagarkar, S. S.; Saha, T.; Desai, A. V.; Talukdar, P.; Ghosh, S. K. Metal-Organic Framework Based Highly Selective Fluorescence Turn-on Probe for Hydrogen Sulphide. *Scientific Reports* **2015**, *4* (1). https://doi.org/10.1038/srep07053.

(193) Dong, X.-Y.; Li, J.-J.; Han, Z.; Duan, P.-G.; Li, L.-K.; Zang, S.-Q. Tuning the Functional Substituent Group and Guest of Metal–Organic Frameworks in Hybrid Membranes for Improved Interface Compatibility and Proton Conduction. *Journal of Materials Chemistry A* **2017**, *5* (7), 3464–3474. https://doi.org/10.1039/C6TA07761G.

(194) Lammert, M.; Bernt, S.; Vermoortele, F.; De Vos, D. E.; Stock, N. Single- and Mixed-Linker Cr-MIL-101 Derivatives: A High-Throughput Investigation. *Inorganic Chemistry* **2013**, *52* (15), 8521–8528. https://doi.org/10.1021/ic4005328.

(195) Bauer, S.; Serre, C.; Devic, T.; Horcajada, P.; Marrot, J.; Férey, G.; Stock, N. High-Throughput Assisted Rationalization of the Formation of Metal Organic Frameworks in the Iron(III) Aminoterephthalate Solvothermal System. *Inorganic Chemistry* **2008**, *47* (17), 7568–7576. https://doi.org/10.1021/ic800538r.

(196) Bernt, S.; Guillerm, V.; Serre, C.; Stock, N. Direct Covalent Post-Synthetic Chemical Modification of Cr-MIL-101 Using Nitrating Acid. *Chemical Communications* **2011**, *47* (10), 2838. https://doi.org/10.1039/c0cc04526h.

(197) Hasan, Z.; Jun, J. W.; Jhung, S. H. Sulfonic Acid-Functionalized MIL-101(Cr): An Efficient Catalyst for Esterification of Oleic Acid and Vapor-Phase Dehydration of Butanol. *Chemical Engineering Journal* **2015**, *278*, 265–271. https://doi.org/10.1016/j.cej.2014.09.025.

(198) Chen, J.; Li, K.; Chen, L.; Liu, R.; Huang, X.; Ye, D. Conversion of Fructose into 5-Hydroxymethylfurfural Catalyzed by Recyclable Sulfonic Acid-Functionalized Metal–Organic Frameworks. *Green Chem.* **2014**, *16* (5), 2490–2499. https://doi.org/10.1039/C3GC42414F.

(199) Brozek, C. K.; Dincă, M. Cation Exchange at the Secondary Building Units of Metal–Organic Frameworks. *Chem. Soc. Rev.* **2014**, *43* (16), 5456–5467. https://doi.org/10.1039/C4CS00002A.

(200) Burrows, A. D. Mixed-Component Metal–Organic Frameworks (MC-MOFs): Enhancing Functionality through Solid Solution Formation and Surface Modifications. *CrystEngComm* **2011**, *13* (11), 3623. https://doi.org/10.1039/c0ce00568a.

(201) Wongsakulphasatch, S.; Nouar, F.; Rodriguez, J.; Scott, L.; Le Guillouzer, C.; Devic, T.; Horcajada, P.; Grenèche, J.-M.; Llewellyn, P. L.; Vimont, A.; et al. Direct Accessibility of Mixed-Metal (III / II) Acid Sites through the Rational Synthesis of Porous Metal Carboxylates. *Chemical Communications* **2015**, *51* (50), 10194–10197. https://doi.org/10.1039/C5CC02550H.

(202) Nouar, F.; Devic, T.; Chevreau, H.; Guillou, N.; Gibson, E.; Clet, G.; Daturi, M.; Vimont, A.; Grenèche, J. M.; Breeze, M. I.; et al. Tuning the Breathing Behaviour of MIL-53 by Cation Mixing. *Chemical Communications* **2012**, *48* (82), 10237. https://doi.org/10.1039/c2cc35348b.

(203) Serre, C.; Millange, F.; Thouvenot, C.; Gardant, N.; Pellé, F.; Férey, G. Synthesis, Characterisation and Luminescent Properties of a New Three-Dimensional Lanthanide Trimesate: M((C_6H_3)–$(CO_2)_3$) (M = Y, Ln) or MIL-78. *J. Mater. Chem.* **2004**, *14* (10), 1540–1543. https://doi.org/10.1039/B312425H.

(204) Mitchell, L.; Williamson, P.; Ehrlichová, B.; Anderson, A. E.; Seymour, V. R.; Ashbrook, S. E.; Acerbi, N.; Daniels, L. M.; Walton, R. I.; Clarke, M. L.; et al. Mixed-Metal MIL-100(Sc,M) (M=Al, Cr, Fe) for Lewis Acid Catalysis and Tandem C□C Bond Formation and Alcohol Oxidation. *Chemistry - A European Journal* **2014**, *20* (51), 17185–17197. https://doi.org/10.1002/chem.201404377.

(205) Adil, K.; Belmabkhout, Y.; Pillai, R. S.; Cadiau, A.; Bhatt, P. M.; Assen, A. H.; Maurin, G.; Eddaoudi, M. Gas/Vapour Separation Using Ultra-Microporous Metal–Organic Frameworks: Insights into the Structure/Separation Relationship. *Chemical Society Reviews* **2017**, *46* (11), 3402–3430. https://doi.org/10.1039/C7CS00153C.

(206) Eddaoudi, M.; Kim, J.; Rosi, N.; Vodak, D.; Wachter, J.; O'Keeffe, M.; Yaghi, O. M. Systematic Design of Pore Size and Functionality in Isoreticular MOFs and Their Application in Methane Storage. *Science* **2002**, *295* (5554), 469–472. https://doi.org/10.1126/science.1067208.

(207) Ming, Y.; Purewal, J.; Yang, J.; Xu, C.; Soltis, R.; Warner, J.; Veenstra, M.; Gaab, M.; Müller, U.; Siegel, D. J. Kinetic Stability of MOF-5 in Humid Environments: Impact of Powder Densification, Humidity Level, and Exposure Time. *Langmuir* **2015**, *31* (17), 4988–4995. https://doi.org/10.1021/acs.langmuir.5b00833.

(208) Deng, H.; Grunder, S.; Cordova, K. E.; Valente, C.; Furukawa, H.; Hmadeh, M.; Gandara, F.; Whalley, A. C.; Liu, Z.; Asahina, S.; et al. Large-Pore Apertures in a Series of Metal-Organic Frameworks. *Science* **2012**, *336* (6084), 1018–1023. https://doi.org/10.1126/science.1220131.

(209) Horcajada, P.; Chevreau, H.; Heurtaux, D.; Benyettou, F.; Salles, F.; Devic, T.; Garcia-Marquez, A.; Yu, C.; Lavrard, H.; Dutson, C. L.; et al. Extended and Functionalized Porous Iron(Iii) Tri- or Dicarboxylates with MIL-100/101 Topologies. *Chemical Communications* **2014**, *50* (52), 6872. https://doi.org/10.1039/c4cc02175d.

(210) Feng, D.; Liu, T.-F.; Su, J.; Bosch, M.; Wei, Z.; Wan, W.; Yuan, D.; Chen, Y.-P.; Wang, X.; Wang, K.; et al. Stable Metal-Organic Frameworks Containing Single-Molecule Traps for Enzyme Encapsulation. *Nature Communications* **2015**, *6*, 5979. https://doi.org/10.1038/ncomms6979.

(211) Ameloot, R.; Vermoortele, F.; Vanhove, W.; Roeffaers, M. B. J.; Sels, B. F.; De Vos, D. E. Interfacial Synthesis of Hollow Metal–Organic Framework Capsules Demonstrating Selective Permeability. *Nature Chemistry* **2011**, *3* (5), 382–387. https://doi.org/10.1038/nchem.1026.

(212) Jeong, G.-Y.; Ricco, R.; Liang, K.; Ludwig, J.; Kim, J.-O.; Falcaro, P.; Kim, D.-P. Bioactive MIL-88A Framework Hollow Spheres via Interfacial Reaction In-Droplet Microfluidics for Enzyme and Nanoparticle Encapsulation. *Chemistry of Materials* **2015**, *27* (23), 7903–7909. https://doi.org/10.1021/acs.chemmater.5b02847.

(213) Lupica-Spagnolo, L.; Ward, D. J.; Marie, J.-J.; Lymperoboulou, S.; Bradshaw, D. Pollen-like ZIF-8 Colloidosomes via Emulsion Templating and Etching. *Chemical Communications* **2018**, *54*, 8506–8509. https://doi.org/10.1039/C8CC03511C.

(214) Yuan, S.; Zou, L.; Qin, J.-S.; Li, J.; Huang, L.; Feng, L.; Wang, X.; Bosch, M.; Alsalme, A.; Cagin, T.; et al. Construction of Hierarchically Porous Metal–Organic Frameworks through Linker Labilization. *Nature Communications* **2017**, *8*, 15356. https://doi.org/10.1038/ncomms15356.

(215) Choi, K. M.; Jeon, H. J.; Kang, J. K.; Yaghi, O. M. Heterogeneity within Order in Crystals of a Porous Metal–Organic Framework. *Journal of the American Chemical Society* **2011**, *133* (31), 11920–11923. https://doi.org/10.1021/ja204818q.

(216) Bradshaw, D.; El-Hankari, S.; Lupica-Spagnolo, L. Supramolecular Templating of Hierarchically Porous Metal–Organic Frameworks. *Chem. Soc. Rev.* **2014**, *43* (16), 5431–5443. https://doi.org/10.1039/C4CS00127C.

(217) Qiu, L.-G.; Xu, T.; Li, Z.-Q.; Wang, W.; Wu, Y.; Jiang, X.; Tian, X.-Y.; Zhang, L.-D. Hierarchically Micro- and Mesoporous Metal-Organic Frameworks with Tunable Porosity. *Angewandte Chemie International Edition* **2008**, *47* (49), 9487–9491. https://doi.org/10.1002/anie.200803640.

(218) Reboul, J.; Furukawa, S.; Horike, N.; Tsotsalas, M.; Hirai, K.; Uehara, H.; Kondo, M.; Louvain, N.; Sakata, O.; Kitagawa, S. Mesoscopic Architectures of Porous Coordination Polymers Fabricated by Pseudomorphic Replication. *Nature Materials* **2012**, *11* (8), 717–723. https://doi.org/10.1038/nmat3359.

(219) Kang, I. J.; Khan, N. A.; Haque, E.; Jhung, S. H. Chemical and Thermal Stability of Isotypic Metal-Organic Frameworks: Effect of Metal Ions. *Chemistry - A European Journal* **2011**, *17* (23), 6437–6442. https://doi.org/10.1002/chem.201100316.

(220) Howarth, A. J.; Liu, Y.; Li, P.; Li, Z.; Wang, T. C.; Hupp, J. T.; Farha, O. K. Chemical, Thermal and Mechanical Stabilities of Metal–Organic Frameworks. *Nature Reviews Materials* **2016**, *1* (3). https://doi.org/10.1038/natrevmats.2015.18.

(221) Burtch, N. C.; Jasuja, H.; Walton, K. S. Water Stability and Adsorption in Metal–Organic Frameworks. *Chemical Reviews* **2014**, *114* (20), 10575–10612. https://doi.org/10.1021/cr5002589.

(222) Low, J. J.; Benin, A. I.; Jakubczak, P.; Abrahamian, J. F.; Faheem, S. A.; Willis, R. R. Virtual High Throughput Screening Confirmed Experimentally: Porous Coordination Polymer Hydration. *Journal of the American Chemical Society* **2009**, *131* (43), 15834–15842. https://doi.org/10.1021/ja9061344.

(223) Lincoln, S. Mechanistic Studies of Metal Aqua Ions: A Semi-Historical Perspective. *Helvetica Chimica Acta* **2005**, *88* (3), 523–545. https://doi.org/10.1002/hlca.200590036.

(224) Burns, R. G. Crystal Field Effects in Chromium and Its Partitioning in the Mantle. *Geochimica et Cosmocimica Acta* **1975**, *39*, 857–864.

(225) He, Y.; Zhou, W.; Qian, G.; Chen, B. Methane Storage in Metal–Organic Frameworks. *Chem. Soc. Rev.* **2014**, *43* (16), 5657–5678. https://doi.org/10.1039/C4CS00032C.

(226) Barea, E.; Montoro, C.; Navarro, J. A. R. Toxic Gas Removal – Metal–Organic Frameworks for the Capture and Degradation of Toxic Gases and Vapours. *Chem. Soc. Rev.* **2014**, *43* (16), 5419–5430. https://doi.org/10.1039/C3CS60475F.

(227) Dedecker, K.; Pillai, R. S.; Nouar, F.; Pires, J.; Steunou, N.; Dumas, E.; Maurin, G.; Serre, C.; Pinto, M. L. Metal-Organic Frameworks for Cultural Heritage Preservation: The Case of Acetic Acid Removal. *ACS Applied Materials & Interfaces* **2018**, *10* (16), 13886–13894. https://doi.org/10.1021/acsami.8b02930.

(228) Horcajada, P.; Gref, R.; Baati, T.; Allan, P. K.; Maurin, G.; Couvreur, P.; Férey, G.; Morris, R. E.; Serre, C. Metal–Organic Frameworks in Biomedicine. *Chemical Reviews* **2012**, *112* (2), 1232–1268. https://doi.org/10.1021/cr200256v.

(229) Dhakshinamoorthy, A.; Garcia, H. Metal–Organic Frameworks as Solid Catalysts for the Synthesis of Nitrogen-Containing Heterocycles. *Chem. Soc. Rev.* **2014**, *43* (16), 5750–5765. https://doi.org/10.1039/C3CS60442J.

(230) Sene, S.; Marcos-Almaraz, M. T.; Menguy, N.; Scola, J.; Volatron, J.; Rouland, R.; Grenèche, J.-M.; Miraux, S.; Menet, C.; Guillou, N.; et al. Maghemite-NanoMIL-100(Fe) Bimodal Nanovector as a Platform for Image-Guided Therapy. *Chem* **2017**, *3* (2), 303–322. https://doi.org/10.1016/j.chempr.2017.06.007.

(231) Zhu, Q.-L.; Xu, Q. Metal–Organic Framework Composites. *Chem. Soc. Rev.* **2014**, *43* (16), 5468–5512. https://doi.org/10.1039/C3CS60472A.

(232) Stassen, I.; Burtch, N.; Talin, A.; Falcaro, P.; Allendorf, M.; Ameloot, R. An Updated Roadmap for the Integration of Metal–Organic Frameworks with Electronic Devices and Chemical Sensors. *Chemical Society Reviews* **2017**, *46* (11), 3185–3241. https://doi.org/10.1039/C7CS00122C.

(233) Ramaswamy, P.; Wong, N. E.; Shimizu, G. K. H. MOFs as Proton Conductors – Challenges and Opportunities. *Chem. Soc. Rev.* **2014**, *43* (16), 5913–5932. https://doi.org/10.1039/C4CS00093E.

(234) Lian, X.; Fang, Y.; Joseph, E.; Wang, Q.; Li, J.; Banerjee, S.; Lollar, C.; Wang, X.; Zhou, H.-C. Enzyme–MOF (Metal–Organic Framework) Composites. *Chemical Society Reviews* **2017**, *46* (11), 3386–3401. https://doi.org/10.1039/C7CS00058H.

(235) Li, P.; Modica, J. A.; Howarth, A. J.; Vargas L., E.; Moghadam, P. Z.; Snurr, R. Q.; Mrksich, M.; Hupp, J. T.; Farha, O. K. Toward Design Rules for Enzyme Immobilization in Hierarchical Mesoporous Metal-Organic Frameworks. *Chem* **2016**, *1* (1), 154–169. https://doi.org/10.1016/j.chempr.2016.05.001.

(236) Li, P.; Chen, Q.; Wang, T. C.; Vermeulen, N. A.; Mehdi, B. L.; Dohnalkova, A.; Browning, N. D.; Shen, D.; Anderson, R.; Gómez-Gualdrón, D. A.; et al. Hierarchically Engineered Mesoporous Metal-Organic Frameworks toward Cell-Free Immobilized Enzyme Systems. *Chem* **2018**, *4* (5), 1022–1034. https://doi.org/10.1016/j.chempr.2018.03.001.

(237) Lian, X.; Chen, Y.-P.; Liu, T.-F.; Zhou, H.-C. Coupling Two Enzymes into a Tandem Nanoreactor Utilizing a Hierarchically Structured MOF. *Chemical Science* **2016**, *7* (12), 6969–6973. https://doi.org/10.1039/C6SC01438K.

(238) Li, P.; Moon, S.-Y.; Guelta, M. A.; Lin, L.; Gómez-Gualdrón, D. A.; Snurr, R. Q.; Harvey, S. P.; Hupp, J. T.; Farha, O. K. Nanosizing a Metal–Organic Framework Enzyme Carrier for Accelerating Nerve Agent Hydrolysis. *ACS Nano* **2016**, *10* (10), 9174–9182. https://doi.org/10.1021/acsnano.6b04996.

(239) Lian, X.; Erazo-Oliveras, A.; Pellois, J.-P.; Zhou, H.-C. High Efficiency and Long-Term Intracellular Activity of an Enzymatic Nanofactory Based on Metal-Organic Frameworks. *Nature Communications* **2017**, *8* (1). https://doi.org/10.1038/s41467-017-02103-0.

(240) Lian, X.; Huang, Y.; Zhu, Y.; Fang, Y.; Zhao, R.; Joseph, E.; Li, J.; Pellois, J.-P.; Zhou, H.-C. Enzyme-MOF Nanoreactor Activates Nontoxic Paracetamol for Cancer Therapy. *Angewandte Chemie International Edition* **2018**, *57* (20), 5725–5730. https://doi.org/10.1002/anie.201801378.

(241) Liang, K.; Ricco, R.; Doherty, C. M.; Styles, M. J.; Bell, S.; Kirby, N.; Mudie, S.; Haylock, D.; Hill, A. J.; Doonan, C. J.; et al. Biomimetic Mineralization of Metal-Organic Frameworks as Protective Coatings for Biomacromolecules. *Nature Communications* **2015**, *6*, 7240. https://doi.org/10.1038/ncomms8240.

(242) Wu, X.; Yang, C.; Ge, J. Green Synthesis of Enzyme/Metal-Organic Framework Composites with High Stability in Protein Denaturing Solvents. *Bioresources and Bioprocessing* **2017**, *4* (1). https://doi.org/10.1186/s40643-017-0154-8.

(243) Zhang, Q.; Zhang, L.; Dai, H.; Li, Z.; Fu, Y.; Li, Y. Biomineralization-Mimetic Preparation of Robust Metal-Organic Frameworks Biocomposites Film with High Enzyme Load for Electrochemical Biosensing. *Journal of Electroanalytical Chemistry* **2018**, *823*, 40–46. https://doi.org/10.1016/j.jelechem.2018.04.015.

(244) Nadar, S. S.; Rathod, V. K. Encapsulation of Lipase within Metal-Organic Framework (MOF) with Enhanced Activity Intensified under Ultrasound. *Enzyme and Microbial Technology* **2018**, *108*, 11–20. https://doi.org/10.1016/j.enzmictec.2017.08.008.

(245) Nadar, S. S.; Rathod, V. K. Facile Synthesis of Glucoamylase Embedded Metal-Organic Frameworks (Glucoamylase-MOF) with Enhanced Stability. *International Journal of Biological Macromolecules* **2017**, *95*, 511–519. https://doi.org/10.1016/j.ijbiomac.2016.11.084.

(246) Li, S.; Dharmarwardana, M.; Welch, R. P.; Benjamin, C. E.; Shamir, A. M.; Nielsen, S. O.; Gassensmith, J. J. Investigation of Controlled Growth of Metal–Organic Frameworks on Anisotropic Virus Particles. *ACS Applied Materials & Interfaces* **2018**, *10* (21), 18161–18169. https://doi.org/10.1021/acsami.8b01369.

(247) Liang, K.; Richardson, J. J.; Doonan, C. J.; Mulet, X.; Ju, Y.; Cui, J.; Caruso, F.; Falcaro, P. An Enzyme-Coated Metal-Organic Framework Shell for Synthetically Adaptive Cell Survival. *Angewandte Chemie* **2017**, *129* (29), 8630–8635. https://doi.org/10.1002/ange.201704120.

(248) Liang, W.; Ricco, R.; Maddigan, N. K.; Dickinson, R. P.; Xu, H.; Li, Q.; Sumby, C. J.; Bell, S. G.; Falcaro, P.; Doonan, C. J. Control of Structure Topology and Spatial Distribution of Biomacromolecules in Protein@ZIF-8 Biocomposites. *Chemistry of Materials* **2018**, *30* (3), 1069–1077. https://doi.org/10.1021/acs.chemmater.7b04977.

(249) Maddigan, N. K.; Tarzia, A.; Huang, D. M.; Sumby, C. J.; Bell, S. G.; Falcaro, P.; Doonan, C. J. Protein Surface Functionalisation as a General Strategy for Facilitating Biomimetic Mineralisation of ZIF-8. *Chem. Sci.* **2018**, *9*, 4217–4223. https://doi.org/10.1039/C8SC00825F.

(250) Wang, Q.; Zhang, X.; Huang, L.; Zhang, Z.; Dong, S. GOx@ZIF-8(NiPd) Nanoflower: An Artificial Enzyme System for Tandem Catalysis. *Angewandte Chemie International Edition* **2017**, *56* (50), 16082–16085. https://doi.org/10.1002/anie.201710418.

(251) Guesh, K.; Caiuby, C. A. D.; Mayoral, Á.; Díaz-García, M.; Díaz, I.; Sanchez-Sanchez, M. Sustainable Preparation of MIL-100(Fe) and Its Photocatalytic Behavior in the Degradation of Methyl Orange in Water. *Crystal Growth & Design* **2017**, *17* (4), 1806–1813. https://doi.org/10.1021/acs.cgd.6b01776.

(252) Gascón, V.; Carucci, C.; Jiménez, M. B.; Blanco, R. M.; Sánchez-Sánchez, M.; Magner, E. Rapid In Situ Immobilization of Enzymes in Metal-Organic Framework Supports under Mild Conditions. *ChemCatChem* **2017**, *9* (7), 1182–1186. https://doi.org/10.1002/cctc.201601342.

(253) Gascón, V.; Castro-Miguel, E.; Díaz-García, M.; Blanco, R. M.; Sanchez-Sanchez, M. *In Situ* and Post-Synthesis Immobilization of Enzymes on Nanocrystalline MOF Platforms to Yield Active Biocatalysts: *In Situ* and Post-Synthesis Immobilization of Enzymes on Nanocrystalline MOFs. *Journal of Chemical Technology & Biotechnology* **2017**, *92* (10), 2583–2593. https://doi.org/10.1002/jctb.5274.

Chapter 2

Cage Inclusion of MP8 into Mesoporous MOFs

Table of Contents

Introduction

This chapter deals with the cage inclusion of the mini-enzyme MP8 into mesoporous MOFs. The cage inclusion, as already discussed, involves the entrapment of small enzyme molecules inside the pores of preformed mesoporous MOFs. Consequently, the size of the selected enzymes must be compatible with the pore openings (windows) and pore dimensions of the MOF. However, as already reported, it is possible to entrap enzyme molecules of slightly larger size compared to the pore dimensions, as enzymes are not rigid molecules and can undergo partial unfolding that allows them to migrate inside the pores.[1] Moreover, in order to limit the diffusional issues of immobilized enzymes, the presence of cavities, that are too small to host the enzymes is considered critical. These cavities can serve for the diffusion of substrates to and from the enzymes. In addition to the structural characteristics of the selected MOFs, another important parameter is their chemical stability and more specifically the water stability that is crucial for both the immobilization procedure and the biocatalytic applications. We thus focused our efforts on the investigation of different mesoporous MOFs for the cage inclusion of MP8. The small size of MP8 (< 3.3 × 1.1 × 1.7 nm) is ideal for this procedure. The cage inclusion approach was preferred, as the 3D confinement has already been shown to enhance the stability and the protection of immobilized enzymes and it may be assumed that this encapsulation can protect MP8 against high concentrations of H_2O_2 and acidic environments. Moreover, the isolation of MP8 molecules inside the pores of mesoporous MOFs can limit its aggregation and possibly enhance its selectivity.

Among the reported mesoporous MOFs, ultra-large frameworks like PCN-333 have attracted much attention for the immobilization of enzymes.[2] Hence, the first part of this chapter deals with PCN-333(Al) and with the attempts to optimize its synthesis and obtain reproducible results. The investigation on the stability of PCN-333(Al) in water will finally result in excluding this MOF as a matrix for the immobilization. The second part deals with the use of the ultra-stable mesoporous MOFs as enzymatic supports. More specifically, MIL-101(Cr) will be investigated for the immobilization of MP8. The study of the MP8@MIL-101(Cr) biocatalyst is presented in a format of an article, recently published.

A. Mesoporous MOFs

PCN-333(Al)

1. Description

The first candidate for this work was the mesoporous PCN-333(Al) (Porous Coordination Network), which has an extended MIL-100 structure, with an MTN topology (Mobil Thirty-Nine). PCN-333 is constructed by the assembly of μ_3-oxo trimers (M^{3+}= Fe, Al, Sc) and the tri-topic ligand 4,4',4''-s-triazine-2,4,6-triyl-tribenzoic acid (TATB), giving rise to a framework with two mesoporous cages of 42 and 55 Å in diameter (Figure 2-1).[2] Contrary to many extended MOFs, PCN-333(Al) has been reported to have a very stable structure in aqueous solutions and in a large pH range (pH 3 and pH 9). This was attributed to the symmetry and the nature of the ligand. TATB as a free anion has an idealized D_{3h} symmetry, due to its planarity. When incorporated into the framework of PCN-333, the symmetry of TATB is reduced to C_{3v}, due to a bowl-shaped bending. Nevertheless, the six oxygen atoms reside in the same plane, thanks to the presence of the triazine ring that give rise to a stable super tetrahedron (Figure 2-2).[3] This could possibly explain the difference in the stability of PCN-333 and the extended form of MIL-100, with the ligand 1,3,5-benzenetribenzoic acid (BTB) (named MIL-100-BTB).[4] With BTB a co-planar symmetry is energetically disfavored due to the repulsions between the H atoms of the central benzene ring and the three peripheral rings,[3] which leads to the fast degradation of the structure in aqueous solutions.[4]

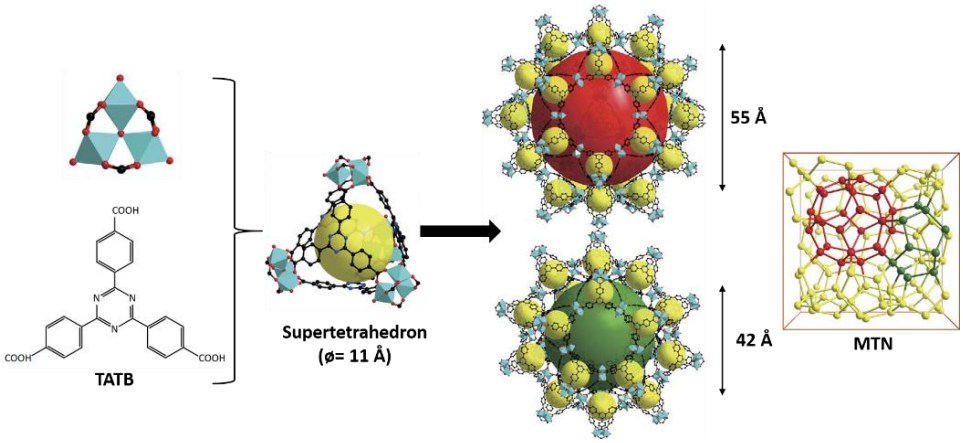

Figure 2-1: Schematic illustration of the construction of PCN-333 framework, with MTN topology. The combination of μ_3-oxo trimers with the ligand TATB forms super tetrahedra (STs) of 11 Å in diameter. The self-assembly of the STs gives rise to two mesoporous cages of 42 and 55 Å. Adapted from[2]

PCN-333(Al) has successfully been used for the inclusion of HRP, Cyt c and MP11 that all showed enhanced activities in organic solvents and good recyclability.[2] Accordingly, the ultra-large pores of PCN-333(Al) should permit high MP8 loadings, while the presence of two different cavities could allow the design of bi-enzymatic systems (*e.g.* co-immobilization of GOx). These results along with the reported water stability of PCN-333(Al), encouraged us to study this ultra-mesoporous MOF for the cage inclusion of MP8.

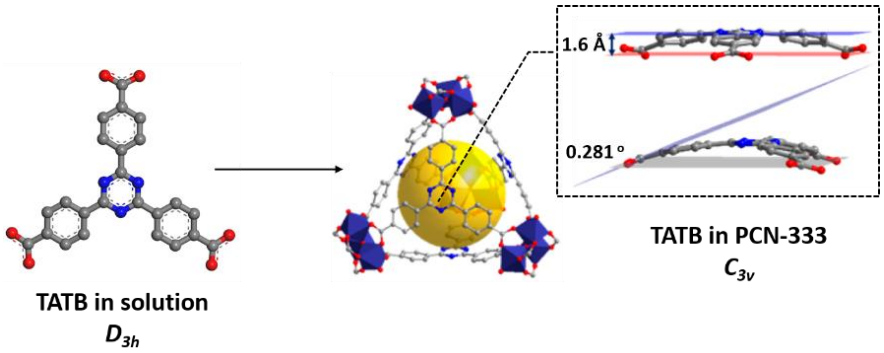

Figure 2-2: Symmetries of TATB in solution (D_{3h}) and in PCN-333 with a bend geometry (C_{3v}). Adapted from[3]

2. Synthesis and characterization of PCN-333(Al)

The synthesis of PCN-333(Al) was initially carried out according to the already reported procedure.[2] We first proceeded with the synthesis of the TATB ligand, as it is not commercially available, and then continued with the synthesis of the MOF. Due to reproducibility issues, a modified synthesis of PCN-333(Al) was finally used, as well as an optimized synthesis pathway for the ligand.

TATB synthesis

The two-step procedure for the synthesis of TATB is illustrated in Figure 2-3. It was obtained following an already reported synthesis that was slightly modified in order to obtain the pure ligand.[2,3] At first, to a 100 mL three-necked flask 27 g of $AlCl_3$ were dissolved in 50 mL dry toluene and heated at 60 °C. 8.3 g of 2,4,6-trichloro-1,3,5-triazine were added in the mixture portionwise over 1 h. The mixture was left overnight under stirring at 60 °C. The resulting reddish sticky oil was poured into 100 mL of ice-cooled distilled water to stop the catalytic activity of $AlCl_3$ and was extracted with $CHCl_3$ (~ 300 mL for 3 extractions). After removing the solvent under reduced pressure, the crude product was dissolved in a CH_2Cl_2/EtOH mixture (100 mL) and was allowed to recrystallize for 1 week. MeOH that was initially reported as a solvent to dissolve the crude product was replaced by CH_2Cl_2/EtOH that allowed both a better dissolution and a better separation from the unreacted precursors. The recrystallization step needed to be performed one more time in order to obtain white crystals of the 2,4,6-tri-p-tolyl-1,3,5-triazine product (~5 g, yield: 32 %).

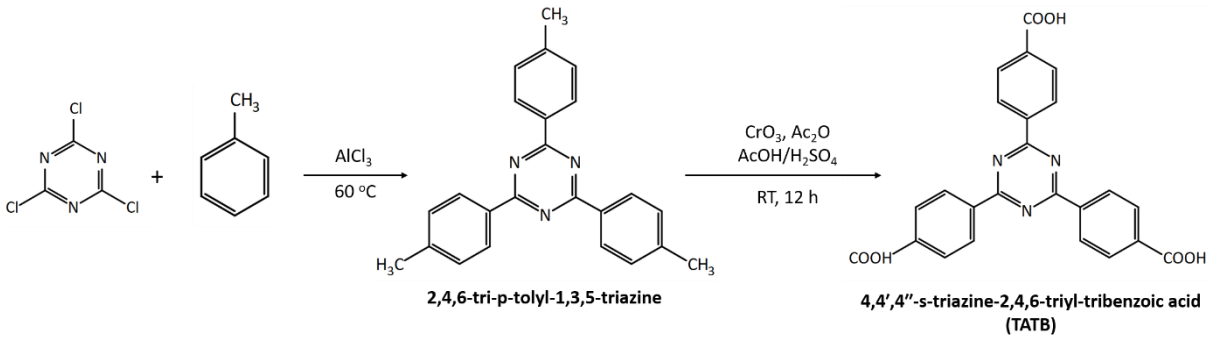

Figure 2-3: Schematic illustration of the two-step synthesis of the ligand TATB.

In the next step, in a 500 mL three-necked flask, 1.5 g of 2,4,6-tri-p-tolyl-1,3,5-triazine were dissolved in 35 mL concentrated acetic acid (AcOH) and 2.2 mL concentrated H_2SO_4 were then added. A solution of 3.6 g CrO_3 in 5 mL of acetic anhydride (Ac_2O) was then added dropwise (exothermic reaction) to the reaction flask that was placed into an ice bath. After 1 h, the ice bath was removed and the mixture was allowed to stir overnight at RT. The resulting dark-green slurry was poured into 125 mL of cold water and stirred for 1 h, in order to remove the excess of chromic acid. The product was separated by centrifugation and washed three more times with water. The light green solid was dissolved in 100 mL NaOH (2 M) and was filtrated to remove the unreacted 2,4,6-tri-p-tolyl-1,3,5-triazine. Finally, the solution was acidified to pH 1 with 6 M HCl, in order to precipitate the white TATB product. Recrystallization in DMF (2 weeks) resulted in pure white crystals of TATB (~1.5 g, yield: 80 %).

The purity of the products was confirmed by ^{1}H NMR spectroscopy. Figure 2-4 shows the ^{1}H NMR spectrum of the 2,4,6-tri-p-tolyl-1,3,5-triazine precursor in $CDCl_3$. The single peak at 2.5 ppm was assigned to the 9 equivalent protons of the methyl groups and the two doublets (6 protons each) were assigned to the ortho and meta protons of the phenyl rings. The ^{1}H NMR spectrum of the TATB ligand in DMSO-d_6 is shown in Figure 2-5. The two doublets were assigned to the ortho and meta protons (6 equivalent per position) of the phenyl rings.

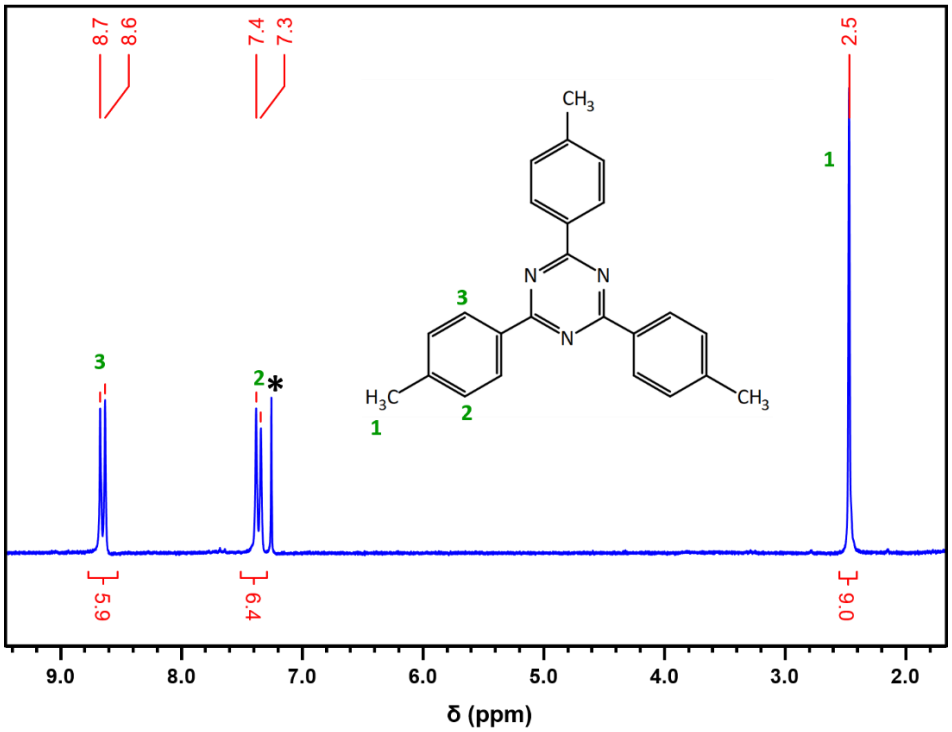

Figure 2-4: ^{1}H NMR spectrum of 2,4,6-tri-tolyl-1,3,5-triazine in $CDCl_3$*.

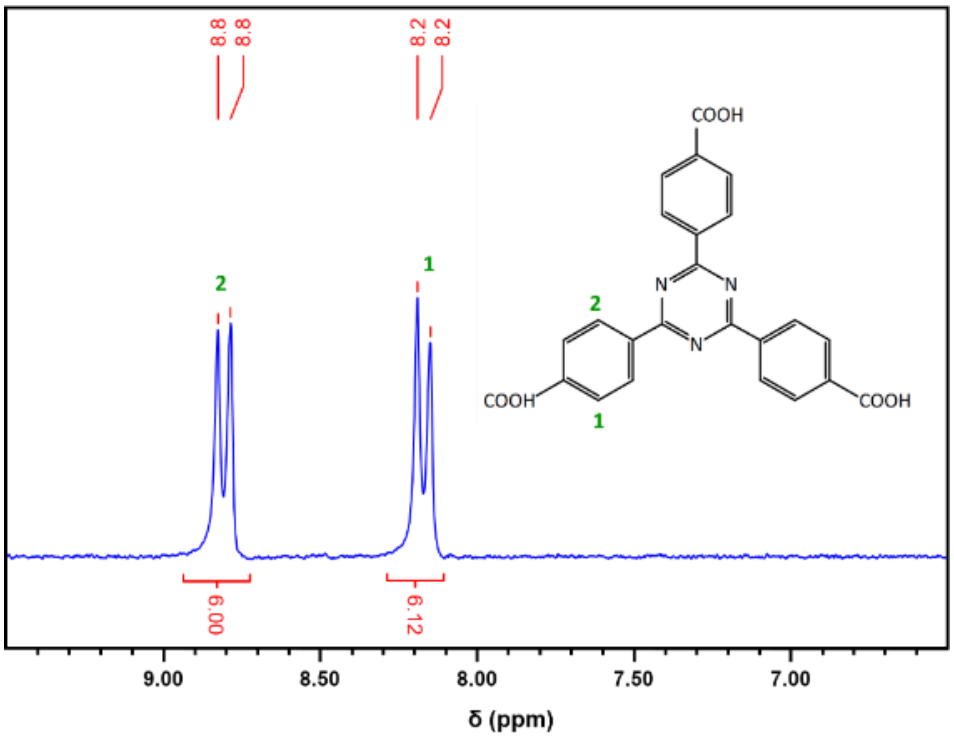

Figure 2-5: ^{1}H NMR spectrum of TATB in DMSO-d_6.

PCN-333(Al) synthesis

PCN-33(Al) (formula: $[Al_3O(OH)(H_2O)_2(TATB)_2]$) was synthesized under solvothermal conditions, by dissolving 50 mg TATB (0.1 mmol) and 120 mg $AlCl_3{\cdot}6H_2O$ (0.5 mmol) in 10 mL DEF (*N,N*-Diethylformamide). 1 mL trifluoroacetic acid (TFA) was added to the mixture (acidic modulator) and the autoclave was sealed and placed in an oven at 135 °C for 48 h. The resulting white solid was centrifuged and then washed several times with DMF. PCN-333(Al) was stored in DMF.[2]

While the reported procedure by Feng et *al.*, resulted in pure products with good crystallinity, the reaction was not reproducible. It was found that pre-heating the oven was a key parameter for the crystallization of PCN-333(Al). Due to these reproducibility issues, the synthesis was optimized, using the conditions reported for the extended MIL-100 series.[4] The use of the acidic modulator, trifluoroacetic acid, was avoided because even though it can enhance the crystallinity of the framework, it is rather toxic. Finally, the modified synthesis was slightly scaled-up compared to the reported one, which allowed the formation of higher amounts of PCN-333(Al).

The modified solvothermal synthesis involved the mixing of 308 mg TATB (0.7 mmol) with 241 mg $AlCl_3{\cdot}6H_2O$ (1 mmol) in 4 mL DMF. The reaction mixture was heated at 100 °C for 10 h, with a temperature ramp of 1 h. The white solid was centrifuged and washed several times with DMF, until it was finally stored in DMF.

Characterization of PCN-333(Al)

The PCN-333(Al) products obtained by the two different synthetic routes were characterized by powder X-ray diffraction (PXRD), infrared spectroscopy (FT-IR), thermogravimetric analysis (TGA) and nitrogen porosimetry.

Figure 2-6 shows the PXRD pattern of the PCN-333(Al) product, obtained using the modified synthesis, compared to that reported by Feng et *al.*[2] and to the calculated pattern of PCN-333(Al). The modified route resulted in a PCN-333(Al) framework with a lower crystallinity, which could be possibly assigned to the absence of trifluoroacetic acid during of the synthesis or to a lower particle size. No SEM analysis of the sample, that would have allowed the validation of the second hypothesis, was performed. Nonetheless, both patterns match the calculated pattern of PCN-333(Al).

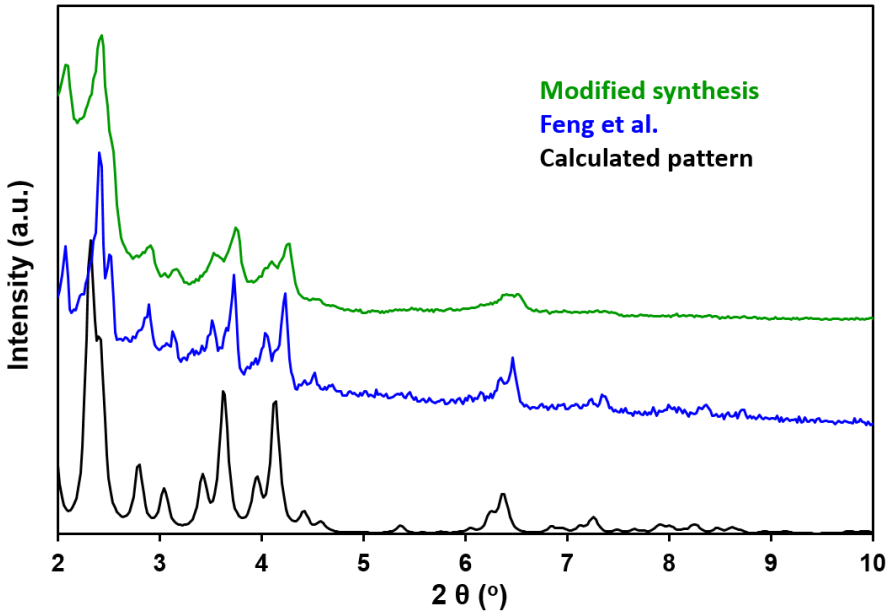

Figure 2-6: Normalized PXRD patterns of the PCN-333(Al) products obtained with the two different synthetic routes; Feng et *al.* synthesis (blue) and the modified synthesis (green), compared with the calculated patterns.

The FT-IR spectra of the two PCN-333(Al) products and of the free TATB are shown in Figure 2-7. A small band at 1700 cm^{-1} is present in the spectra of both products. It is characteristic of a ν(C=O) stretching mode that could be assigned to traces of unreacted ligand molecules or to DMF molecules in the pores of the MOFs. The complexation of the ligand to the metal center is confirmed by the presence of two new bands: the asymmetric $\nu(C\text{-}O)_{as}$=1600 cm^{-1} and the symmetric $\nu(C\text{-}O)_{s}$=1430 cm^{-1} stretching modes. Other vibration bands, characteristic of the free TATB, the ν(C-O)=1350 cm^{-1} stretching mode and the ν(C-O)=1280 cm^{-1} bending mode were not observed in the spectrum of PCN-333(Al)).

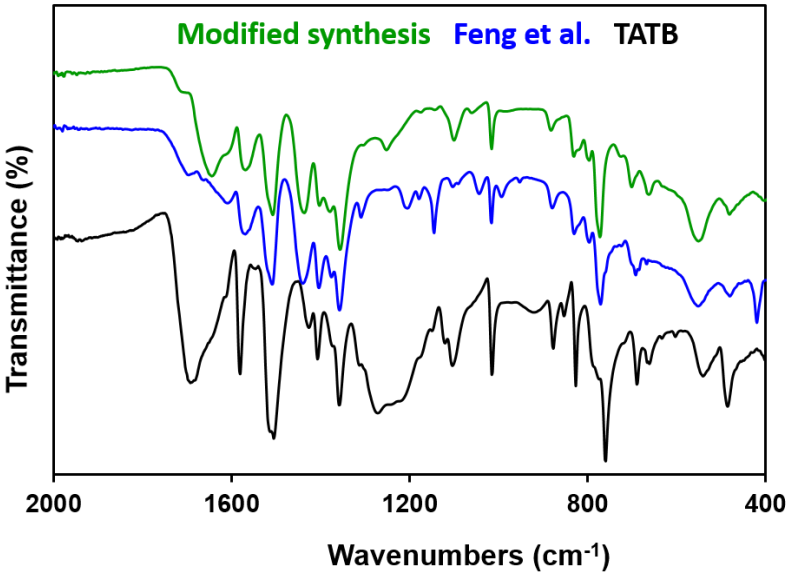

Figure 2-7: FT-IR spectra of the free TATB (black) and the two PCN-333(Al) products; Feng et *al.* (blue) and modified synthesis (green).

The TGA curves for the two PCN-333(Al) products are shown in Figure 2-8. The first weight loss (≤ 100 °C) that corresponds to the removal of adsorbed solvent molecules is almost negligible for both products. The second weight loss that is observed after 100 °C and continues up to 350 °C corresponds to the release of coordinated solvent molecules, as well as solvent molecules and free ligand molecules entrapped in the pores. The degradation of the ligand and thus the destruction of the structure is observed for both cases at around 450 °C, leaving a final Al_2O_3 residue. The table in Figure 2-8 shows the percentages of the ligand and metal oxide of the two products, without taking into account the water molecules or impurities on the frameworks. The experimental values indicate traces of metal oxide impurities in both products, which are however close to the calculated values. The calculated values were extracted by the formula: $Al_3OH(H_2O)_3O(TATB)_2$.

Finally, the material prepared following the modified procedure was characterized by N_2 porosimetry whereas the sorption measurement could not be performed with the sample prepared by the Feng et *al.* procedure, due to the very low amounts of product obtained (< 10 mg). As seen in Figure 2-9, under the reported activation conditions (150 °C/24 h, under secondary vacuum), a very low BET surface area was obtained (659 m^2/g), compared to the reported one (4000 m^2/g).

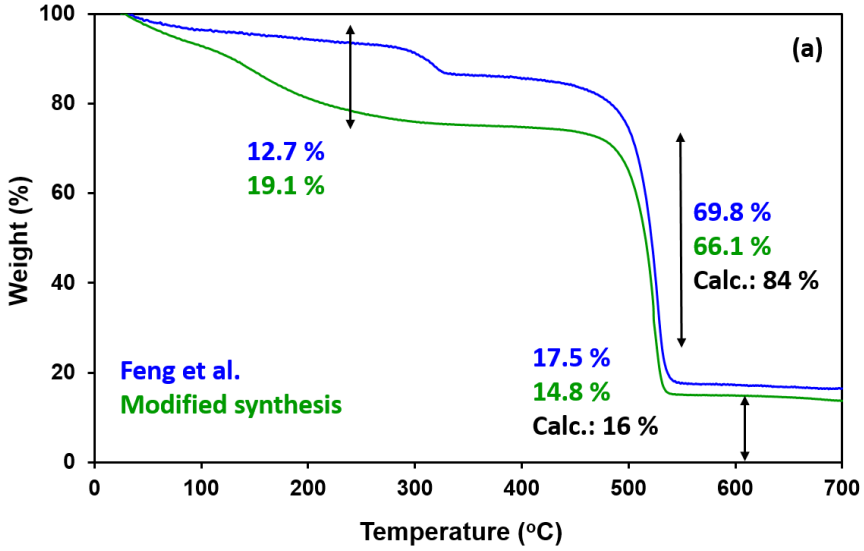

(b)

Normalized values (no solvent/impurities)	Ligand (%)	Al_2O_3 (%)
Calculated	84	16
Feng et al.	80	20
Modified synthesis	82	18

Figure 2-8: (a) TGA curves of the two PCN-333(Al) products under O_2 flow; Feng et *al.* (blue) and modified synthesis (green); (b) Table with normalized values taking into account only the percentages of the ligand and the metal oxide.

We therefore used as an alternative activation method, supercritical CO_2 drying, a method that has been extensively used to access the total internal surface area of relatively unstable structures and for MOFs whose porosity is lost after solvent removal.[5–7] Briefly, the solvent (DMF) that remains within the pores and stabilizes the MOF structure was exchanged with dry EtOH, which is miscible with CO_2. The EtOH-exchanged powder was then placed in a chamber and the dry EtOH was exchanged with liquid CO_2 for a period of 5 h. After the complete CO_2 exchange, the sample was sealed in the chamber and the temperature was raised to 40 °C, causing the increase of the pressure at around 88.4 atm, above the CO_2 critical point (T = 31 °C; P = 73 atm),[5] and was maintained under these conditions for 1 h. Finally, the pressure of the chamber was slowly decreased down to atmospheric pressure and the N_2 sorption of the sample was measured. This procedure allows a direct transition from the supercritical phase to the gaseous phase, which avoids the strong capillary forces and surface tension that are responsible for the decrease of the porosity.[7] This supercritical CO_2 activation resulted in a measured BET surface area of 2300 m^2/g, which was significantly higher than the one obtained with the conventional activation (659 m^2/g), but still much lower than the reported one (4000 m^2/g).[2]

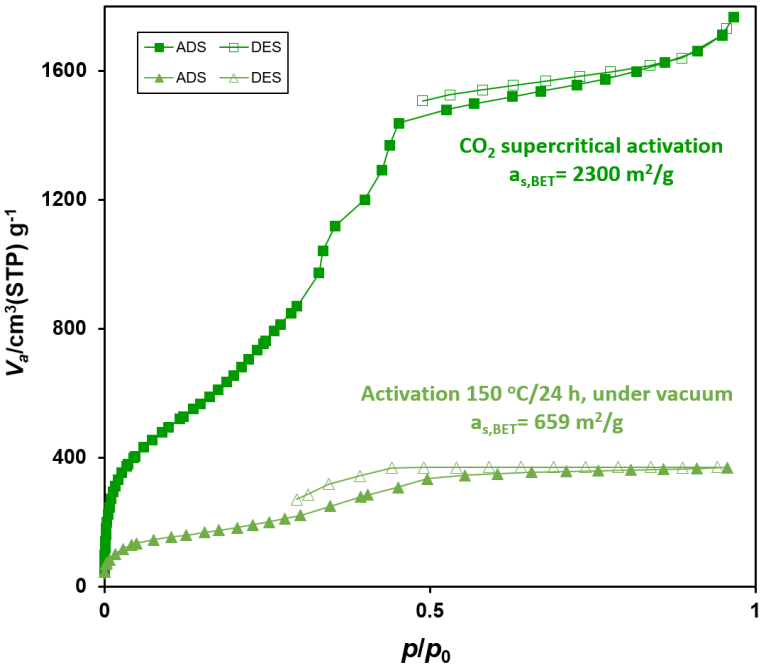

Figure 2-9: N_2 adsorption/desorption isotherms of PCN-333(Al) at 77 K; sample activation: 150 °C/24 h, under vacuum (light blue) and CO_2 supercritical activation (dark blue).

Stability of PCN-333(Al)

As discussed above, due to the nature of TATB, PCN-333(Al) was reported to have an excellent chemical stability compared to that of its MIL-100-BTB analog. Given that the presence of modulators can change the structural properties and thus the stability of MOF's frameworks,[8–10] the PCN-333(Al) obtained by the route reported by Feng et *al.* was selected for the stability tests.

A common risk of ultra-large mesoporous MOF frameworks is the decrease of the porosity after the release of solvent molecules from the pores. We thus evaluated the stability of the PCN-333(Al) framework after drying at 100 °C overnight. As seen in Figure 2-9, no change in the PXRD diagram was observed, which confirms the previously stated importance of the triazine ring for the stability of the framework. Since PCN-333(Al) was selected as a potential support for the MP8 enzyme, it was crucial to confirm its stability in water. Briefly, 3 solutions containing each 20 mg of MOF in 10 mL H_2O were prepared. The stability was monitored for 10 min, 30 min and overnight (under stirring). The powders were recovered by centrifugation, dried at 100 °C for 1 h and then analyzed by PXRD. Figure 2-10 shows the obtained PXRD patterns. After only 10 min in H_2O, the intensity of the first peaks of PCN-333(Al) decreases drastically. This is even more apparent after 30 min in H_2O. These changes in the intensity of the peaks at small angles are similar to those that have already been observed for other mesoporous MOFs, in which the pores were occupied by large amounts of guest molecules (in this case H_2O), which creates local disorder.[11] Finally, when in contact with H_2O overnight, no diffraction peaks were observed in the diagram, which may suggest that the structure of PCN-333(Al) was destroyed.

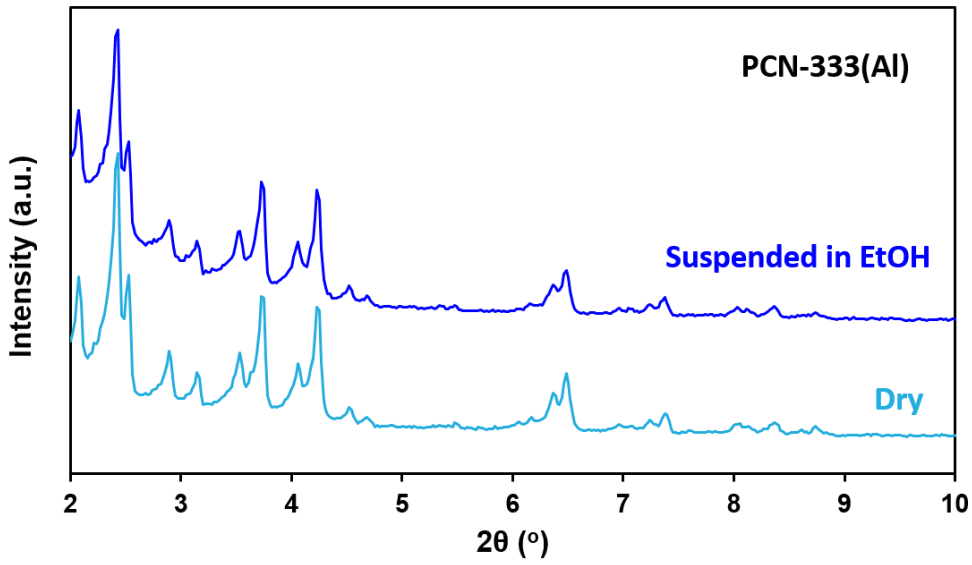

Figure 2-10: Normalized PXRD patterns of PCN-333(Al) powder suspended in EtOH and dried at 100 °C, overnight.

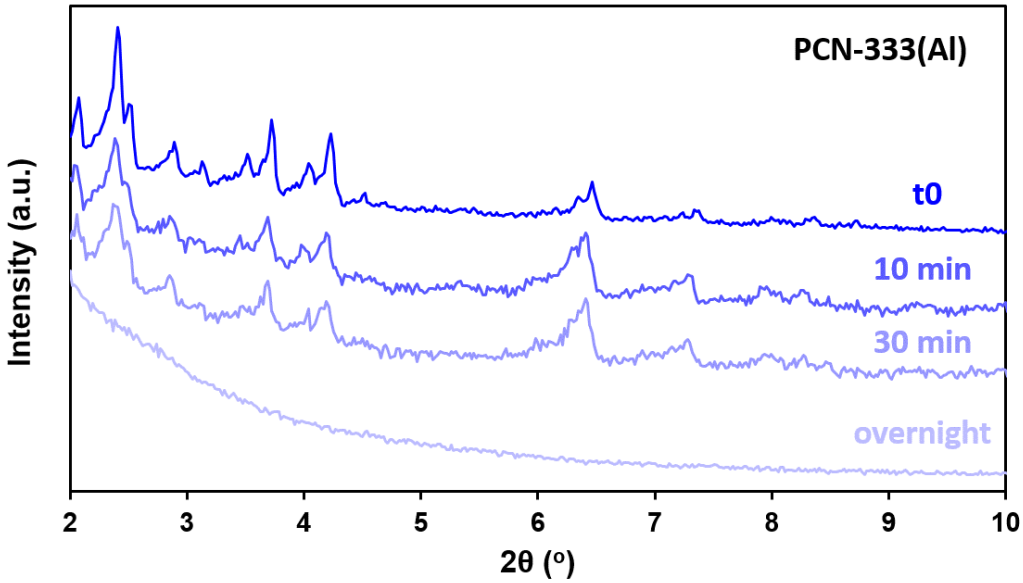

Figure 2-11: Normalized PXRD patterns of PCN-333(Al) after contact with water for different times.

PXRD data without indexing are not sufficient to suggest the progressive degradation of the PCN-333(Al) framework into an amorphous solid. Additional characterizations would be required to confirm the poor stability of PCN-333(Al), like N_2 porosimetry sorption measurements (possible decrease of porosity), SEM (textural changes of the particles), ICP analysis (concentration of Al^{3+} leached in H_2O) *etc*… However, the observed poor quality of the PXRD data (severe decrease of intensity of Bragg peaks) is not consistent with the reported stability of PCN-333(Al).[2] Moreover, this behavior in the presence of water constitutes a strong issue for the use of this material for the immobilization of the enzyme and the catalytic tests. The apparent low stability of extended PCN-333(Al) framework, along with the need for time-consuming organic synthesis for the preparation of the ligand and the use of toxic, carcinogenic and corrosive compounds (*e.g.* 2,4,6-trichloro-1,3,5-triazine and CrO_3) motivated

us to exclude this material and use instead ultra-stable mesoporous MOFs such as MIL-101 (Cr) for further studies.[11]

MIL-101(Cr)

The next candidate for the cage inclusion immobilization was MIL-101(Cr), a chromium terephthalate mesoporous MOF that shows excellent chemical and thermal stability.[11] Moreover, it is synthesized from commercially available and inexpensive reactants. Different synthetic routes have been used for the synthesis of MIL-101(Cr),[11–13] including a 5 min microwave-assisted hydrothermal synthesis (developed previously in the lab) that results in ~70 nm nanoparticles.[14] Details on the synthesis of MIL-101(Cr) as well as its use for the cage inclusion of MP8 are given in the article that follows.

Enzyme encapsulation in mesoporous Metal-Organic Frameworks for selective biodegradation of harmful dye molecules

Introduction and contributions

This work is described in the format of a research communication article, recently published in Angewandte Chemie International Edition (doi.org/10.1002/anie.201811327).

The following paper describes the cage inclusion of microperoxidase 8 in nanoparticles of MIL-101(Cr). MP8 was selected due to its exceptional, dual enzymatic activity (peroxidase-like activity and cytochrome P450-like activity) that is essential for the degradation of environmental pollutants such as the oxidative degradation of toxic organic dyes (*e.g.* methyl orange). However, MP8 suffers from several drawbacks: deterioration of the catalytic activity under acidic pH and oxidative conditions, dimerization of MP8 at concentrations above 2 µM, as well as low substrate selectivity. The objective of this work was to combine MP8 with MIL-101(Cr) in order to optimize the stability and the catalytic properties of the enzyme. The MP8 encapsulation in the mesoporous MOF led to a biocatalyst with enhanced long-term, recyclable catalytic activity under acidic or oxidative conditions. This was attributed to the isolation and confinement of MP8 inside the cavities of MIL-101(Cr), along with the excellent adsorption properties of MIL-101(Cr) that induced the selective and efficient degradation of dyes, through a charge-based pre-concentration mechanism.

In this work, most of the synthesis and characterizations of nanoMIL-101(Cr) and the composite MP8@nanoMIL-101(Cr) were performed by me. The N_2 sorption measurements were performed by Dr. A. Tissot. The SEM images were recorded by Dr. C. Livage and Dr. M. Benzaqui. The selective adsorption of dye molecules by MIL-101 materials has been studied initially by Dr. Q. Zhang. The ζ-potential measurements were performed by L. Benahmed that also helped me with the catalytic tests. The preparation, purification and characterization of MP8 were carried out by Dr. R. Ricoux and myself. The MALDI-TOF mass spectroscopy was performed by V. Guerineau. The ICP-OES measurements were carried out by F. Bourdreux. Dr. C. Sicard, Prof. N. Steunou, Prof. J.-P. Mahy, Dr. C. Serre and Dr. R. Ricoux strongly supervised the work and Dr. C. Sicard, with the help and corrections of all authors, wrote the article.

GDCh Communications Angewandte International Edition Chemie

MOFs and Enzymes Hot Paper

International Edition: DOI: 10.1002/anie.201811327
German Edition: DOI: 10.1002/ange.201811327

Enzyme Encapsulation in Mesoporous Metal–Organic Frameworks for Selective Biodegradation of Harmful Dye Molecules

Effrosyni Gkaniatsou, Clémence Sicard, Rémy Ricoux,* Linda Benahmed, Flavien Bourdreux, Qi Zhang, Christian Serre, Jean-Pierre Mahy, and Nathalie Steunou*

In memory of Gérard Férey

Abstract: *Microperoxidase-8, a small, peroxidase-type enzyme was immobilized into nanoparticles of the mesoporous and ultra-stable metal–organic framework (MOF) MIL-101(Cr). The immobilized enzyme fully retained its catalytic activity and exhibited enhanced resistance to acidic conditions. The biocatalyst was reusable and showed a long-term stability. By exploiting the properties of the MOF's framework, we demonstrated, for the first time, that the MOF matrix could act in synergy with the enzyme (Microperoxidase-8) and enhance selectivity the oxidation reaction of dyes. The oxidation rate of the harmful negatively charged dye (methyl orange) was significantly increased after enzyme immobilization, probably as a result of the pre-concentration of the methyl orange reactant owing to a charge matching between this dye and the MOF.*

Enzymes are biomolecules with remarkable catalytic properties essential for specific applications, such as production of biochemicals and biofuels, and for biosensing and bioremediation purposes.[1] Despite many advances in enzyme engineering, they remain expensive and/or fragile entities. As a result, their use in industrial context often requires their immobilization on a solid support to increase their stability and recovery. Many supports have been developed in the last decades, including, but not limited to, biopolymers/synthetic polymers, sol-gel materials, mesoporous silica, carbon materials,[2] and recently metal–organic frameworks (MOFs).[3] MOFs are a class of crystalline hybrid porous material characterized by a vast chemical functionality, exhibiting a large variety of structural features (surface area, pore size, shape, flexibility). These have sparked a great interest in many applications, such as gas storage and separation, heat transfer, biomedicine, sensing and catalysis.[4] As immobilization matrices, they seem promising since the biological activity of immobilized enzymes was preserved, even under unnatural environments (high temperature, solvent), and long-term stability was observed.[5] Among the MOF properties, their hybrid nature and multimodal porosity have appeared as key parameters for successful biocatalysis, as they allow efficient mass transfer, and eventually the co-entrapment of co-factors.[6] In few studies, the MOF matrix acted as a selective diffusion barrier of reactants by size exclusion.[3f,7] Despite these encouraging results, the role of MOF materials on the bioreactor performances has so far been mostly limited to a stabilizing host scaffold.

Microperoxidase-8 (MP8, Figure 1a), is a mini enzyme that contains a heme prosthetic group together with amino acid residues 14–21 of horse cytochrome c. This heme-octapeptide simultaneously combines two types of catalytic activities: a high peroxidase-like activity as well as a cytochrome P450-like activity.[8] However, it suffers from several limitations. Deterioration of the catalytic activity occurs both under harsh conditions (acidic pH or oxidative media) and at MP8 concentrations higher than 2 μM due to the heme dimerization.[9] Moreover, the distal coordination position of the iron atom of MP8 is completely exposed to the solvent and, thus lacks of a specific catalytic pocket, which results in low substrate selectivity.

Herein, we show that the encapsulation of MP8 in the mesoporous cages of a polycarboxylate MOF (MIL-101(Cr)) can be a valuable strategy to enhance the catalytic activity of MP8 under acidic or oxidative conditions. We also demonstrate that the MOF matrix not only performs as a protective host support able to maintain long-term, recyclable catalytic activity but can also enhance the catalytic performance of the bioreactor due to its excellent adsorption properties. Furthermore, since very large amounts of commercial dyes are produced in textile and paper industries,[10] which makes their

[*] E. Gkaniatsou, Dr. C. Sicard, L. Benahmed, F. Bourdreux, Dr. Q. Zhang, Prof. N. Steunou
Institut Lavoisier de Versailles, UVSQ, CNRS
Université Paris-Saclay
45 avenue des Etat-Unis, Versailles (France)
E-mail: clemence.sicard@uvsq.fr
Dr. R. Ricoux, Prof. J.-P. Mahy
Laboratoire de Chimie Bioorganique et Bioinorganique, Institut de Chimie Moléculaire et des Matériaux d'Orsay, UMR 8182
Université Paris Sud, Université Paris-Saclay
Orsay (France)
E-mail: remy.ricoux@u-psud.fr
Dr. C. Serre
Institut des Matériaux Poreux de Paris, FRE 2000 CNRS Ecole Normale Supérieure, Ecole Supérieure de Physique et de Chimie Industrielles de Paris, PSL research university
Paris (France)
Dr. Q. Zhang
Current address: Collaborative Innovation Center of Advanced Energy Materials, School of Materials and Energy, Guangdong University of Technology
Guangzhou 510006 (China)
Supporting information and the ORCID identification number(s) for the author(s) of this article can be found under: https://doi.org/10.1002/anie.201811327.

GDCh Communications Angewandte International Edition Chemie

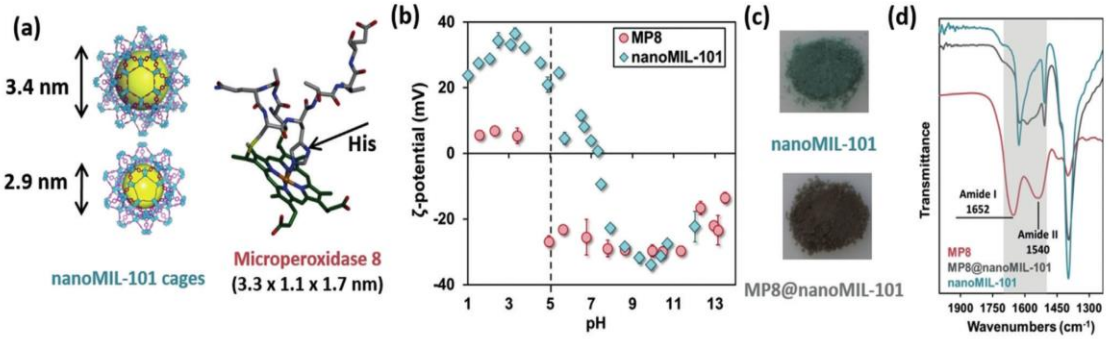

Figure 1. a) Cages of nanoMIL-101 (yellow sphere indicates cage volume) and molecular structure of microperoxidase-8 which contains an Fe^{III} porphyrin and the amino acid residues 14 to 21 of Cytochrome c; Fe orange, N blue. The imidazole group of the histidine residue (His18) acts as the fifth axial ligand of the Fe^{III} (Structure data were obtained from the solution structure of PDB: 1OCD);[13] b) ζ-potential measurements of nanoMIL-101 (blue diamonds) and MP8 (red circles) as a function of pH; c) Images of the powder of nanoMIL-101 (top) and MP8@nanoMIL-101 (bottom); d) FT-IR spectra of MP8 (red), MP8@nanoMIL-101 (grey), and nanoMIL-101 (blue).

removal crucial for environmental matters, we targeted the oxidative degradation of model organic dyes (harmful Methyl Orange). Remarkably, we demonstrated that the MOF-based matrix can supplement a higher reaction rate to the enzymatic catalytic reaction due to the selective substrate pre-concentration through a charge-based mechanism.

MP8 was obtained by the hydrolytic digestion of cytochrome c (synthesis conditions in Supporting Information and characterization of purified MP8 by MALDI-TOF mass spectrometry and UV/Vis spectroscopy in Figure S1).[11] MIL-101(Cr) was selected as an immobilization matrix due to its high chemical stability and its very large hierarchical porosity (cages of 2.9 nm and 3.4 nm),[12] compatible with MP8 size ($<3.3\times1.1\times1.7$ nm), while retaining accessible diffusion pathways for substrates, once the enzyme is immobilized. Notably, the windows to access the cages are smaller in sizes (1.2×1.6 nm and 1.2 nm), but it has previously been shown that heme-based enzymes could undergo conformational changes similar to translocation mechanisms to diffuse through smaller windows into larger voids.[14] A simple microwave assisted hydrothermal synthesis was employed (synthesis conditions in Supporting Information) to obtain nanoparticles of MIL-101(Cr)[15] and thus favour diffusion kinetics.[16] To take full advantage of the impact of the framework and provide an enhanced protection, a 3-dimensional confinement of the enzyme was preferred over a surface immobilisation. The encapsulation was accomplished by simply mixing a solution of nanoMIL-101 with a solution of MP8 for 48 h at 37 °C. To ensure strong electrostatic interactions between the MP8 molecules and the MOF particles, the pH of the mixture was adjusted to 5, where the MIL-101 nanoparticles are positively charged and MP8 negatively charged as shown in Figure 1b. The immobilized catalyst (MP8@nanoMIL-101) was washed with water to remove MP8 molecules that may have remained weakly adsorbed on the outer surface of nanoMIL-101. The presence of MP8 within the powder could be directly observed by the resulting colour change from green to brown-reddish as illustrated in Figure 1c. The MP8@nanoMIL-101 was characterized by powder X-ray diffraction (PXRD, Figure S2), showing that the crystalline structure of MIL-101(Cr) was preserved after encapsulation. The immobilization of MP8 was confirmed by the presence of characteristic vibrations bands of amide I and II in FTIR spectrum of MP8@nanoMIL-101 displayed in Figure 1d. The amount of enzyme within MP8@MIL-101 was determined to be of circa 5% w/w by inductively coupled plasma atomic emission spectroscopy (ICP-AES) based on the Fe/Cr ratio (sample preparation in Supporting Information and detailed amounts in Table S1 and S2). The same MP8 content was confirmed by energy dispersive X-ray (Table S3) and with UV/Vis spectra of the remaining MP8 quantities in the supernatant (Table S4). NanoMIL-101 and MP8@nanoMIL-101 were further characterized by nitrogen porosimetry at 77 K (Figure S3), leading to BET surface areas of 2550 m^2g^{-1} and 1510 m^2g^{-1}, respectively. This loss of surface area of about 1000 m^2g^{-1}, that is, 39%, was consistent with the presence of MP8 within the pores of the MOF. A similar content of MP8 (5% w/w, see Table S1 and S2) was also obtained when larger particles (micrometre size) of MIL-101 were considered (Figure S4), thereby suggesting that MP8 molecules were inserted within the porosity and not adsorbed at the outer surface. To further confirm the confinement of MP8 molecules inside the pores of nanoMIL-101, the accessibility of the Fe^{III} atom of MP8 was assessed by following the coordination of an imidazole molecule (ImH) to the sixth axial position of the Fe^{III} on the distal face of the heme (Figure 1a).[17] As seen in Figure S5a and S6a, with increasing imidazole concentrations, the maximum absorbance wavelength of MP8 Soret band shifts gradually from 396 nm to 404 nm, as a result of the complexation reaction of the ImH with the heme moiety of MP8, forming MP8(ImH).[18] To reach saturation of MP8(ImH) complex formation, MP8@MIL-101 reacted with almost 7 times more imidazole than the free MP8 (3.7 mM and 0.57 mM, respectively). This higher amount suggests diffusional limitations, in agreement with the inclusion of MP8 inside the porosity of nanoMIL-101. Importantly, the calculated dissociation constants of the MP8(ImH) complex were 0.37 and 0.10 mM (Figure S5b and S6b) for MP8@nanoMIL-101 and free MP8, respectively. These relatively close values

indicate that the MP8 binding sites are not altered and remain fully accessible after encapsulation.

No peroxidase activity was detected in the presence of nanoMIL-101 alone as catalyst. Both free and immobilized MP8 catalysed the oxidation of ABTS showing similar trends with increasing both reaction rates and converted ABTS amounts with increasing pH (Figure 2a and Figure S8). At pH 8, the concentration of $ABTS^{\bullet+}$ was higher for immobilized MP8@nanoMIL-101. For the free MP8, as illustrated in Figure S9, the absorbance at 420 nm of $ABTS^{\bullet+}$ reached a maximum and then decreased due to over oxidation.[19] This phenomenon was not observed in the case of MP8@nanoMIL-101, which may result from stabilization of $ABTS^{\bullet+}$ through strong interactions (coordination on the Cr metal sites) with the MOF framework, as reported before for ABTS encapsulation into an iron mesoporous polycarboxylate based MOF.[6b] At pH 6–7, free MP8 oxidized higher amounts of ABTS than immobilized MP8@nanoMIL-101. On the opposite, at pH 5 the amount of $ABTS^{\bullet+}$ was higher for immobilized MP8@nanoMIL-101. Since high concentrations of H_2O_2 and acidic conditions are known to be detrimental to MP8 catalytic peroxidase activity,[20] the protective role of the MOF matrix against such harmful conditions was further investigated by varying H_2O_2 concentration (0.1–1.8 mM), at pH 7 (Figure 2b, Figures S10 and S11) and pH 5 (Figures 2c, S12 and S13).

At pH 7, for the entire H_2O_2 range, in 300 seconds, higher amounts of ABTS were obtained with free MP8, as shown in

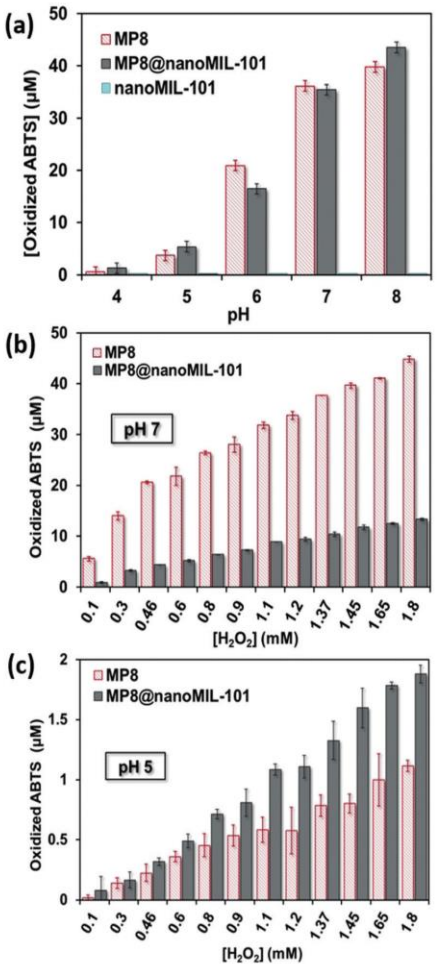

Figure 2. a) Catalytic oxidation of ABTS after 180 s as a function of pH by free MP8 (red), immobilized MP8@nanoMIL101 (grey), and nanoMIL-101 (blue); b) catalytic oxidation of ABTS after 300 s as a function of H_2O_2 at pH 7 by free MP8 (red), immobilized MP8@nanoMIL101 (grey); c) catalytic oxidation of ABTS after 300 s as a function of H_2O_2 at pH 5 by free MP8 (red), immobilized MP8@nanoMIL-101 (grey). Error bars are the standard deviation of three measurements.

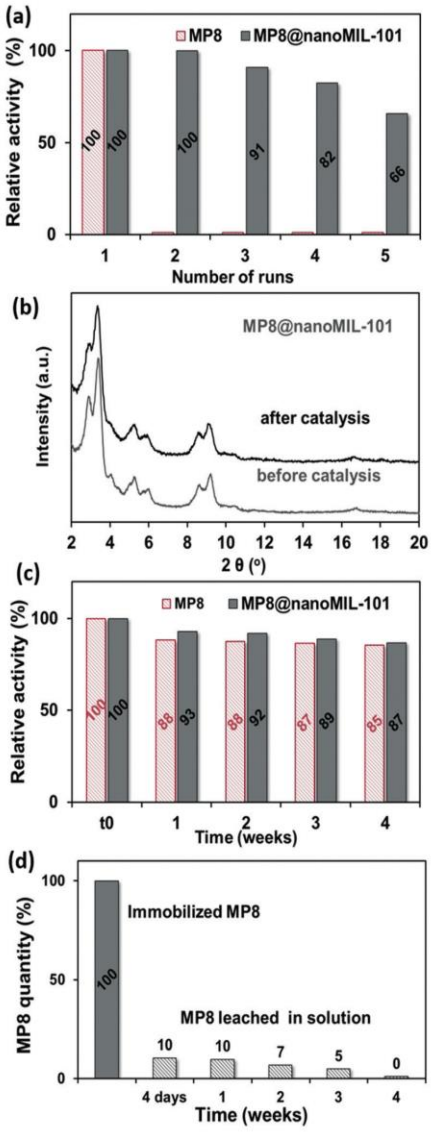

Figure 3. a) Relative catalytic activity of MP8@nanoMIL-101 over 5 catalytic cycles; b) PXRD of MP8@nanoMIL-101 before and after 5 catalytic cycles; c) Stability of free MP8 and immobilized MP8@MIL-101 over time d) Amount of MP8 leached from the MP8@MIL101 material over one month.

GDCh Communications Angewandte International Edition Chemie

Figure 2b. The reaction kinetics (Figure S10 and S11) were faster for free MP8 with a maximum $ABTS^{\bullet+}$ amount reached in less than 100 seconds, whereas immobilized MP8@nanoMIL-101 did not reach the maximum $ABTS^{\bullet+}$ amount even after 300 seconds. This was attributed to slower diffusion of the substrate to the immobilized enzyme, in accordance with numerous reports on bio-immobilization matrices.[2] However, for a longer period of time (1 hour) at high H_2O_2 concentration (0.9 mM) displayed in Figure S14, a higher amount of $ABTS^{\bullet+}$ was obtained for immobilized MP8@nanoMIL-101, exceeding the amount attained with the free MP8. Such results are consistent with a possible oxidative degradation of the heme moiety of the free MP8 while the active site of the encapsulated MP8 is preserved. At pH 5, the protonation of the histidine coordinated to the heme-Fe in the axial position (Figure 1a) leads to the cleavage of the Fe–histidine bond, thereby reducing the MP8 catalytic activity. The improved catalytic activity of the MP8@nanoMIL-101 at pH 5 clearly suggests that the MIL-101 matrix provides an efficient protection for MP8 outside its optimum pH range. As already reported,[21] the enzyme encapsulation may provide a confined micro-environment with lower proton concentrations, which likely limits the protonation of the axial histidine of MP8.

The possibility of recycling the material was also evaluated. Since the separation of free MP8 from the reaction mixture is not possible, the activity of free MP8 was not maintained after 1 cycle. As displayed in Figure 3a, 66% of the initial activity of MP8@nanoMIL-101 was preserved after 5 catalytic cycles.The PRXD pattern of MP8@nanoMIL-101 after the 5 catalytic cycles, in Figure 3b, shows the preservation of the MOF structure. The long-term stability of the material, stored at 4°C, was assessed over 1 month both in terms of catalytic activity and stability (experimental details are given in Supporting Information). The results, shown in Figures 3c and 3d, demonstrate a minimal loss of catalytic activity over time (less than 15%) as well as minimal leaching of MP8 that stabilizes after a week to reach a cumulated amount of 32% after 4 weeks (determined from UV/Vis spectra of the supernatant).

Further catalytic experiments were performed toward the oxidative degradation of model organic dyes. Dyes with different electrostatic charges were selected: cationic Methylene Blue (MB), neutral Sudan II and anionic Methyl Orange (MO), as shown in Figure 4 and Figure S15. The separation of MB/MO mixtures have previously been reported with various MOFs, including MIL-101(Cr).[22] These dyes have similar molecular sizes but opposite electrostatic charges, their separation has been mainly attributed to the difference of electrostatic affinity with the charged MOF framework. MIL-101(Cr) particles are positively charged within the 5–7 pH range, and therefore selectively adsorbs the negatively charged MO over the positively charged MB. Thus our idea was to determine if coupling the adsorption selectivity of the MOF matrix with the MP8 oxidative catalytic activity could lead to an enhanced dye degradation process with high substrate selectivity. The catalytic activity of MP8@MIL-101 towards the oxidation of MB, Sudan II and MO was thus, investigated (Figures 4 and Figure S15). For the oxidation of the positively charged dye (MB, Figure 4a), the reaction rate observed with immobilized MP8@MIL-101(Cr) was almost negligible when compared to that observed with free MP8. On the contrary, similar experiments carried out with negatively charged dye (MO, Figure 4b) led to much higher reaction rates compared with the free MP8. This can be explained by the electrostatic attractive interactions between MO and the MOF matrix, while repulsive interactions are expected between MB and MIL-101(Cr) This may strongly favour diffusion of MO within the pores of the MOF, leading to a pre-concentration of MO at the vicinity of the enzyme. The reaction rate for the neutral dye (Sudan II) was similar for free and immobilized MP8 (Figure S15) in agreement with the much lower affinity with MIL-101(Cr). Hence, the MOF matrix contributes to the material's overall catalytic activity

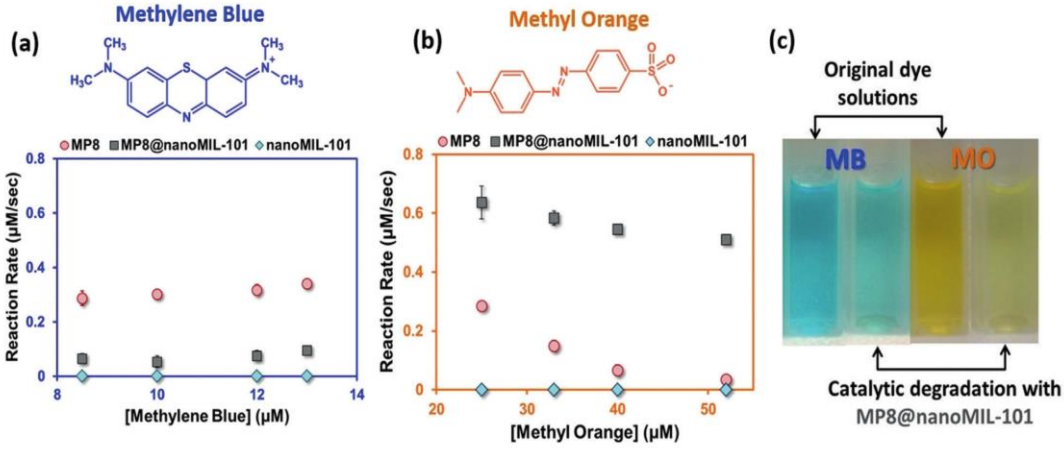

Figure 4. a) Reaction rate of degradation of Methylene Blue (MB, positive) by free MP8 (red circles), immobilized MP8@nanoMIL-101 (grey squares), and nanoMIL-101 (blue diamonds); b) Reaction rate of degradation of Methyl Orange (MO, negative) by free MP8 (red circles), immobilized MP8@nanoMIL-101 (grey squares), and nanoMIL-101 (blue diamonds); c) Solutions of MB and MO before and after the catalytic degradation with MP8@nanoMIL-101.

by providing a charge-based selective adsorption of reactants, leading to enhanced reaction rate.

In conclusion, we have shown that MP8 could be entrapped and retained in a mesoporous robust MOF with minimal leaching, high catalytic activity, and long-term stability. In addition, the entrapped enzyme was protected under acidic or oxidative conditions by its confinement within the MOF matrix. This work also demonstrated for the first time, that the MOF matrix could act in synergy with the enzyme by selectively enhancing the oxidation reaction of dyes. This enhancement was attributed to the pre-concentration of reactants through charge matching between the dye and the MOF. This work expands the use of MOFs as bio-immobilization matrices beyond simple solids to an active component in catalytic processes.

Acknowledgements

This work was supported by the ANR-11-LABEX-0039 (labex charm3at). We thank Dr. M. Benzaqui and C. Livage for the SEM experiments, Dr. A. Tissot for nitrogen sorption measurements and V. Guerineau for technical assistance in mass spectrometry.

Conflict of interest

The authors declare no conflict of interest.

Keywords: biocatalysis · enzymes · immobilization · metal–organic frameworks (MOFs) · oxidation

How to cite: *Angew. Chem. Int. Ed.* **2018**, *57*, 16141–16146
Angew. Chem. **2018**, *130*, 16373–16378

[1] a) G. Rocchitta, A. Spanu, S. Babudieri, G. Latte, G. Madeddu, G. Galleri, S. Nuvoli, P. Bagella, M. I. Demartis, V. Fiore, R. Manetti, P. A. Serra, *Sensors* **2016**, *16*, 780–800; b) O. Kirk, T. V. Borchert, C. C. Fuglsang, *Curr. Opin. Biotechnol.* **2002**, *13*, 345–351.

[2] a) R. A. Sheldon, S. van Pelt, *Chem. Soc. Rev.* **2013**, *42*, 6223–6235; b) M. Hartmann, X. Kostrov, *Chem. Soc. Rev.* **2013**, *42*, 6277–6289; c) Z. Zhou, M. Hartmann, *Chem. Soc. Rev.* **2013**, *42*, 3894–3912; d) H. H. P. Yiu, P. A. Wright, *J. Mater. Chem.* **2005**, *15*, 3690–3700; e) D. Avnir, T. Coradin, O. Lev, J. Livage, *J. Mater. Chem.* **2006**, *16*, 1013–1030; f) E. M. Forsberg, C. Sicard, J. D. Brennan, *Annu. Rev. Anal. Chem.* **2014**, *7*, 337–359.

[3] a) V. Lykourinou, Y. Chen, X.-S. Wang, L. Meng, T. Hoang, L.-J. Ming, R. L. Musselman, S. Ma, *J. Am. Chem. Soc.* **2011**, *133*, 10382–10385; b) H. Deng, S. Grunder, K. E. Cordova, C. Valente, H. Furukawa, M. Hmadeh, F. Gandara, A. C. Whalley, Z. Liu, S. Asahina, H. Kazumori, M. O'Keeffe, O. Terasaki, J. F. Stoddart, O. M. Yaghi, *Science* **2012**, *336*, 1018–1023; c) F. Lyu, Y. Zhang, R. N. Zare, J. Ge, Z. Liu, *Nano Lett.* **2014**, *14*, 5761–5765; d) K. Liang, R. Ricco, C. M. Doherty, M. J. Styles, S. Bell, N. Kirby, S. Mudie, D. Haylock, A. J. Hill, C. J. Doonan, P. Falcaro, *Nat. Commun.* **2015**, *6*, 7240; e) D. Feng, T. F. Liu, J. Su, M. Bosch, Z. Wei, W. Wan, D. Yuan, Y. P. Chen, X. Wang, K. Wang, X. Lian, Z. Y. Gu, J. Park, X. Zou, H. C. Zhou, *Nat. Commun.* **2015**, *6*, 5979; f) J. Huo, J. Aguilera-Sigalat, S. El-Hankari, D. Bradshaw, *Chem. Sci.* **2015**, *6*, 1938–1943; g) S. Patra, T. H. Crespo, C. Serre, A. Permyakova, C. Sicard, A. Chausse, N. Steunou, L. Legrand, *J. Mater. Chem. B* **2015**, *3*, 8983–8992.

[4] a) G. Maurin, C. Serre, A. Cooper, G. Ferey, *Chem. Soc. Rev.* **2017**, *46*, 3104–3107; b) H. Furukawa, K. E. Cordova, M. O'Keeffe, O. M. Yaghi, *Science* **2013**, *341*, 1230444; c) K. Adil, Y. Belmabkhout, R. S. Pillai, A. Cadiau, P. M. Bhatt, A. H. Assen, G. Maurin, M. Eddaoudi, *Chem. Soc. Rev.* **2017**, *46*, 3402–3430; d) M. F. de Lange, K. J. Verouden, T. J. Vlugt, J. Gascon, F. Kapteijn, *Chem. Rev.* **2015**, *115*, 12205–12250; e) M. Giménez-Marqués, T. Hidalgo, C. Serre, P. Horcajada, *Coord. Chem. Rev.* **2016**, *307*, 342–360; f) L. E. Kreno, K. Leong, O. K. Farha, M. Allendorf, R. P. Van Duyne, J. T. Hupp, *Chem. Rev.* **2012**, *112*, 1105–1125; g) P. García-García, M. Müller, A. Corma, *Chem. Sci.* **2014**, *5*, 2979–3007.

[5] a) E. Gkaniatsou, C. Sicard, R. Ricoux, J. P. Mahy, N. Steunou, C. Serre, *Mater. Horiz.* **2017**, *4*, 55–63; b) C. Doonan, R. Ricco, K. Liang, D. Bradshaw, P. Falcaro, *Acc. Chem. Res.* **2017**, *50*, 1423–1432; c) X. Lian, Y. Fang, E. Joseph, Q. Wang, J. Li, S. Banerjee, C. Lollar, X. Wang, H. C. Zhou, *Chem. Soc. Rev.* **2017**, *46*, 3386–3401; d) M. B. Majewski, A. J. Howarth, P. Li, M. R. Wasielewski, J. T. Hupp, O. K. Farha, *CrystEngComm* **2017**, *19*, 4082–4091.

[6] a) P. Li, J. A. Modica, A. J. Howarth, E. L. Vargas, P. Z. Moghadam, R. Q. Snurr, M. Mrksich, J. T. Hupp, O. K. Farha, *Chem* **2016**, *1*, 154–169; b) S. Patra, S. Sene, C. Mousty, C. Serre, A. Chausse, L. Legrand, N. Steunou, *ACS Appl. Mater. Interfaces* **2016**, *8*, 20012–20022; c) P. Li, Q. Chen, T. C. Wang, N. A. Vermeulen, B. L. Mehdi, A. Dohnalkoya, N. D. Browning, D. Shen, R. Anderson, D. A. Gomez-Gualdron, F. M. Cetin, J. Jagiello, A. M. Asiri, J. F. Stoddart, O. K. Farha, *Chem* **2018**, *4*, 1022–1034.

[7] a) Y. Chen, V. Lykourinou, T. Hoang, L. J. Ming, S. Ma, *Inorg. Chem.* **2012**, *51*, 9156–9158; b) F.-K. Shieh, S.-C. Wang, C.-I. Yen, C.-C. Wu, S. Dutta, L.-Y. Chou, J. V. Morabito, P. Hu, M.-H. Hsu, K. C. Wu, C.-K. Tsung, *J. Am. Chem. Soc.* **2015**, *137*, 4276–4279.

[8] a) A. M. Osman, M. A. Posthumus, C. Veeger, P. J. van Bladeren, C. Laane, I. M. Rietjens, *Chem. Res. Toxicol.* **1998**, *11*, 1319–1325; b) R. Ricoux, J. L. Boucher, D. Mansuy, J. P. Mahy, *Eur. J. Biochem.* **2001**, *268*, 3783–3788.

[9] O. Q. Munro, H. M. Marques, *Inorg. Chem.* **1996**, *35*, 3752–3767.

[10] T. Robinson, G. McMullan, R. Marchant, P. Nigam, *Bioresour. Technol.* **2001**, *77*, 247–255.

[11] J. Aron, D. A. Baldwin, H. M. Marques, J. M. Pratt, P. A. Adams, *J. Inorg. Biochem.* **1986**, *27*, 227–243.

[12] G. Ferey, C. Mellot-Draznieks, C. Serre, F. Millange, J. Dutour, S. Surble, I. Margiolaki, *Science* **2005**, *309*, 2040–2042.

[13] P. X. Qi, R. A. Beckman, A. J. Wand, *Biochemistry* **1996**, *35*, 12275–12286.

[14] Y. Chen, V. Lykourinou, C. Vetromile, T. Hoang, L.-J. Ming, R. W. Larsen, S. Ma, *J. Am. Chem. Soc.* **2012**, *134*, 13188–13191.

[15] A. Demessence, P. Horcajada, C. Serre, C. Boissière, D. Grosso, C. Sanchez, G. Férey, *Chem. Commun.* **2009**, 7149–7151.

[16] P. Li, S. Y. Moon, M. A. Guelta, L. Lin, D. A. Gomez-Gualdron, R. Q. Snurr, S. P. Harvey, J. T. Hupp, O. K. Farha, *ACS Nano* **2016**, *10*, 9174–9182.

[17] S. D. Lauzon, D. Mansuy, J.-P. Mahy, *Eur. J. Biochem.* **2002**, *269*, 470–480.

[18] S. Othman, A. Le Lirzin, A. Desbois, *Biochemistry* **1994**, *33*, 15437–15448.

[19] E. N. Kadnikova, N. M. Kostic, *J. Mol. Catal. B* **2002**, *18*, 39–48.

[20] a) J.-S. Wang, A.-L. Tsai, J. Heldt, G. Palmer, E. V. Warts, *J. Biol. Chem.* **1992**, *267*, 15310–15318; b) J. Cheek, D. W. Low, H. B. Gray, J. H. Dawson, *Biochem. Biophys. Res. Commun.* **1998**, *253*, 195–198.

[21] H. Frenkel-Mullerad, D. Avnir, *J. Am. Chem. Soc.* **2005**, *127*, 8077 – 8081.

[22] a) E. Haque, J. W. Jun, S. H. Jhung, *J. Hazard. Mater.* **2011**, *185*, 507 – 511; b) M. M. Tong, D. H. Liu, Q. Y. Yang, S. Devautour-Vinot, G. Maurin, C. L. Zhong, *J. Mater. Chem. A* **2013**, *1*, 8534 – 8537; c) Q. X. Yang, S. S. Ren, Q. Q. Zhao, R. Lu, C. Hang, Z. J. Chen, H. G. Zheng, *Chem. Eng. J.* **2018**, *333*, 49 – 57.

Manuscript received: October 2, 2018
Accepted manuscript online: October 11, 2018
Version of record online: November 8, 2018

Angewandte Chemie
Eine Zeitschrift der Gesellschaft Deutscher Chemiker

Supporting Information

Enzyme Encapsulation in Mesoporous Metal–Organic Frameworks for Selective Biodegradation of Harmful Dye Molecules

Effrosyni Gkaniatsou, Clémence Sicard, Rémy Ricoux,* Linda Benahmed, Flavien Bourdreux, Qi Zhang, Christian Serre, Jean-Pierre Mahy, and Nathalie Steunou*

anie_201811327_sm_miscellaneous_information.pdf

1. Synthesis

- ***nanoMIL-101(Cr):***

MIL-101(Cr) nanoparticles were synthesized following a reported microwave-assisted hydrothermal synthesis.[1] 2 g of $Cr(NO_3)_3 \cdot 9H_2O$ and 0.825 g of terephthalic acid were added in a 100 mL Teflon reactor and dissolved in 25 mL of H_2O.The reaction mixture was heated up to 200°C for 1 min, with a temperature ramp of 4 min. The resulting nanoparticles were then filtered, to eliminate the excess of unreacted ligand and the filtrate was centrifuged (14500 rpm, 50 min). Finally, to fully remove any traces of $Cr(NO_3)_3$ and unreacted ligand from the pores, the nanoparticles were washed three times in boiling H_2O, centrifuged and washed again three times in boiling ethanol (abs.). The purified nanoparticles were kept in ethanol suspensions at RT.

- ***microMIL-101(Cr):***

Microparticles of MIL-101(Cr) were synthesized based on a reported hydrothermal synthesis.[2]

- ***Microperoxidase 8:***

Microperoxidase 8 (MP8) was prepared by the hydrolytic digestion of Cytochrome c (Cyt c), described previously in the literature.[3] Briefly, 400 mg of Cyt c were mixed with 10.4 mg of pepsin and dissolved in 5 mL of H_2O. The pH of the solution was adjusted to 2.6 with HCl (1M). The mixture was incubated for 1 h at 37°C, followed by the addition of 10.4 mg of pepsin and the re-adjustment of the pH. The incubation continued for 5 h, by which point the main product of the reaction was microperoxidase 11 (MP11). The peptic activity was stopped by raising the pH to 9, using NH_4HCO_3 solution. 8 mg of trypsin were finally added for the digestion of MP11 to MP8 and the mixture was incubated at 37°C overnight. MP8 was collected from the reaction mixture by gel filtration chromatography (biogel P6; 4 × 100 cm). The purified MP8 was lyophilized and stored at 4°C. The concentration of the MP8 solutions were calculated by using the reported extinction coefficient, $\varepsilon_{396} = 1.57 \times 10^5$ $M^{-1} \cdot cm^{-1}$.[3]

- ***Encapsulation of MP8 into nano/microMIL-101:***

5 mg of MIL-101 suspended in 1 mL EtOH was mixed with 1 mg MP8 dissolved in 1 mL H_2O. The pH of the mixture was adjusted at 5. The mixture was incubated at 37°C for 48 h. The immobilized catalyst (MP8@nano/microMIL-101) was washed with H_2O and centrifuged (14500 rpm, 50 min), until the supernatant was clear. The composite was stored in H_2O suspension at 4°C.

2. Experimental Conditions

- ***ζ-potential:***

The ζ-potential of MIL-101 nanoparticles as a function of pH was measured with suspensions of 0.1 mg/mL in H_2O. The desired pH (1-12) was adjusted with HCl or NaOH solutions. Before each measurement, the sample was placed in an ultrasonic bath for 15 min to assure complete dispersion of the nanoparticles.

- ***Determination of the MP8 loading by ICP-AES:***

The enzyme loading was measured by detecting the Fe present in the MP8 molecules and the Cr present in MIL-101.

Sample treatment: Typically, a sample was heated at 100 ^{o}C overnight to evaporate the containing solvent. Afterwards, 1 mL of HCl (37%) was added and the sample was heated in a closed vial at 80 ^{o}C, overnight (16 h) for total mineralization. The sample was diluted to 40 mL with ultrapure H_2O before the analysis.

- ***Accessibility study:***

The coordination of imidazole (ImH) to the Fe(III) of the free and the immobilized MP8 was monitored via the spectral evolution of the absorbance from 350 to 650 nm. The reactions were performed with 1 μM MP8 (free and immobilized) and increasing concentrations of ImH in phosphate buffer (0.01 M) at pH 7. With each addition of ImH the initial spectrum of MP8 (λ_{max}= 396 nm) was progressively replaced by a new spectrum (λ_{max}= 404 nm), due to the formation of the MP8(ImH) complex. The plot of $1/\Delta A_{404}$ versus 1/[ImH] was fitted to a linear function and confirmed the binding of one ImH ligand to the Fe(III), as previously described in the literature.[4,5] The dissociation constants were calculated using the Brault and Rouge equation.[6]

- ***Evaluation of the MP8 catalytic activity:***

The catalytic activity of the free and the immobilized MP8 was evaluated by its capacity to catalyze the oxidation of ABTS, in the presence of H_2O_2. The activity was measured by monitoring the increase of the absorbance at 420 nm over time, due to the formation of the oxidized product, $ABTS^{\cdot+}$ (ε_{420}=3.6 × 10^4 M^{-1}·cm^{-1}).[7]

Typically, the reactions were performed with 2 mM ABTS, 0.35 μM MP8 (free and immobilized), 0.9 mM H_2O_2 in citric acid-sodium citrate buffer (0.01 M) at pH 5 or in phosphate buffer (0.01 M) at pH 7 at room temperature and in a total volume of 3 mL. The total reaction time was fixed to 180 s. The reaction rates were calculated by the slope of the absorbance (at 420 nm) over time for the first 10 sec of the reaction. The catalytic activity of MP8 and nanoMIL-101 were also evaluated with similar amount of MP8 and nanoMIL101 than in the MP8@nanoMIL101 composite, respectively. The error bars corresponds to the standard deviation of three measurements.

- ***Oxidation of the ABTS substrate as a function of pH:***

The above mentioned procedure was followed to study the effect of the pH on the catalytic activity of the free and the immobilized MP8, and the reactions were performed in citric acid-sodium citrate buffer for pH 4-6 (0.01 M) and phosphate buffer for pH 7-8 (0.01 M).

- ***Oxidation of the ABTS substrate at pH 7 and 5 as a function of H_2O_2 concentration:***

The above mentioned procedure and the reaction were performed with 0.1-1.8 mM H_2O_2 in phosphate buffer (0.01 M) at pH 7 or in citric acid-sodium citrate buffer (0.01 M) at pH 5. The total reaction time was fixed to 300 sec.

- ***Recycling study:***

The recycling of MP8@nanoMIL-101 was performed using 4 μM of the immobilized MP8@nanoMIL-101, 0.8 mM ABTS, 0.5 mM H_2O_2 in 10 mL of phosphate buffer (0.01 M) at pH 7 and at room temperature. After 5 min of reaction, the mixture was separated by centrifugation (14500 rpm, 20 min). The supernatant was analyzed by UV-vis, in order to quantify the amount of oxidized ABTS. The recovered MP8@nanoMIL-101 was washed twice with buffer solution and then used for the second catalytic cycle, by adding similar amounts of reactants. The above procedure was repeated for an overall of five catalytic cycles. The relative activity of the biocatalyst corresponds to the ratio of each cycle's activity over the activity of the first cycle.

- ***Stability study:***

The stability of the free MP8 and the immobilized MP8@nanoMIL101 catalysts under storage (4 ^{o}C, aqueous media) was evaluated based on their ability to catalyze the oxidation of ABTS. The reactions were performed with 2 mM ABTS, 0.35 μM MP8 (free and immobilized) and 0.9 mM H_2O_2 in phosphate buffer (0.01 M) at pH 7, at room temperature. The total reaction time was fixed to 5 min.

- ***Leaching study:***

For each measurement the MP8@nanoMIL-101 was removed via centrifugation and the supernatant was collected for UV-vis analysis. The immobilized catalyst was redispersed in H_2O and stored at 4^{o}C until the next measurement. The MP8 quantity (mass %) corresponds to the ratio of the detected MP8 quantity, leached in solution at a given time over the initial MP8 quantity immobilized in nanoMIL-101 The study was performed over 4 weeks with the same sample.

- ***Catalytic degradation of dyes:***

The catalytic degradation of Methylene Blue, Sudan II and Methyl Orange by the free MP8 and the immobilized MP8@nanoMIL101 was evaluated by measuring the decrease of the absorbance of the respective absorption band over time (ε_{660}= 7.85 × 10^5 $M^{-1}\cdot cm^{-1}$, ε_{499}=1.98 × 10^5 $M^{-1}\cdot cm^{-1}$ and ε_{456}= 2.78 × 10^5 $M^{-1}\cdot cm^{-1}$, respectively). The reactions were performed with 1 μM MP8 (free and immobilized), 0.9 mM H_2O_2 and increasing concentrations of dye, in a mixture of H_2O:MeOH (50:50), at room temperature and in a total volume of 3 mL. The catalytic activity of nanoMIL-101 was also evaluated with similar amount of nanoMIL-101 than in the MP8@MIL101 composite). The total reaction time was fixed to 7 min. The reaction rates were calculated by the slope of the respective absorbance over time for the first 10 sec of the reaction.

3. Characterizations

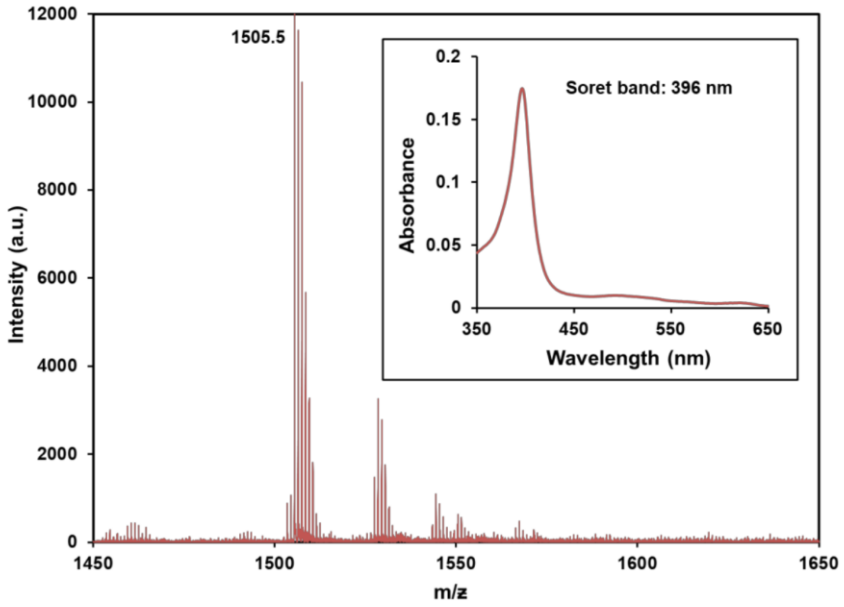

Figure S1 MALDI-TOF mass spectrum of the purified MP8. Inset: UV-vis spectrum of purified MP8 with a characteristic Soret band at 396 nm.

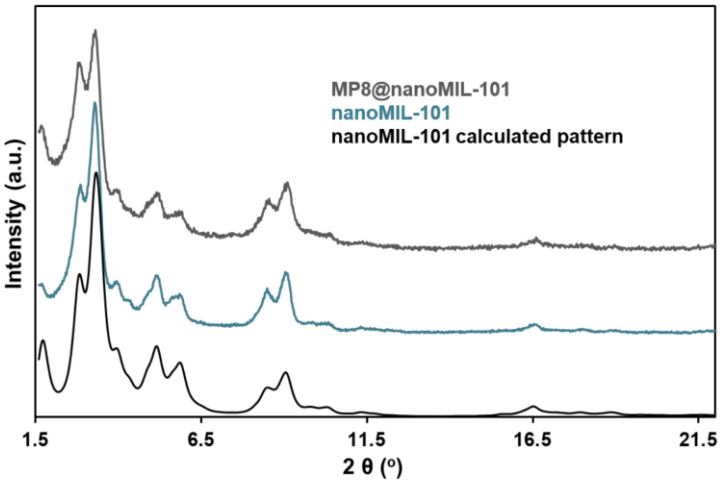

Figure S2 Powder X-Ray diffractions patterns of MIL-101 nanoparticles calculated (black), before (blue) and after (grey) immobilization of the MP8 molecules.

Table S1: MP8 loading obtained by ICP-AES:

Composite	Size	MP8 in composite (w/w %)
MP8@nanoMIL-101	70 nm	5.0 ± 0.3
MP8@microMIL-101	1 µm	5.4 ± 0.2

Table S2: Detailed results obtained by ICP-AES

Sample	Cr	Fe	MOF	MP8	Composite
	mg				
MP8	0.001±0.001	0.017±0.001	-	0.47±0.03	-
nanoMIL-101	0.64±0.02	0.001±0.001	2.942±0.004	-	-
MP8@nanoMIL-101	0.633±0.008	0.01±0.01	3.887±0.003	0.206±0.002	4.09±0.05
MP8@nanoMIL-101 supernatant	0.019	0.001	0.117±0.001	0.037	-
microMIL-101	0.96±0.02	0.003	4.44±0.09	-	-
MP8@microMIL-101	0.96±0.02	0.009	4.40±0.07	0.249±0.004	4.65±0.06
MP8@microMIL-101 supernatant	0.005±0.001	0.003	0.023±0.008	0.097±0.004	-

Table S3: Results obtained by EDX

	Experimental (w/w %)
Cr	99.3±0.3
Fe	0.7±0.3
Fe:Cr ratio	0.007

Table S4: UV-Vis results of the MP8 solution used for the immobilization and the supernatants solutions of MP8@nanoMIL-101 (washing solutions)

	Absorbance	Dilution factor	Mass MP8 (mg)
MP8	0.16	230	0.26
Supernatant after encapsulation	0.43	0	0.01

Encapsulated MP8 = 0.25mg into 5 mg nanoMIL-101 (5 % w/w)

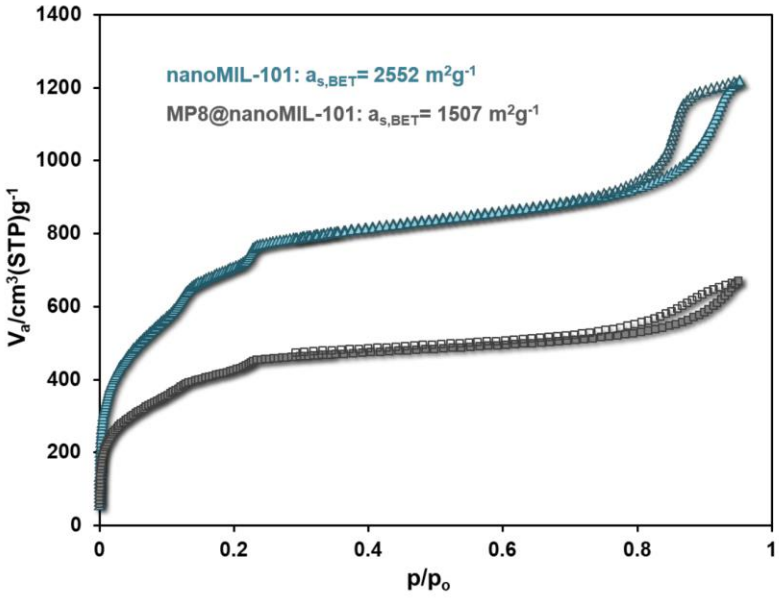

Figure S3 N_2 sorption isotherms of MP8@nanoMIL-101(grey) and nanoMIL-101(blue) at 77 K with calculated BET surface areas of 1507 m^2/g and 2552 m^2/g, respectively.

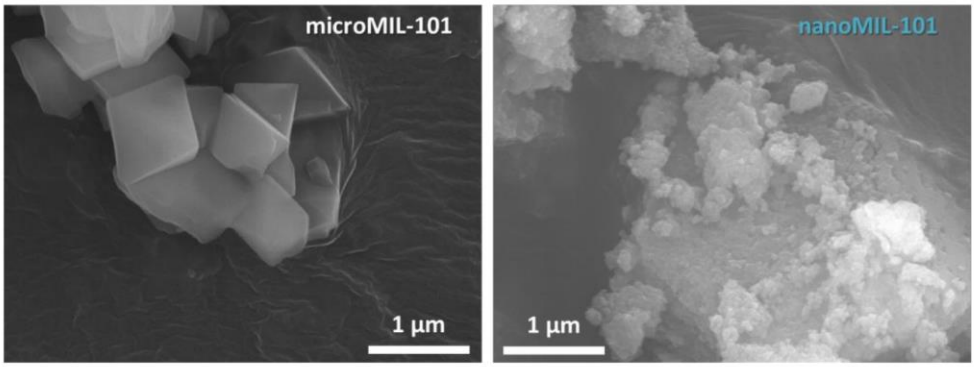

Figure S4 On the left, SEM image of microMIL-101 with average size ≈ 1 µm. On the right, SEM image of nanoMIL-101 with average size ≈ 70 nm.

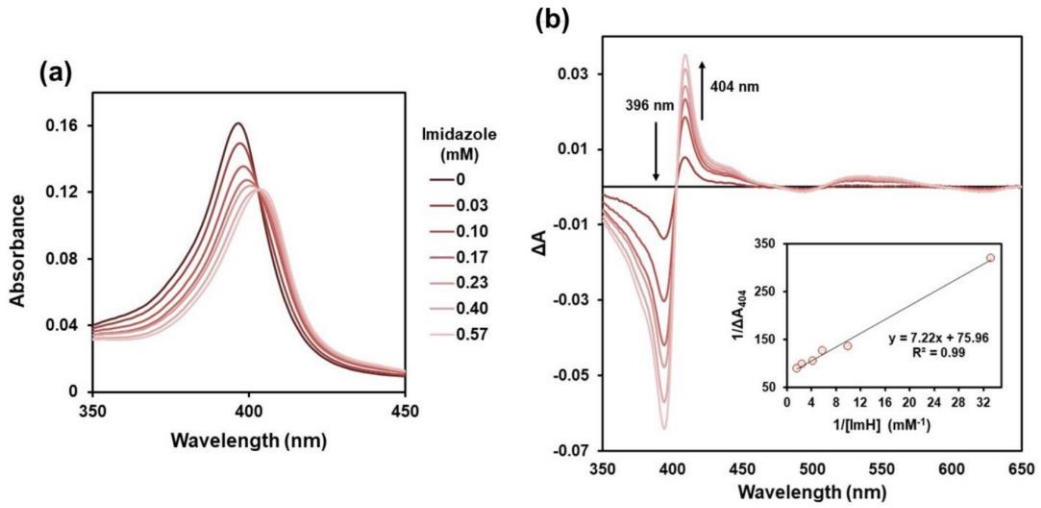

Figure S5 (a) Spectral evolution of MP8 in the presence of 0-0.57 mM ImH (dark to ligh red); (b) Differential UV-vis spectra of MP8 in the presence of ImH, showing the decrease of the MP8 Soret band at 396 nm and the increase of the MP8(ImH) Soret band at 404 nm. Inset: Plot of 1/ΔA (at 404 nm) as a function of 1/[ImH] with a first order linear fit.

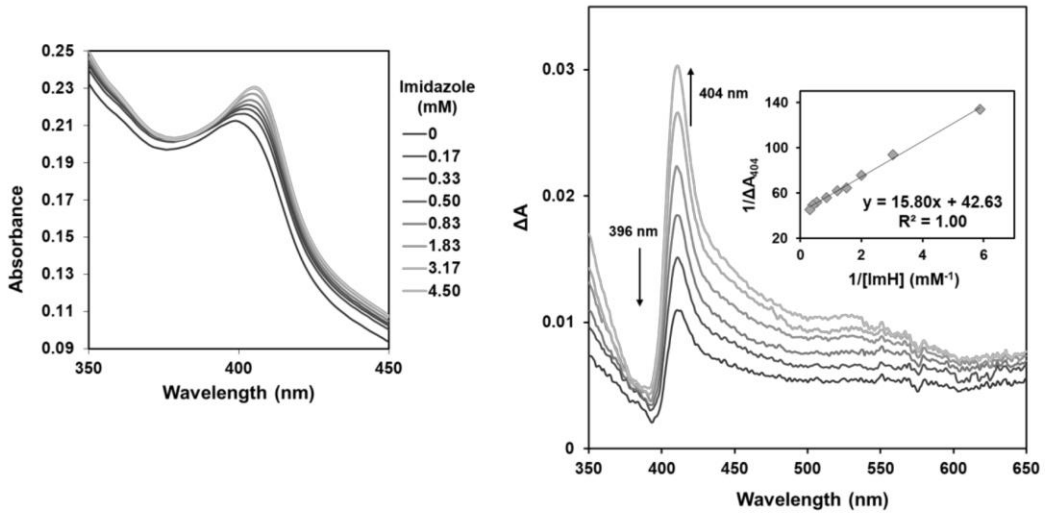

Figure S6 (a) Spectral evolution of MP8@nanoMIL-101 in the presence of 0-3.17 mM ImH (from black to light grey; (b) Differential UV-vis spectra of MP8@nanoMIL-101 in the presence of ImH, showing the decrease of the MP8 Soret band at 396 nm and the increase of the MP8(ImH) Soret band at 404 nm. Inset: Plot of 1/ΔA at 404 nm as a function of 1/[ImH] with a first order linear fit.

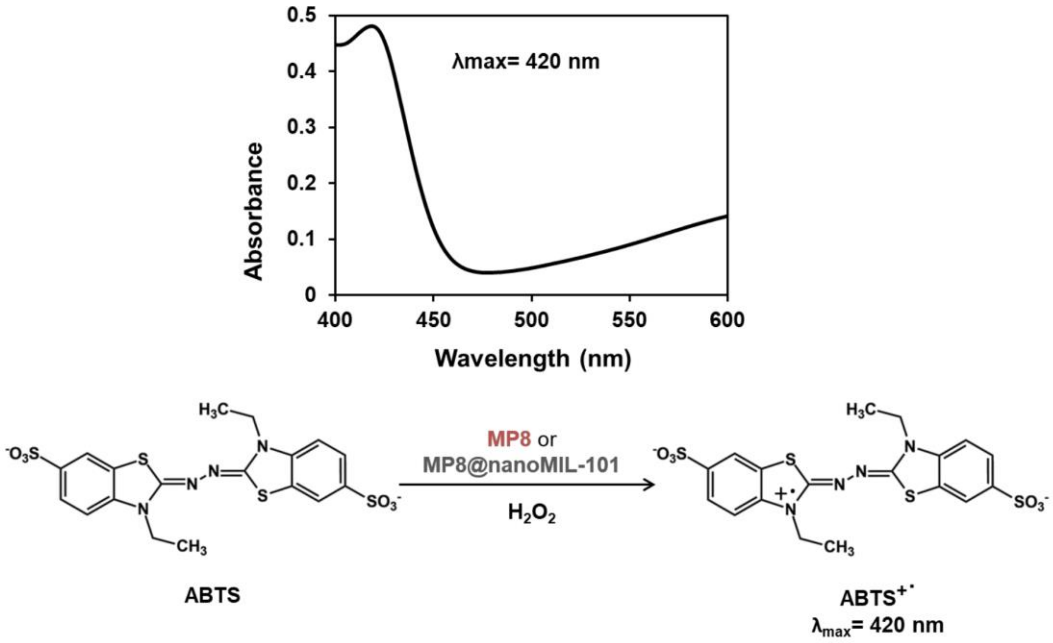

Figure S7 Catalytic oxidation of ABTS in the presence of H_2O_2. The radical cation $ABTS^{+\cdot}$ shows a maximum absorbance at 420 nm.

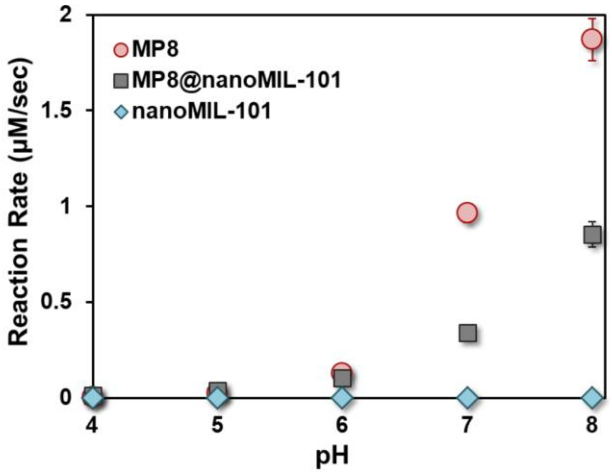

Figure S8 Reaction rate of ABTS oxidation by the free, MP8 (red circles), the immobilized MP8@nanoMIL-101 (grey square) and nanoMIL-101(blue diamond). The errors bars correspond to the standard deviation of three measurements.

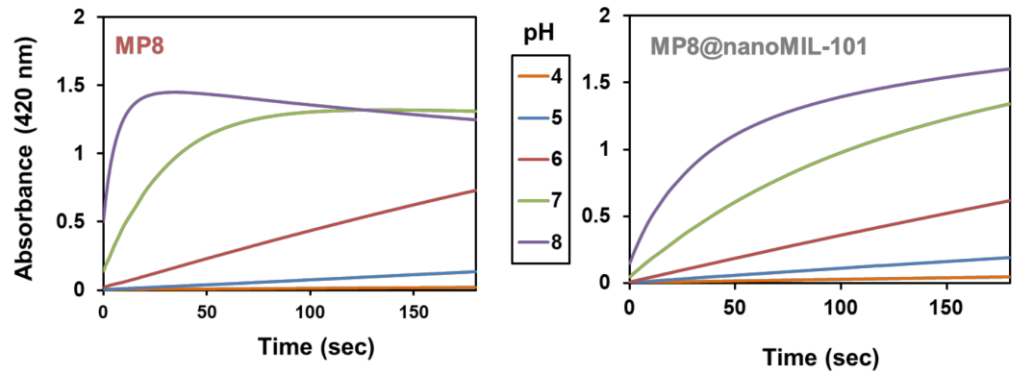

Figure S9 Time course oxidation of ABTS by free MP8 (left), and immobilized MP8@nanoMIL-101 (right) for a pH range 4-8.

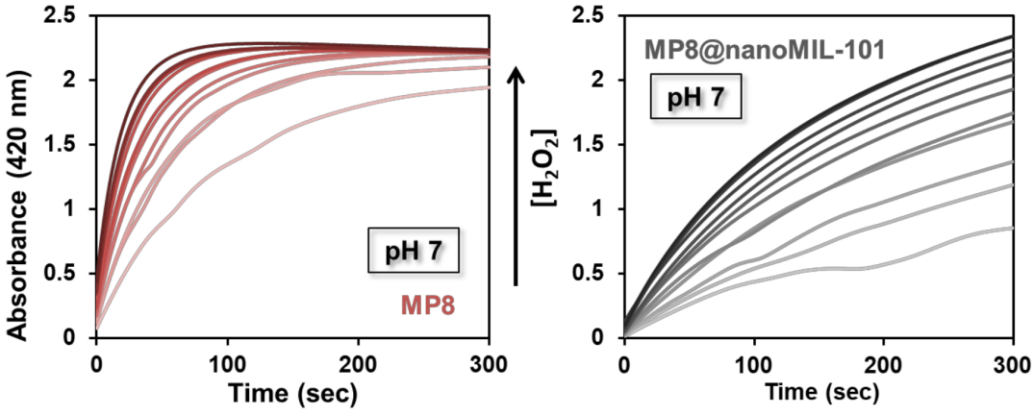

Figure S10 Time course of ABTS oxidation by the free MP8 (on the left) and the immobilized MP8@nanoMIL-101 (on the right) as a function of H_2O_2 concentration (0.1-1.8 mM) at pH 7.

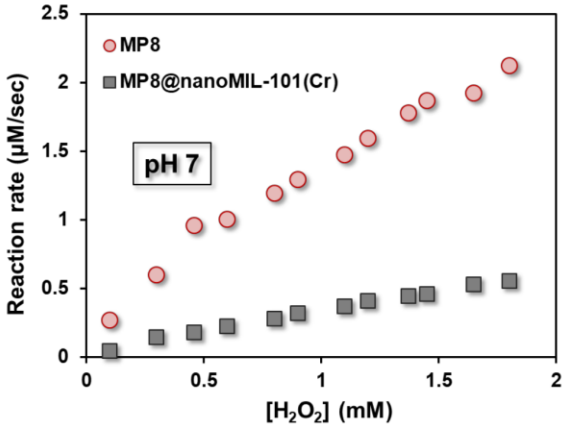

Figure S11 Reaction rate of ABTS oxidation by the free MP8 (red circle) and the immobilized MP8@nanoMIL101 (grey square) at pH 7. The errors bars correspond to the standard deviation of three measurements.

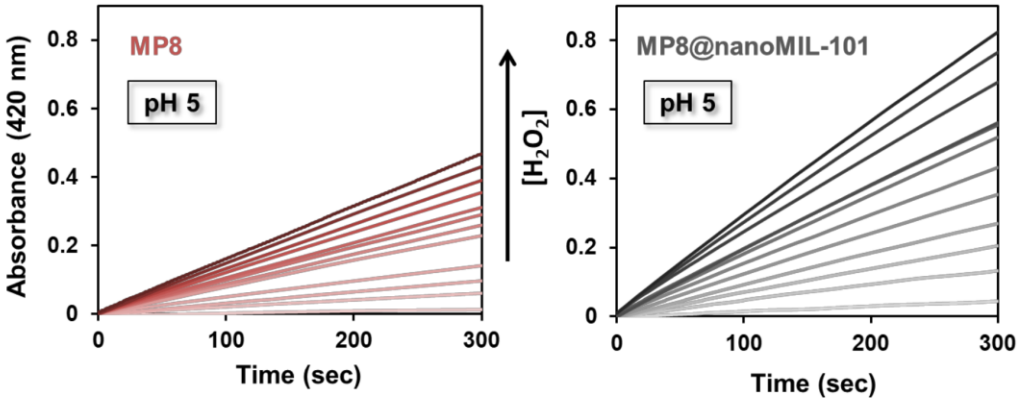

Figure S12 Time course of ABTS oxidation by the free MP8 (red, on the right) and the immobilized MP8@MIL101 (grey, on the left) as a function of H_2O_2 concentration (0.1-1.8 mM) at pH 5.

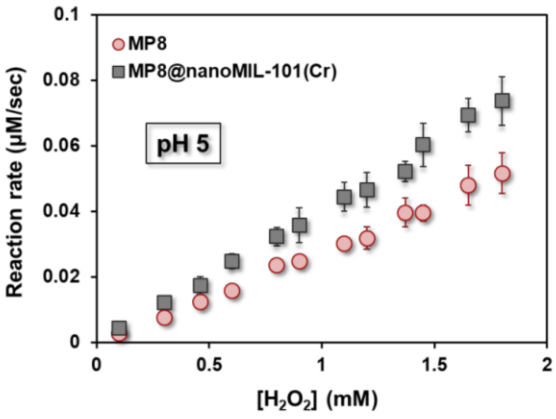

Figure S13 Reaction rate of ABTS oxidation by the free MP8 (red circle) and the immobilized MP8@nanoMIL101 (grey square) at pH 5. The errors bars correspond to the standard deviation of three measurements.

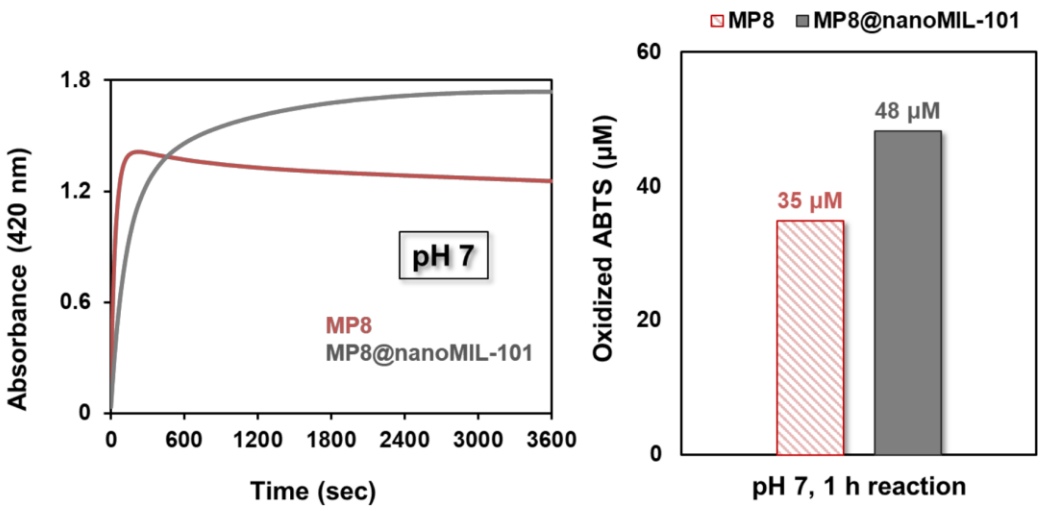

Figure S12 Left: Time course of ABTS oxidation by the free MP8 (red line) and the immobilized MP8@nanoMIL-101 (grey line) during 1 h of reaction at pH 7 and $[H_2O_2]$ = 0.9 mM. Right: Amounts of oxidized ABTS by the free MP8 (red column) and the immobilized MP8@nanoMIL-101 (grey column) during 1 h of reaction at pH 7 and $[H_2O_2]$ = 0.9 mM.

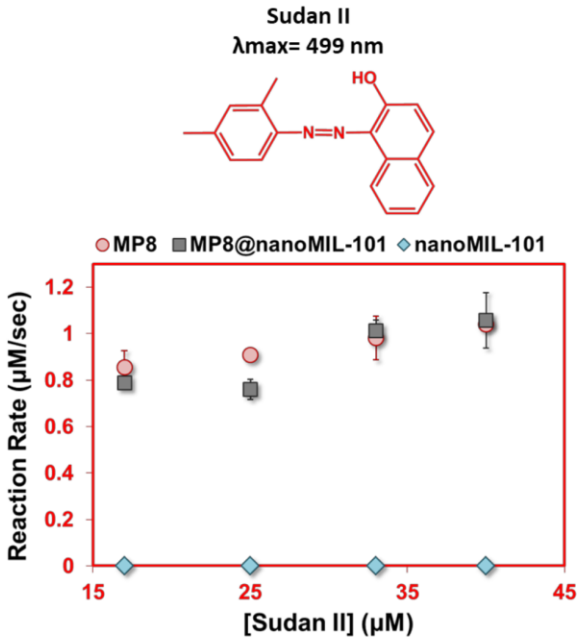

Figure S13 Reaction rate of Sudan II degradation by the free, the immobilized MP8 and nanoMIL-101. The reactions were performed with 1 μM MP8 (free and immobilized) and same amount of nanoMIL-101 as in the composite, 0.9 mM H_2O_2 and increasing concentrations of dye, in a mixture of H2O:MeOH (50:50), at room temperature.

4. Instrumentation

- ***X-ray powder diffraction (XRPD)***

XRPD patterns were collected on a Bruker D8 Advance diffractometer with a Debye-Scherrer geometry, equipped with a Ge(111) monochromator producing $CuK\alpha_1$ radiation (λ= 1.540598 Å) and a LynxEye detector.

- ***Fourier transform infrared spectroscopy (FTIR)***

FTIR spectra were collected on a ThermoScientificNicolet 6700 FT-IR.

- ***N_2 adsorption***

The sorption measurements were performed at 77 K on a BEL Japan Belsorp Max apparatus using N_2 as the probing gas, after an overnight activation at 120°C under primary vacuum (BEL Japan, Belsorp Prep).

- ***Dynamic light scattering (DLS) / ζ-potential***

DLS and ζ-potential studies were performed on a Malvern Instrument Zetasizer Nano ZS.

- ***Inductively coupled plasma optical emission spectroscopy (ICP-AES)***

The measurements were performed with an Agilent 720 Series with axially-viewed plasma and with a Cr/Fe calibration curve of 50-30,000 ppb.

- ***Matrix-assisted laser desorption/ionization-time of flight mass spectrometry (MALDI-TOF MS)***

MALDI-TOF MS was performed on a Bruker Daltonics UltrafleXtreme spectrometer.

- ***Ultraviolet-visible spectroscopy (UV-vis)***

UV/vis spectra were collected on a PerkinElmer LAMBDA 750 UV/Vis/NIR Spectrophotometer

References

[1] A. Demessence, C. Boissière, D. Grosso, P. Horcajada, C. Serre, G. Férey, G. J. A. A. Soler-Illia, C. Sanchez, *Journal of Materials Chemistry* **2010**, *20*, 7676.
[2] G. Ferey, *Science* **2005**, *309*, 2040–2042.
[3] J. Aron, D. A. Baldwin, H. M. Marques, J. M. Pratt, P. A. Adams, *Journal of Inorganic Biochemistry* **1986**, *27*, 227–243.
[4] S. de Lauzon, D. Mansuy, J.-P. Mahy, *The FEBS Journal* **2002**, *269*, 470–480.
[5] P. R. Vashi, H. M. Marques, *Journal of Inorganic Biochemistry* **2004**, *98*, 1471–1482.
[6] D. Brault, M. Rougee, *Biochemical and biophysical research communications* **1974**, *57*, 654–659.
[7] T. Kenzom, P. Srivastava, S. Mishra, *Applied and Environmental Microbiology* **2014**, *80*, 7484–7495.

B. Conclusions

In this chapter, we focused our efforts on the investigation of different mesoporous MOFs to be used for the cage inclusion of microperoxidase 8. A 3D confinement of MP8 was preferred, as this procedure has already been shown to enhance the stability and protect immobilized enzymes. Moreover, the small size of MP8 was compatible with this approach.

The first candidate for this work was the mesoporous PCN-333(Al), which has an extended MIL-100 structure. This MOF was selected due to its large cavities (42 and 55 Å) and its reported high stability in water (essential for biocatalytic applications). The reported synthetic procedure was not always reproducible, which forced us to optimize the synthetic conditions. However, based on the poor PCN-333(Al) stability in water, it was not found suitable for the immobilization of MP8. Therefore, the ultra-stable mesoporous MIL-101(Cr) was selected instead as an immobilization matrix for MP8. MIL-101(Cr) contains two mesopores (29 and 34 Å) that can host the MP8 molecules. Nanoparticles of MIL-101(Cr) were thus used for the immobilization of MP8. The immobilized enzyme showed an enhanced stability under acidic environments and in the presence of oxidizing agents and was found to be reusable several times, which highlighted the protection of the enzyme by the 3D framework. Finally, the selective adsorption of dye molecules by the MIL-101(Cr), provided an enhanced catalytic activity for the biodegradation of harmful dye molecules (like methyl orange) through a charge-based pre-concentration mechanism.

These results are promising for the use of Metal-Organic Frameworks as enzymatic matrices and encourage for the research of new, stable mesoporous frameworks. A more extensive study though is required to better define and possibly tune the interactions between the enzymes and the MOF frameworks. As we will see in the following chapter, the ligand functionalization of MIL-101(Cr) can influence the immobilization and reactivity of the enzymes, highlighting the importance of interactions between the enzymes and the support.

C. References

(1) Chen, Y.; Lykourinou, V.; Vetromile, C.; Hoang, T.; Ming, L.-J.; Larsen, R. W.; Ma, S. How Can Proteins Enter the Interior of a MOF? Investigation of Cytochrome *c* Translocation into a MOF Consisting of Mesoporous Cages with Microporous Windows. *Journal of the American Chemical Society* **2012**, *134* (32), 13188–13191. https://doi.org/10.1021/ja305144x.

(2) Feng, D.; Liu, T.-F.; Su, J.; Bosch, M.; Wei, Z.; Wan, W.; Yuan, D.; Chen, Y.-P.; Wang, X.; Wang, K.; et al. Stable Metal-Organic Frameworks Containing Single-Molecule Traps for Enzyme Encapsulation. *Nature Communications* **2015**, *6*, 5979. https://doi.org/10.1038/ncomms6979.

(3) Park, J.; Feng, D.; Zhou, H.-C. Structure-Assisted Functional Anchor Implantation in Robust Metal–Organic Frameworks with Ultralarge Pores. *Journal of the American Chemical Society* **2015**, *137* (4), 1663–1672. https://doi.org/10.1021/ja5123528.

(4) Horcajada, P.; Chevreau, H.; Heurtaux, D.; Benyettou, F.; Salles, F.; Devic, T.; Garcia-Marquez, A.; Yu, C.; Lavrard, H.; Dutson, C. L.; et al. Extended and Functionalized Porous Iron(Iii) Tri- or Dicarboxylates with MIL-100/101 Topologies. *Chemical Communications* **2014**, *50* (52), 6872. https://doi.org/10.1039/c4cc02175d.

(5) Nelson, A. P.; Farha, O. K.; Mulfort, K. L.; Hupp, J. T. Supercritical Processing as a Route to High Internal Surface Areas and Permanent Microporosity in Metal–Organic Framework Materials. *Journal of the American Chemical Society* **2009**, *131* (2), 458–460. https://doi.org/10.1021/ja808853q.

(6) Totten, R. K.; Kim, Y.-S.; Weston, M. H.; Farha, O. K.; Hupp, J. T.; Nguyen, S. T. Enhanced Catalytic Activity through the Tuning of Micropore Environment and Supercritical CO_2 Processing: Al(Porphyrin)-Based Porous Organic Polymers for the Degradation of a Nerve Agent Simulant. *Journal of the American Chemical Society* **2013**, *135* (32), 11720–11723. https://doi.org/10.1021/ja405495u.

(7) Mondloch, J. E.; Karagiaridi, O.; Farha, O. K.; Hupp, J. T. Activation of Metal–Organic Framework Materials. *CrystEngComm* **2013**, *15* (45), 9258. https://doi.org/10.1039/c3ce41232f.

(8) Hu, Z.; Castano, I.; Wang, S.; Wang, Y.; Peng, Y.; Qian, Y.; Chi, C.; Wang, X.; Zhao, D. Modulator Effects on the Water-Based Synthesis of Zr/Hf Metal–Organic Frameworks: Quantitative Relationship Studies between Modulator, Synthetic Condition, and Performance. *Crystal Growth & Design* **2016**, *16* (4), 2295–2301. https://doi.org/10.1021/acs.cgd.6b00076.

(9) Van de Voorde, B.; Stassen, I.; Bueken, B.; Vermoortele, F.; De Vos, D.; Ameloot, R.; Tan, J.-C.; Bennett, T. D. Improving the Mechanical Stability of Zirconium-Based Metal–Organic Frameworks by Incorporation of Acidic Modulators. *Journal of Materials Chemistry A* **2015**, *3* (4), 1737–1742. https://doi.org/10.1039/C4TA06396A.

(10) Morris, W.; Wang, S.; Cho, D.; Auyeung, E.; Li, P.; Farha, O. K.; Mirkin, C. A. Role of Modulators in Controlling the Colloidal Stability and Polydispersity of the UiO-66 Metal–Organic Framework. *ACS Applied Materials & Interfaces* **2017**, *9* (39), 33413–33418. https://doi.org/10.1021/acsami.7b01040.

(11) Férey, G.; Mellot-Draznieks, C.; Serre, C.; Millange, F.; Gutour, J.; Surblé, S.; Margiolaki, I. A Chromium Terephthalate-Based Solid with Unusually Large Pore Volumes and Surface Area. *Science* **2005**, *309* (5743), 2040–2042. https://doi.org/10.1126/science.1116275.

(12) Jiang, D.; Burrows, A. D.; Edler, K. J. Size-Controlled Synthesis of MIL-101(Cr) Nanoparticles with Enhanced Selectivity for CO2 over N2. *CrystEngComm* **2011**, *13* (23), 6916–6919. https://doi.org/10.1039/c1ce06274c.

(13) Yang, J.; Zhao, Q.; Li, J.; Dong, J. Synthesis of Metal–Organic Framework MIL-101 in TMAOH-Cr(NO3)3-H2BDC-H2O and Its Hydrogen-Storage Behavior. *Microporous and Mesoporous Materials* **2010**, *130* (1–3), 174–179. https://doi.org/10.1016/j.micromeso.2009.11.001.

(14) Demessence, A.; Horcajada, P.; Serre, C.; Boissière, C.; Grosso, D.; Sanchez, C.; Férey, G. Elaboration and Properties of Hierarchically Structured Optical Thin Films of MIL-101(Cr). *Chemical Communications* **2009**, No. 46, 7149. https://doi.org/10.1039/b915011k.

Chapter 3

Influence of MIL-101(Cr) functionalization on enzymatic immobilization and catalysis

Table of Contents

Introduction

This chapter deals with the functionalization of MIL-101(Cr) and with its influence on the encapsulation of microperoxidase 8 (MP8) and its catalytic activity. Two different approaches have been investigated, the ligand functionalization and the metal functionalization of the framework. For the first approach, two functionalized ligands have been selected, 2-amino-terephthalic acid and 2-sulfo-terephthalic acid. The functionalized MOFs have then been used for the encapsulation of MP8. The catalytic activity of the obtained bio-hybrid materials was examined first by the oxidation of a typical peroxidase chromogenic substrate (ABTS) and, second, *via* a more challenging reaction, the oxidation of organosulfur compounds. The resulting catalytic activities have been compared to those of MP8@MIL-101(Cr) and of the free enzyme. Concerning the functionalization of the metal cluster, the objective was the partial substitution of the inorganic chromium(III) Secondary Building Unit (SBU) with iron(III) in order to obtain a stable mesoporous and catalytically active structure (as Lewis acid and/or peroxidase-like catalyst). The attempts to obtain pure phases of MIL-101(Cr/Fe), using greener and milder synthetic conditions will be presented, along with the chemical stability study of the MOF.

A. Ligand functionalization in MIL-101(Cr)

Introduction and contributions

This work is presented in the format of a research article that will soon be submitted for publication.

The following paper describes our studies on the effect of ligand functionalization in MIL-101(Cr) on the immobilization process of MP8 and on the resulting catalytic activities. Two different functionalized MOFs were selected, MIL-101(Cr)-NH_2 and MIL-101(Cr)-SO_3H and were compared to the non-functionalized MIL-101(Cr). The choice of the functional groups was based on their difference in polarity, acidity and the particles' surface charge that could lead to different interactions with the MP8 molecules. MP8 loadings higher than those in MIL-101(Cr) were observed in the functionalized MOFs, which could be due to the enhanced adsorption of some enzyme molecules at the external surface of the MOFs through additional specific interactions (H-bonding, additional electrostatic interactions *etc*…). The catalytic activity of the composites and of the free MP8 was evaluated both in the oxidation of a typical peroxidase substrate (ABTS) and in a more challenging reaction, the oxidation of thioanisole derivatives by hydrogen peroxide. MP8@MIL-101(Cr) and MP8@MIL-101(Cr)-NH_2 showed similar catalytic activities, due to the similar microenvironment of their structures in terms of surface charge and acidity, whereas MP8@MIL-101(Cr)-SO_3H showed a poor catalytic activity probably due to its high acidity, which may have led to the deactivation of MP8.

In this work, the preparation, purification and characterization of MP8 were carried out by Dr. R. Ricoux and myself. Most of the synthesis and characterizations of MIL-101(Cr)-X and the composites MP8@MIL-101(Cr)-X were performed by me. The Raman measurements were performed by Dr. I. Stenger. The synthesis optimization of MIL-101(Cr)-SO_3H was carried out by N. Ayoub. S. Salas assisted me with the catalytic tests of ABTS. The SEM images were recorded by Dr. F. Nouar. Dr. R. Ricoux and Kalani Kariyawasam-Bowithanthri assisted me with the sufloxidation reactions. The ICP-OES measurements were carried out by F. Bourdreux. Dr C. Sicard, Dr. R. Ricoux Prof. J.-P. Mahy, Prof. N. Steunou and Dr. C. Serre strongly supervised the work and Dr. C. Sicard and I, with the help and corrections of all authors, wrote the article.

Influence of MIL-101(Cr)-X functionalization on enzymatic immobilization and their efficiency for sulfoxidation reactions

Effrosyni Gkaniatsou, Rémy Ricoux,* Narjès Ayoub, Samanta Salas, Kalani Kariyawasam-Bowithanthri, Ingrid Stenger, Christian Serre, Jean-Pierre Mahy, Nathalie Steunou, Clémence Sicard*

N. Ayoub, S. Salas, E. Gkaniatsou, Dr. C. Sicard, Pr. N. Steunou
Institut Lavoisier de Versailles, UVSQ, CNRS, Université Paris-Saclay, Versailles, France.
clemence.sicard@uvsq.fr

Dr. I. Stenger
Groupe d'étude de la matière condensée, UVSQ, CNRS, Université Paris-Saclay, Versailles, France.

K. Kariyawasam-Bowithanthri, Dr. R. Ricoux, Pr. J.P. Mahy
Laboratoire de Chimie Bioorganique et Bioinorganique, Institut de Chimie Moléculaire et des Matériaux d'Orsay, UMR 8182, Université Paris Sud, Université Paris-Saclay, Orsay, France.
remy.ricoux@u-psud.fr

Dr. C. Serre
Institut des Matériaux Poreux de Paris, FRE 2000 CNRS Ecole Normale Supérieure, Ecole Supérieure de Physique et de Chimie Industrielles de Paris, PSL Research University, Paris, France.

1. Introduction

Organosulfur compounds are common pollutants of wastewaters and fossil fuels. Their presence in the latter is a significant issue as their combustion results in the emission of toxic SOx compounds. Therefore, desulfurization is often required and vast research has been conducted on the topic.[1,2] Among the developed techniques, oxidation has appeared as sustainable process that can also yield compounds that are of great importance for the synthesis of fine chemicals, biological active compounds, chiral auxiliaries *etc.*[3–6] A variety of catalysts has been employed over the years for such transformations, like polyoxometallates,[7] Schiff-base complexes[8] and titanium oxide.[9] Among them, peroxidase enzymes represent a very promising class of bio-catalysts, as they combine environmental friendly operational conditions and high selectivity.[10,11] However, a drawback of most peroxidases is their low operational stability, as a result of an easy oxidative degradation by H_2O_2 (natural co-substrate) and denaturation under acidic conditions.[12] Their difficult recovery and reusability may also hamper their application. These problems can be circumvented by their immobilization on solid supports, which provides the benefits of heterogeneous catalysis (recycling, shaping…) and may protect the enzyme from the operational conditions. Traditional inorganic and organic supports (sol-gel glasses, synthetic polymers, biopolymers) have been used to enhance the activity of peroxidases, during the oxidation of sulfides.[13–15] The combination of several supports may however be required to obtain hybrid matrices that address stability and leaching issues.[16,17] Besides, most of these materials do not present any long-range order, thereby limiting any control over the distribution of enzymes.

Recently, Metal-Organic Frameworks (MOFs), a class of hybrid crystalline porous materials, have been highlighted as promising immobilization matrices.[18–21] MOFs are built-up from the assembly of inorganic units and polytopic organic ligands. They combine the advantages of organic and inorganic supports, providing specific interactions with enzymes and robust structures. Their high surface area and porosity can ensure homogeneous immobilization of biomolecules with high loadings. Several immobilization techniques have been developed, but the entrapment of enzymes inside the porosity of preformed MOFs (*i.e*. cage inclusion) has been largely preferred for biocatalytic applications, since the 3D confinement of enzymes provides enhanced protection and stabilization.[22–24] The first studies were mainly focused on the biocatalysis of model reactions, with typical chromogenic substrates (e.g. 3,5-dit-butyl-catechol (DTBC), p-nitrophenyl butyrate (PNPB), 2,2'-azino-bis(3-ethylbenzothiazoline-6-sulphonic acid) (ABTS), *etc.*).[22,25,26] Only very recently, more challenging reactions such as nerve agent detoxification[27] and tumor specific prodrug activation[28] have been reported.

In this work, Microperoxidase 8 (MP8), a small heme octapeptide, was selected as a mini peroxidase enzyme that was shown to be able to catalyze the oxidation of sulfides in the presence of H_2O_2.[29] MP8 derives from the hydrolytic digestion of bovine Cytochrome c (Cyt c) and contains the amino acid residues 14 to 21 of Cyt c and the heme prosthetic group, whose iron(III) ion is bound to His 17 of this octapeptide. MP8 possesses a dual catalytic activity (peroxidase- and Cytochrome P450-like reactions) that allows the selective oxidation of

organosulfur compounds.[29] However, the catalytic activity of MP8 is usually hampered by high concentrations of H_2O_2 and acidic conditions.[30] We have recently demonstrated that MP8 encapsulation in nanoparticles of MIL-101(Cr) enabled its protection and stabilization, under these conditions.[31] It was thus of interest to investigate the activity of MP8 encapsulated in MIL-101(Cr) for the catalysis of a more challenging reaction such as sulfoxidation. Accordingly, the oxidation of sulfides such as thioanisole derivatives by hydrogen peroxide was studied. The reactivity of para-substituted thioanisole derivatives is known to increase with electron donating groups and decrease with electron withdrawing groups as a result of the modulation of the electronic density on the sulfur atom.[32] Several thioanisole derivatives bearing substituting groups: -H, $-OCH_3$ (strong activator *via* resonance effect), $-CH_3$ (weak activator *via* inductive effect) and $-NO_2$ (strong deactivator *via* resonance and inductive effect) were thus selected to study their influence on the catalytic activity of free and immobilized MP8.

Furthermore, while some key parameters for designing optimized MOF-enzyme systems have been highlighted, the influence of pending functional groups in the MOF frameworks on the stability and activity of encapsulated enzymes has been rarely investigated. Functional groups may promote stabilizing interactions between the MOF and the enzyme, enabling higher loadings and/or enhancing its catalytic activity. Among the important factors for the selection of MOF matrices for the cage inclusion of enzymes, three criteria appeared as critical. The size matching between the enzyme size and the pores apertures is a prerequisite for a successful immobilization. The presence of interconnected hierarchical porosity that allows enzyme encapsulation in larger pores, while preserving a free porosity for the diffusion of substrates was shown to lead to biocatalysts with superior performances than isolated 1-D channel porous system.[25] Finally, MOFs nanoparticles have been shown to favor substrate diffusion compared to micron-sized MOFs.[33] All of the aforementioned requirements are fulfilled by the water stable nanoMIL-101(Cr) material.[34] MIL-101(Cr) has a high hierarchical, interconnected mesoporosity (cages of 2.9 nm and 3.4 nm) (Figure 3-1), compatible with the size of MP8 (3.3 × 1.1 × 1.7 nm). Once the enzyme is immobilized, part of the porosity can remain accessible for the diffusion of substrates. Interestingly, various functionalized MIL-101(Cr) analogs (some of at the nanoscale) had already been reported.[35–37] Among them, we focused on MIL-101(Cr) bearing hydrophilic substituents to induce a good affinity with the hydrophilic MP8 enzyme.[38] On the contrary, hydrophobic environments can promote the denaturation of hydrophilic enzymes.[39] MIL-101(Cr)-NH_2 was selected due to the potential interactions between the MOF's amino groups and the four free carboxylic acid groups of MP8. To complement the study, another functionalized MOF, MIL-101(Cr)-SO_3H was taken for its different acidic properties. MP8 was encapsulated in the three MOFs. MP8@MIL-101(Cr)-X (X = H, NH_2, SO_3H) materials were structurally characterized and Raman spectroscopy was employed to investigate the structure of the MP8 molecules after their immobilization. The catalytic activity of the MP8@MIL-101(Cr)-X along with the protecting effect of the MOF matrices against acidic conditions were evaluated first toward the oxidation of a typical peroxidase substrate, 2,2´-azino-bis(3-ethylbenzothiazoline-6-sulphonic acid) (ABTS). Their catalytic

activity toward the oxidation of thioanisole derivatives with various electron donating and electron withdrawing groups was also studied in a second time.

2. Experimental Section

Materials

All chemicals were purchased from commercial sources and used without any further purification: $Cr(NO_3)_3 \cdot 9H_2O$ (98.5% Alfa Aesar), terephthalic acid (98 %, Sigma Aldrich), 2-animoterephthalic acid (> 98 %, TCI Chemicals), 2-sulfoterephthalic acid monosodium salt (> 98 %, TCI Chemicals), Cytochrome c from bovine heart (≥ 95 %, Sigma-Aldrich). Thioanisole (> 99 % TCI Chemicals), 4-nitrothioanisole (99 %, ACROS Organics), 4-methylthioanisole (> 99 %, TCI Chemicals), and 4-methoxythioanisole (99 %, ACROS Organics).

Synthesis of MOFs

MIL-101(Cr) was synthesized following a reported microwave-assisted hydrothermal synthesis.[34] MIL-101(Cr)-NH_2 was synthesized following a reported hydrothermal synthesis.[35] For the synthesis of MIL-101(Cr)-SO_3H, 400 mg of $Cr(NO_3)_3 \cdot 9H_2O$ (1 mmol) and 840 mg of 2-sulfoterephthalic acid (3 mmol, BDC-SO_3H) were added in a 15 mL Teflon reactor and dissolved in 5 mL of a 27 mM tetramethylammonium hydroxide (TMAOH) solution. The reaction mixture was heated under autogenous pressure at 190 °C for 24 h. After cooling at room temperature, the solid product was isolated by centrifugation and washed three times with H_2O and three times with absolute ethanol. The resulting particles were kept as a suspension in ethanol.

Synthesis of Microperoxidase 8

MP8 was prepared and purified as described previously in the literature.[40] Briefly, 400 mg of Cyt c were mixed with 10.4 mg of pepsin and dissolved in 5 mL of H_2O. The pH of the solution was adjusted to 2.6 with HCl (1 M). The mixture was incubated for 1 h at 37°. After a second addition of 10.4 mg of pepsin, the pH was adjusted to 2.6. The incubation continued for 5 h and the main product of the reaction was microperoxidase 11 (MP11). The pepsin activity was quenched by raising the pH to 9 with NH_4HCO_3 solution (1 M). 8 mg of trypsin were then added for the digestion of MP11 to MP8 and the mixture was incubated at 37°C overnight. MP8 was collected from the reaction mixture by gel filtration chromatography (biogel P6; 4 × 100 cm). The purified MP8 was lyophilized and stored at 4°C. The concentration of the MP8 solutions were calculated using the reported extinction coefficient, $\varepsilon_{396} = 1.57 \times 10^5\ M^{-1} \cdot cm^{-1}$.[40]

Characterizations

Powder X-ray diffraction was carried out with a Siemens D5000 diffractometer (θ-2θ), with Cu radiation. Infrared spectra were collected with a ThermoScientificNicolet 6700 FT-IR. Thermogravimetric analyses (TGA) were performed on a Mettler Toledo TGA/DSC 1, STAR®System apparatus under O_2 flow between room temperature and 700 °C, with a heating speed of 3 °C/min. Micro-Raman spectra were collected on a Horiba Jobin Yvon Labram HR 8500 (confocal) spectrometer, with an excitation wavelength of 488 nm and P=1.175 mW.

Scanning electron microscopy (SEM) images were recorded on a JEOL JSM-7001F microscope, using gold-coated samples. Dynamic light scattering (DLS)/ζ-potential measurements were performed on a Malvern Instrument Zetasizer Nano ZS. Inductively coupled plasma optical emission spectroscopy (ICP-OES) was carried out with an Agilent 720 Series with axially-viewed plasma and with a Cr/Fe calibration curve of 50-30,000 ppb. Ultraviolet–visible (UV-vis) spectra were collected on a PerkinElmer LAMBDA 750 UV/Vis/NIR Spectrophotometer. Gas chromatography analyses were performed with a SHIMADZU GC-2014A, equipped with a Zebron ZB Semi Volatiles column (30 m × 0.25 mm × 0.25 mm).

ζ-potential measurements

The ζ-potential of MP8 and MIL-101(Cr)-X particles as a function of pH were measured with aqueous suspensions of 0.1 mg/mL. Prior to each measurement, the sample was sonicated in an ultrasonic bath for 15 min for complete dispersion of the nanoparticles.

Immobilization of MP8 into MIL-101(Cr)-X

An aqueous solution of MP8 (1 mg/mL) was mixed with the respective MIL-101(Cr)-X particles, suspended in ethanol (5 mg/mL). The pH of the mixtures was adjusted at pH 5 for MIL-101(Cr) and MIL-101(Cr)-NH_2, and at pH 3 for MIL-101(Cr)-SO_3H. The mixtures were incubated at 37°C and gently shaken for 48 h. The immobilized MP8@MIL-101(Cr)-X catalysts were washed several times with H_2O to remove loosely bound enzyme molecules from the MOF surface and were stored at 4°C in aqueous suspensions. The MP8 loadings were evaluated by inductively coupled plasma - optical emission spectrometry (ICP-OES), through the quantification of Cr and Fe concentrations derived from the MOFs and the enzyme, respectively (samples preparation is described in SI).

Imidazole coordination studies

The reactions were performed with 1 μM catalyst (free MP8, MP8@MIL-101(Cr) and MP8@MIL-101(Cr)-SO_3H) in the presence of increasing concentrations of imidazole (ImH) in phosphate buffer (0.01 M) at pH 7. With ImH addition, the initial maximum absorbance wavelength of MP8-Fe(III) (λ_{max}= 396 nm) progressively shifted to λ_{max}= 404 nm, due to the formation of the MP8-Fe(III)(ImH) complex.[41]

Oxidation of ABTS by free MP8 and MP8@MIL-101(Cr)-X

The catalytic activity of the free MP8 and MP8@MIL-101-X was evaluated using a typical peroxidase substrate 2,2´-azino-bis(3-ethylbenzothiazoline-6-sulphonic acid) (ABTS), which was catalytically oxidized in the presence of H_2O_2 into the $ABTS^{\cdot+}$. The activity was measured by monitoring the increase in absorbance at 420 nm over time, due to the formation of $ABTS^{\cdot+}$ (ε_{420}=3.6 × 10^4 M^{-1}·cm^{-1}).[42] The reactions were typically performed with 2 mM ABTS, 0.35 μM MP8 (free MP8 and MP8@MIL-101-X), 0.1-1.8 mM H_2O_2 in citrate buffer (0.01 M) at pH 5 or in phosphate buffer (0.01 M) at pH 7 at room temperature with a total volume of 3 mL. The total reaction time was fixed to 300 sec. The reaction rates were calculated by the slope of the absorbance (at 420 nm) over time for the first 20 sec of the reaction.

Sulfoxidation reactions catalyzed by free and immobilized MP8@MIL-101-X

Typically, the reactions were performed with 1 mM of the respective thioanisole substrate (thioanisole, 4-nitrothioanisole, 4-methylthioanisole, and 4-methoxythioanisole), 1 µM MP8 (either as free MP8 or MP8@MIL-101-X), and 0.5 mM H_2O_2 in a mixture 80:20 v/v phosphate buffer (0.01 M, pH 7):CH_3CN, at room temperature, under stirring with a total volume of 0.5 mL. The total reaction time was fixed to 1 h. Acetophenone was added after 1 h as the internal standard for GC analysis. The sulfoxidized products were collected by extracting the organic phase with ethyl acetate and analyzed by GC. Retention times of respective sulfoxides: 7.4 min (thioanisole), 9.2 min (4-nitrothioanisole), 8.4 min (4-methylthioanisole) and 9.6 min (4-methoxythioanisole) and 4 min for internal standard.

3. Results and Discussion

MIL-101(Cr)-X

MIL-101(Cr) and two functionalized forms were selected, MIL-101(Cr)-NH_2 and MIL-101(Cr)-SO_3H, based on their difference in polarity and acidity as well as the surface charge of particles. These physico-chemical properties of MOFs may affect their interaction with MP8. MIL-101(Cr) and MIL-101(Cr)-NH_2 (Figure 3-1) were synthesized following already reported protocols.[34,35] For MIL-101(Cr)-SO_3H, a novel synthetic protocol was developed to avoid the use of toxic chemicals (e.g. Cr(VI) - CrO_3[43] or hydrofluoric acid[44]) and reduce the reaction time. The synthetic conditions were based on the protocol of MIL-101(Cr) reported by Yang *et al*, involved the use of tetramethylammonium hydroxide (TMAOH) as a base to increase the reaction pH to 6, improve the solubility of terephthalic acid and thus the sample crystallinity.[45] The nature of the chromium precursor ($Cr(NO_3)_3{\cdot}9H_2O$) as well as the metal cation:ligand:TMAOH molar ratio were found to be key parameters for the successful synthesis of MIL-101(Cr)-SO_3H.

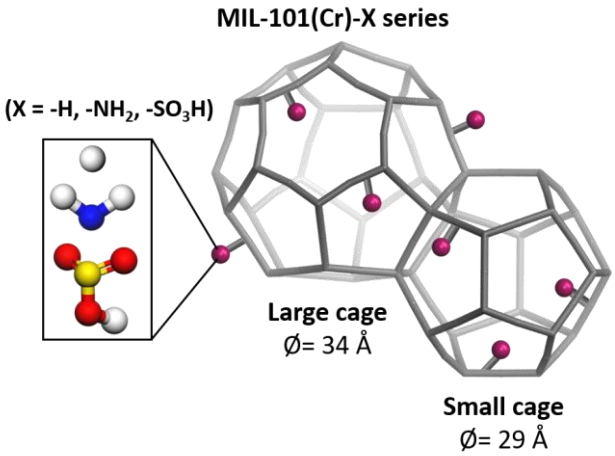

Figure 3-1: Structure of MIL-101(Cr)-X (X= -H, NH_2, -SO_3H) with an MTN topology, containing interconnected cages with diameters of 34 and 29 Å, respectively.

As indicated from the X-ray powder diffraction (XPRD) patterns in Figure 3-2, the diffraction peaks of MIL-101(Cr)-X are in agreement with the calculated pattern of MIL-101(Cr). The main

difference between the MIL-101(Cr)-X analogs concerns the crystallinity that was lower for MIL-101(Cr)-NH_2 and higher for MIL-101(Cr)-SO_3H. The broad peaks are consistent with the small particle size: ~50 nm for MIL-101(Cr), ~ 70 nm MIL-101(Cr)-NH_2 and ~200 nm for MIL-101(Cr)-SO_3H, as indicated by SEM images in Figure S1. The particle size of these MOFs are in the nanoscale, which favors the diffusion kinetics of the reactants in the catalytic process.[23,33] MIL-101(Cr)-SO_3H was further characterized by elemental analysis (C: 29.4 ± 0.3 % and S: 6.4 ± 0.1 %), indicating that 64 % of the ligands in the MOF's framework contained the sulfonic groups. The incomplete substitution can be explained by the partial degradation of some sulfonic groups during the synthesis of the MOF. Moreover, the purity of the starting ligand (98%) could also influence this substitution, since the functionalized and non-modified ligand may not present the same reactivity.

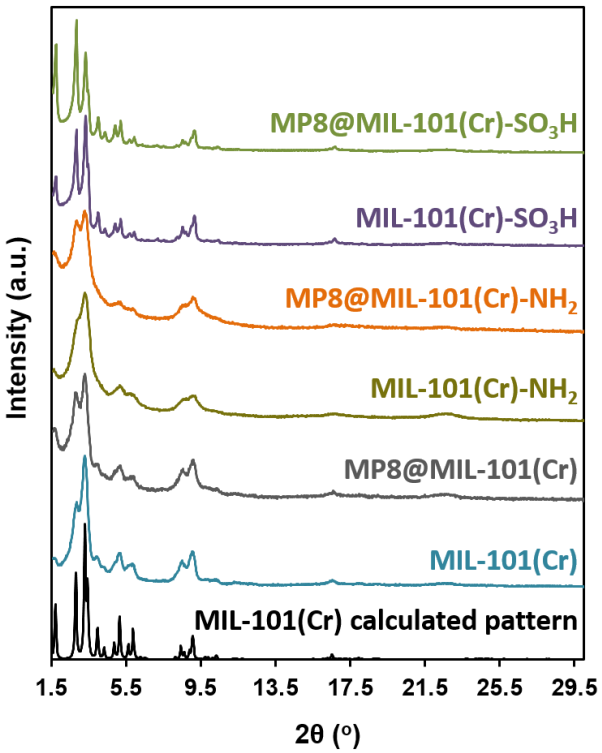

Figure 3-2: PXRD patterns prior and after immobilization of MP8 of MIL-101(Cr), MIL-101(Cr)-NH_2, MIL-101(Cr)-SO_3H and the calculated pattern of MIL-101(Cr).

MP8 immobilization within MIL-101(Cr)-X

Prior to the immobilization, the possible electrostatic interactions between MP8 molecules and MOF particles were evaluated by measuring the ζ-potential as a function of pH, as shown in Figure 3-3. MIL-101(Cr) and MIL-101(Cr)-NH_2 were positively charged under acidic conditions. This positive charge may be attributed to the carboxylic acid groups and the water molecules coordinated to the open metal sites.[46] For MIL-101(Cr)-NH_2 the positive charge under acidic conditions can also arise from the protonation of the amino group. The point of zero charge was found to be 7 for MIL-101(Cr) and 8 for MIL-101(Cr)-NH_2. The particle charge of MIL-101(Cr)-SO_3H was negative over the whole pH range due to the presence of the negatively charged SO_3^- groups. In the case of MP8 (Figure 3-4), a positive charge was observed

at pH ≤ 4, due to the protonation of the proximal His18 in agreement with the $pK\alpha_1$ = 4.4 reported in the literature.[47] Above this pH, MP8 showed a negative charge since the carboxylic acid groups of the enzyme and the water molecule, coordinated to the sixth axial position of Fe(III), were deprotonated (Figure S2).

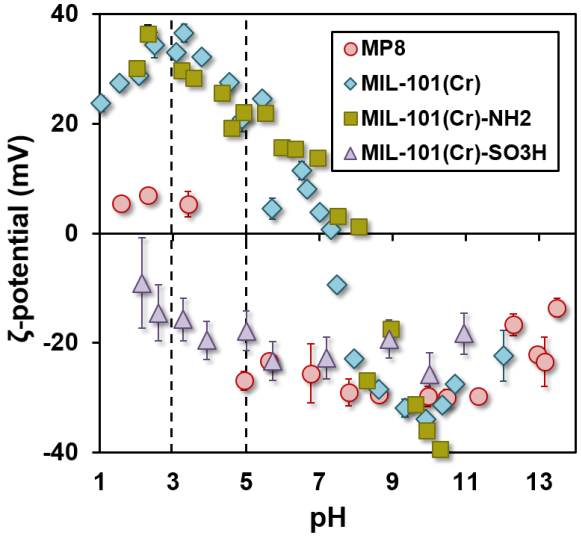

Figure 3-3: ζ-potential measurements of MP8 (red circles), MIL-101(Cr) (blue diamonds), MIL-101(Cr)-NH_2 (green squares) and MIL-101(Cr)-SO_3H (purple triangles) as a function of pH. Errors bars are the standard deviation of three measurements.

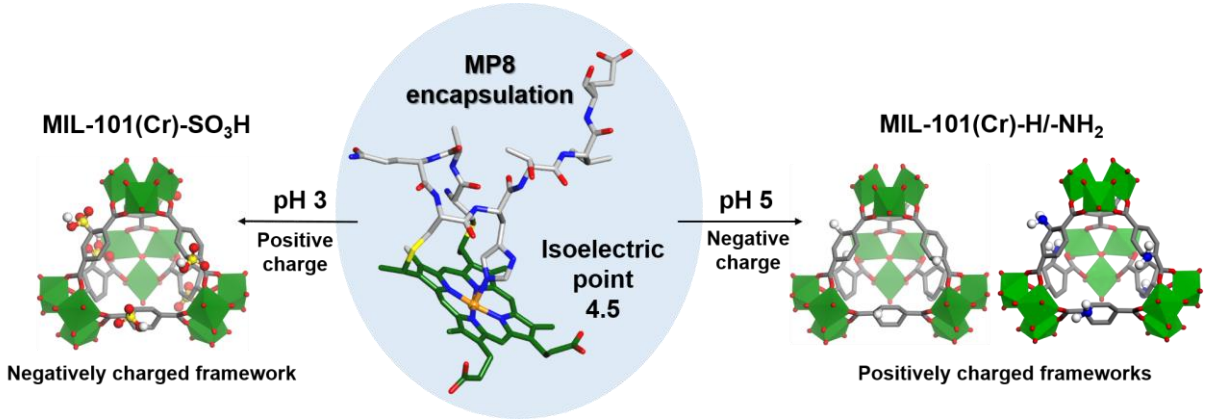

Figure 3-4: Molecular structure of microperoxidase 8, containing an Fe(III) porphyrin and the amino acid residues 14-21 of Cytochrome c (Structural data were obtained from the structure resolution of PDB·1OCD).[48] Schematic representation of the immobilization process: at pH 3, MP8 is positively charged and can be immobilized in the negatively charged MIL-101(Cr)-SO_3H, whereas at pH 5 MP8 is negatively charged and can be immobilized in the positively charged MIL-101(Cr) and MIL-101(Cr)-NH_2.

The MP8 immobilization was performed by simply mixing MP8 with MIL-101(Cr)-X at room temperature for 48 hours. Based on the ζ-potential measurements, the pH was fixed to 5, where attractive electrostatic interactions between MP8 and MIL-101(Cr), MIL-101(Cr)-NH_2 are present. The MP8 loadings of the resulting MP8@MIL-101(Cr)-X materials were determined experimentally by inductively coupled plasma atomic emission spectroscopy (ICP-OES) based on the ratio of Fe and Cr found in MP8 and MIL-101(Cr)-X. The MP8 loadings were also confirmed from the remaining MP8 amounts in the supernatants measured by UV-Vis

spectroscopy. As seen in Table 3-1, at pH 5, a 5 % w/w loading of MP8 was measured in the MP8@MIL-101(Cr) material, while a higher content of 8.1 % w/w was found in MP8@MIL-101(Cr)-NH_2. The encapsulation of MP8 in MP8@MIL-101(Cr)-SO_3H at pH 5 was not successful. This is consistent with repulsive coulombic interactions between MP8 and MIL-101(Cr)-SO_3H, since they were both negatively charged at pH 5. The immobilization was thus performed at pH 3, where opposite charges between MP8 and MIL-101(Cr)-SO_3H were observed (Figures 3-3 and Figure 3-4). The obtained MP8@MIL-101(Cr)-SO_3H showed a higher loading of 7.2 % w/w, demonstrating that coulombic interactions are an important driving force in the immobilization procedure. The higher loading of MP8 in functionalized MOFs than in the bare MIL-101(Cr) was not expected when considering the reduced free volume of the cages of functionalized MOFs resulting from the presence of the pending functional groups. Therefore, this higher enzyme loadings may result from the presence of strongly anchored MP8 molecules at the external surface of MOFs, due to specific interactions (H-bonding, additional electrostatic interactions *etc*…) between the -NH_2/NH_3^+ and - SO_3^- groups and the enzyme molecules. These results are in agreement with previous immobilization studies, in which the amino-functionalization of porous matrices resulted in higher enzyme loadings.[49] On the contrary, any MP8 molecules loosely bound at the external surface of the bare MIL-101(Cr) could be successfully removed by the washing procedure of the particles, leaving only the MP8 molecules that were confined inside the porosity.

Table 3-1: MP8 loading in MIL-101(Cr)-X determined by ICP-OES

Catalyst	MP8 loading (w/w %)
MP8@MIL-101(Cr)	5.0 ± 0.3
MP8@MIL-101(Cr)-NH_2	8.1 ± 0.5
MP8@MIL-101(Cr)-SO_3H (pH 2)	7.2 ± 0.1
MP8@MIL-101(Cr)-SO_3H (pH 5)	-

Characterization of MP8@MIL-101(Cr)-X

As revealed from the PXRD patterns shown in Figure 3-2, the crystalline structure of MIL-101(Cr)-X was preserved after immobilization of MP8 molecules. The UV-vis spectra (Figure S3) showed the characteristic Soret band of MP8 at 396 nm for MP8@MIL-101(Cr) and MIL-101(Cr)-SO_3H, which confirmed the presence of immobilized MP8 molecules. The MP8 Soret band could not be clearly distinguished in MP8@MIL-101(Cr)-NH_2 as it superimposed with a broad band arising from the MOF in the 356-400 nm range. From the FT-IR spectra (Figure S4), once immobilized in the MIL-101(Cr)-X particles, the characteristic amide I, amide II and amide III vibrations of MP8 (1652, 1540 and 1413 cm^{-1}, respectively) could not be clearly observed, as they overlap with the carboxylate vibration bands ($\nu(CO)_{as}$ 1628, $\nu(CO)_s$ 1394 cm^{-1}) of the MOFs. However, a slight broadening of the bands in 1620-1510 cm^{-1} region was observed for MIL-101(Cr) and MIL-101(Cr)-NH_2 that may be attributed to the presence of MP8 molecules. Raman spectroscopy was employed in order to further examine the presence of MP8 molecules in the MOF particles and investigate possible interactions. Figure 3-5 shows the

Raman spectra of free MP8, MIL-101(Cr)-X and MP8@MIL-101(Cr)-X and the detailed attributions of the bands are reported in Table S1. The spectra of MP8@MIL-101(Cr)-X showed the presence of characteristic vibration modes of both the MP8 and MIL-101(Cr)-X and thus confirmed the immobilization of MP8 in all MOF particles. Note that, due to the low crystallinity of MIL-101(Cr)-NH_2, its vibration bands are broad and cannot be clearly identified. MIL-101(Cr), MIL-101(Cr)-NH_2, and MIL-101(Cr)-SO_3H exhibited vibrations characteristic of the carboxylate stretching mode (1615, 1580 and 1607 cm^{-1}, respectively) and two stretching modes of the *v*(C=C) of the aromatic system (1453/1154 cm^{-1}, 1393/1139 and 1445/1143 cm^{-1}, respectively). The spectra of MIL-101(Cr) and MIL-101(Cr)-SO_3H display also the symmetric stretching band *v*(Cr-O) of the chromium trimers (869 and 811 cm^{-1}, respectively).[50] In the case of MIL-101(Cr)-SO_3H, two additional bands at 1100 cm^{-1} and 763 cm^{-1} can be assigned to the *v*(S=O) and *v*(C-S) modes of the sulfonic groups. The frequencies of the skeletal stretching modes of the heme in MP8 are located in the high-frequency region between 1300 and 1600 cm^{-1}.[41] The bands related to the Fe(III) coordination and spin state, v_{10}, v_3, and v_2, are summarized in Table 3-2 (Figure S5).[51] In the spectrum of free MP8, these vibration bands were indicative of the presence of both penta-coordinated high-spin (5C-HS) and hexa-coordinated low-spin (6C-LS) iron species. The 5C-HS form corresponds to the monomeric form of MP8, whereas the 6C-LS form could be attributed to intermolecular bonding between MP8 molecules (large aggregates).[41,52] The oxidation state marker band, v_4, was surprisingly observed for free MP8 at 1359 cm^{-1}, which is characteristic of a reduced Fe(II)MP8, instead of ~1370 cm^{-1} as expected for Fe(III)MP8.[53] The reduction of Fe(III) center to Fe(II) in free MP8 was possibly due to the laser irradiation of the sample, as similar changes have been reported for other heme containing enzymes.[54] The v_{10}, v_3, and v_2 modes of MP8@MIL-101(Cr)-X are characteristic of iron 5C-HS species, although not all modes were visible due to overlapping with the MIL-101(Cr)-X modes. It may suggest that the immobilized MP8 molecules were mainly in the monomeric form and thus their dispersion in the MOF frameworks avoided their aggregation. Moreover, the v_4 modes of MP8@MIL-101(Cr) and MP8@MIL-101(Cr)-SO_3H indicated a Fe(III) oxidation state for MP8 (1371 cm^{-1}) that is thus not reduced under the laser irradiation, suggesting a protection of MP8 by its encapsulation into the MOF. Other characteristic modes of MP8, v_{29} and v_{21} (1398 and 1313 cm^{-1}), were slightly shifted in the cases of MIL-101(Cr) (1405 and 1309 cm^{-1}) and MIL-101(Cr)-SO_3H (1404 and 1309 cm^{-1}), indicating interactions between the MP8 molecules and the frameworks.[55]

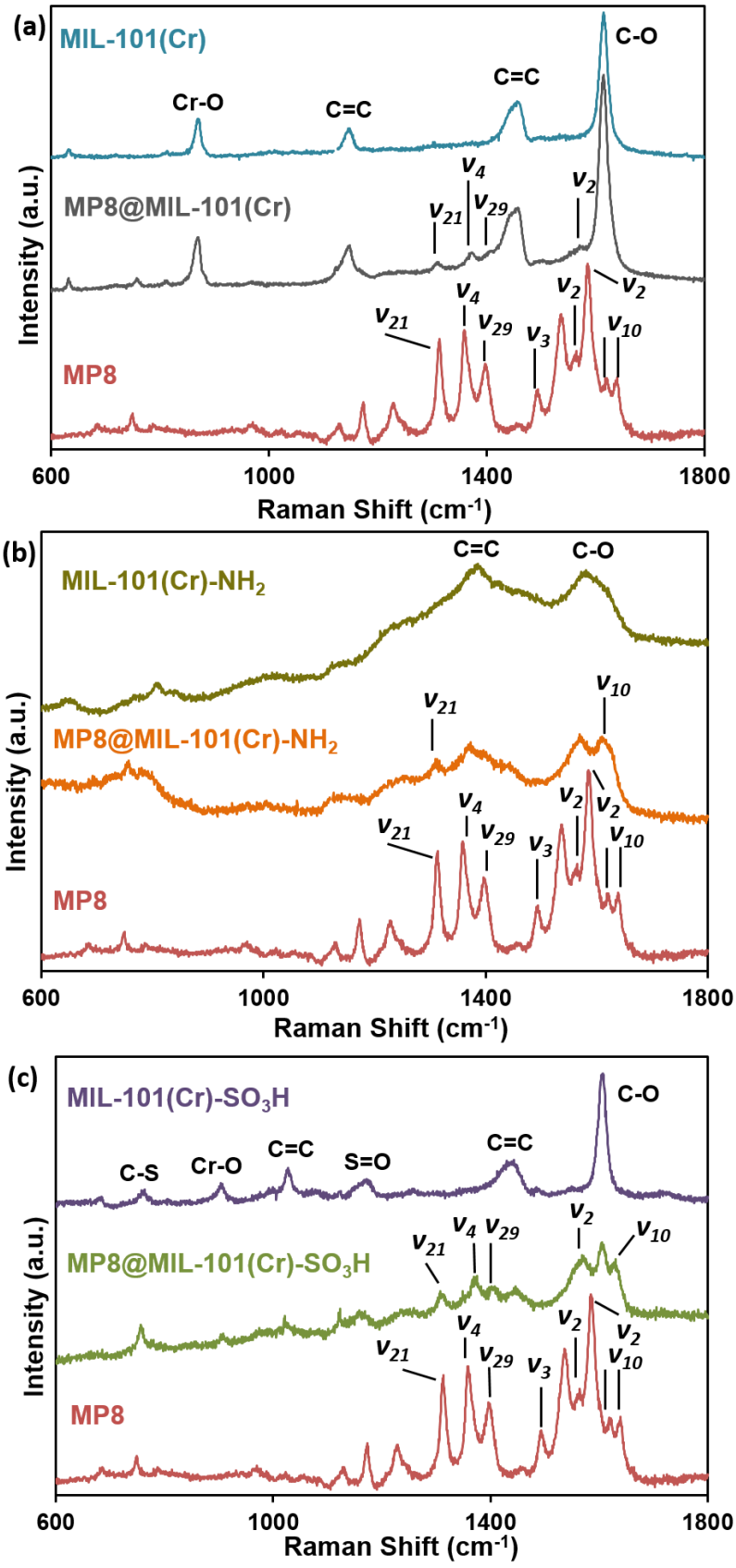

Figure 3-5: Raman spectra of (a) free MP8 (red), MP8@MIL-101(Cr) (grey) and MIL-101(Cr) (blue); (b) free MP8 (red), MP8@MIL-101(Cr)-NH_2 (orange) and MIL-101(Cr)-NH_2 (brown); (c) free MP8 (red), MP8@MIL-101(Cr)-SO_3H (green) and MIL-101(Cr)-SO_3H (purple).

Table 3-2: High-frequency Raman modes (cm^{-1}) of free MP8 and immobilized MP8@MIL-101(Cr), MP8@MIL-101(Cr)-NH_2 and MP8@MIL-101(Cr)-SO_3H

Catalyst	Hexacoordinated low-spin state			Pentacoordinated high-spin state			ν_4
	ν_{10}	ν_3	ν_2	ν_{10}	ν_3	ν_2	
MP8	1639	-	1585	1620	1456	1565	1359 (Fe^{2+})
MP8@MIL-101(Cr)	Overlap ν(C-O)	Overlap ν(C=C)	-	Overlap ν(C-O)	Overlap ν(C=C)	1572	1371 (Fe^{3+})
MP8@MIL-101(Cr)-NH_2	-	-	Overlap ν(C-O)	1622	1451	Overlap ν(C-O)	-
MP8@MIL-101(Cr)-SO_3H	-	Overlap ν(C=C)	-	1629	Overlap ν(C=C)	1568	1371 (Fe^{3+})

Accessibility of immobilized MP8

The sixth axial position of Fe(III) in MP8 is generally occupied by a water molecule and it can easily be replaced by ligands with high binding affinity for the Fe(III) such as imidazole (ImH). ImH has been used in previous studies[56] to evaluate the accessibly of the Fe center of MP8 as its coordination to the Fe(III) results in a spectral evolution that can be easily monitored by UV-vis spectroscopy. The Soret band at 396 nm of free MP8 gradually red shifts to 404 nm due to the formation of MP8Fe(III)(ImH) complex. The accessibility of Fe(III) was evaluated for free MP8, and for the immobilized MP8@MIL-101(Cr) and MP8@MIL-101(Cr)-SO_3H. MP8@MIL-101(Cr)-NH_2 was not studied due to its poor crystallinity. For all samples, a red shift was observed upon addition of imidazole, in agreement with the formation of MP8Fe(III)(ImH), thereby indicating that the Fe center of MP8 remained accessible upon immobilization (Figure S6). The amounts of imidazole needed to reach the complete coordination of the MP8 Fe(III) center was 0.57, 3.7 and 7.83 mM for MP8, MP8@MIL-101(Cr) and MP8@MIL-101(Cr)-SO_3H, respectively. The higher amount of imidazole required for the immobilized MP8 suggested diffusional limitations, which was consistent with the inclusion of MP8 inside the mesoporosity of MIL-101(Cr)-X. However, the imidazole concentration required for the complete MP8 complexation in MP8@MIL-101(Cr)-SO_3H was two-times higher than that of MP8@MIL-101(Cr), suggesting important diffusion limitations in MIL-101(Cr)-SO_3H. It is possible that the presence of some MP8 molecules at the external surface of this MOF limit the diffusion of imidazole in the internal surface of the MOF and thus its coordination to the MP8 molecules that are confined in the cavities.

Evaluation of the catalytic activity of MP8@MIL-101(Cr)-X

The catalytic activity of free and immobilized MP8 molecules with similar MP8 content was evaluated using a typical peroxidase reaction: the oxidation of the chromogenic substrate ABTS to $ABTS^{\cdot+}$ (λ_{max} = 420 nm) in the presence of H_2O_2. No catalytic activity was detected for the three MOFs. Figure 3-6 shows the amounts of $ABTS^{\cdot+}$ formed after 300 sec, as well as the initial reaction rates, with increasing concentrations of H_2O_2 at pH 7. Free MP8 oxidized faster the ABTS and led to higher concentrations of oxidized substrate than MP8 immobilized into

the MOFs (kinetics of the catalytic reactions in Figure S7) after 300 s. This is in agreement with previous studies in which immobilized enzymes have shown slower kinetics due to diffusion barriers from the host matrix.[57] The amounts of $ABTS^{\cdot+}$ formed, as well as the rates of oxidation were similar for MP8@MIL-101(Cr) and MP8@MIL-101(Cr)-NH_2. However, considering the higher MP8 loading in MIL-101(Cr)-NH_2, the specific activity per gram of material is expected to be higher for MP8@MIL-101(Cr)-NH_2 than that of MP8@MIL-101(Cr) when similar amounts of MP8@MIL-101(Cr)-X materials are used. On the contrary, the catalytic activity of MP8@MIL-101(Cr)-SO_3H was low as shown by the moderate amounts of $ABTS^{\cdot+}$ converted and the almost negligible reaction rates. The acidic conditions (pH 3) necessary for the MP8 immobilization in MIL-101(Cr)-SO_3H may have led to the cleavage of the Fe(III)-His18 bond as a result of the protonation of the nitrogen atom bound to the iron and may be responsible for the loss of catalytic activity. Moreover, the presence of sulfonic acid groups of low pka (~ -7) did not favor the coordination of the His18 to the Fe(III) once MP8 was immobilized in MIL-101(Cr)-SO_3H. High H_2O_2 concentrations are known to be detrimental to the MP8 catalytic activity.[58] The MOF frameworks may provide protection against the oxidative degradation of MP8 due to the slower diffusion of reactant and thus may reduce local H_2O_2 concentrations, enhancing the catalytic activity. Importantly, by increasing the H_2O_2 concentration, the difference of the formed $ABTS^{\cdot+}$ amounts between free MP8 and immobilized MP8 in MIL-101(Cr) and MIL-101(Cr)-NH_2 decreased. For example, while at 0.1 mM H_2O_2, MP8@MIL-101(Cr) oxidized only 16.5 % and MP8@MIL-101(Cr)-NH_2 10.9 % $ABTS^{\cdot+}$ compared to free MP8 (100%), at 1.8 mM they oxidized 29.6 % and 25.8 % respectively. Thus, this increase in $ABTS^{\cdot+}$ amounts for immobilized MP8, at high H_2O_2 may indicate the protective effect of the frameworks. Since the reaction kinetics were slower for the MP8@MIL-101(Cr)-X, the oxidation of ABTS was also assessed for longer reaction times (1 hour). Figure 3-7 illustrated the $ABTS^{\cdot+}$ amounts formed after 1 hour, as well as the reaction kinetics for the free and the immobilized MP8 with 0.9 mM H_2O_2 and at pH 7. As observed, even though free MP8 reached the maximum $ABTS^{\cdot+}$ amount (35 µM) in less than 10 min, MP8@MIL-101(Cr) and MP8@MIL-101(Cr)-NH_2 oxidized higher amounts of ABTS in 1 h (48 µM). Furthermore, for free MP8, the absorbance of $ABTS^{\cdot+}$ decreased with time as a result of its over-oxidation to $ABTS^{2+}$ by H_2O_2.[59] Neither MP8@MIL-101(Cr) nor MP8@MIL-101(Cr)-NH_2 showed this effect, probably due to the stabilization of $ABTS^{\cdot+}$ by the MOFs framework, as previously reported.[60]

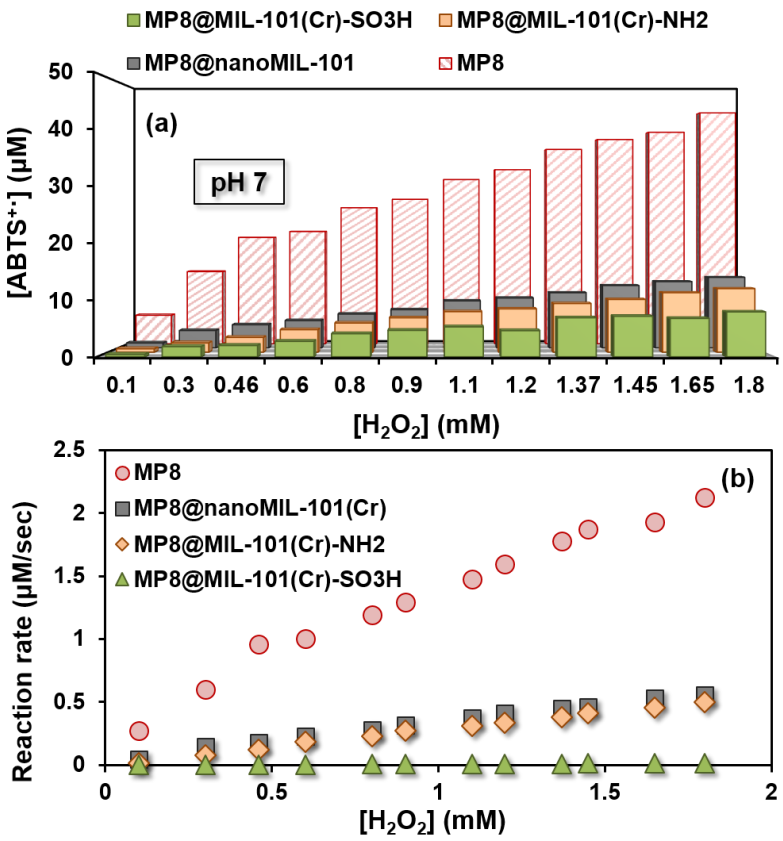

Figure 3-6: (a) $ABTS^{\bullet+}$ amounts and (b) reaction rates for the oxidation of ABTS in the presence of increasing concentration of H_2O_2 (0.1-1.8 mM) for similar amounts of free MP8 and MP8@MIL-101(Cr)-X in phosphate buffer at pH 7 for 300 sec of reaction. Errors bars are the standard deviation of three measurements.

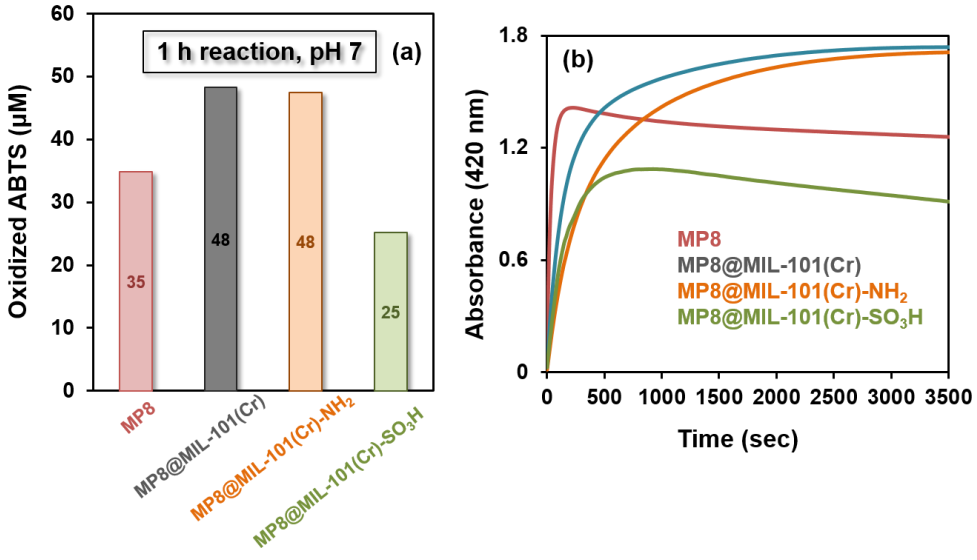

Figure 3-7: (a) $ABTS^{\bullet+}$ amounts with 0.9 mM H_2O_2, equivalent amounts of free MP8 and MP8@MIL-101(Cr)-X in phosphate buffer, pH 7 for 1 h reaction time, (b) the respective reaction kinetics.

In a previous work,[31] it has been demonstrated that the MOF framework could protect MP8 molecules under acidic conditions (pH 5) as a result of a confined micro-environment in the pores that limited the protonation of the axial His18. The protective role of the framework

was also examined for MIL-101(Cr)-NH_2 and MIL-101(Cr)-SO_3H. Figure 3-8 displays the $ABTS^{\cdot+}$ amounts after 300 s and the reaction rates of oxidation with increasing concentrations of H_2O_2, at pH 5 (kinetics of the catalytic reactions in Figure S8). MIL-101(Cr) and MIL-101(Cr)-NH_2 had a similar catalytic activity and both immobilized enzymes could catalyze the oxidation of higher amount of ABTS with faster reaction rates than free MP8, showing the protective role of the MOF framework toward MP8 catalytic activity. MP8@MIL-101(Cr)-SO_3H showed the lowest catalytic activity due to the acidic pore environment, as discussed above.

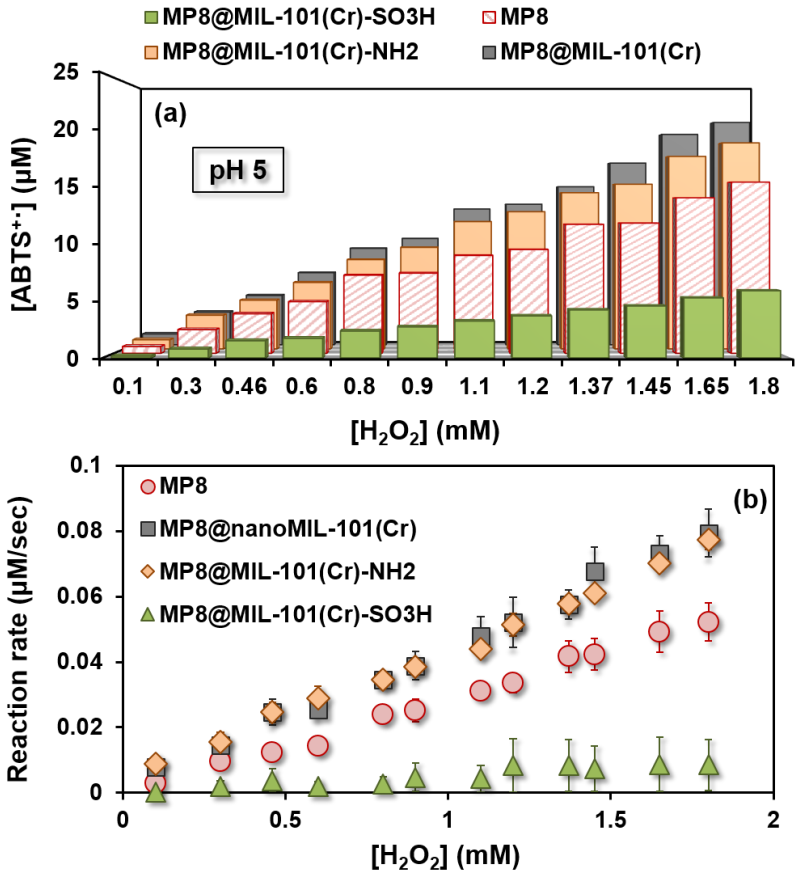

Figure 3-8: (a) $ABTS^{\cdot+}$ amounts and (b) reaction rates of the oxidation of ABTS in the presence of increasing concentration of H_2O_2 (0.1-1.8 mM) by equivalent amounts of free MP8 and MP8@MIL-101(Cr)-X at citrate buffer, pH 5 for 300 sec of reaction.

Catalytic oxidation of thioanisole derivatives to sulfoxides

The ability of free and immobilized MP8 to catalyze the sulfoxidation of different para-substituted thioanisole derivatives, in presence of H_2O_2 was investigated (Figure 3-9) and the obtained products were quantified by gas chromatography. The reactivity of para-substituted thioanisole derivatives for the electrophilic oxygen transfer reaction is known to increase with electron donating group (EDG), with the order 4-methoxythioanisole (strong activator *via* resonance effect) > 4-methylthioanisole (weak activator *via* inductive effect) > thioanisole > 4-nitrothioanisole (strong deactivator *via* resonance and inductive effect).[32]

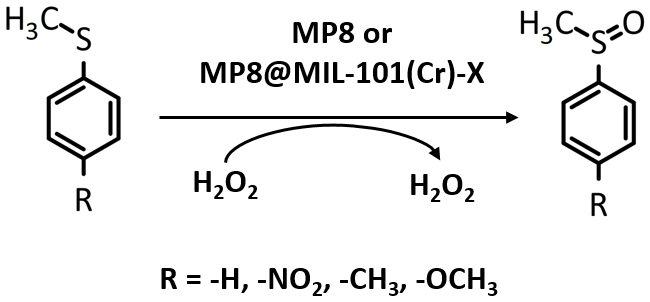

Figure 3-9: Oxidation of thioanisole derivatives catalyzed by free MP8 or MP8@MIL-101(Cr)-X, in presence of H_2O_2.

No product was detected in the absence of MP8 in a medium containing H_2O_2 and MIL-101(Cr)-X. As seen in Table 3-3 and Figure 3-10, the immobilized MP8@MIL-101(Cr)-X catalyzed the chemo-selective oxidation of thioanisole derivatives into the respective sulfoxides. MP8@MIL-101(Cr)-X catalysts led to lower yields in sulfoxides than the free MP8, in agreement with diffusional limitation as previously explained. The catalytic activity of the bio-catalysts followed the order MP8 > MP8@MIL-101(Cr) / MP8@MIL-101(Cr)-NH_2 > MP8@MIL-101(Cr)-SO_3H, also in agreement with the catalytic activity observed for the oxidation of ABTS. The most efficient conversion was achieved with the 4-methoxythioanisole derivative, bearing a strong EDG, that may activate the electrophilic oxygen transfer reaction as previously shown.[61] The 4-methylthioanisole derivative and thioanisole were also successfully converted. The sulfoxidation of the 4-nitrothioanisole was very limited when compared to the other thioanisole derivatives, as its phenyl ring was substituted with a strong electron withdrawing group (EWG, NO_2 that deactivated the sulfur atom for the electrophilic oxygen transfer reaction). While for free MP8 the impact of EDG groups led to a tremendous increase of the conversion of the thioanisole derivatives (+ 372 % increase in presence of -OCH_3), the impact was much less important for MIL-101(Cr)-X (+177 % and + 151 % increase in presence of -OCH_3 for MIL-101(Cr) and MIL-101(Cr)-NH_2, respectively). The MOF frameworks thus seem to reduce the impact of the substituting groups on MP8's reactivity for the sulfoxidation reactions. Based on the current results, it is not possible to explain this effect and further investigation is required.

Table 3-3: Amount of oxidized thioanisole derivatives obtained after 1 hour by the catalytic conversion with free MP8 and MP8@MIL-101(Cr)-X

	Oxidized product (µM)			
Thioanisole derivative	**MP8**	**MP8@MIL-101(Cr)**	**MP8@MIL-101(Cr)-NH_2**	**MP8@MIL-101(Cr)-SO_3H**
-H	43± 15	36 ± 8	35 ± 9	16 ± 7
-NO_2	3 ± 3	4 ± 3	4 ± 3	-
-CH_3	74 ± 12	47 ± 6	44 ± 3	32 ± 6
-OCH_3	161 ± 1	64 ± 2	53 ± 2	45 ± 5

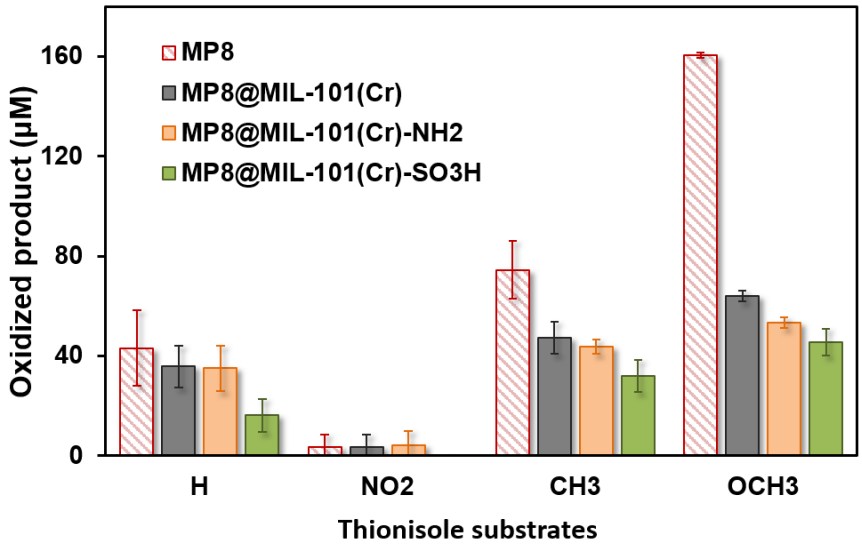

Figure 3-10: Sulfoxidized amounts of thioanisole derivatives with 0.5 mM H_2O_2 by equivalent amounts of free MP8 and MP8@MIL-101(Cr)-X, at 80:20 phosphate buffer (pH 7):CH_3CN for 1 h of reaction.

4. Conclusions

In conclusion, MIL-101(Cr), bearing different functionalized groups (-NH_2 and -SO_3H) were used for the immobilization of Microperoxidase 8 (MP8), with preservation of their crystalline structures. The electrostatic interaction between the MP8 molecules and the MOF matrix was found to be a key parameter for successful immobilization. Moreover, the presence of functional groups resulted in higher immobilized amounts of MP8 compared to the bare MIL-101(Cr). This may be attributed to specific interactions between the MP8 molecules and the functionalized groups that enabled strong adsorption of MP8 at the external surface of the functionalized MOFs. Raman spectroscopy was found to be an interesting tool to probe MP8 structure. The immobilized MP8 molecules were found to be dispersed in the MIL-101(Cr)-X matrices as monomers without aggregation. Furthermore, the shifts observed in the characteristic bands of MP8, suggested interactions between the enzyme molecules and the MOF matrices. The presence of the MOF frameworks seemed to protect the MP8 iron(III) from reduction by the laser irradiation. The catalytic activity was found to be similar for MP8@MIL-101(Cr) and MP8@MIL-101(Cr)-NH_2 at identical MP8 contents. However, MIL-101(Cr)-NH_2 immobilized higher amounts of enzyme and thus the specific activity per gram of material is expected to be increased. On the contrary, MP8@MIL-101(Cr)-SO_3H showed a very low catalytic activity. The acidic conditions for the encapsulation and the acidic environment of the MOF matrix may have caused the deprotonation of the histidine residue in MP8, which is detrimental for its catalytic activity. Similarly to the already reported protective nature of MP8@MIL-101(Cr), MP8@MIL-101(Cr)-NH_2 efficiently enhanced MP8's catalytic activity under acidic conditions. MP8@MIL-101(Cr) and MP8@MIL-101(Cr)-NH_2 were successfully used for the oxidation of thioanisole derivatives to sulfoxides. Similarly to free MP8, the immobilized enzymes were more reactive when sulfides bearing EDG groups were used.

However, the influence of the para-substituted groups on immobilized MP8 reactivity was much less important compared to free MP8.

Ackowledgements

This work was supported by the ANR-11-LABEX-0039 (labex charm3at). We thank Dr. M. Benzaqui and C. Livage for the SEM experiments, F. Bourdreux for ICP-OES measurements.

5. Supporting Information

Determination of the MP8 loading by ICP-AOS

The enzyme loading was measured by detecting the Fe present from the MP8 molecules and the Cr from the MIL-101(Cr)-X by ICP - OES.

Sample treatment: Typically, a sample was heated at 100 °C overnight to evaporate the remaining solvent. Afterwards, 1 mL of HCl (37%) was added and the sample was heated in a closed vial at 80 °C, overnight (16 h) for total mineralization. The sample was diluted to 40 mL with ultrapure H_2O before the analysis.

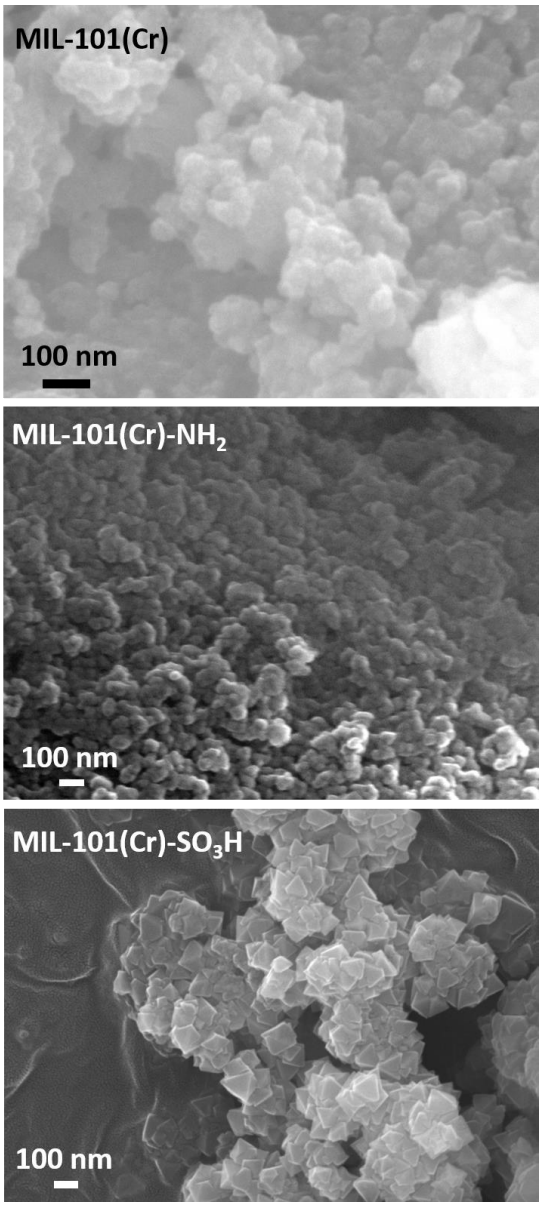

Figure S1: SEM images of MIL-101(Cr) (~ 50nm), MIL-101(Cr)-NH_2 (~ 70 nm) and MIL-101(Cr)-SO_3H (~ 200 nm).

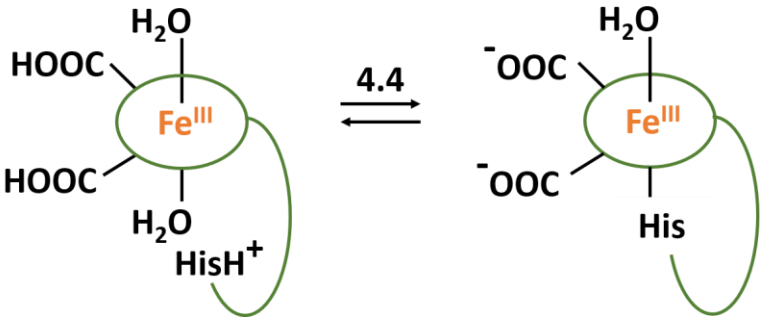

Figure S2: Schematic representation of His18 coordination to the Fe(III) of MP8 as a function of pH.

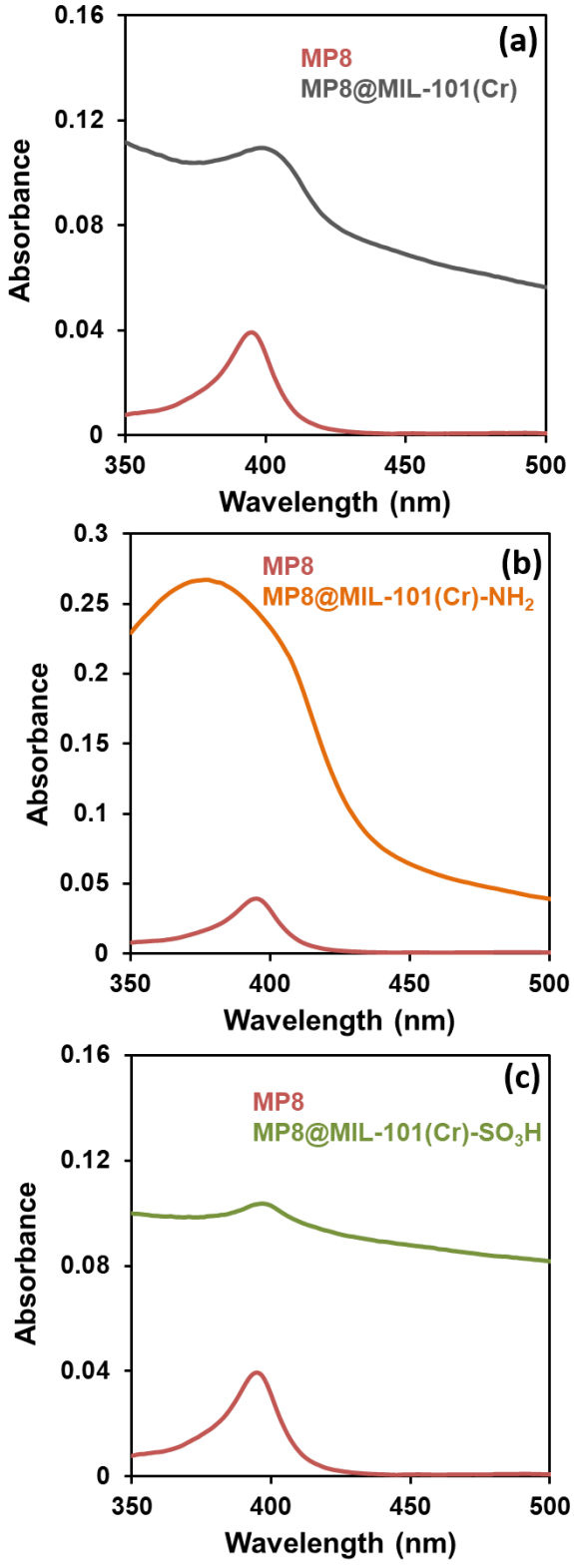

Figure S3: UV-vis spectra of (a) free MP8 and MP8@MIL-101(Cr),(b) free MP8 and MP8@MIL-101(Cr)-NH_2 and (c) free MP8 and MP8@MIL-101(Cr)-SO_3H.

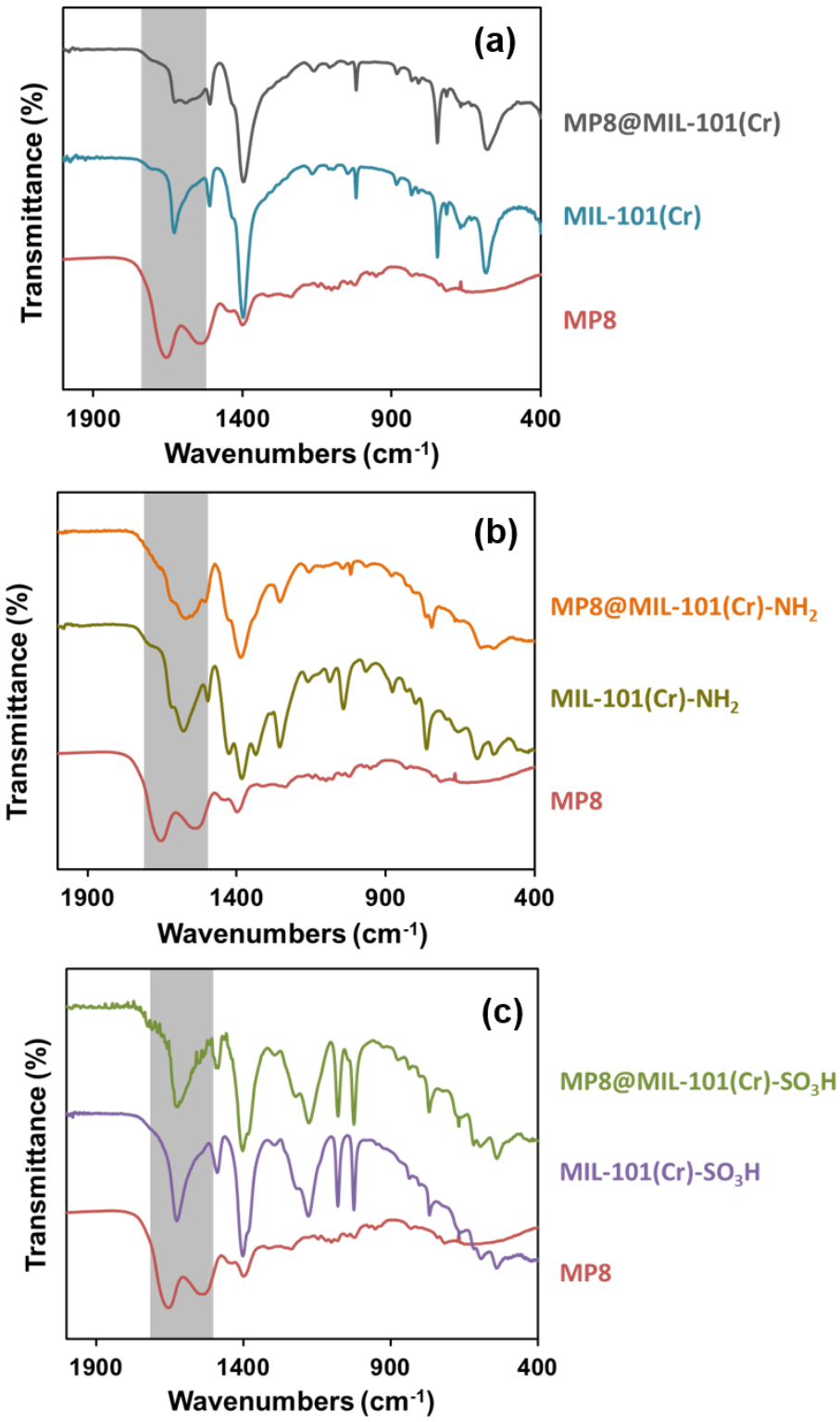

Figure S4: FT-IR spectra of (a) free MP8, MIL-101(Cr) and MP8@MIL-101(Cr),(b) free MP8, MIL-101(Cr)-NH_2 and MP8@MIL-101(Cr)-NH_2 and (c) free MP8, MIL-101(Cr)-SO_3H and MP8@MIL-101(Cr)-SO_3H.

Table S1: Raman modes (cm^{-1}) of free MP8, immobilized MP8@MIL-101(Cr)-X and MIL-101(Cr)-X

Sample	MP8 vibration bands						MIL-101(Cr)-X vibration bands				
	ν_{10}	ν_2	ν_3	ν_{29}	ν_4	ν_{21}	ν(C-O)	ν(C=C)	ν(Cr-O)	ν(S=O)	ν(C-S)
MP8	1639/ 1620	1585/ 1565	1456	1398	1359	1312					
MP8@MIL-101(Cr)	Overlap ν(C-O)	1527	Overlap ν(C=C)	1405	1371	1309	1614	1457/ 1152	871		
MP8@MIL-101(Cr)-NH_2	1622	Overlap ν(C-O)	-	Overlap ν(C=C)	-	1319	1579	1984			
MP8@MIL-101(Cr)-SO_3H	1629	1568	Overlap ν(C=C)	1404	1371	1309	1610	1451/ 1030	912	1169	754
MIL-101(Cr)							1615	1453/ 1154	869		
MIL-101(Cr)-NH_2							1580	1393			
MIL-101(Cr)-SO_3H							1607	1445/ 1143	811	1100	763

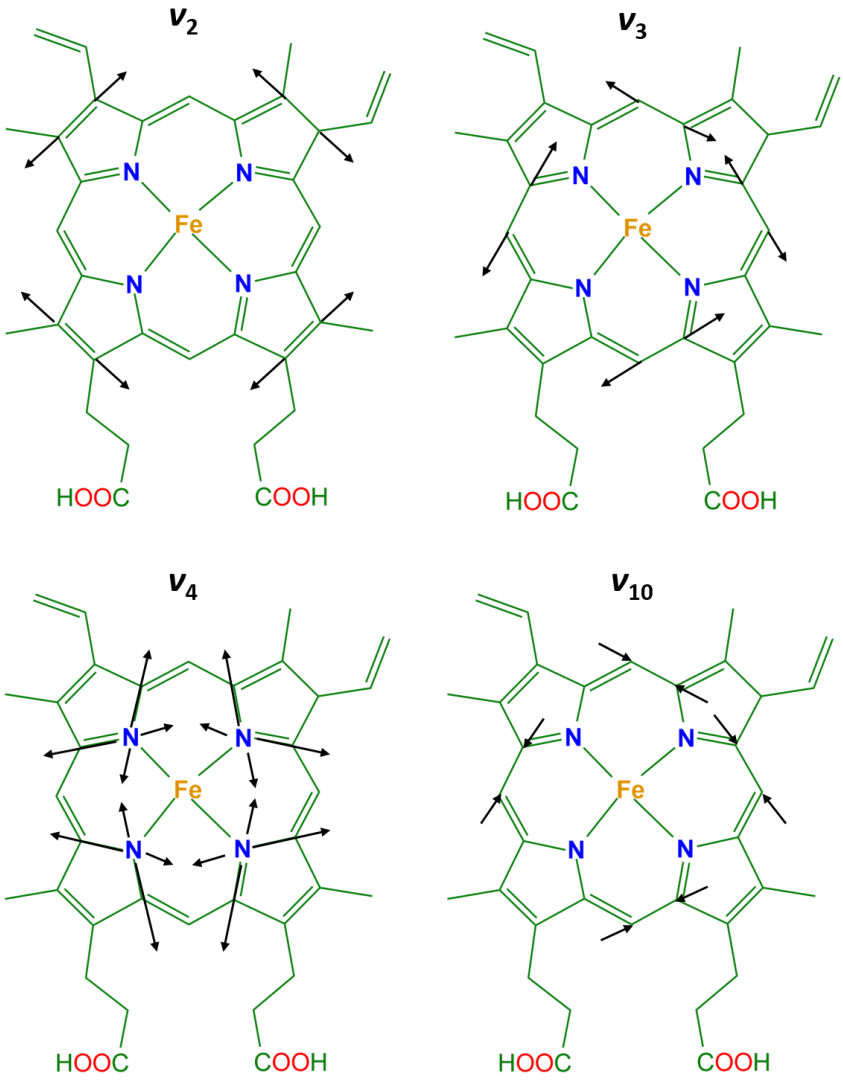

Figure S5: Characteristic skeletal stretching modes of the heme in MP8.

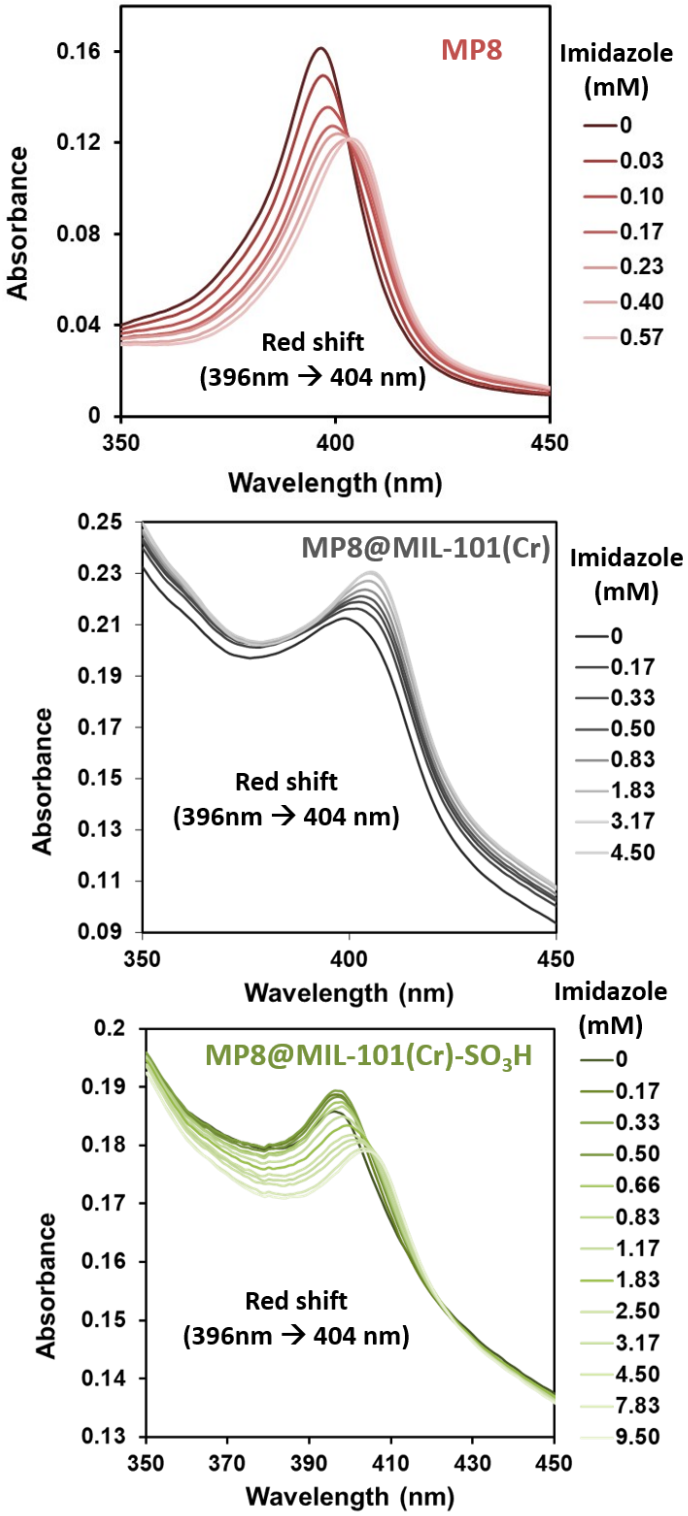

Figure S6: Spectral evolution of MP8 Soret band in the presence of increasing concentrations of imidazole for free MP8 (top), MP8@MIL-101(Cr) (middle) and MP8@MIL-101(Cr)-SO_3H (bottom).

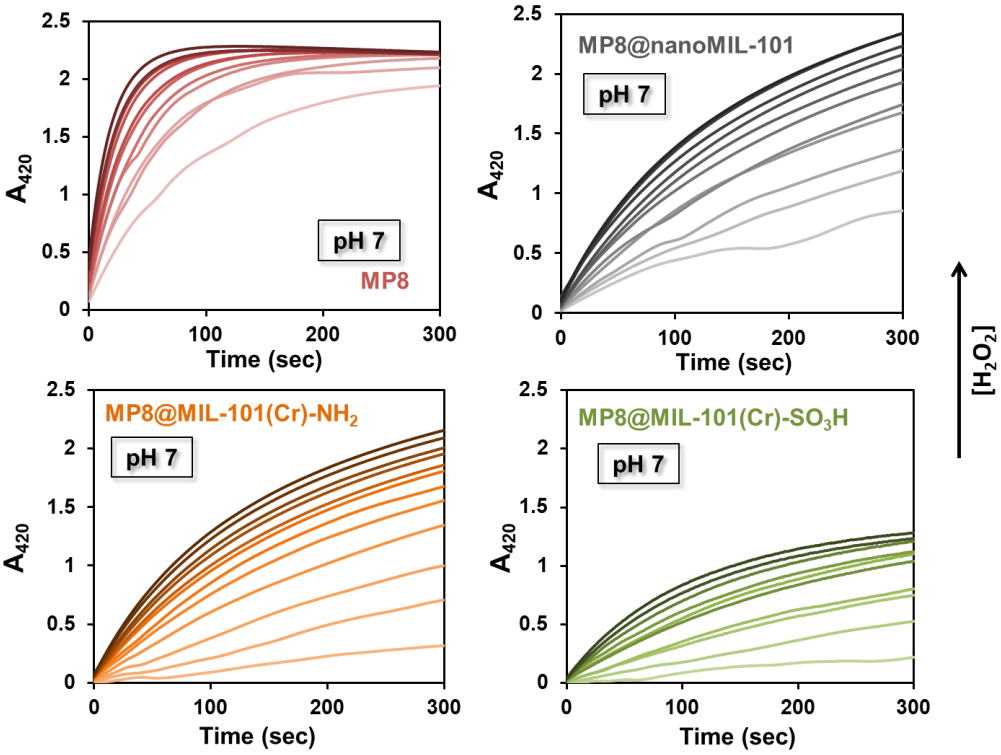

Figure S7: Time course of ABTS oxidation by free MP8 (red), MP8@MIL-101(Cr) (grey), MP8@MIL-101(Cr)-NH_2 (orange) and MP8@MIL-101(Cr)-SO_3H (green) as a function of H_2O_2 concentration (0.1-1.8 mM) at pH 7.

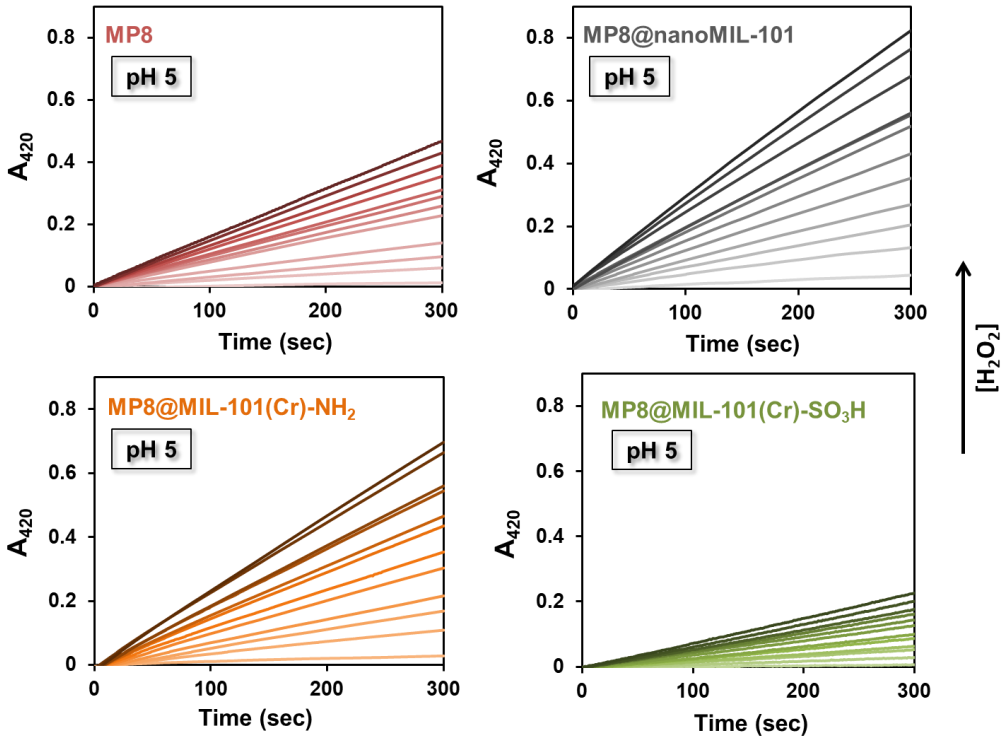

Figure S8: Time course of ABTS oxidation by the free MP8 (red), MP8@MIL-101(Cr) (grey), MP8@MIL-101(Cr)-NH_2 (orange) and MP8@MIL-101(Cr)-SO_3H (green) as a function of H_2O_2 concentration (0.1-1.8 mM) at pH 5.

B. Metal functionalization in MIL-101(Cr): MIL-101(Cr/Fe)

Even though the structure of MIL-101(Cr) stands among the most stable MOF structures, its Fe^{3+}-based form, MIL-101(Fe) shows very poor chemical stability.[62] Nonetheless, the use of Fe-based MOFs is of interest due to their inherent catalytic activity (see chapter 1) that, coupled with MP8, may result in synergetic properties. For that reason, we were interested in studying the use of the mixed-metal MIL-101(Cr/Fe) as enzymatic support.

MIL-101(Cr/Fe) combines the properties induced both by the Cr ions (stability) and by the substituent Fe ions (catalytic activity). A possible way to obtain the mixed-cation MIL-101 is the post-synthetic cation exchange, through the reaction of MIL-101(Cr) with an iron salt under reflux.[63] However, when possible, direct syntheses are generally preferred, as they are usually easier to control and more cost-effective. Vu *et al.* reported the direct hydrothermal synthesis of the mixed MIL-101(Cr/Fe), by replacing 25 wt% of the total $Cr(NO_3)_3{\cdot}9H_2O$ by $Fe(NO_3)_3{\cdot}9H_2O$.[64] FT-IR and XPS analyses demonstrated that Fe^{3+} was indeed incorporated in the structure and not encapsulated in the pores as iron oxides, which was also supported by the measured high specific surface area (3000 m^2/g). MIL-101(Cr/Fe) was successfully used for the photo-degradation of a commercially azo-dye, *via* a Fenton mechanism, using H_2O_2 as oxidant.[64] While these results are promising, the reported synthetic route for MIL-101(Cr/Fe) uses hydrofluoric acid (HF) as an acidic modulator.[64] HF has been extensively used in the past as a mineralizing agent, since it favors the formation of well crystalline MOF phases.[65] However, HF is a highly hazardous material (highly toxic and corrosive) and thus not acceptable for green and sustainable syntheses that are targeted nowadays. Consequently, the synthesis optimization was a mandatory step in order to avoid the use of HF, while producing a pure and well crystallized MIL-101(Cr/Fe).

1. Optimization of the synthesis of MIL-101(Cr/Fe)

Important efforts have been made lately to replace HF by other less toxic and less dangerous acidic modulators such as HCl, acetic acid (AcOH) or to avoid completely the use of modulators.[66,67] Inspired by such works, we first tried to follow a direct protocol similar to that reported, but we replaced HF by AcOH or performed the synthesis without additives. Figure 3-11 shows the PXRD patterns of the obtained samples. The use of additive did not seem to have a significant impact on the products' crystallinity. When mixtures of Cr and Fe nitrates were used, mixtures of MIL-101/MIL-88B were obtained (MIL-88B Bragg peaks are at 9.4° and 10.5°). As described in the first chapter, MIL-101 and MIL-88B are two polymorphs, *i.e.* distinct phases composed of the same building units (metal trimers and terephthalic acid), and it is often possible to have a mixture of these two MOFs. The use of AcOH and the lower Fe ratios (3Cr:1Fe) seemed to enhance the crystallization of MIL-101, based on the relative intensities of the MIL-101 Bragg peaks. This suggests that the higher reactivity of the Fe ions (more reactive than Cr ions) led to the formation of the two MOF phases. A possible way to address this difference in reactivity is the use of a less reactive Fe source such as metal iron. Fe^0 has already successfully been used for the preparation of the mixed metal MIL-53(Cr/Fe).[68]

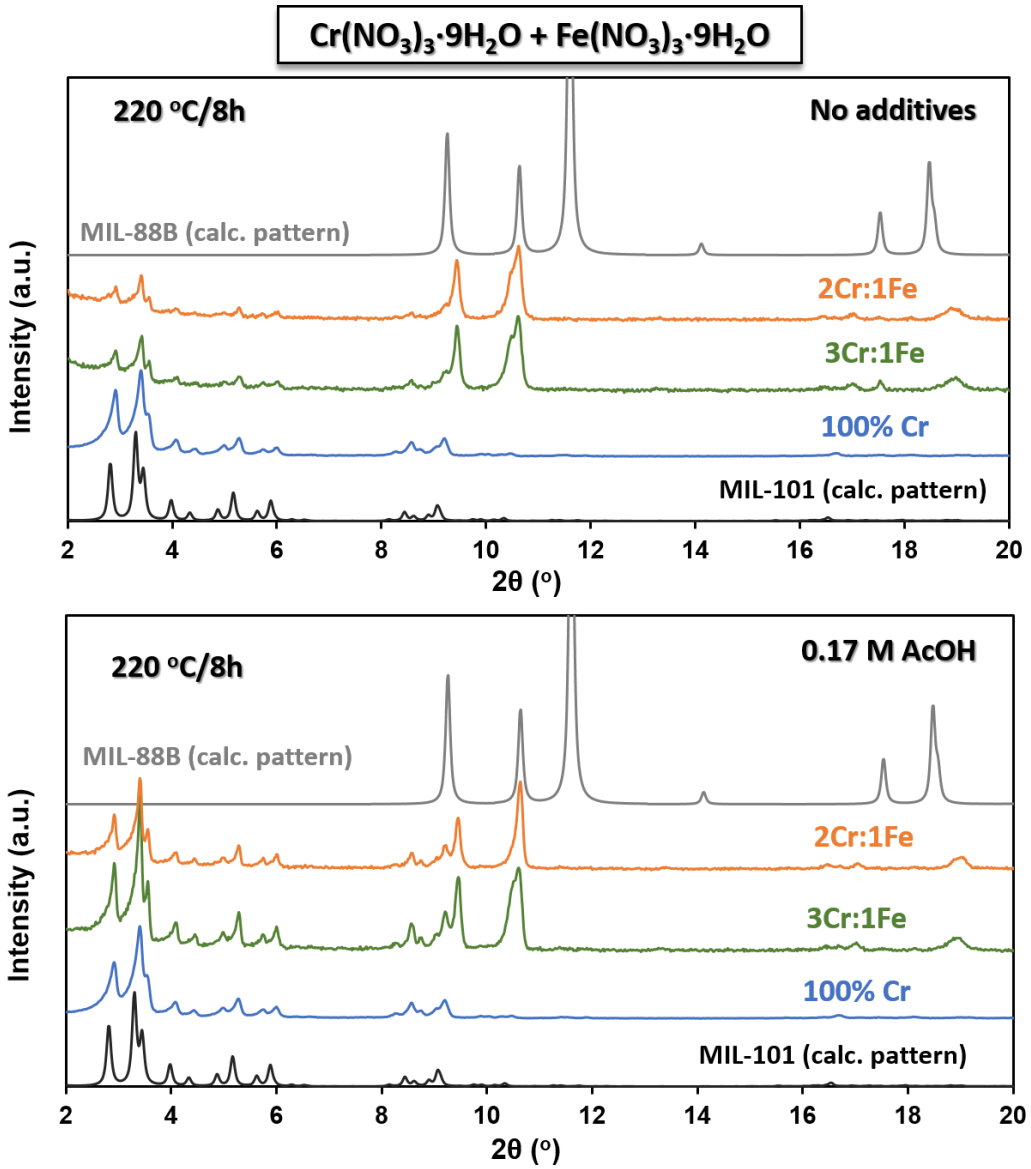

Figure 3-11: Normalized PXRD patterns of the obtained products using different ratios of the metal sources $Cr(NO_3)_3{\cdot}9H_2O$ and $Fe(NO_3)_3{\cdot}9H_2O$. Hydrothermal conditions: 220 °C for 8 h; without additives (top) and with 0.17 M AcOH (down).

Based on the conditions that seem to favor MIL-101 formation (use of AcOH and low Fe contents), we performed a second series of reactions, using Fe^0 as an iron source. As seen in Figure 3-12, the use a Fe^0 seemed to importantly limit the formation of the MIL-88B phase, which was nevertheless present in all the products. The use of a 4Cr:1Fe ratio was more favorable for the synthesis of MIL-101, than a 3Cr:1Fe ratio. AcOH concentrations ≥ 0.35 M also limited drastically the formation of MIL-88B, but did not fully prevented its formation.

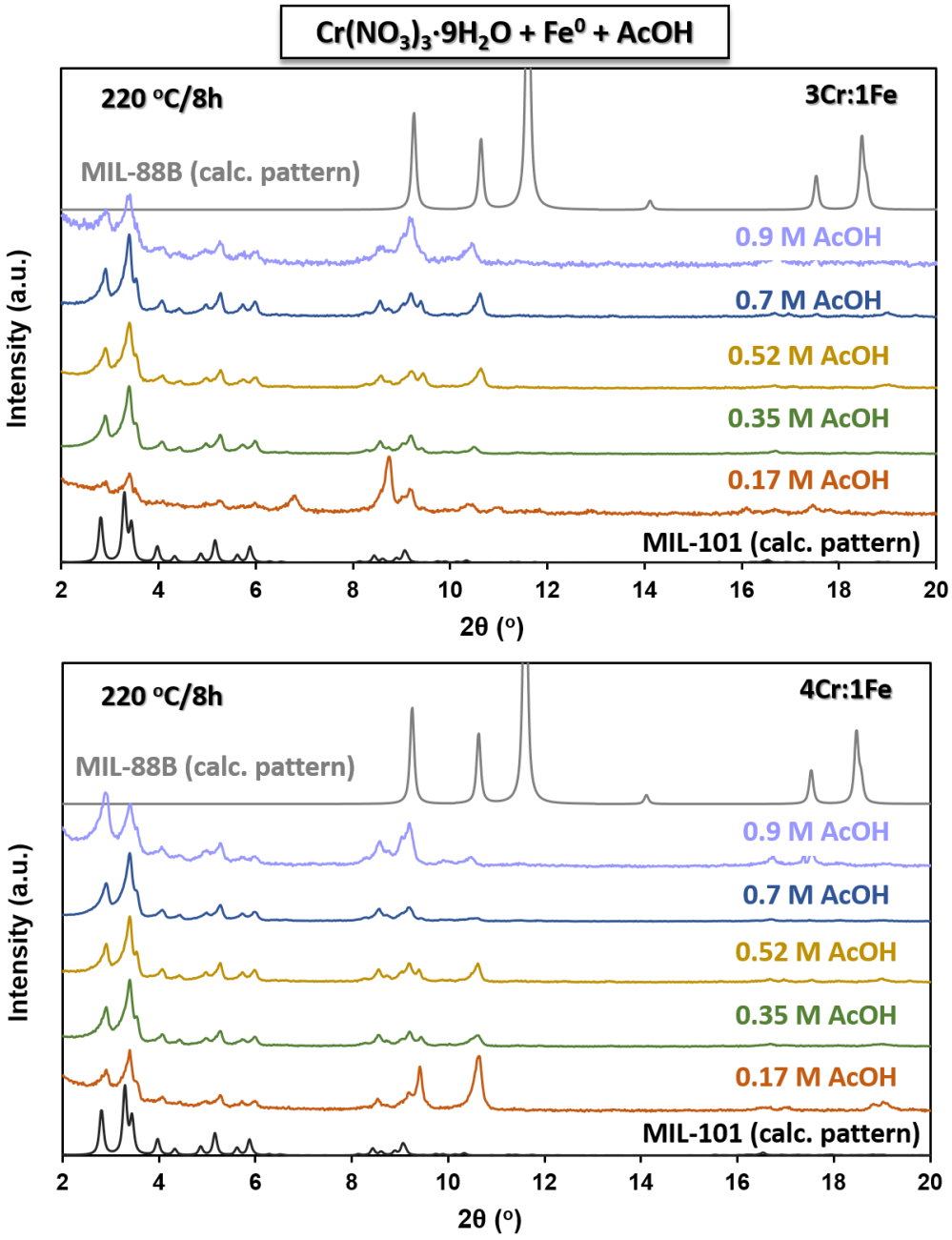

Figure 3-12: Normalized PXRD patterns of the obtained products using as metal sources $Cr(NO_3)_3{\cdot}9H_2O$ and Fe^0 with different concentrations of AcOH (0.17-0.9 M). Hydrothermal conditions: 220 °C for 8 h; metal ratio 3Cr:1Fe (top) and 4:Cr:Fe (down).

A third series of reactions was performed using the conditions previously reported for the preparation of the mixed metal MIL-53(Cr/Fe) that allowed the incorporation of Fe in the structure of a Cr-based MOF.[68] The MIL-53 phase is generally prepared from a Cr^{3+} or a Fe^{3+} source and terephthalic acid (similarly to MIL-101). MIL-53 is a thermodynamically stable phase (chains of M^{3+} and 1D micropores), whereas MIL-101 is a kinetically favored phase (M^{3+} trimers and 3D mesopores).[69] It was thus hypothesized that by decreasing the reported reaction time from 96 h to 48 h, it would be possible to promote only the formation of MIL-101. However, as seen in Figure 3-13, none of the tested conditions (varying AcOH

concentrations) gave the pure MIL-101 phase, as shown by the presence of MIL-88B Bragg peaks at 9.4º and 10.5º and MIL-53 Bragg peaks at 12.3º and 17.0º in all the patterns.

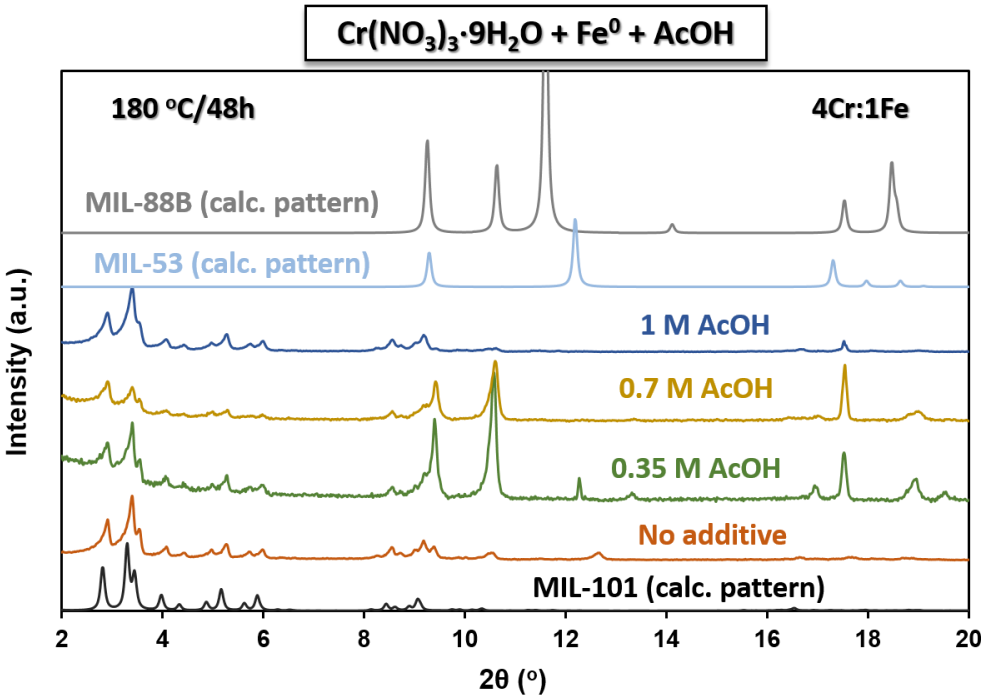

Figure 3-13: Normalized PXRD patterns of the obtained products using as metal sources $Cr(NO_3)_3 \cdot 9H_2O$ and Fe^0, with different concentrations of AcOH (0.35-0.7 M) and metal ratio 4Cr:Fe. Hydrothermal conditions: 180 ºC for 48 h.

The use of AcOH resulted in all the above series of reactions in mixture of phases, MIL-101/MIL-88B and MIL-101/MIL-88B/MIL-53. It was thus concluded that this acidic modulator was not adequate for the formation of a pure MIL-101(Cr/Fe) phase. Similar results were also obtained without the use of additives. Besides acidic modulators, basic additives have also been studied for the synthesis of MIL-101 materials, like NaOH, KOH and trimethylammonium hydroxide (TMAOH).[70] Their use has been reported to enhance the solubility of the terephthalic acid and the nucleation process, as the pH conditions are shifted around pH 6, thus promoting the synthesis of MIL-101. However, more basic conditions should be avoided because they would lead to the formation of oxides.[45] MIL-101(Cr) synthesized in the presence of low concentrations of TMAOH showed a good crystallinity, high specific surface areas and the formation of pure phases.[45,71] It was hence of interest to investigate the use of this base for the formation of the mixed metal MIL-101(Cr/Fe).

As shown in Figure 3-14, the concentration of TMAOH varies linearly with the purity of MIL-101. At very low concentration (0.012 M), a small MIL-53 impurity (main Bragg peaks at 10.6º and 12.7º) was observed, which seemed to decrease with increasing concentrations of TMAOH (based on relative intensities of the Bragg peaks). At 0.07 M of TMAOH, no Bragg peak characteristic of MIL-53 was observed. When the TMAOH concentration was further increased, the crystallinity of the product significantly decreased until an amorphous solid was

obtained at 0.09 M of TMAOH. These results are in agreement with the previous studies that showed the effect of the TMAOH concentration on the crystallinity of MIL-101.[14]

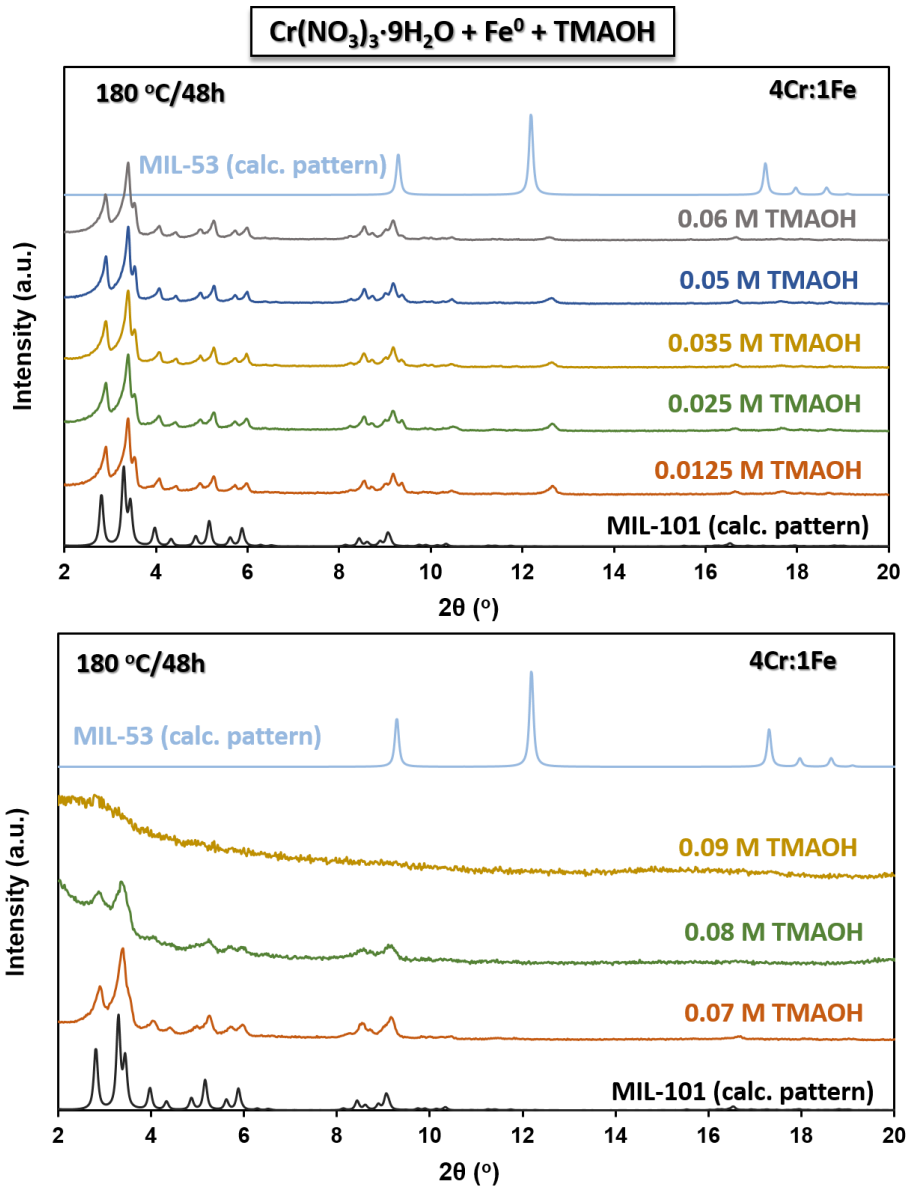

Figure 3-14: Normalized PXRD patterns of the obtained products using as metal sources $Cr(NO_3)_3 \cdot 9H_2O$ and Fe^0, with different concentrations of TMAOH and metal ratio 4Cr:Fe. Hydrothermal conditions: 180 °C for 48 h; [TMAOH] = 0.0125-0.06 M (left) and 0.07-0.09 M (right).

From the PXRD data shown in Figure 3-14, the MIL-101(Cr/Fe) sample prepared with 0.07 M TMAOH appeared to be promising and this MOF was thus selected for further characterization (Figure 3-15). However, the N_2 sorption measurement of the product revealed a very low BET surface area (1974 m^2/g), compared to that of a pure MIL-101(Cr) product (~3000 m^2/g) (synthesized without TMAOH). This poor specific surface area could neither be attributed to an inadequate activation of the sample (remaining unreacted ligand), nor to the presence of iron oxides, as the TGA analysis of the sample was similar to the pure MIL-101(Cr). SEM images revealed that the product contained crystals of different morphologies, which may justify the low surface area.

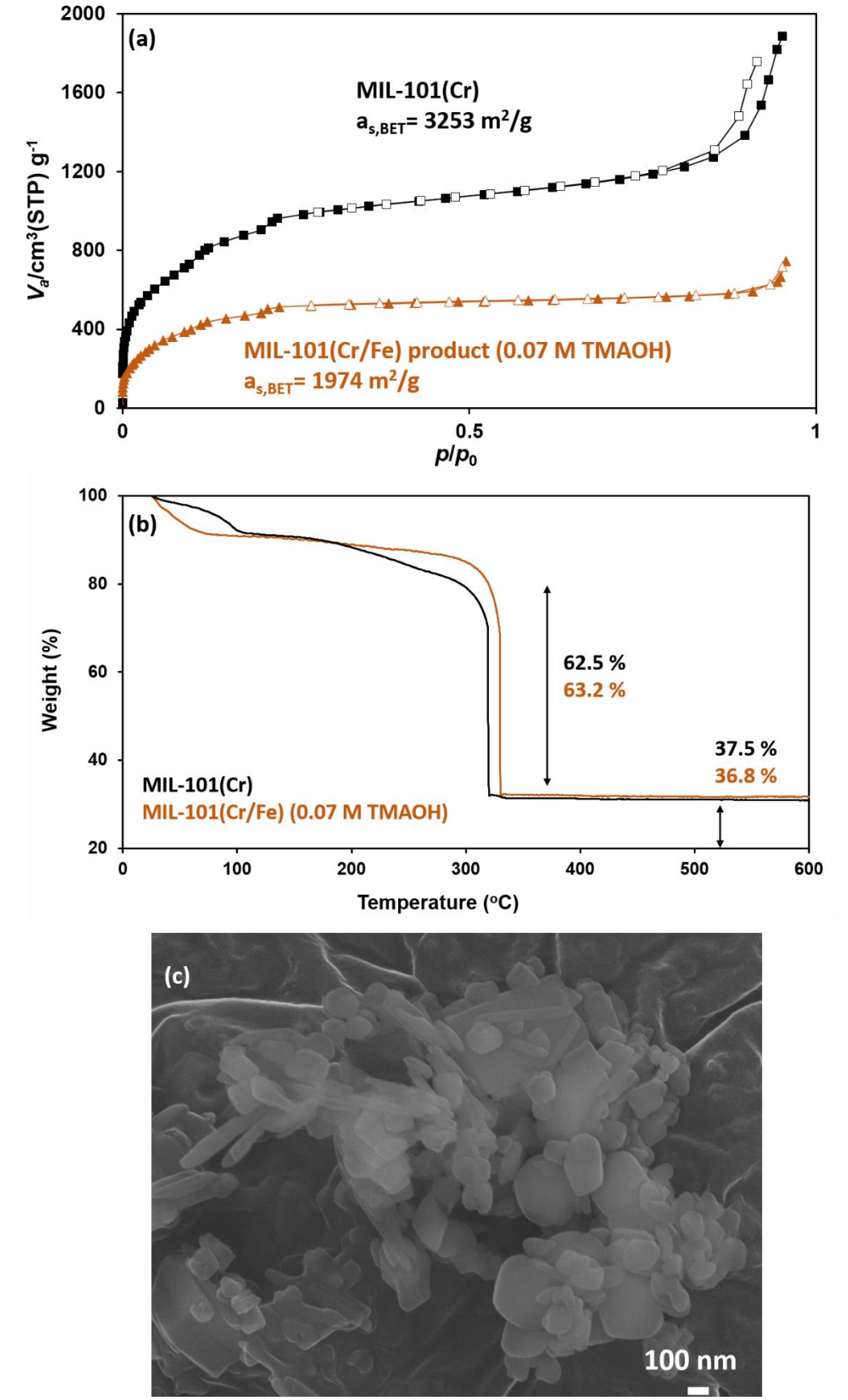

Figure 3-15: (a) N_2 sorption measurements of MIL-101(Cr) and MIL-101(Cr/Fe) (0.07 M TMAOH); (b) TGA curves of MIL-101(Cr) and MIL-101(Cr/Fe) (0.07 M TMAOH) under O_2 flow; (c) SEM image of MIL-101(Cr/Fe) (0.07 M TMAOH).

Finally, by further reducing the reaction temperature to 150 °C it was possible to isolate pure MIL-101(Cr/Fe) products, with different Cr/Fe compositions. In this case, 1.5 mmol terephthalic acid was mixed with 1 mmol metal source (ratios 3Cr:1Fe and 4Cr:1Fe) in 10 mL TMAOH (0.06 M) and heated at 150 °C for 48 h. The obtained solids were isolated by centrifugation (20 min, 14500 rpm) and washed several times with water and EtOH (abs.). In order to remove the residual ligand molecules from the pores, the solids were treated with a solution of KF (0.1 M) for 1 h. The purified products were dried at 150 °C, prior to their characterization. Attempts to further increase the Fe content resulted in amorphous solids (data not shown).

2. Characterization of the mixed metal MIL-101(Cr/Fe)

The mixed metal MOFs were synthetized starting from 3Cr:1Fe and 4Cr:1Fe ratios. However, the incorporation of the Fe^{3+} cations was found to be lower in both cases, as 4Cr:1Fe and 5.9Cr:1Fe ratios were determined respectively from the EDX data (see below). Therefore, the isolated mixed metal MOFs will be referred to as MIL-101(Cr/Fe) (4:1) and MIL-101(Cr/Fe) (5.9:1).

As expected, the incorporation of Fe^{3+} cations was reflected in the color of the products. While the powder of the pure MIL-101(Cr) had a dark green color, MIL-101(Cr) (4:1) showed a light brown color and MIL-101(Cr/Fe) (5.9:1) had a light green-brown powder (Figure 3-16).

Figure 3-16: Photos of the powders of MIL-101(Cr), MIL-101(Cr/Fe) (4:1) and MIL-101(Cr/Fe) (5.9:1).

Figure 3-17 shows the PXRD patterns of the obtained MIL-101(Cr/Fe) (4:1), MIL-101(Cr/Fe) (5.9:1) and the calculated pattern of MIL-101(Cr). Both products showed characteristic diffraction peaks of MIL-101, without any additional peaks, which confirmed the formation of a single MOF phase. Both MOFs showed a reduced crystallinity compared to the reported pure MIL-101(Cr) phase possibly, because Fe^{3+} cations introduced a certain disorder in the frameworks. Accordingly, MIL-101(Cr) (4:1), which has a higher Fe content, showed a less crystalline structure than MIL-101(Cr/Fe) (5.9:1).

The FT-IR spectra of the two mixed metal MIL-101(Cr/Fe) are shown in Figure 3-18. No stretching band corresponding to the carboxyl groups of the free ligand, (ν(C=O)= 1700 cm^{-1}) was present in the spectrum of MIL-101(Cr/Fe) (5.9:1), but a small residual band was present in the spectrum of MIL-101(Cr/Fe) (4:1), indicating traces of unreacted terephthalic acid. The complexation of the ligand with the metal ions is depicted by bands at ~1600 cm^{-1} and ~ 1440

cm^{-1} corresponding respectively to the asymmetric $\nu(C\text{-}O)_{as}$ and symmetric $\nu(C\text{-}O)_{s}$ stretching modes. The broader bands of MIL-101(Cr/Fe) (4Cr:1Fe) are consistent with the lower crystallinity of this sample.

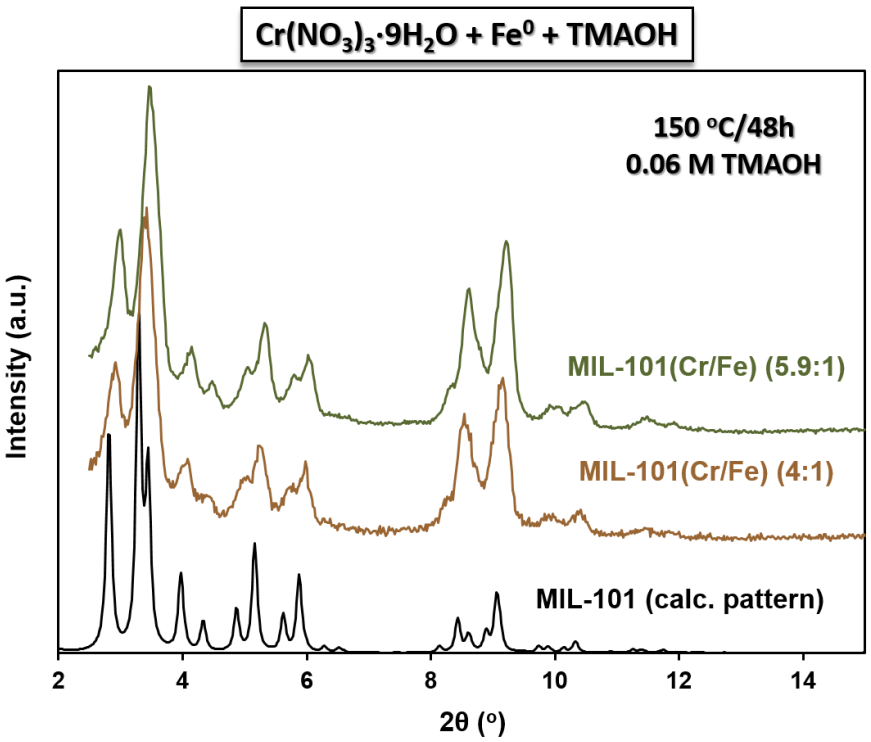

Figure 3-17: Normalized PXRD patterns of MIL-101(Cr/Fe) (4:1) and MIL-101(Cr/Fe) (5.9:1), compared with the calculated pattern of MIL-101(Cr).

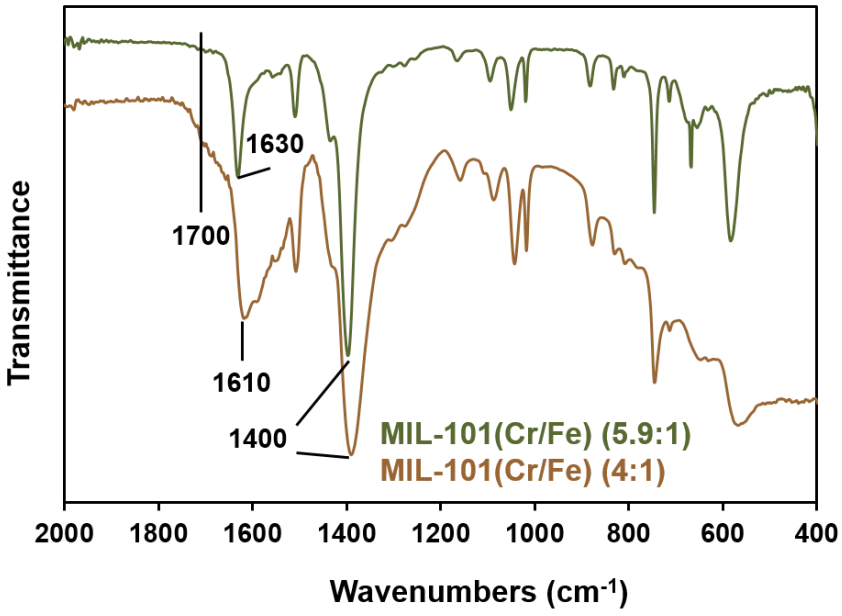

Figure 3-18: FT-IR spectra of MIL-101(Cr/Fe) (4:1) and MIL-101(Cr/Fe) (5.9:1).

The TGA curves of the two mixed metal MOFs are compared with that of MIL-101(Cr) in Figure 3-19. Note that MIL-101(Cr) was synthesized hydrothermally, without the use of TMAOH. The

chemical formulas of the MOFs deduced from the EDX results are $Cr_{2.4}Fe_{0.6}OH(H_2O)_2O[(O_2C)\text{-}C_6H_4\text{-}(CO_2)]_3$, $Cr_{2.57}Fe_{0.43}OH(H_2O)_2O[(O_2C)\text{-}C_6H_4\text{-}(CO_2)]_3$ for MIL-101(Cr/Fe) (4:1) and MIL-101(Cr/Fe) (5.9:1) respectively, whereas that corresponding to the pure MIL-101(Cr) is $Cr_3OH(H_2O)_2O[(O_2C)\text{-}C_6H_4\text{-}(CO_2)]_3$.[72] The first weight loss (≤ 100 °C) corresponds to the removal of adsorbed solvent molecules (H_2O and EtOH). The second weight loss between 100 and 300 °C is attributed to the release of coordinated solvent molecules and free terephtalate molecules entrapped in the pores of the MOFs. The degradation of the structures is observed around 300 °C, which is similar to the degradation temperature of the pure MIL-101(Cr),[72] indicating that the incorporation of Fe^{3+} cations, did not affect the thermal stability of the frameworks. The percentage of Cr_2O_3 residue obtained in the case of MIL-101(Cr) (31 %) is slightly lower than then global percentage of the oxide residues (Cr_2O_3 + Fe_2O_3) formed in the case of the mixed metal MOFs: 34.7 % for MIL-101(Cr/Fe) (4:1) (27.8 % Cr_2O_3 + 6.9 % Fe_2O_3) and 32.1 % for MIL-101(Cr/Fe) (5.9:1) (27.5 % Cr_2O_3 + 4.6 % Fe_2O_3). This may indicate that a part of the metal precursors used for the synthesis of the MOFs may have formed oxides that could not be removed during the activation of the samples (washing procedure).

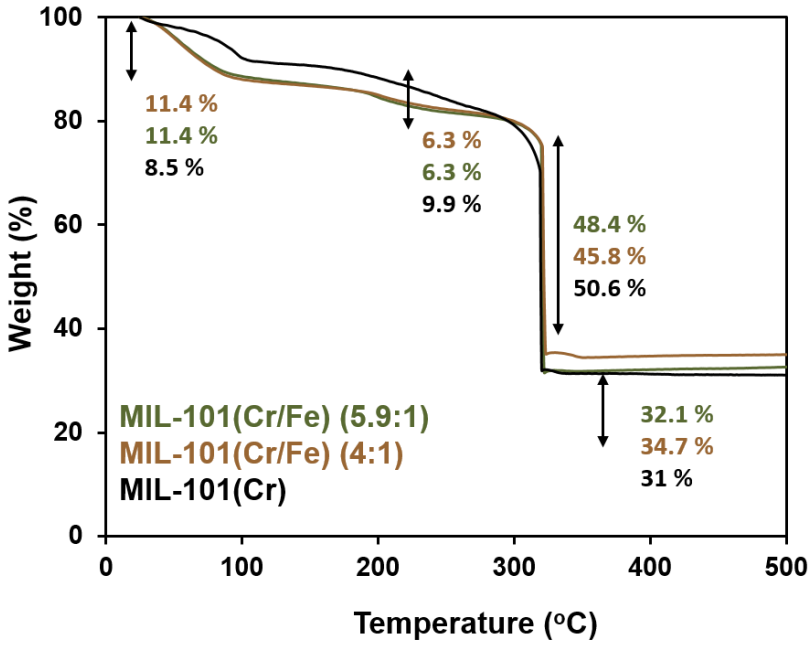

Figure 3-19: TGA curves of MIL-101(Cr/Fe) (4:1), MIL-101(Cr/Fe) (5.9:1) and MIL-101(Cr), under O_2 flow.

Figure 3-20 shows the N_2 sorption isotherms of MIL-101(Cr/Fe) (4:1) and MIL-101(Cr/Fe) (5.9:1) at 77 K. Both mixed metal MOFs exhibit secondary uptakes at p/p_0 ~0.1 and p/p_0 ~0.2, which are characteristic of the two microporous windows (pentagonal and hexagonal) of the two mesoporous cages. The apparent BET surface areas are 2660 and 3040 m^2/g for MIL-101(Cr/Fe) (4:1) and MIL-101(Cr/Fe) (5.9:1), respectively. Both mixed metal MOFs exhibit lower surfaces areas than that reported for the pure MIL-101(Cr) (~3500 m^2/g),[72] which could be due to the presence of traces of metal oxides and unreacted ligand molecules in the pores.

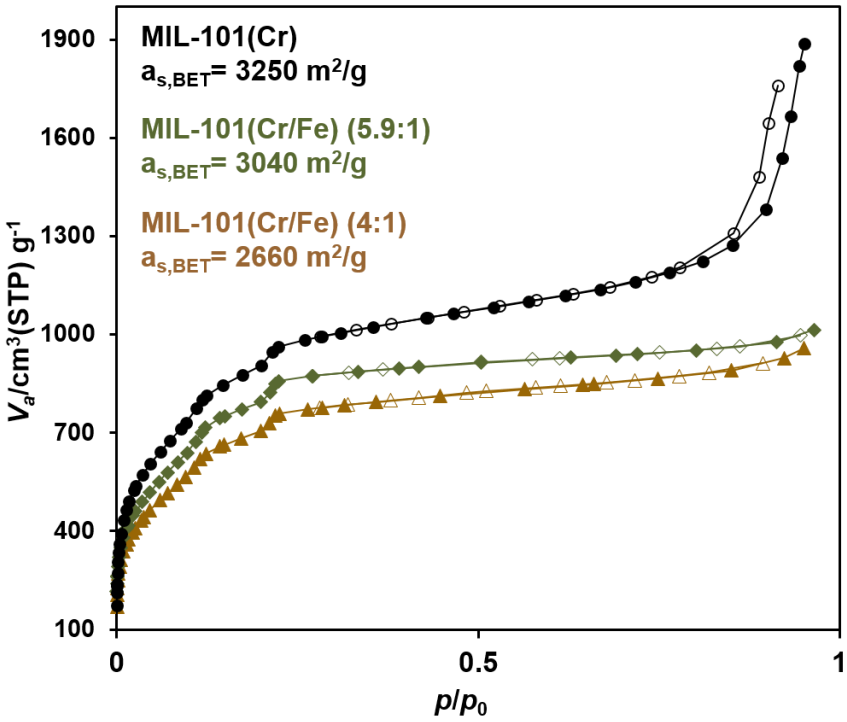

Figure 3-20: N_2 sorption isotherms of MIL-101 (Cr) (black cycles), MIL-101(Cr/Fe) (4:1) (brown triangles) and MIL-101(Cr/Fe) (5.9:1) (green diamonds) at 77 K.

The particles of the mixed metal MOFs did not show a well-defined morphology and were much aggregated. Nonetheless, both MOFs showed uniform particles of around 100 nm. Figure 3-21 shows the SEM images of the two mixed metal MOFs and the Cr and Fe atomic composition based on EDX analysis. MIL-101(Cr/Fe) (4:1) contains 81 ± 2% Cr and 19± 2.0 % Fe, whereas MIL-101(Cr/Fe) (5.9:1) contains 85 ± 1 % Cr and 15 ± 1 % Fe.

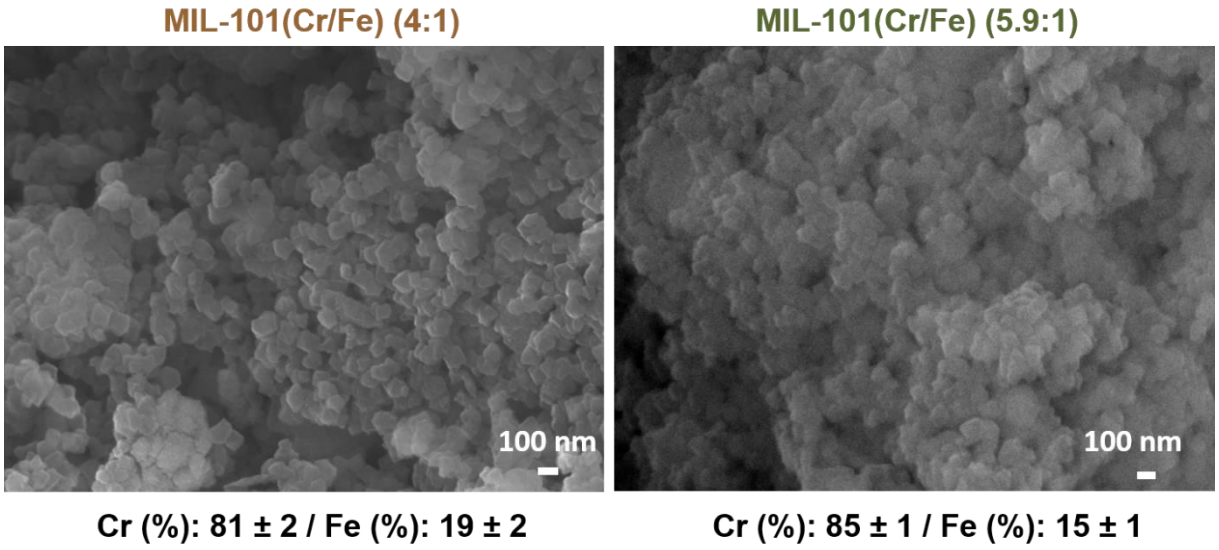

Figure 3-21: SEM-EDX analysis of MIL-101(Cr/Fe) (4:1) and MIL-101(Cr/Fe) (5.9:1).

The Mössbauer spectrometry on the MIL-101(Cr/Fe) materials was performed by Dr. Jean-Marc Greneche at the Institut des Molécules et Matériaux du Mans (UMR CNRS 6283), at the Le Mans Université.

^{57}Fe Mössbauer spectrometry was used to gain information about the oxidation and the spin state of Fe, along with its electronic environment, in order to confirm that the detected Fe of the mixed MOFs was indeed incorporated in their crystal structures and exclude the possibility of Fe being under the forms of Fe oxides or hydroxides. The transmission Mössbauer spectra of MIL-101(Cr/Fe) (4:1) recorded at 300 K and 77 K, consist of quadrupolar doublets with broadened and overlapped lines, indicative of different environments of Fe atoms (Figure 3-22). They were first recorded at 4 mm/s to check that the samples did not contain any HS Fe(II) species and then at 2 mm/s. Figure 3-22 illustrates only the spectra recorded at 2 mm/s. Different fitting models could be applied with 2 components (top of figure) or 3 components (bottom of figure), resulting in the same mean values of isomer shift (0.33 and 0.48 mm/s at 300 K and 77 K, respectively) and quadrupolar splitting (0.68 and 0.74 mm/s at 300 K and 77 K, respectively). These values are consistent with the presence of HS Fe(III) in an octahedral environmental, suggesting that they may be located in the octahedral units of the inorganic building blocks.[73–75] This is further supported by the similarity between the Mössbauer spectra of the mixed MIL-101(Cr/Fe) (4:1) and the reported spectrum of MIL-100(Fe) (Figure 3-23).[75] The isomer shift values of MIL-100(Fe) are significantly higher (0.42 and 0.54 mm/s at 300 K and 77 K, respectively). This difference could result from the amount of fluorine ions contained in the structure, as the presence of F ions in the Fe environment leads to higher isomer shifts than Fe surrounded by O.[68] MIL-100(Fe) synthesis was performed in presence of KF and it has been previously demonstrated that the resulting structure has one fluorine atom per Fe trimer. However, in the case of MIL-101 (Cr/Fe) the synthesis was performed without fluorine which can usually be replaced by hydroxyl ions in the structure.[76] The present mean values of isomer shift are rather typical of Fe^{3+} surrounded by oxygen or hydroxyl groups, in fair agreement with the absence of KF during the synthesis of MIL-101(Cr/Fe). When the content of Fe incorporated in the synthesis was decreased (ratio Cr/Fe 5.9:1), no significant differences were observed in the Mössbauer spectrum (Figure 3-24), except for a slight increase of the quadrupolar doublet asymmetry. The presence of water molecules in the framework influences the Mössbauer spectra and may be responsible for this difference. It is important to emphasize that the lack of resolution of the hyperfine structure does not allow to exclude the presence of some iron(III) oxides in MIL-101(Ce/Fe) samples, similarly to the case of MIL 100(Fe).

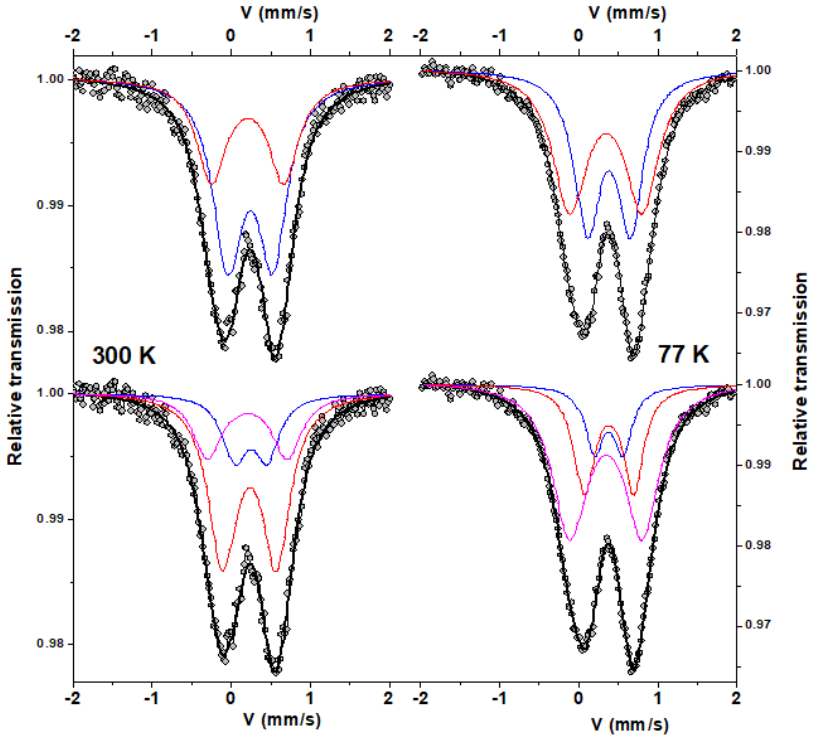

Figure 3-22: Mössbauer transmission spectra of MIL-101(Cr/Fe) (4:1), recorded at 300 K and 77 K with 2 fitting models (see text).

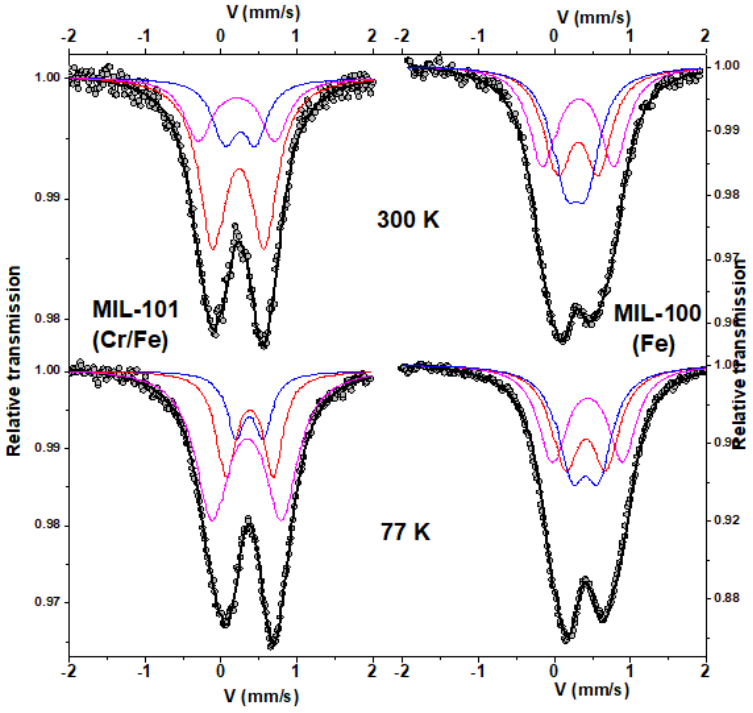

Figure 3-23: Mössbauer transmission spectra of MIL-101(Cr/Fe) (4:1) and MIL-100(Fe), recorded at 300 K and 77 K.

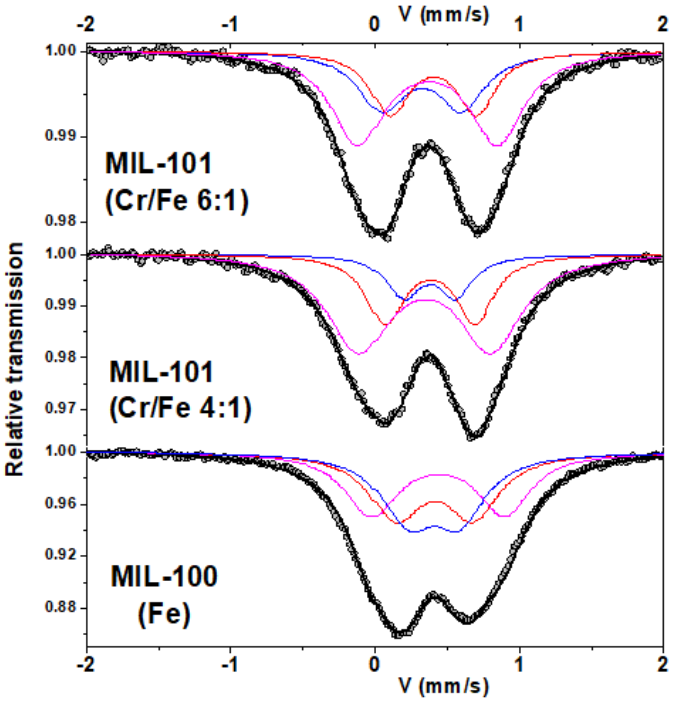

Figure 3-24: Mössbauer transmission spectra of MIL-101(Cr/Fe) (5.9:1), MIL-101(Cr/Fe) (4:1) and MIL-100(Fe), recorded at 77 K.

While the thermal stability of the mixed metal MIL-101(Cr/Fe) MOFs was not affected by the incorporation of the Fe atoms, it was also important to evaluate the chemical stability of the MOFs and especially in water, as these materials have been designed to be used for biocatalytic applications. For the water stability tests, 50 mg of MIL-101(Cr/Fe) (4:1) were dispersed in 5 mL H_2O and left under stirring at RT or reflux for 24 h. The powders were then recovered by centrifugation and dried at 100 ^oC for 1 h, prior to their characterization by PXRD. As observed in Figure 3-25 no change was observed in the PXRD patterns neither at RT nor under reflux conditions, indicating the chemical robustness of MIL-101(Cr) (4:1) in water.

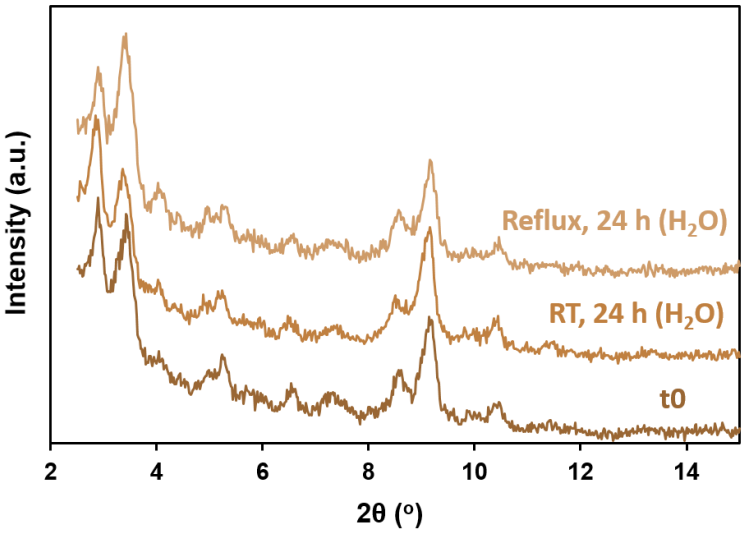

Figure 3-25: Normalized PXRD patterns of MIL-101(Cr/Fe) (4:1) after contact with water at RT and reflux for 24 h.

Prior to the utilization of the mixed-metal MOFs as potential catalytically active immobilization matrices, it was important to fully evaluate their catalytic activity. Some preliminary catalytic results of the MIL-101(Cr/Fe) (4:1) are presented in Annex 1, concerning the Lewis acid catalyzed reactions, Prins coupling and ring opening of epoxides.

C. Conclusions

In this chapter, we focused our efforts on the functionalization of MIL-101(Cr) and on studying the effects that could have on the encapsulation of MP8 on its resulting catalytic activity. Two different studies were performed: the ligand functionalization and the metal functionalization.

Concerning the first study, the terephthalic acid of MIL-101(Cr) was replaced by its functionalized analogs, 2-aminotephthalic acid and 2-sulfoterepththalic acid. The choice of the ligands was based on their difference in polarity, acidity and surface charge of the MOF particles that could have different effects on MP8 immobilization and activity. Higher amounts of MP8 were immobilized in the functionalized MOFs than in MIL-101(Cr), possibly because of additional specific interactions (H-bonding, additional electrostatic interactions *etc*…) that stabilized some enzyme molecules at the external surface of the MOFs. The catalytic activity the immobilized MP8 was evaluated both with a typical substrate (ABTS) and a more challenging catalytic conversion, the oxidation of thioanisole derivatives bearing electron donating, EDG (-CH_3, -OCH_3) or electron withdrawing, EWG (-NO_2) groups. MP8@MIL-101(Cr) and MP8@MIL-101(Cr)-NH_2 showed similar activities, due to the similar microenvironment of their structures in terms of surface charge and acidity. MP8@MIL-101(Cr)-SO_3H showed poor activity probably due to its high acidity that could result in the protonation of the His18 residue, which is essential for the activity of MP8. Similar to what was observed with free MP8, the immobilized enzymes were more reactive when sulfides bearing EDG groups were used. However, their reactivity was less influenced than with free MP8, suggesting a minimized influence of the nucleophilic character of the substrate when immobilized MP8 was used.

For the metal functionalization of MIL-101(Cr), the goal was to partially substitute the inorganic Cr(III) SBU with Fe(III) in order to obtain a more stable mesoporous structure, which could be catalytically active either as Lewis acid catalyst or as peroxidase-like catalyst. The combination of this MOF with MP8 could be envisioned for coupling complementary catalytic activities. An optimization of the synthesis was performed in order to avoid toxic reactants used in the reported protocols. Two MOFs with different Cr(III)/Fe(III) ratios, MIL-101(Cr/Fe) (4:1) and MIL-101(Cr/Fe) (5.9:1) were obtained and characterized. Both MOFs showed good chemical stability and Lewis acid catalytic activity.

D. References

(1) Pires, S. M. G.; Simões, M. M. Q.; Santos, I. C. M. S.; Rebelo, S. L. H.; Paz, F. A. A.; Neves, M. G. P. M. S.; Cavaleiro, J. A. S. Oxidation of Organosulfur Compounds Using an Iron(III) Porphyrin Complex: An Environmentally Safe and Efficient Approach. *Applied Catalysis B: Environmental* **2014**, *160–161*, 80–88. https://doi.org/10.1016/j.apcatb.2014.05.003.

(2) Sharma, V. K.; Luther, G. W.; Millero, F. J. Mechanisms of Oxidation of Organosulfur Compounds by Ferrate(VI). *Chemosphere* **2011**, *82* (8), 1083–1089. https://doi.org/10.1016/j.chemosphere.2010.12.053.

(3) Holland, H. L. Chiral Sulfoxidation by Biotransformation of Organic Sulfides. *Chemical Reviews* **1988**, *88*, 473–485.

(4) Carreno, M. C. Applications of Sulfoxides to Asymmetric Synthesis of Biologically Active Compounds. *Chemical Reviews* **1995**, *95*, 1717–1760.

(5) Fernández, I.; Khiar, N. Recent Developments in the Synthesis and Utilization of Chiral Sulfoxides. *Chemical Reviews* **2003**, *103* (9), 3651–3706. https://doi.org/10.1021/cr990372u.

(6) Wojaczyńska, E.; Wojaczyński, J. Enantioselective Synthesis of Sulfoxides: 2000−2009. *Chemical Reviews* **2010**, *110* (7), 4303–4356. https://doi.org/10.1021/cr900147h.

(7) Wang, R.; Zhang, G.; Zhao, H. Polyoxometalate as Effective Catalyst for the Deep Desulfurization of Diesel Oil. *Catalysis Today* **2010**, *149* (1–2), 117–121. https://doi.org/10.1016/j.cattod.2009.03.011.

(8) Khorshidifard, M.; Rudbari, H. A.; Askari, B.; Sahihi, M.; Farsani, M. R.; Jalilian, F.; Bruno, G. Cobalt(II), Copper(II), Zinc(II) and Palladium(II) Schiff Base Complexes: Synthesis, Characterization and Catalytic Performance in Selective Oxidation of Sulfides Using Hydrogen Peroxide under Solvent-Free Conditions. *Polyhedron* **2015**, *95*, 1–13. https://doi.org/10.1016/j.poly.2015.03.041.

(9) Lang, X.; Leow, W. R.; Zhao, J.; Chen, X. Synergistic Photocatalytic Aerobic Oxidation of Sulfides and Amines on TiO_2 under Visible-Light Irradiation. *Chemical Science* **2015**, *6* (2), 1075–1082. https://doi.org/10.1039/C4SC02891K.

(10) Dai, L.; Klibanov, A. M. Peroxidase-Catalyzed Asymmetric Sulfoxidation in Organic Solvents versus in Water. *Biotechnology and Bioengineering* **2000**, *70* (3), 353–357. https://doi.org/10.1002/1097-0290(20001105)70:3<353::AID-BIT13>3.0.CO;2-0.

(11) van de Velde, F.; Arends, I. W. C. .; Sheldon, R. A. Biocatalytic and Biomimetic Oxidations with Vanadium. *Journal of Inorganic Biochemistry* **2000**, *80* (1–2), 81–89. https://doi.org/10.1016/S0162-0134(00)00043-X.

(12) Velde, F. van de; Rantwijk, F. van; Sheldon, R. A. Improving the Catalytic Performance of Peroxidases in Organic Synthesis. *Trends in Biotechnology* **2001**, *19* (2), 73–80. https://doi.org/10.1016/S0167-7799(00)01529-8.

(13) Ferrer, M. L.; Levy, D.; Gomez-Lor, B.; Iglesias, M. High Operational Stability in Peroxidase-Catalyzed Non-Aqueous Sulfoxidations by Encapsulation within Sol–Gel Glasses. *Journal of Molecular Catalysis B: Enzymatic* **2004**, *27* (2–3), 107–111. https://doi.org/10.1016/j.molcatb.2003.11.001.

(14) Šulek, F.; Fernández, D. P.; Knez, Ž.; Habulin, M.; Sheldon, R. A. Immobilization of Horseradish Peroxidase as Crosslinked Enzyme Aggregates (CLEAs). *Process Biochemistry* **2011**, *46* (3), 765–769. https://doi.org/10.1016/j.procbio.2010.12.001.

(15) van de Velde, F.; Lourenço, N. D.; Bakker, M.; van Rantwijk, F.; Sheldon, R. A. Improved Operational Stability of Peroxidases by Coimmobilization with Glucose Oxidase. *Biotechnology and Bioengineering* **2000**, *69* (3), 286–291. https://doi.org/10.1002/1097-0290(20000805)69:3<286::AID-BIT6>3.0.CO;2-R.

(16) Hwang, E. T.; Gu, M. B. Enzyme Stabilization by Nano/Microsized Hybrid Materials: Enzyme Stabilization by Nano/Microsized Hybrid Materials. *Engineering in Life Sciences* **2013**, *13* (1), 49–61. https://doi.org/10.1002/elsc.201100225.

(17) Mousty, C.; Prevot, V. Hybrid and Biohybrid Layered Double Hydroxides for Electrochemical Analysis. *Analytical and Bioanalytic Chemistry* **2013**, *405*, 3513–3523. https://doi.org/10.1007/s00216-013-6797-1.

(18) Lian, X.; Fang, Y.; Joseph, E.; Wang, Q.; Li, J.; Banerjee, S.; Lollar, C.; Wang, X.; Zhou, H.-C. Enzyme–MOF (Metal–Organic Framework) Composites. *Chemical Society Reviews* **2017**, *46* (11), 3386–3401. https://doi.org/10.1039/C7CS00058H.

(19) Doonan, C.; Riccò, R.; Liang, K.; Bradshaw, D.; Falcaro, P. Metal–Organic Frameworks at the Biointerface: Synthetic Strategies and Applications. *Accounts of Chemical Research* **2017**, *50* (6), 1423–1432. https://doi.org/10.1021/acs.accounts.7b00090.

(20) Majewski, M. B.; Howarth, A. J.; Li, P.; Wasielewski, M. R.; Hupp, J. T.; Farha, O. K. Enzyme Encapsulation in Metal–Organic Frameworks for Applications in Catalysis. *CrystEngComm* **2017**, *19* (29), 4082–4091. https://doi.org/10.1039/C7CE00022G.

(21) Gkaniatsou, E.; Sicard, C.; Ricoux, R.; Mahy, J.-P.; Steunou, N.; Serre, C. Metal–Organic Frameworks: A Novel Host Platform for Enzymatic Catalysis and Detection. *Materials Horizons* **2017**, *4* (1), 55–63. https://doi.org/10.1039/C6MH00312E.

(22) Lykourinou, V.; Chen, Y.; Wang, X.-S.; Meng, L.; Hoang, T.; Ming, L.-J.; Musselman, R. L.; Ma, S. Immobilization of MP-11 into a Mesoporous Metal–Organic Framework, MP-11@mesoMOF: A New Platform for Enzymatic Catalysis. *Journal of the American Chemical Society* **2011**, *133* (27), 10382–10385. https://doi.org/10.1021/ja2038003.

(23) Lian, X.; Erazo-Oliveras, A.; Pellois, J.-P.; Zhou, H.-C. High Efficiency and Long-Term Intracellular Activity of an Enzymatic Nanofactory Based on Metal-Organic Frameworks. *Nature Communications* **2017**, *8* (1). https://doi.org/10.1038/s41467-017-02103-0.

(24) Li, P.; Chen, Q.; Wang, T. C.; Vermeulen, N. A.; Mehdi, B. L.; Dohnalkova, A.; Browning, N. D.; Shen, D.; Anderson, R.; Gómez-Gualdrón, D. A.; et al. Hierarchically Engineered Mesoporous Metal-Organic Frameworks toward Cell-Free Immobilized Enzyme Systems. *Chem* **2018**, *4* (5), 1022–1034. https://doi.org/10.1016/j.chempr.2018.03.001.

(25) Li, P.; Modica, J. A.; Howarth, A. J.; Vargas L., E.; Moghadam, P. Z.; Snurr, R. Q.; Mrksich, M.; Hupp, J. T.; Farha, O. K. Toward Design Rules for Enzyme Immobilization in Hierarchical Mesoporous Metal-Organic Frameworks. *Chem* **2016**, *1* (1), 154–169. https://doi.org/10.1016/j.chempr.2016.05.001.

(26) Lian, X.; Chen, Y.-P.; Liu, T.-F.; Zhou, H.-C. Coupling Two Enzymes into a Tandem Nanoreactor Utilizing a Hierarchically Structured MOF. *Chemical Science* **2016**, *7* (12), 6969–6973. https://doi.org/10.1039/C6SC01438K.

(27) Li, P.; Moon, S.-Y.; Guelta, M. A.; Harvey, S. P.; Hupp, J. T.; Farha, O. K. Encapsulation of a Nerve Agent Detoxifying Enzyme by a Mesoporous Zirconium Metal–Organic Framework Engenders Thermal and Long-Term Stability. *Journal of the American Chemical Society* **2016**, *138* (26), 8052–8055. https://doi.org/10.1021/jacs.6b03673.

(28) Lian, X.; Huang, Y.; Zhu, Y.; Fang, Y.; Zhao, R.; Joseph, E.; Li, J.; Pellois, J.-P.; Zhou, H.-C. Enzyme-MOF Nanoreactor Activates Nontoxic Paracetamol for Cancer Therapy. *Angewandte Chemie International Edition* **2018**, *57* (20), 5725–5730. https://doi.org/10.1002/anie.201801378.

(29) Ricoux, R.; Korri-Youssoufi, H.; Mahy, J. P. Microperoxidase 8 as a Powerful Tool for Biological Applications. *Journal of Biological Sciences* **2005**, *5* (1), 44–49.

(30) Marques, H. M. Insights into Porphyrin Chemistry Provided by the Microperoxidases, the Haempeptides Derived from Cytochrome C. *Dalton Transactions* **2007**, No. 39, 4371. https://doi.org/10.1039/b710940g.

(31) Gkaniatsou, E.; Sicard, C.; Ricoux, R.; Benahmed, L.; Bourdreux, F.; Zhang, Q.; Serre, C.; Mahy, J.-P.; Steunou, N. Enzyme Encapsulation in Mesoporous Metal-Organic Frameworks for Selective Biodegradation of Harmful Dye Molecules. *Angewandte Chemie International Edition* **2018**. https://doi.org/10.1002/anie.201811327.

(32) Kamata, K.; Hirano, T.; Ishimoto, R.; Mizuno, N. Sulfoxidation with Hydrogen Peroxide Catalyzed by [SeO4{WO(O2)2}2]2−. *Dalton Transactions* **2010**, *39* (23), 5509. https://doi.org/10.1039/c002318c.

(33) Li, P.; Moon, S.-Y.; Guelta, M. A.; Lin, L.; Gómez-Gualdrón, D. A.; Snurr, R. Q.; Harvey, S. P.; Hupp, J. T.; Farha, O. K. Nanosizing a Metal–Organic Framework Enzyme Carrier for Accelerating Nerve Agent Hydrolysis. *ACS Nano* **2016**, *10* (10), 9174–9182. https://doi.org/10.1021/acsnano.6b04996.

(34) Demessence, A.; Horcajada, P.; Serre, C.; Boissière, C.; Grosso, D.; Sanchez, C.; Férey, G. Elaboration and Properties of Hierarchically Structured Optical Thin Films of MIL-101(Cr). *Chemical Communications* **2009**, No. 46, 7149. https://doi.org/10.1039/b915011k.

(35) Jiang, D.; Keenan, L. L.; Burrows, A. D.; Edler, K. J. Synthesis and Post-Synthetic Modification of MIL-101(Cr)-NH2via a Tandem Diazotisation Process. *Chemical Communications* **2012**, *48* (99), 12053. https://doi.org/10.1039/c2cc36344e.

(36) Lammert, M.; Bernt, S.; Vermoortele, F.; De Vos, D. E.; Stock, N. Single- and Mixed-Linker Cr-MIL-101 Derivatives: A High-Throughput Investigation. *Inorganic Chemistry* **2013**, *52* (15), 8521–8528. https://doi.org/10.1021/ic4005328.

(37) Buragohain, A.; Couck, S.; Van Der Voort, P.; Denayer, J. F. M.; Biswas, S. Synthesis, Characterization and Sorption Properties of Functionalized Cr-MIL-101-X (X=–F, –Cl, –Br, –CH3, –C6H4, –F2, –(CH3)2) Materials. *Journal of Solid State Chemistry* **2016**, *238*, 195–202. https://doi.org/10.1016/j.jssc.2016.03.034.

(38) Deng, H.; Grunder, S.; Cordova, K. E.; Valente, C.; Furukawa, H.; Hmadeh, M.; Gandara, F.; Whalley, A. C.; Liu, Z.; Asahina, S.; et al. Large-Pore Apertures in a Series of Metal-Organic Frameworks. *Science* **2012**, *336* (6084), 1018–1023. https://doi.org/10.1126/science.1220131.

(39) Koutsopoulos, S.; Patzsch, K.; Bosker, W. T. E.; Norde, W. Adsorption of Trypsin on Hydrophilic and Hydrophobic Surfaces. *Langmuir* **2007**, *23* (4), 2000–2006. https://doi.org/10.1021/la062238s.

(40) Aron, J.; Baldwin, D. A.; Marques, H. M.; Pratt, J. M.; Adams, P. A. Hemes and Hemoproteins: 1: Preparation and Analysis of the Heme-Containing Octapeptide (Microperoxidase-8) and Identification of the Monomeric Form in Aqueous Solution. *Journal of Inorganic Biochemistry* **1986**, *27* (4), 227–243. https://doi.org/10.1016/0162-0134(86)80064-2.

(41) Othman, S.; Le Lirzin, A.; Desbois, A. Resonance Raman Investigation of Imidazole and Imidazolate Complexes of Microperoxidase: Characterization of the Bis (Histidine) Axial Ligation in c-Type Cytochromes. *Biochemistry* **1994**, *33* (51), 15437–15448.

(42) Kenzom, T.; Srivastava, P.; Mishra, S. Structural Insights into 2,2′-Azino-Bis(3-Ethylbenzothiazoline-6-Sulfonic Acid) (ABTS)-Mediated Degradation of Reactive Blue 21 by Engineered Cyathus Bulleri Laccase and Characterization of Degradation Products. *Applied and Environmental Microbiology* **2014**, *80* (24), 7484–7495. https://doi.org/10.1128/AEM.02665-14.

(43) Akiyama, G.; Matsuda, R.; Sato, H.; Takata, M.; Kitagawa, S. Cellulose Hydrolysis by a New Porous Coordination Polymer Decorated with Sulfonic Acid Functional Groups. *Advanced Materials* **2011**, *23* (29), 3294–3297. https://doi.org/10.1002/adma.201101356.

(44) Juan-Alcañiz, J.; Gielisse, R.; Lago, A. B.; Ramos-Fernandez, E. V.; Serra-Crespo, P.; Devic, T.; Guillou, N.; Serre, C.; Kapteijn, F.; Gascon, J. Towards Acid MOFs – Catalytic Performance of Sulfonic Acid Functionalized Architectures. *Catalysis Science & Technology* **2013**, *3* (9), 2311. https://doi.org/10.1039/c3cy00272a.

(45) Yang, J.; Zhao, Q.; Li, J.; Dong, J. Synthesis of Metal–Organic Framework MIL-101 in TMAOH-Cr(NO3)3-H2BDC-H2O and Its Hydrogen-Storage Behavior. *Microporous and Mesoporous Materials* **2010**, *130* (1–3), 174–179. https://doi.org/10.1016/j.micromeso.2009.11.001.

(46) Zhao, X.; Wang, K.; Gao, Z.; Gao, H.; Xie, Z.; Du, X.; Huang, H. Reversing the Dye Adsorption and Separation Performance of Metal–Organic Frameworks via Introduction of −SO_3H Groups. *Industrial & Engineering Chemistry Research* **2017**, *56* (15), 4496–4501. https://doi.org/10.1021/acs.iecr.7b00128.

(47) Marques, H. M.; Baldwin, D. A.; Pratt, J. M. Hemes and Hemoproteins. 3. the Reaction of Microperoxidase-8 with Cyanide: Comparison with Aquocobalamin and Hemoproteins. *Journal of Inorganic Biochemistry* **1987**, *29* (1), 77–91. https://doi.org/10.1016/0162-0134(87)80014-4.

(48) Qi, P. X.; Beckman, R. A.; Wand, A. J. Solution Structure of Horse Heart Ferricytochrome c and Detection of Redox-Related Structural Changes by High-Resolution 1H NMR†,‡. *Biochemistry* **1996**, *35*, 12275–12286.

(49) Hartono, S. B.; Qiao, S. Z.; Liu, J.; Jack, K.; Ladewig, B. P.; Hao, Z.; Lu, G. Q. M. Functionalized Mesoporous Silica with Very Large Pores for Cellulase Immobilization. *The Journal of Physical Chemistry C* **2010**, *114* (18), 8353–8362. https://doi.org/10.1021/jp102368s.

(50) Weckhuysen, B. M.; Wachs, I. E. *In Situ* Raman Spectroscopy of Supported Chromium Oxide Catalysts: $^{18}O_2$ – $^{16}O_2$ Isotopic Labeling Studies. *The Journal of Physical Chemistry B* **1997**, *101* (15), 2793–2796. https://doi.org/10.1021/jp963101l.

(51) Biju, V.; Pan, D.; Gorby, Y. A.; Fredrickson, J.; McLean, J.; Saffarini, D.; Lu, H. P. Combined Spectroscopic and Topographic Characterization of Nanoscale Domains and Their Distributions of a Redox Protein on Bacterial Cell Surfaces. *Langmuir* **2007**, *23* (3), 1333–1338. https://doi.org/10.1021/la061343z.

(52) Lefevre-Groboillot, D.; Dijols, S.; Boucher, J.-L.; Mahy, J.-P.; Ricoux, R.; Desbois, A.; Zimmermann, J.-L.; Mansuy, D. *N* -Hydroxyguanidines as New Heme Ligands: UV−Visible, EPR, and Resonance Raman Studies of the Interaction of Various Compounds Bearing a CNOH Function with Microperoxidase-8 †. *Biochemistry* **2001**, *40* (33), 9909–9917. https://doi.org/10.1021/bi010561i.

(53) Othman, S.; Le Lirzin, A.; Desbois, A. A Heme C-Peptide Model System for the Resonance Raman Study of c-Type Cytochromes: Characterization of the Solvent-Dependence of Peptide-Histidine-Heme Interactions. *Biochemistry* **1993**, *32* (37), 9781–9791. https://doi.org/10.1021/bi00088a033.

(54) Karu, T. I.; Pyatibrat, L. V.; Kolyakov, S. F.; Afanasyeva, N. I. Absorption Measurements of a Cell Monolayer Relevant to Phototherapy: Reduction of Cytochrome c Oxidase under near IR Radiation. *Journal of Photochemistry and Photobiology B: Biology* **2005**, *81* (2), 98–106. https://doi.org/10.1016/j.jphotobiol.2005.07.002.

(55) Chen, Y.; Han, S.; Li, X.; Zhang, Z.; Ma, S. Why Does Enzyme Not Leach from Metal–Organic Frameworks (MOFs)? Unveiling the Interactions between an Enzyme Molecule and a MOF. *Inorganic Chemistry* **2014**, *53* (19), 10006–10008. https://doi.org/10.1021/ic501062r.

(56) de Lauzon, S.; Mansuy, D.; Mahy, J.-P. Coordination Chemistry of Iron (III)–Porphyrin–Antibody Complexes. *The FEBS Journal* **2002**, *269* (2), 470–480.

(57) Zhou, Z.; Hartmann, M. Progress in Enzyme Immobilization in Ordered Mesoporous Materials and Related Applications. *Chemical Society Reviews* **2013**, *42* (9), 3894. https://doi.org/10.1039/c3cs60059a.

(58) Valderrama, B.; Ayala, M.; Vazquez-Duhalt, R. Suicide Inactivation of Peroxidases and the Challenge of Engineering More Robust Enzymes. *Chemistry & biology* **2002**, *9* (5), 555–565.

(59) Kadnikova, E. N.; Kostić, N. M. Oxidation of ABTS by Hydrogen Peroxide Catalyzed by Horseradish Peroxidase Encapsulated into Sol–Gel Glass.: Effects of Glass Matrix on Reactivity. *Journal of Molecular Catalysis B: Enzymatic* **2002**, *18* (1–3), 39–48.

(60) Patra, S.; Sene, S.; Mousty, C.; Serre, C.; Chaussé, A.; Legrand, L.; Steunou, N. Design of Laccase–Metal Organic Framework-Based Bioelectrodes for Biocatalytic Oxygen Reduction Reaction. *ACS Applied Materials & Interfaces* **2016**, *8* (31), 20012–20022. https://doi.org/10.1021/acsami.6b05289.

(61) Kobayashi, S.; Nakano, M.; Kimura, T.; Schaap, P. A. On the Mechanism of the Peroxidase-Catalyzed Oxygen-Transfer Reactiont. *Biochemistry* **1987**, *26*, 5019–5022.

(62) Burtch, N. C.; Jasuja, H.; Walton, K. S. Water Stability and Adsorption in Metal–Organic Frameworks. *Chemical Reviews* **2014**, *114* (20), 10575–10612. https://doi.org/10.1021/cr5002589.

(63) Evans, J. D.; Sumby, C. J.; Doonan, C. J. Post-Synthetic Metalation of Metal–Organic Frameworks. *Chem. Soc. Rev.* **2014**, *43* (16), 5933–5951. https://doi.org/10.1039/C4CS00076E.

(64) Vu, T. A.; Le, G. H.; Dao, C. D.; Dang, L. Q.; Nguyen, K. T.; Dang, P. T.; Tran, H. T. K.; Duong, Q. T.; Nguyen, T. V.; Lee, G. D. Isomorphous Substitution of Cr by Fe in MIL-101 Framework and Its Application as a Novel Heterogeneous Photo-Fenton Catalyst for Reactive Dye Degradation. *RSC Adv.* **2014**, *4* (78), 41185–41194. https://doi.org/10.1039/C4RA06522K.

(65) Loiseau, T.; Férey, G. Crystalline Oxyfluorinated Open-Framework Compounds: Silicates, Metal Phosphates, Metal Fluorides and Metal-Organic Frameworks (MOF). *Journal of Fluorine Chemistry* **2007**, *128* (4), 413–422. https://doi.org/10.1016/j.jfluchem.2006.09.009.

(66) Jiang, D.; Burrows, A. D.; Edler, K. J. Size-Controlled Synthesis of MIL-101(Cr) Nanoparticles with Enhanced Selectivity for CO2 over N2. *CrystEngComm* **2011**, *13* (23), 6916–6919. https://doi.org/10.1039/c1ce06274c.

(67) Rallapalli, P. B. S.; Raj, M. C.; Senthilkumar, S.; Somani, R. S.; Bajaj, H. C. HF-Free Synthesis of MIL-101(Cr) and Its Hydrogen Adsorption Studies. *Environmental Progress & Sustainable Energy* **2016**, *35* (2), 461–468. https://doi.org/10.1002/ep.12239.

(68) Nouar, F.; Devic, T.; Chevreau, H.; Guillou, N.; Gibson, E.; Clet, G.; Daturi, M.; Vimont, A.; Grenèche, J. M.; Breeze, M. I.; et al. Tuning the Breathing Behaviour of MIL-53 by Cation Mixing. *Chemical Communications* **2012**, *48* (82), 10237. https://doi.org/10.1039/c2cc35348b.

(69) Devic, T.; Serre, C. High Valence 3p and Transition Metal Based MOFs. *Chem. Soc. Rev.* **2014**, *43* (16), 6097–6115. https://doi.org/10.1039/C4CS00081A.

(70) Zhao, T.; Jeremias, F.; Boldog, I.; Nguyen, B.; Henninger, S. K.; Janiak, C. High-Yield, Fluoride-Free and Large-Scale Synthesis of MIL-101(Cr). *Dalton Transactions* **2015**, *44* (38), 16791–16801. https://doi.org/10.1039/C5DT02625C.

(71) Wickenheisser, M.; Herbst, A.; Tannert, R.; Milow, B.; Janiak, C. Hierarchical MOF-Xerogel Monolith Composites from Embedding MIL-100(Fe,Cr) and MIL-101(Cr) in Resorcinol-Formaldehyde Xerogels for Water Adsorption Applications. *Microporous and Mesoporous Materials* **2015**, *215*, 143–153. https://doi.org/10.1016/j.micromeso.2015.05.017.

(72) Férey, G.; Mellot-Draznieks, C.; Serre, C.; Millange, F.; Gutour, J.; Surblé, S.; Margiolaki, I. A Chromium Terephthalate-Based Solid with Unusually Large Pore Volumes and Surface Area. *Science* **2005**, *309* (5743), 2040–2042. https://doi.org/10.1126/science.1116275.

(73) Férey, G.; Millange, F.; Morcrette, M.; Serre, C.; Doublet, M.-L.; Grenèche, J.-M.; Tarascon, J.-M. Mixed-Valence Li/Fe-Based Metal–Organic Frameworks with Both Reversible Redox and Sorption Properties. *Angewandte Chemie International Edition* **2007**, *46* (18), 3259–3263. https://doi.org/10.1002/anie.200605163.

(74) Abeykoon, B.; Grenèche, J.-M.; Jeanneau, E.; Chernyshov, D.; Goutaudier, C.; Demessence, A.; Devic, T.; Fateeva, A. Tuning the Iron Redox State inside a Microporous Porphyrinic Metal Organic Framework. *Dalton Transactions* **2017**, *46* (2), 517–523. https://doi.org/10.1039/C6DT04208B.

(75) Horcajada, P.; Surblé, S.; Serre, C.; Hong, D.-Y.; Seo, Y.-K.; Chang, J.-S.; Grenèche, J.-M.; Margiolaki, I.; Férey, G. Synthesis and Catalytic Properties of MIL-100(Fe), an Iron(III) Carboxylate with Large Pores. *Chem. Commun.* **2007**, No. 27, 2820–2822. https://doi.org/10.1039/B704325B.

(76) Vimont, A.; Goupil, J.-M.; Lavalley, J.-C.; Daturi, M.; Surblé, S.; Serre, C.; Millange, F.; Férey, G.; Audebrand, N. Investigation of Acid Sites in a Zeotypic Giant Pores Chromium(III) Carboxylate. *Journal of the American Chemical Society* **2006**, *128* (10), 3218–3227. https://doi.org/10.1021/ja056906s.

Chapter 4

In-situ synthesis of MOFs and enzyme immobilization

Table of Contents

Introduction

This chapter deals with the "*in-situ* synthesis" approach for the immobilization of enzyme molecules. It is a one-step and sustainable process in which, the MOF synthesis is taking place simultaneously with the immobilization of the enzymes, resulting in the entrapment of enzymes by aggregates of MOF particles. As the enzyme molecules are surrounded by the MOF particles, they can be stabilized and protected under non-natural environments, similarly to what occurs for the inclusion of enzymes in MOF cages. Moreover, there is no limitation on the MOFs' pore size, as the enzymes are not occupying the MOF porosity. The MOF porosity is left free for the diffusion of substrates and therefore there is reduced diffusion limitations to the enzyme's active site. The challenging part of this approach is to perform the synthesis of MOFs under mild conditions (T≤ 37 ^{o}C, aqueous solutions, and physiological pH) to be compatible with the preservation of enzymes' catalytic activity. Most MOFs are obtained under high temperatures and pressures and in organic solvents or acidic conditions (discussed in the first chapter). As a result, in most cases synthesis optimization is required to obtain MOFs under milder conditions. The selection of potential MOFs for the "in-situ synthesis" must be made taking into account several key parameters: (i) the MOF precursors must at least partially soluble in water, and the MOFs must be (ii) composed of reactive cations in order to synthesize them under atmospheric pressure; (iii) chemically and water stable and finally (iv) relatively hydrophilic to minimize the denaturation of hydrophilic enzymes and maintain a humid environment when non-aqueous media are required for catalytic applications.

Based on these parameters, two chemically stable MOF structures were selected for the "*in-situ* synthesis" process, MIL-53(Al)-FA a microporous, hydrophilic MOF and MIL-100(Fe) a mesoporous, amphiphilic MOF that is known to be highly biocompatible. The first part of this chapter presents the efforts made to obtain MIL-53(Al)-FA in water under ambient temperature and pressure. The obtained MIL-53(Al)-FA was then used for the immobilization of proteins. The study was performed with bovine serum albumin (BSA), as a model protein that is relatively robust and commercially available at low costs. The systems were thoroughly characterized to gain information on their structural characteristics and on the localization of the immobilized biomolecules. While the "*in-situ* synthesis" approach using MIL-53(Al)-FA has been studied from the beginning of this PhD project, the required synthesis optimization and the complexity of the system did not permit the completion of this work, which still remains under investigation. Thus, some preliminary results obtained for the encapsulation of the model and commercially available enzyme, Horseradish peroxidase (HRP) and the catalytic efficiency of the resulting HRP@MIL-53(Al)-FA materials, are briefly presented. Despite the extensive optimization of MIL-53(Al)-FA, the synthesis pH remained acidic, as this is necessary for the formation of MIL-53(Al)-FA. Therefore, an alternative approach for the immobilization of pH sensitive enzymes is also presented. It involves the synthesis of hybrid MIL-53(Al)-FA/alginate beads materials. Finally, the use of MIL-100(Fe) as an immobilization matrix will be briefly discussed.

A. MIL-53(Al)-FA

MIL-53(Al)-FA (or Basolite A520) is one of the few commercialized MOFs, used as a adsorbent of CH_4 by BASF, thanks to its low-cost and non-toxic components (aluminum sulfate and fumaric acid) and to its excellent water stability and its relatively high surface area (~1100 m^2/g).[1] Moreover, fumaric acid is soluble in water (7 g/L at 25 °C), which should make possible the synthesis of this MOF in water under ambient conditions. All these characteristics render MIL-53(Al)-FA a perfect candidate for the "*in-situ* synthesis" immobilization. The structure of MIL-53(Al)-FA is presented in Figure 4-1. Its 3D framework is composed by 1D chains of corner sharing Al(III) octahedra linked together by fumarate ligands, giving a microporous structure with 1D channels of 5.7 × 6.0 Å free aperture.[2]

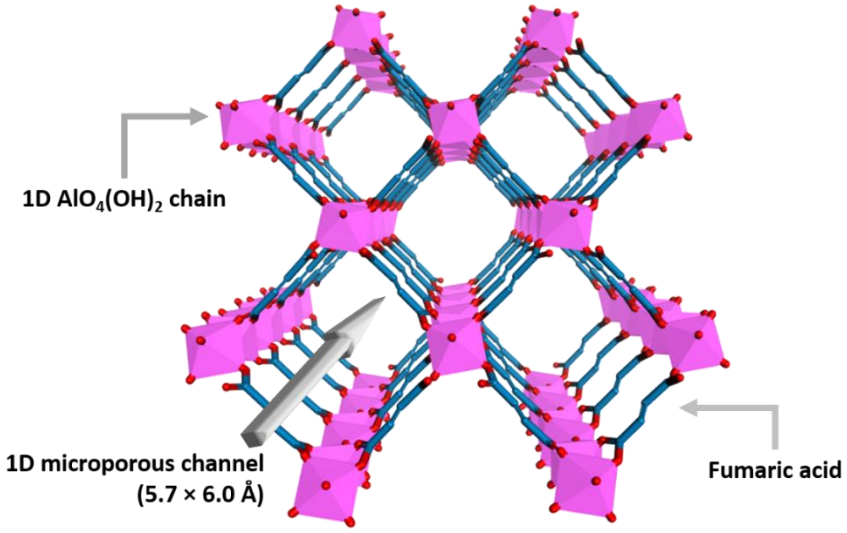

Figure 4-1: Structure of MIL-53(Al)-FA (or Basolite A520).

1. Synthesis Optimization

This work has been performed by myself with the contribution of <u>Stellina Giannopoulou</u> (Master 2 student) and <u>Chrysoula Kartsiouka</u> (bachelor student) as part of their internship at the Institut Lavoisier de Versailles.

The synthesis optimization of MIL-53(Al)-FA was based on the conditions reported in the BASF patent and the PhD work of Elsa Alvarez:[3] 0.105 mol $Al_2(SO_4)_3 \cdot 18H_2O$ (0.16 M) dissolved in 300 mL H_2O were heated at 60 °C. A mixture of 0.209 mol fumaric acid (0.32 M) and 0.630 mol NaOH (0.95 M) dissolved in 360 mL H_2O was heated at 60 °C and then added to the aluminium sulfate solution. The formed white suspension was collected by filtration.

In order to adapt the patent synthesis to milder temperature conditions, the concentration of the reactants was decreased, to achieve a better solubility. Moreover, various aluminum precursors, as well as various metal cation:ligand:base molar ratios were tested. The temperature of the syntheses was fixed at RT or 37 °C (use of incubator) and the reaction time was extended from 16 to 72 h. Table 4-1 summarizes the tested synthetic conditions.

Table 4-1: Parameters studied for the synthesis of MIL-53(Al)-FA, in H_2O and ambient conditions.

Parameters	Tested Conditions	Optimal Conditions
Al precursors	$Al_2(SO_4)_3{\cdot}18H_2O$, $Al(NO_3)_3{\cdot}9H_2O$, $Al(NH_4)(SO_4)_2{\cdot}12H_2O$, $Al(OH)_3$, $Al(OH)(C_2H_3O_2)_2$, Al_2O_3, $NaAlO_2$	$Al_2(SO_4)_3{\cdot}18H_2O$ & $NaAlO_2$
Al concentration (M)	0.05, 0.075	0.05 & 0.075 (respectively)
Molar ratio metal cation:ligand:NaOH	1:2:6, 1:2:6, 1:2:7, 1:2:7.5, 1:2:8,1:2:0, 1.5:2:0, 2:2:0, 2.5:2:0, 2:2:0.5	1:2:6 & 1.5:2:0 (respectively)
Temperature (°C)	RT, 37 °C	RT
Time (h)	16, 48, 72	48

A key parameter for the synthesis of MIL-53(Al)-FA is the pH of the solution. As seen from the Pourbaix diagram of aluminium (Figure 4-2), Al^{3+} is soluble in water, under acidic conditions (pH ≤ 4) or under basic conditions (pH > 10). However, the coordination of aluminium is pH dependent.[4] At low pH, the dominant species of aluminium is $[Al(H_2O)_6]^{3+}$, in which the Al^{3+} ion is coordinated by six water molecules in an octahedral geometry.[5] With the increase of the pH, some of the coordinated water molecules lose a proton, resulting to coordinated hydroxyl ions. They are more strongly attracted to the Al atom, which leads to a lower effective Al ionic radius and reduces the space for other coordinating species. Therefore, at basic pH (pH > 10) the coordination number of Al decreases to four and the dominant species in aqueous solution are the tetrahedra is $Al(OH)4^{-5}$, in which the Al^{3+} ion is coordinated by four hydroxylates in a tetrahedral geometry(Figure 4-2).[5] A control of the pH is also important for the viability of the encapsulated enzymes (quaternary structure and resulting catalytic activity), as acidic conditions are known to denaturate many of them. It was thus crucial to maintain the pH of the reaction around 4, in order to promote the synthesis of the 1D chains of Al octahedra of MIL-53(Al)-FA. In the meantime, as it is also crucial not to expose enzyme molecules to very acidic conditions, some attempts were made to obtain the MIL-53(Al)-FA at pH~5.

Precursors choice: Different aluminium precursors were tested in order to replace $Al_2(SO_4)_3{\cdot}18H_2O$ (patent synthesis) and to increase the pH of the reaction to render the synthesis more compatible for pH-sensitive enzymes. $Al(NH_4)(SO_4)_2{\cdot}12H_2O$, $Al(NO_3)_3{\cdot}9H_2O$, and $Al(OH)(C_2H_3O_2)_2$ were selected due to their slightly lower acidity compared to that of $Al_2(SO_4)_3{\cdot}18H_2O$. $Al(OH)_3$ and Al_2O_3 were chosen as they could dissolve progressively upon reaction with fumaric acid, resulting in the formation of the MOF. However, the low reaction temperature did not permit their slow dissolution and were thus disregarded as precursors. $Al(OH)(C_2H_3O_2)_2$ was discarded as Al^{3+} sources since it was not possible to remove the unreacted precursor by washing the obtained solid with water. $Al(NO_3)_3{\cdot}9H_2O$ and $Al(NH_4)(SO_4)_2{\cdot}12H_2O$, even though they were both soluble in water, did not induce a sufficient crystallization of MIL-53(Al)-FA. The increase of the reaction pH to 5 using these precursors caused an important decrease in the crystallinity of the samples, highlighting the need of lower pH conditions. Finally, it was possible to obtain well crystallized MIL-53(Al)-FA, with two

different metal precursors: $Al_2(SO_4)_3 \cdot 18H_2O$ and $NaAlO_2$. Therefore, two synthetic routes were developed.

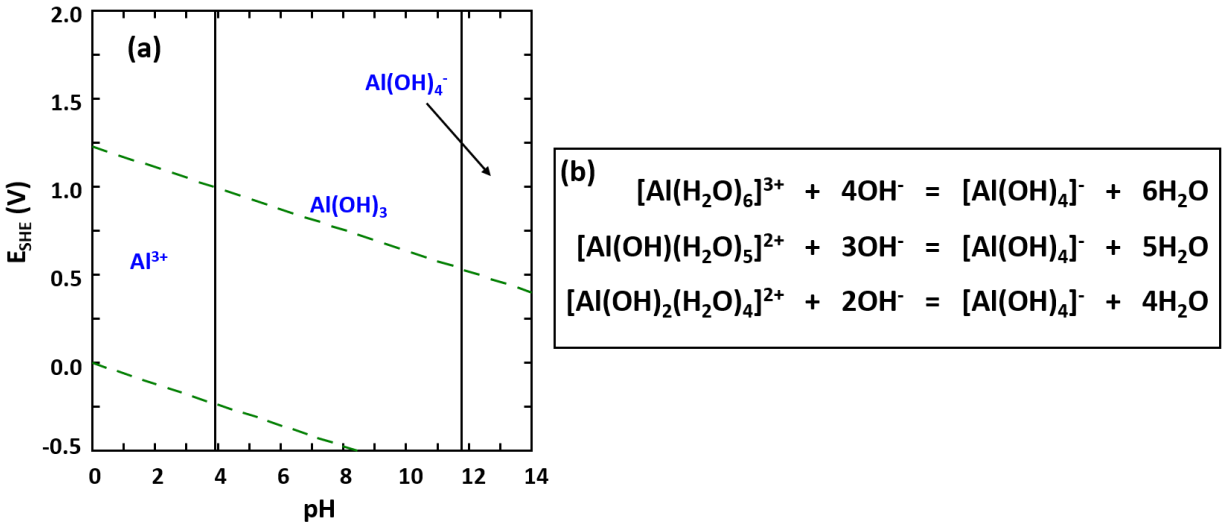

Figure 4-2: (a) Pourbaix diagram of aluminum calculated for $[Al^{3+}]$ = 0.001 M, at 25 °C, using the Hydra/Medousa software. Green dashed lines represent the redox couples O_2/H_2O and H_2O/H_2; (b) pH-dependent equilibria of soluble Al species in water.

Molar ratio of reactants: Similarly to the investigation of different aluminium precursors, different molar ratios of reactants were tested in order to tune the reaction pH around 5. However, this increase led either to amorphous phases or to very poorly crystallized MIL-53(Al)-FA particles. The optimal metal cation:ligand:NaOH ratios 1:2:6 & 1.5:2:0 for the two synthetic routes with $Al_2(SO_4)_3 \cdot 18H_2O$ and $NaAlO_2$, respectively, resulted in a pH value of ~ 4.

Reaction Temperature: No difference in crystallinity and surface area were observed by increasing the temperature from RT to 37 °C. Therefore, the temperature was set at RT.

Reaction time: The crystallization of MIL-53(Al)-FA started immediately after the mixing of the metal precursor and the ligand (for both precursors). However, as we were aiming to study the structural characteristics of the MOF and its composites with different biomolecules, a well-crystallized structure, with possibly a lower number of defects was preferred and the reaction time was set at 48 h. No noticeable differences in crystallinity and surface area could be observed by increasing the reaction time over 48 h. Note that in case of highly pH-sensitive enzymes, shorter reaction times should be preferred, in order to limit as much as possible the duration of the exposure of the biomolecules to the slightly acidic conditions of the synthesis (pH 4) that could affect their catalytic activities.

Synthetic route based on $Al_2(SO_4)_3 \cdot 18H_2O$: The first synthetic route is very similar to the already reported one and involves the use of aluminium sulfate (0.05 M). More specifically, 1 mmol of $Al_2(SO_4)_3 \cdot 18H_2O$ was dissolved in 10 mL H_2O (pH 3.3), under stirring at RT. 2 mmol of fumaric acid and 6 mmol of NaOH were then dissolved in 10 mL H_2O (pH 12) and the resulting solution was added to the aluminium sulfate solution (pH ~3.7). The mixture was left under stirring at RT for 48 h. The obtained white solid was recovered by centrifugation (1000 rpm, 3

min) and was then washed 6 times with H_2O, to remove any unreacted precursors. The pure MIL-53(Al)-FA was dried overnight at 100°C. Yield =81.1 %

Synthetic route based on $NaAlO_2$: The second procedure was obtained with sodium aluminate (0.075 M). Briefly, 1.5 mmmol $NaAlO_2$ was dissolved in 20 mL H_2O (pH 10). In this case, there was no need for NaOH, as the dissolution of $NaAlO_2$ in water produces basic $Al(OH)_4^-$. 2 mmol fumaric acid were added directly (as powder) in the metal solution (pH ~4.4) and the mixture was left stirring at RT for 48 h. The obtained white solid was recovered by centrifugation and purified as described above. Yield= 67.3 %

2. Characterization of MIL-53(Al)-FA products

Figure 4-3 shows the normalized PXRD diagrams of the two MIL-53(Al)-FA products, obtained in H_2O at RT after 48 h of reaction, along with that of the MOF obtained from the synthesis described in the patent and the calculated pattern. The diagrams of both products match with the diagram obtained from the patent synthesis, indicating the formation of the MIL-53(Al)-FA phase. The width of the characteristic Bragg peaks (10.5, 15, 21, 30, 31.6, 42.5 43.8 °) is much larger than that obtained from the patent synthesis, especially for the MOF obtained with $Al_2(SO_4)_3{\cdot}18H_2O$. This could arise either from a low crystallinity of the MOF and/or from a small particle size. However, it is not possible to conclude on that point, considering the strong aggregation of the particles, as shown by the SEM images below (Figure 4-7). The use of $AlNaO_2$ seems to result in a better crystallized product, compared to that obtained from $Al_2(SO_4)_3{\cdot}18H_2O$. Nonetheless, Basolite A520 (or MIL-53(Al)-FA) is well-known to give poorly crystallized particles,[2] and a decrease of the crystallinity could be expected with the decrease of the reaction temperature from 60 °C (patent conditions) to RT. The successful formation of MIL-53(Al)-FA by both synthetic routes was also confirmed by solid-state ^{27}Al NMR spectroscopy (see Annex 2).

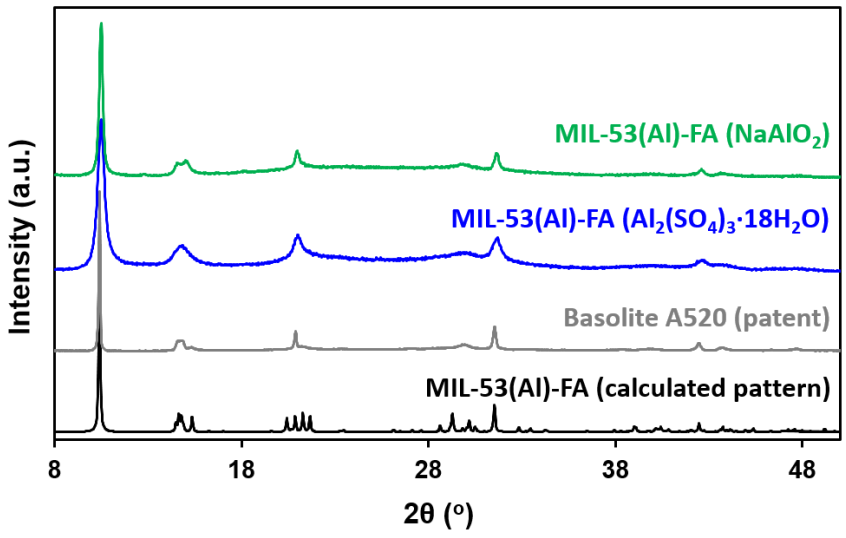

Figure 4-3: Normalized XRD patterns of the calculated pattern of MIL-53(Al)-FA (black), Basolite A520, synthesized based on the patent conditions (grey), MIL-53(Al)-FA, synthesized with $Al_2(SO_4)_3{\cdot}18H_2O$ in water at room temperature (blue) and MIL-53(Al)-FA, synthesized with $NaAlO_2$ in water at room temperature (green).

The FT-IR spectra of the two MIL-53(A)-FA products, along with that of Basolite A520 are shown in Figure 4-4. The stretching band of the C=O bond of the carboxylic acid groups of the free ligand, ν(C=O) = 1700 cm^{-1} is present only in the case of the MIL-53(Al)-FA ($Al_2(SO_4)_3 \cdot 18H_2O$) product, indicating the presence of small amounts of remaining unreacted fumaric acid. The asymmetric $\nu(C\text{-}O)_{as}$ and symmetric $\nu(C\text{-}O)_s$ stretching modes of the coordinated carboxylate groups are found around 1600 cm^{-1} and 1400 cm^{-1} respectively, for all three products. The spectrum of MIL-53(Al)-FA ($Al_2(SO_4)_3 \cdot 18H_2O$) shows broader IR bands than those of the other samples, which is consistent with a lower crystallinity of the sample.

Figure 4-5 shows the TGA curves of the MIL-53(A)-FA products and of Basolite A520. The calculated weight losses were based on the formula $AlOH(C_4O_4H_2) \cdot xH_2O$ (x~4).[2] Both MIL-53(Al)-FA products show a lower decomposition temperature (~380 °C), than Basolite A520 (~400 °C). Moreover, Basolite A520 and MIL-53(Al)-FA ($Al_2(SO_4)_3 \cdot 18H_2O$) lead to higher amounts of residues than the calculated values, indicating the presence of hydroxides or oxides in the samples. On the contrary, the oxide residue of MIL-53(Al)-FA ($NaAlO_2$) is close to the calculated value, which is consistent with the formation of a MOF with high purity.

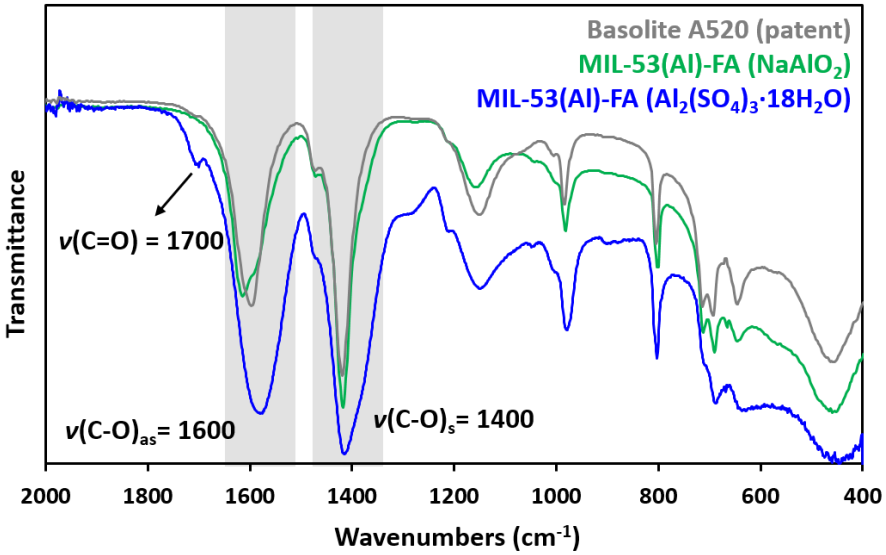

Figure 4-4: FT-IR spectra of Basolite A520 (patent) (grey), MIL-53(Al)-FA ($NaAlO_2$) (green) and MIL-53(Al)-FA ($Al_2(SO_4)_3 \cdot 18H_2O$) (blue).

The N_2 adsorption isotherms are shown in Figure 4-6. All products display a type I isotherm, characteristic of microporous materials, and the calculated BET surface areas are close to 1000 m^2/g, independently of the synthetic conditions. Given that MIL-53(Al)-FA ($NaAlO_2$) led to a better crystallinity compared to the $Al_2(SO_4)_3 \cdot 18H_2O$ product, based on the PXRD diagrams and a to higher purity of its structure, based on the TG analysis, it would be expected to have a slightly higher BET surface area than the other two products. However, it should be noticed that the standard error of TGA measurements is around ± 5% and, thus, it is possible that the amounts of the residual oxides could be over or under estimated. Similarly, the BET analysis also has a value of incertitude.

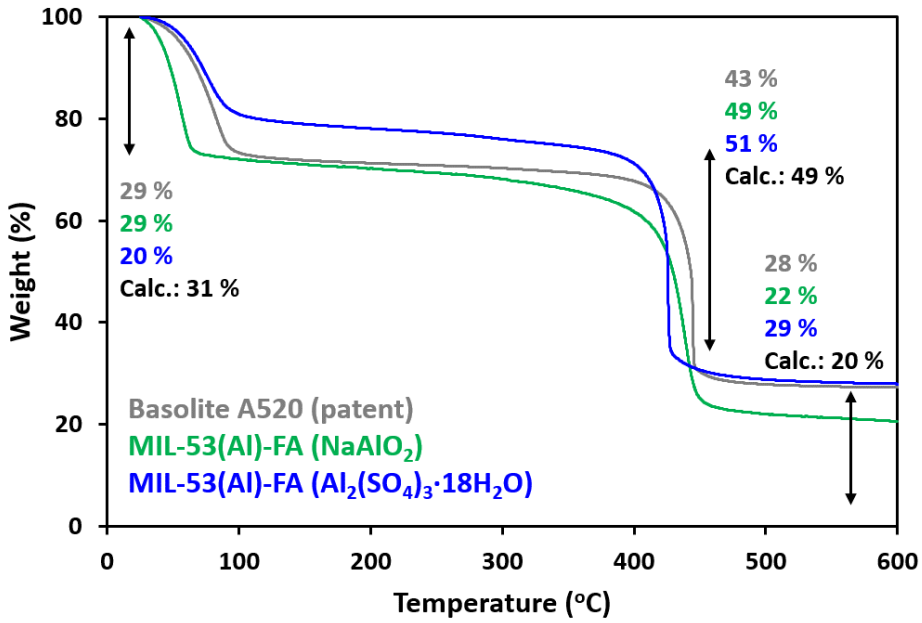

Figure 4-5: TGA curves of Basolite A520 (patent) (grey), MIL-53(Al)-FA ($NaAlO_2$) (green) and MIL-53(Al)-FA ($Al_2(SO_4)_3 \cdot 18H_2O$) (blue), measured under O_2 flow.

The SEM images of the two MIL-53(Al)-FA products and Basolite A520 are presented in Figure 4-7. No morphological information could be extracted for MIL-53(Al)-FA ($Al_2(SO_4)_3 \cdot 18H_2O$), as in this case, the particles are very aggregated and their size is extremely small. MIL-53(Al)-FA ($NaAlO_2$) forms larger particles, which however, do not have a specific form. These results are not surprising as Basolite A520 obtained following the patent synthesis also forms particles with non-specific morphology.[2]

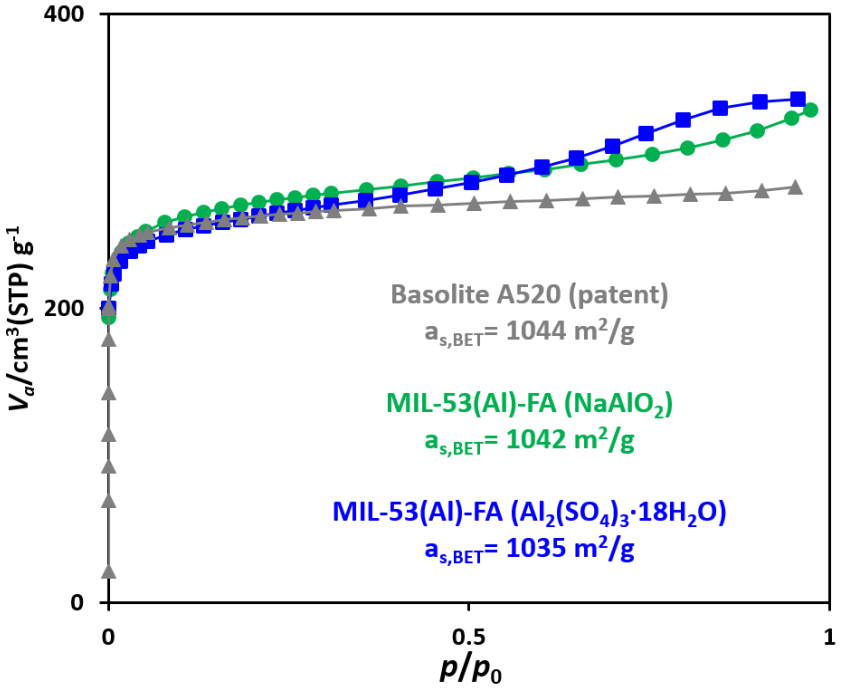

Figure 4-6: N_2 adsorption isotherms of Basolite A520 (patent) (grey), MIL-53(Al)-FA ($NaAlO_2$) (green) and MIL-53(Al)-FA ($Al_2(SO_4)_3 \cdot 18H_2O$) (blue) at 77 K; sample activation: 150 °C/24 h, under vacuum.

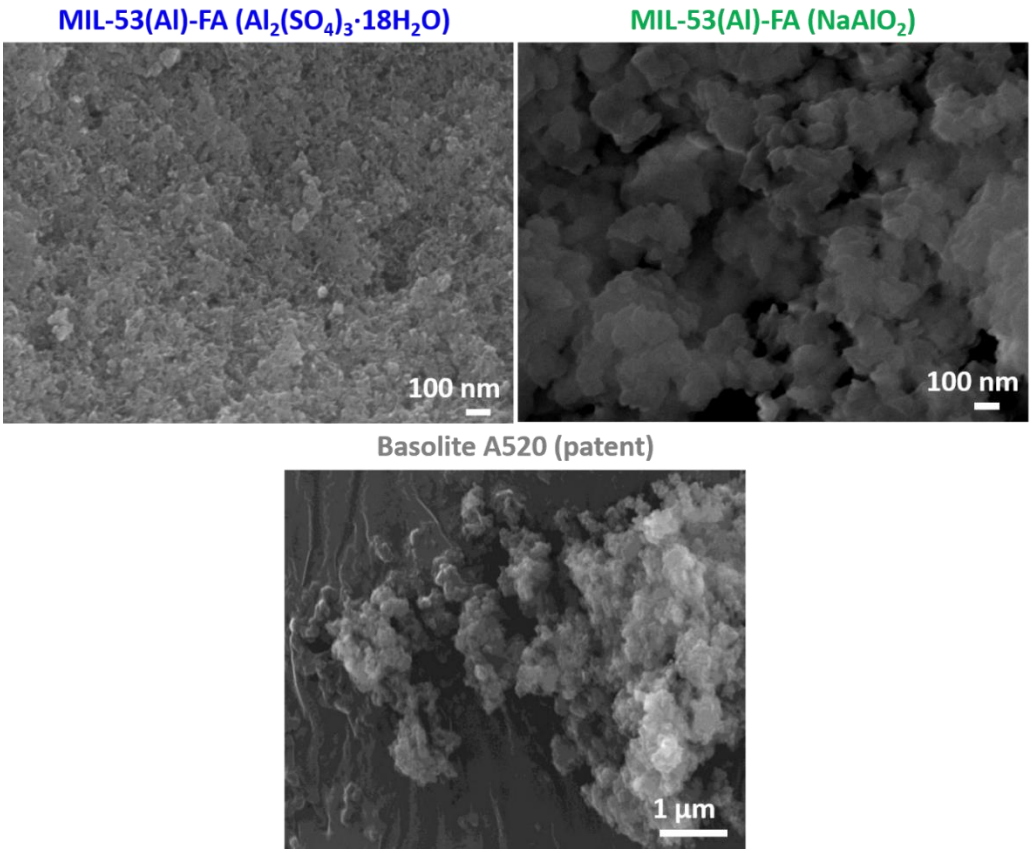

Figure 4-7: SEM images of MIL-53(Al)-FA ($Al_2(SO_4)_3 \cdot 18H_2O$) on the top left and MIL-53(Al)-FA ($NaAlO_2$) on the top right and Basolite A520 (patent)[2] on the bottom.

3. *In-situ* immobilization of BSA protein in MIL-53(Al)-FA

The *in-situ* immobilization of the protein BSA (Bovine Serum Albumin) was performed with the $Al_2(SO_4)_3 \cdot 18H_2O$ precursor, as this synthetic procedure was developed prior to the $NaAlO_2$ procedure. Nonetheless, it would be of interest to test the $NaAlO_2$ precursor for the *in-situ* immobilization of biomolecules in the future, as it results into products with higher crystallinity.

BSA was chosen first as a model biomolecule, for its properties, including its large size (~66 kDa), its robustness and cheap commercial availability. In addition, it has already been extensively used to study similar systems (mostly with ZIF-8), in which BSA seems to attract and concentrate metal cations and ligands, thus facilitating the MOF synthesis.[6–8] At a first stage, the goal of the study was mainly to investigate the immobilization process and the structural characteristics of the bio-hybrid materials, thus the use of a catalytically active biomolecule was not required. It should however be noticed that different biomolecules may have different interactions with the MOF precursors and thus result to different structural characteristics or even modify the crystallization process of the material.

The first *in-situ* experiments were performed with a fluorophore-tagged biomolecule, FITC-BSA (FITC-BSA= fluorescein isothiocyanate conjugate of BSA), as the immobilization of FITC-BSA and its localization in the MOF matrix could be followed by fluorescence microscopy. For

the immobilization, 5 mg of FITC-BSA (as powder) were added to the ligand/base aqueous solution and the synthetic procedure was identical to that described above. The obtained solid was washed six times with water and left to dry at RT.

As seen in Figure 4-8, the immobilization of the FITC-BSA can be confirmed by the color change of the powder from white to yellow, due to the presence of the tagged biomolecule. The supernatant and the washing solution of the FITC-BSA@MIL-53(Al)-FA were uncolored, which may indicate the full immobilization of the biomolecule. The composite was then analyzed by confocal laser scanning microscopy (CLSM) in order to investigate the localization of FITC-BSA in the MOF powder. As seen in Figure 4-8(b), the composite shows green fluorescence that confirms the presence of FITC-BSA in the MOF powder.

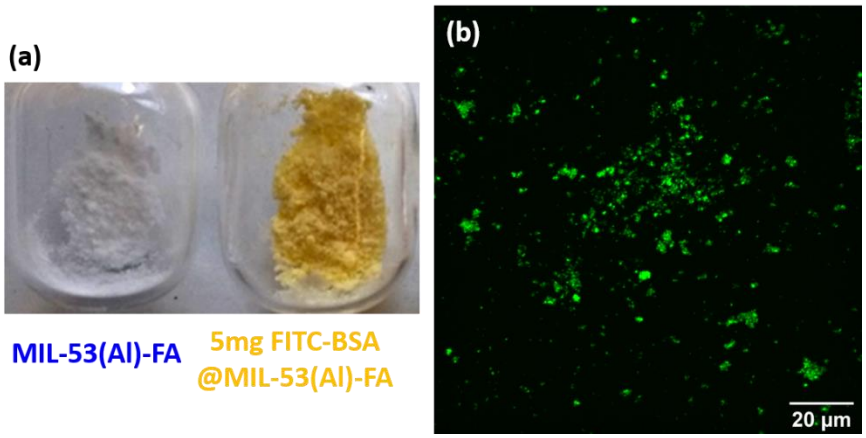

Figure 4-8: (a) Powders of MIL-53(Al)-FA (white) and 5mg FITC-BSA@MIL-53(Al)-FA (yellow), synthesized in H_2O at RT; (b) CLSM image of 5mg FITC-BSA@MIL-53(Al)-FA showing the contribution of the FITC-labeled protein.

The PXRD diagram of the composite superimposes with that of MIL-53(Al)-FA, suggesting that the crystal structure of the MOF was preserved upon the association with FITC-BSA (Figure 4-9).

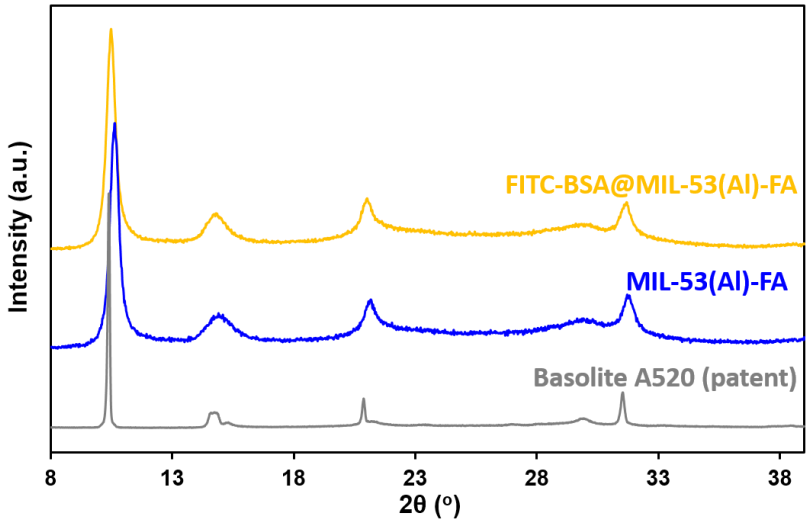

Figure 4-9: Normalized PXRD patterns of Basolite A520 (patent) (grey), MIL-53(Al)-FA (blue) and FITC-BSA@MIL-53(Al)-FA (yellow).

The composite was further characterized by IR spectroscopy, TG analysis and N_2 porosimetry. However, since the amount of immobilized FITC-BSA was rather low (~0.01 mg biomolecule/mg MIL-53(Al)-FA), no difference was observed between the analyses of the composite and those of the parent MOF (Figure 4-10). It was thus concluded that higher amounts of FITC-BSA were required for a complete characterization of the system. The use of FITC-BSA in large quantities is problematic, due to its high cost. Nonetheless, one more experiment was performed with FITC-BSA, as it allows the visualization of the protein by confocal microscopy. Specifically, we proceeded with the immobilization of 50 mg FITC-BSA in MIL-53(Al)-FA *via* the *in-situ* approach and for comparison, 50 mg FITC-BSA were immobilized with pre-formed particles of MIL-53(Al)-FA, in order to investigate any differences on the localization of the protein. The CLSM images of 50 mg FITC-BSA@MIL-53(Al)-FA and 50 mg FITC-BSA@MIL-53(Al)-FA (post-synthesis) are shown in Figure 4-11. Both composites presented green fluorescence, deriving from the FITC-conjugated protein. The protein was homogeneously dispersed in both samples, but its exact localization was not possible due to the small size of the MOF particles and the extensive aggregation. The morphology of the samples showed important differences. In the case of the *in-situ* composite, extended aggregates of very small particles were present forming a kind of network, whereas the post-synthesis sample displayed separated aggregates of larger particles. Interestingly, variations were also found in the thickness of the two composites. While the aggregates of the post-synthesis sample presented important thickness (z~ 8 μm), the *in-situ* composite presented very thin aggregates (z = 1.8 μm) (Figure 4-12). These results may indicate that BSA modified the formation of the MOF particles, possibly by providing multiple nucleation sites for the MOF resulting in small nanoparticles that aggregated in larger particles. To fully evaluate the role of BSA and the induced changes in the formation of MIL-53(Al)-FA, we continued our studies with BSA non-conjugate with FITC for reasons of cost.

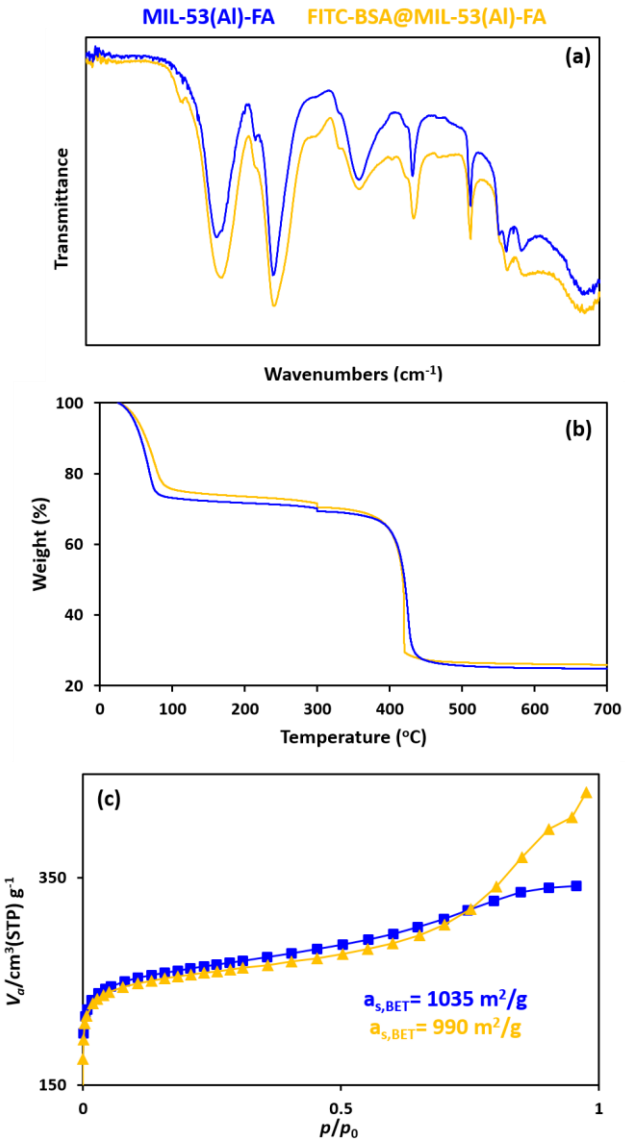

Figure 4-10: (a) FT-IR spectra, (b) TGA curves, under O_2 flow and (c) N_2 adsorption isotherms at 77 K of MIL-53(Al)-FA (blue) and FITC-BSA@ MIL-53(Al)-FA (yellow).

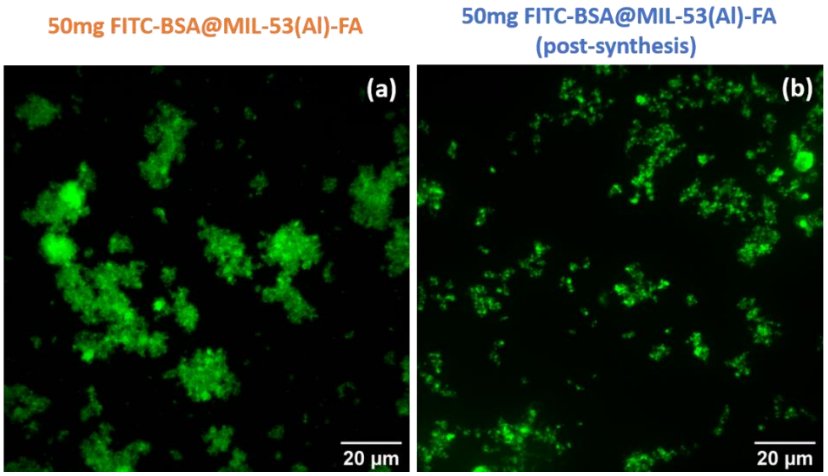

Figure 4-11: CLSM image of (a) 50mg FITC-BSA@MIL-53(Al)-FA and (b) 50mg FITC-BSA@MIL-53(Al)-FA (post-synthesis) showing the contribution of the FITC-labeled protein.

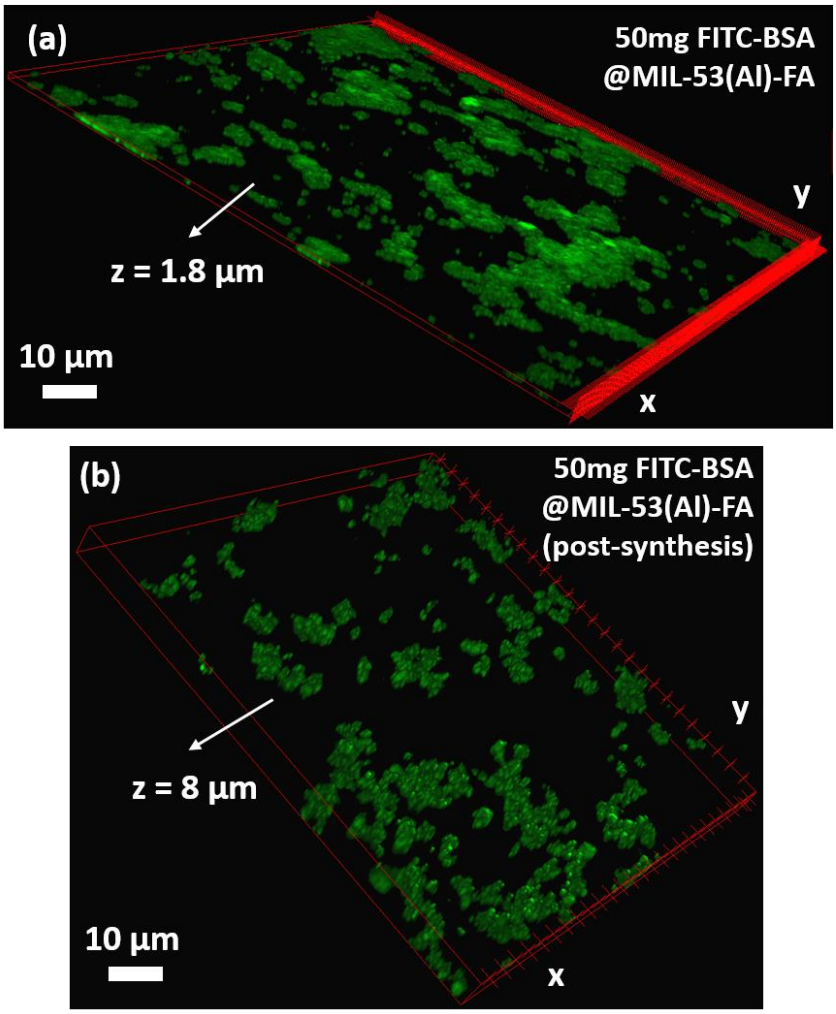

Figure 4-12: 3D view of (a) 50mg FITC-BSA@MIL-53(Al)-FA and (b) 50mg FITC-BSA@MIL-53(Al)-FA (post-synthesis), demonstrating the thickness of the samples (z). The images were constructed by the confocal microscopy measurements.

The immobilization procedure for BSA was similar to that described above. Different amounts of BSA (50, 200 and 400 mg) were added to the fumaric acid/NaOH aqueous solution (2mmol/6mmol) and then mixed with the $Al_2(SO_4)_3 \cdot 18H_2O$ aqueous solution (1 mmol). After 48 h, the solids were recovered by centrifugation (3 min, 10000 rpm) and washed six times with H_2O. The purified products were then dried overnight at 100 °C. The immobilized BSA amounts were estimated approximately by subtracting the weight of the MIL-53(Al)-FA, obtained without BSA from the weight of the composite. In order to evaluate the entrapment effect of this procedure, a control reaction was also performed, in which 200 mg of BSA were mixed with a pre-formed sample of MIL-53(Al)-FA for 48 h (200 mg BSA@MIL-53(Al)-FA, post synthesis). The amount of BSA adsorbed at the outer surface of the MOF was calculated in the same manner. As seen in Table 4-2, for all composites almost all the amount of the added BSA was immobilized. This translates into extremely high loadings (over 116 % wt BSA) by comparison with those already reported for MOF bio-hybrids (≤ 10 %)[9–11]. One explanation could be that the presence of BSA favors strongly the formation of the MOF and increases the overall mass of MIL-53(Al)-FA formed, compared to its synthesis in the absence of

biomolecule. However, the important increase of the composites' mass could not be attributed only to that effect, as this would lead to unrealistic changes to the MOF's yield (over 2-fold increase of MIL-53(Al)-FA mass). Besides, the theoretical yield (100 %) of reaction is 411 mg, thus the rest of the composites' mass can only be attributed to BSA. The high loading of the composite prepared *via* post-synthesis (58.8 wt %) is valid and cannot be due to the change of the reaction yield, as preformed particles were used. Such immobilization systems are very complex and little understood, as a variety of factors may influence the loading (nature of biomolecule and matrix, isoelectric points, specific interactions, kinetics of MOF synthesis…). It is thus not easy to explain the significant differences in the BSA loadings of MIL-53(Al) with the commonly used MOFs (ZIF-8). Some of the ZIF-8 based articles state that the biomolecules promote the crystallization of ZIF-8, which does not occur with the same kinetics without the biomolecules. This phenomenon requires low biomolecules amounts to favor the local crystallization of the MOF and may be one the reasons to explain the lower loadings. As already noted in the introduction, this work is not completed and a more adequate and precise quantification of the immobilized amounts of BSA needs to be performed. The chemical composition of the samples and the UV-Vis spectra of the supernatants will be investigated to enable a more precise quantification of the BSA loadings.

Table 4-2: Approximate BSA loading (wt % of MOF) of composites.

Sample	Composite (mg)	BSA weight (mg)	BSA loading (mg/mg, wt %)
MIL-53(Al)-FA	-	-	-
50mg BSA@MIL-53(Al)-FA	382 ± 12	48 ± 11	14
200mg BSA@MIL-53(Al)-FA	533 ±62	199 ± 38	60
200mg BSA@MIL-53(Al)-FA (post synthesis)	529 ± 49	196 ± 26	60
400mg BSA@MIL-53(Al)-FA	719 ± 46	385 ± 22	116

Figure 4-13 shows the PRXD diagrams of the composites, along with those of MIL-53(Al)-FA and Basolite A520. All samples showed a similar broadening of the Bragg peaks, compared to Basolite A520, which could be attributed to a lower crystallinity and/or to a smaller particle size. Nonetheless, the crystal structure of the MOF was not affected by the presence of high amounts of BSA. This was not the case for other immobilization systems (like ZIF-8), in which the crystallization of the MOF was totally hampered in the presence of high amounts of biomolecules.[6]

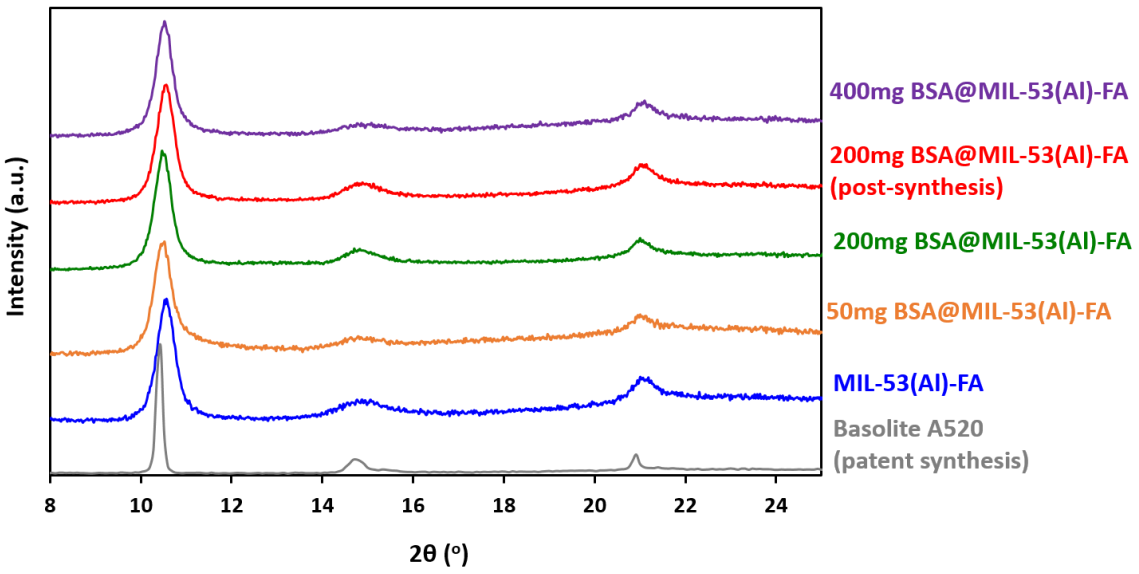

Figure 4-13: Normalized PXRD diagrams of Basolite A520 (grey), MIL-53(Al)-FA (blue), 50mg BSA@MIL-53(Al)-FA (orange), 200mg BSA@MIL-53(Al)-FA (green), 200mg BSA@MIL-53(Al)-FA (post-synthesis) (red) and 400mg BSA@MIL-53(Al)-FA (purple).

Figure 4-14 shows the characteristic vibrations of the peptide bonds found in proteins that can be detected by IR spectroscopy. The amide I vibration (~1650 cm^{-1}) is mainly attributed to the *v*(C=O) stretching mode of the amide groups, with a minor contribution of the *v*(N-H) bending mode.[12] This vibration is strongly dependent on the secondary structure of the protein that derives from hydrogen bonding between one amino hydrogen atom and one carbonyl oxygen atom in the polypeptide chain and reflects the backbone conformation and the hydrogen-bonding pattern (α-helix, β-sheet, *etc.*).[13] It is thus, commonly used for structural analysis of the protein backbone. The amide II vibration (~1550 cm^{-1}) is assigned to the *v*(C-N) stretching mode with a small contribution of the *v*(N-H) bending vibration.[12] The amide II vibration can also be used to extract structural information about the secondary structure of the protein but to a lesser extent when compared to the amide I vibration. Finally, the amide III (1400-1200 cm^{-1}) vibration is the combination of the *v*(N-H) bending and the *v*(C-N) stretching modes. This vibration is more complex, as it depends on the side chain structure (chemical groups attached to the alpha-carbon atoms of the peptide backbone), but in certain cases it can also give information about the secondary structure of proteins.[12]

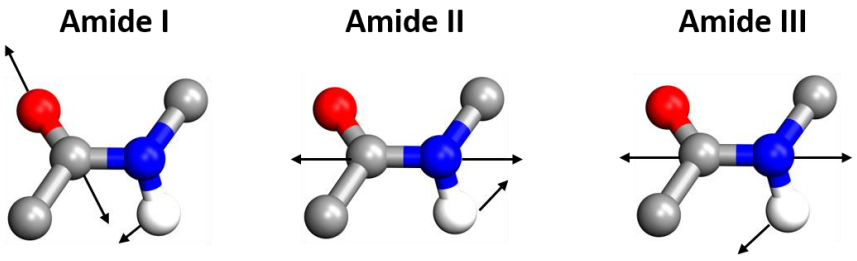

Figure 4-14: Schematic illustration of the characteristic vibrations of the peptide bonds found in protein molecules, like BSA.

The IR spectra of the composites are shown in Figure 4-15. The asymmetric (~1580 cm^{-1}) and symmetric (~1400 cm^{-1}) stretching modes of the carboxylates are overlapping with the amide vibrations, thus it was not possible to extract any structural information about the immobilized BSA. However, as the loading of BSA increased, a clear broadening of the vibration bands at 1700-1500 cm^{-1} was observed, which suggested a significant contribution of the amide I & II vibration bands is this region. This is consistent with the presence of BSA in the composites. At the highest BSA loading (400 mg), the appearance of a double band was observed (1600 & 1580 cm^{-1}) that could be assigned to the amide I vibration of the immobilized BSA and to the $\nu(CO)_{as}$ of MIL-53(Al)-FA. A similar double band was also observed in the case of the post-synthesis sample. The amide III vibration was not easily detectable. However, in the cases of the post-synthesis sample and the 400 mg BSA@MIL-53(Al)-FA, the broadening of the vibration around 1380 cm^{-1} may arise from the overlapping of $\nu(CO)_s$ of the MOF and the amide III vibrations.

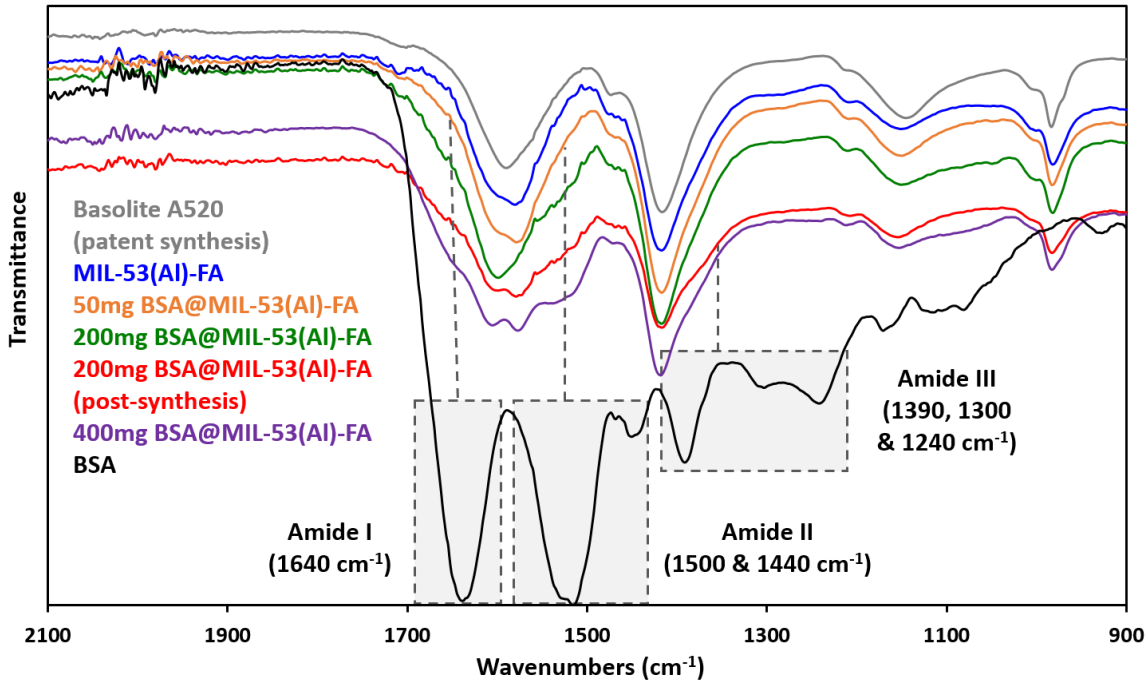

Figure 4-15: FT-IR spectra of Basolite A520 (grey), MIL-53(Al)-FA (blue), 50mg BSA@MIL-53(Al)-FA (orange), 200mg BSA@MIL-53(Al)-FA (green), 200mg BSA@MIL-53(Al)-FA (post-synthesis) (red), 400mg BSA@MIL-53(Al)-FA (purple) and free BSA (black).

The presence of BSA in MIL-53(Al)-FA samples is also consistent with the ^{13}C MAS NMR spectra of the composites as they showed resonances of α-carbons, aliphatic carbons and carbonyl carbons of the peptide bonds, characteristic of the BSA molecule. Moreover, the BSA did not seem to affect the structure of the MOF, based on the ^{27}Al MAS NMR spectra of the composites, which are identical to the parent MOF. (for details see Annex 2).

The composites were also analyzed by TGA (Figure 4-16). While in the absence of BSA, the destruction of the MIL-53(Al)-FA structure due to the decomposition of the coordinated fumarate is observed around 350 °C, in the presence of BSA the decomposition temperature

decreases with increasing amounts of BSA. The presence of BSA is consistent with the increase in the organic loss and the gradual decomposition of the organic part, due to the gradual decomposition of BSA (200-520 °C). By normalizing the residual Al_2O_3 content in all the composites to the oxide content of MIL-53(Al)-FA, it was possible to quantify the amounts of immobilized BSA (indicated in the graphs). The loadings extracted by TGA were in close agreement with the estimated amounts by simple weighing of the composites. The small differences can be possibly assigned to the standard error of both the TGA measurements and of the previously quantified amounts by simple weighing. Nonetheless, the values are close enough to confirm the previously calculated high loadings of BSA in MIL-53(Al)-FA, but a more precise quantification (elemental analysis, UV-vis of the supernatants) would be indispensable in the future.

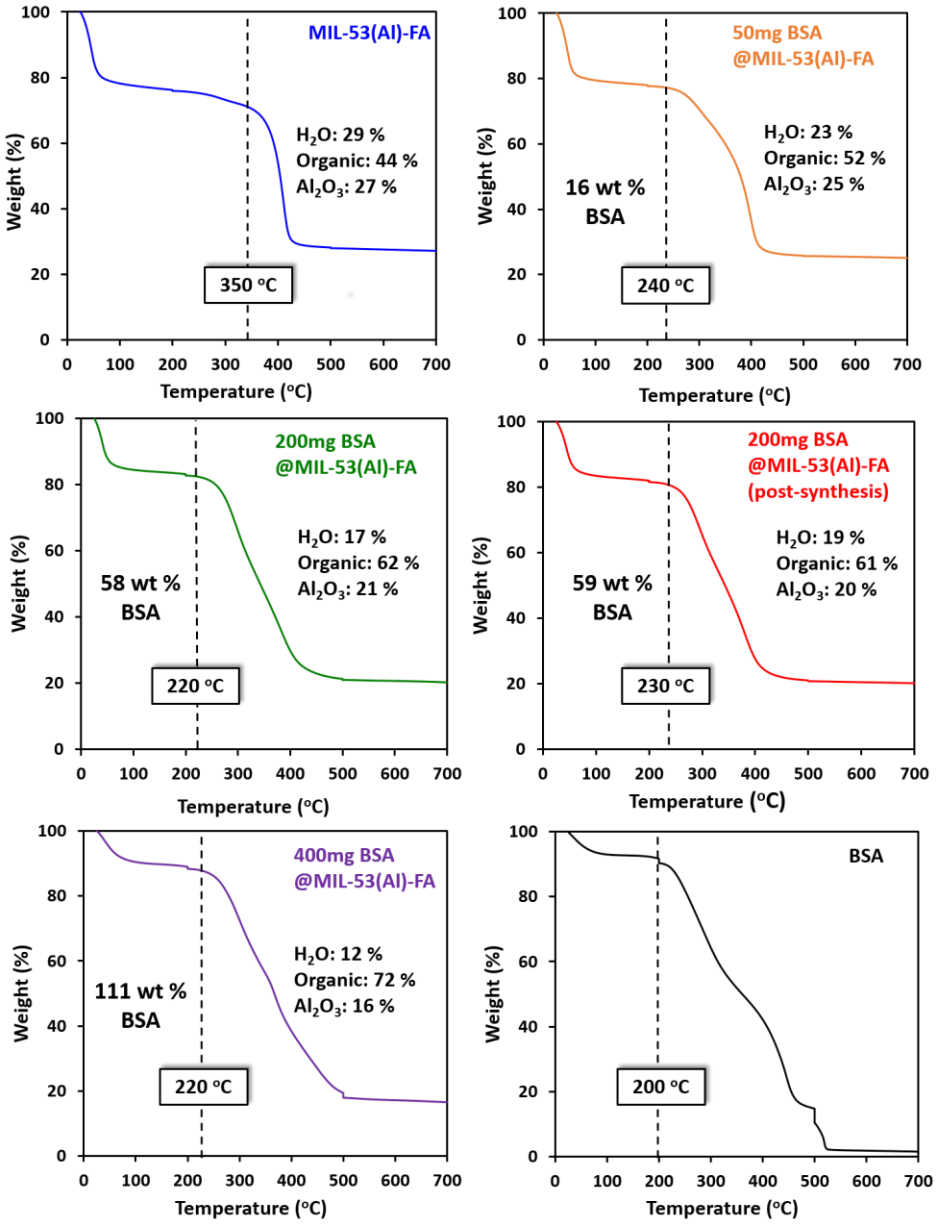

Figure 4-16: TGA curves of MIL-53(Al)-FA (blue), 50mg BSA@MIL-53(Al)-FA (orange), 200mg BSA@MIL-53(Al)-FA (green), 200mg BSA@MIL-53(Al)-FA (post-synthesis) (red), 400mg BSA@MIL-53(Al)-FA (purple) and free BSA (black). The dotted line marks the decomposition temperature of the samples.

The N_2 sorption isotherms of the composites are shown in Figure 4-17. All the composites prepared with the *in-situ* synthesis process, showed a decreased surface area that could be attributed to BSA molecules, blocking some of the micropores of the structure. The post-synthesis immobilization of BSA in MIL-53(Al)-FA resulted in a non-porous material, due to the total blockage of the external surface of the MOF by BSA molecules. The calculated BET surface areas were based on normalized weights of the materials (subtracting the weight of BSA). However, the accuracy of the BET surface values is not high, according to the approximate content of BSA. Interestingly, the isotherms of the *in-situ* synthesis samples show a type I isotherm, characteristic of a microporous material and similar to the adsorption isotherm of MIL-53(Al)-FA, but the desorption isotherms present a hysteresis loop. Hysteresis is usually associated with capillary condensation in mesoporous structures and can have different shapes (similarly to the type of isotherms) depending on the shape of the pores. All three composites prepared with the *in-situ* process show a H4 hysteresis loop, associated with narrow slit-like pores.[14] This is typically observed in the case of large defects in the structure or important interparticle spaces that are generated through the aggregation of MOF nanoparticles.[15,16]

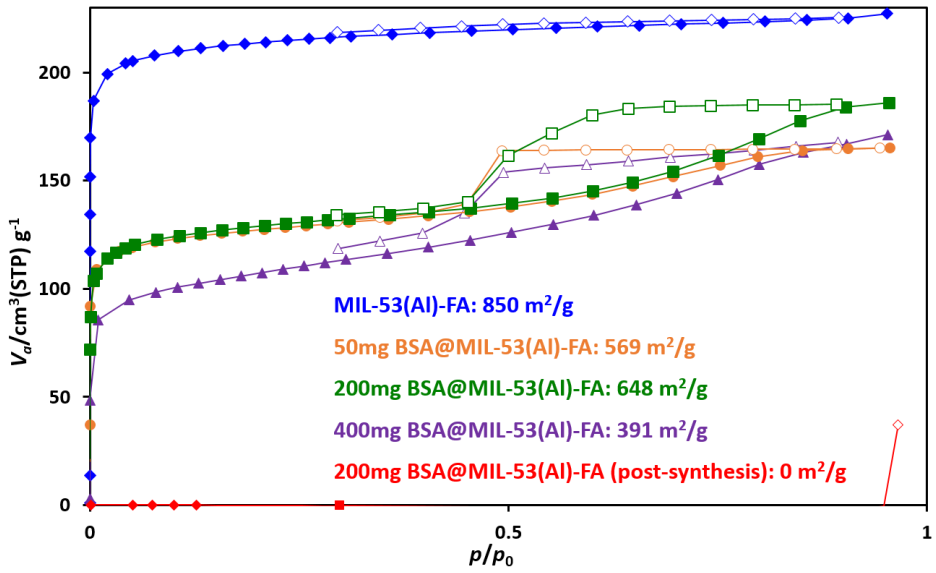

Figure 4-17: N_2 sorption isotherms of MIL-53(Al)-FA (blue diamonds), 50mg BSA@MIL-53(Al)-FA (orange circles), 200mg BSA@MIL-53(Al)-FA (green squares), 400mg BSA@MIL-53(Al)-FA (purple triangles) and 200mg BSA@MIL-53(Al)-FA (post-synthesis) (red diamonds), measured at 77 K. Filled symbols correspond to the adsorption process and unfilled symbols to the desorption process. Sample activation: 150 °C for 16 h, under secondary vacuum.

Figure 4-18 shows the pore-size distribution calculated from the N_2 sorption data. While Basolite A520 and MIL-53(Al)-FA did not present any mesopores, in agreement with the microporous structure of the MOF (0.6 nm), the presence of BSA has induced the formation of larger pores in the composites with radius of 2.4, 3.0 and 1.7 nm for 50mg BSA@ MIL-53(Al)-FA, 200mg BSA@ MIL-53(Al)-FA and 400mg BSA@ MIL-53(Al)-FA, respectively. Due to the large size of these formed pores, it is very unlikely that they derive from defects in the crystal structure, as it would require important parts of the structure missing. A more probable explanation is that the presence of BSA molecules results into important interparticle spaces

in the range of mesopores. It seems possible that the presence of BSA influences the crystallization and/or morphology of the material. In particular, the BSA surface may provide nucleation sites for the MOF synthesis and thus small nanoparticles may be formed that are aggregated and/or are retained together on the BSA surface. However, only the N_2 porosimetry and the calculated pore-size distribution cannot be enough to conclude on these results. As we will see below, electronic microscopy techniques and *in-situ* FT-IR analysis were employed in order to examine more extensively the morphology and porosity of the composites.

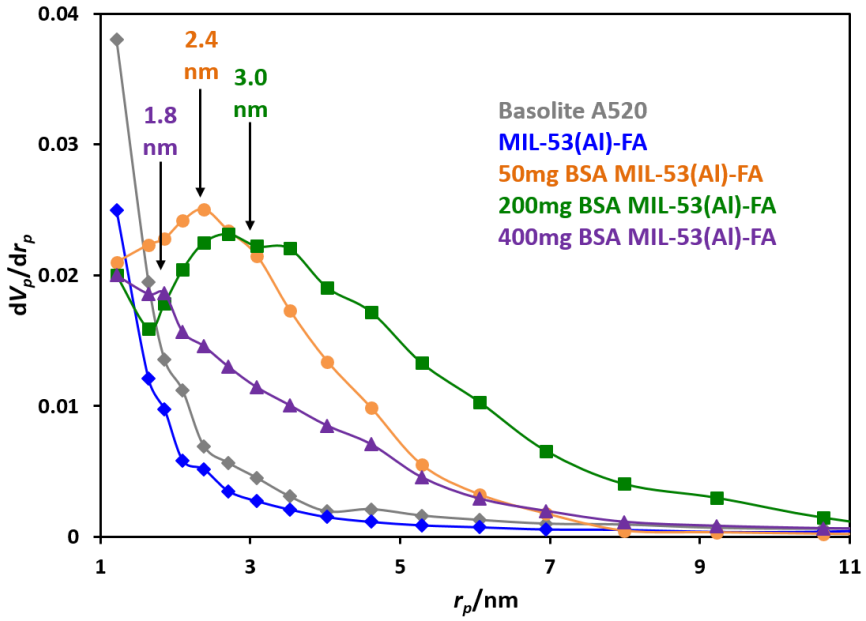

Figure 4-18: Calculated pore size distribution of mesopores *via* the BJH method for Basolite A520 (grey diamonds), MIL-53(Al)-FA (blue diamonds), 50mg BSA@MIL-53(Al)-FA (orange circles), 200mg BSA@MIL-53(Al)-FA (green squares) and 400mg BSA@MIL-53(Al)-FA (purple triangles).

The composites were characterized by transmission electron microscopy (TEM), Scanning transmission electron microscopy (STEM) and Energy-dispersive X-ray spectroscopy (XEDS) to investigate their morphology and the distribution of BSA in the MOF matrix. The TEM, STEM and EDX characterizations were performed by Prof. Nicolas Menguy at the Institut de Minéralogie, de Physique des Matériaux et de Cosmochimie at Sorbonne Université.

Figure 4-19 shows the STEM image of MIL-53(Al)-FA. No important morphological information could be extracted, due to the extended aggregation of the particles and their small size. Figure 4-20 presents the TEM images of BSA@MIL-53(Al)-FA composites. All samples showed extended aggregated networks, in which it was not possible to distinguish isolate particles and obtain information on their morphology. No significant morphological differences could be observed between the samples, but interestingly in the case of 50 mg BSA@MIL-53(Al)-FA and 200 mg BSA@MIL-53(Al)-FA the aggregated networks presented non-uniform mesoporous cavities that may be due to interparticle spaces. This could not be clearly evidenced on the 400 mg BSA@MIL-53(Al)-FA and the post-synthesis sample, suggesting that mesoporous cavities were less present in those samples.

XEDS analysis was performed in order to investigate the presence of BSA, by detecting the N atoms of the protein molecules. In the MIL-53(Al)-FA, three main elements were detected, Al, C and O that derive from the structure of the MOF (metal clusters and organic ligands) (Figure 4-21). Concerning the composites with BSA, four main elements were detected, Al, C, O and N. The detected N atoms may thus confirm the presence of BSA in the composites. (Figures 4-22/4-24). Furthermore, with increasing amounts of BSA, the detected N atoms also increased, following the order 400mg BSA@MIL-53(Al)-FA > 200mg BSA@MIL-53(Al)-FA (post-synthesis) > 50mg BSA@MIL-53(Al)-FA. It should however be noted that the elemental maps are not quantitative, but they demonstrate a general distribution of the elements in the samples. All elements were distributed homogeneously in the samples, which indicates that there is no phase separation between the BSA molecules and the MOF particles. Note that the apparent heterogeneous distribution of the O, C and N atoms in the composite 400mg BSA@MIL-53(Al)-FA is an effect of shadowing. (Figure 4-24) Backscatter electrons depend on the atomic mass of the elements. Thus, the lighter O, C and N atoms are less likely to diffuse through the sample and reach the detector compared to the Al atoms, resulting in a different elemental distribution. The detected Cu derives from the sample holder, the S atoms may be due to the use of $Al_2(SO_4)_3 \cdot 18H_2O$ for the synthesis of the MOF, while the small trace of Si could be attributed to impurities during the sample preparation (use of glassware).

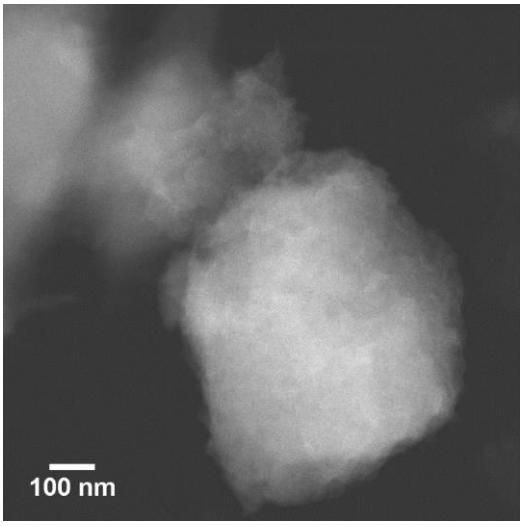

Figure 4-19: High-resolution STEM image of MIL-53(Al)-FA.

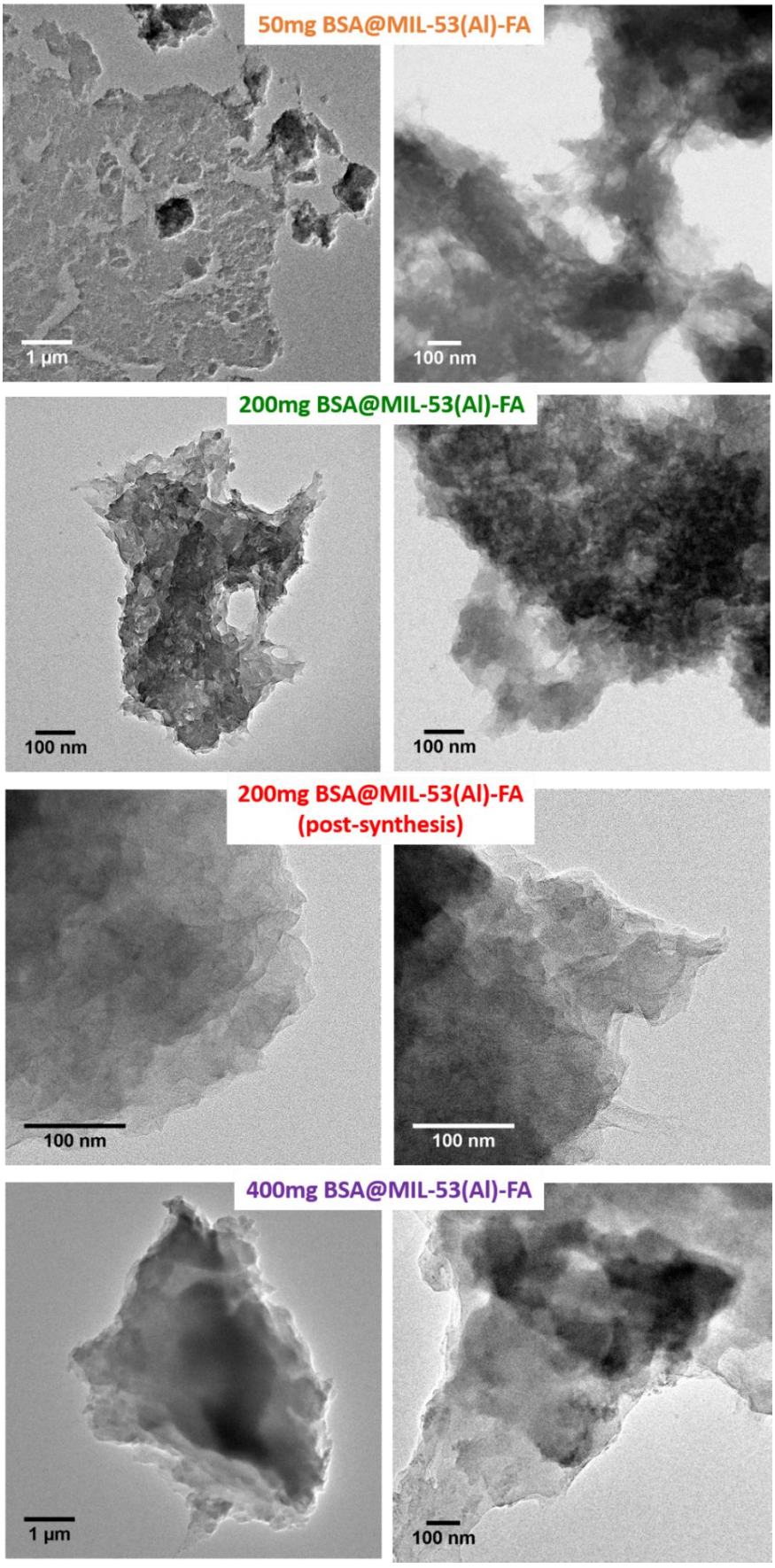

Figure 4-20: High resolution TEM images of 50mg BSA@MIL-53(Al)-FA (orange), 200mg BSA@MIL-53(Al)-FA (green), 200mg BSA@MIL-53(Al)-FA (post-synthesis) (red) and 400mg BSA@MIL-53(Al)-FA (purple)

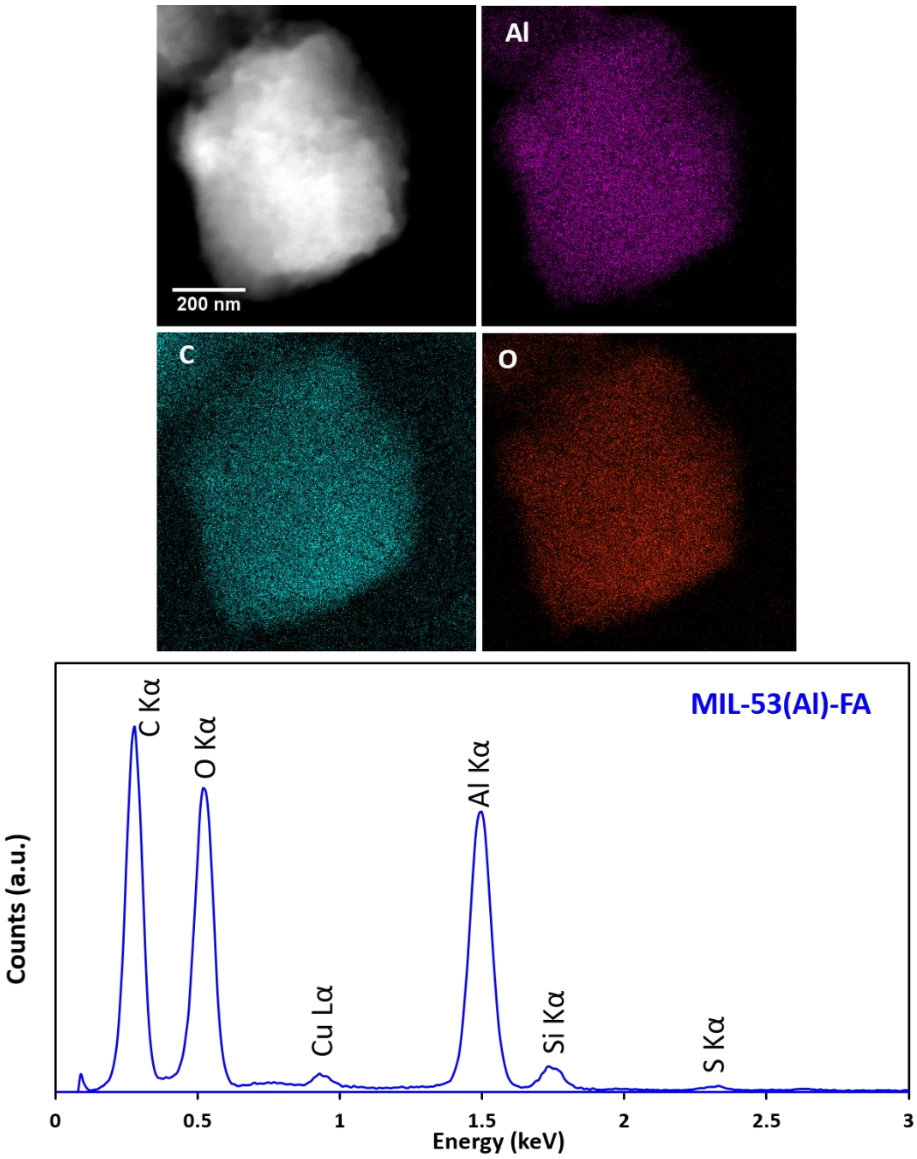

Figure 4-21: STEM-XEDS elemental mapping of MIL-53(Al)-FA acquired using energy windows related respectively to Al-Kα (magenta area), C-Kα (cyan area), O-Kα (red area) and N-Kα (green area) lines. Elemental maps are not quantitative.

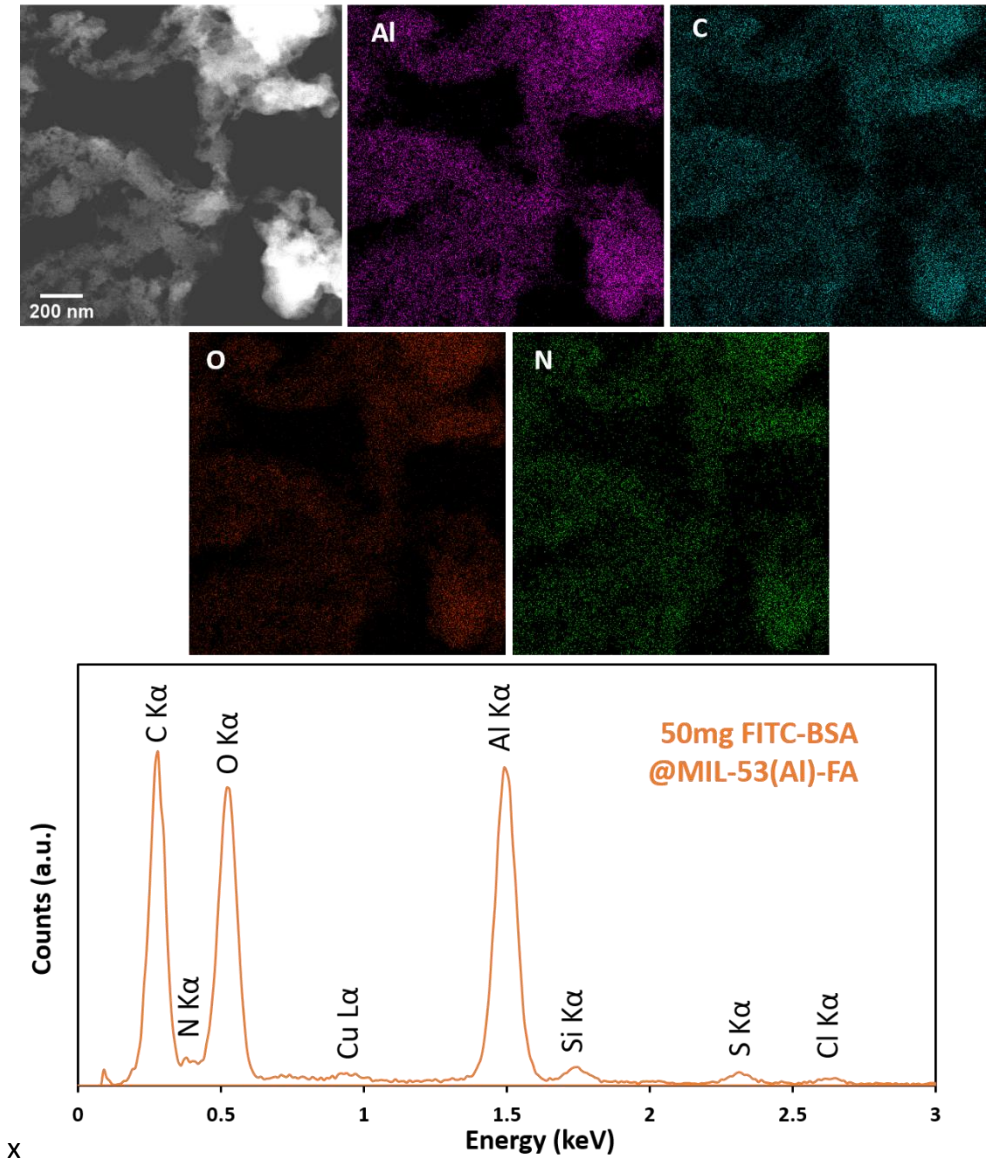

Figure 4-22: STEM-XEDS elemental mapping of 50mg BSA@MIL-53(Al)-FA acquired using energy windows related respectively to Al-Kα (magenta area), C-Kα (cyan area), O-Kα (red area) and N-Kα (green area) lines. Elemental maps are not quantitative.

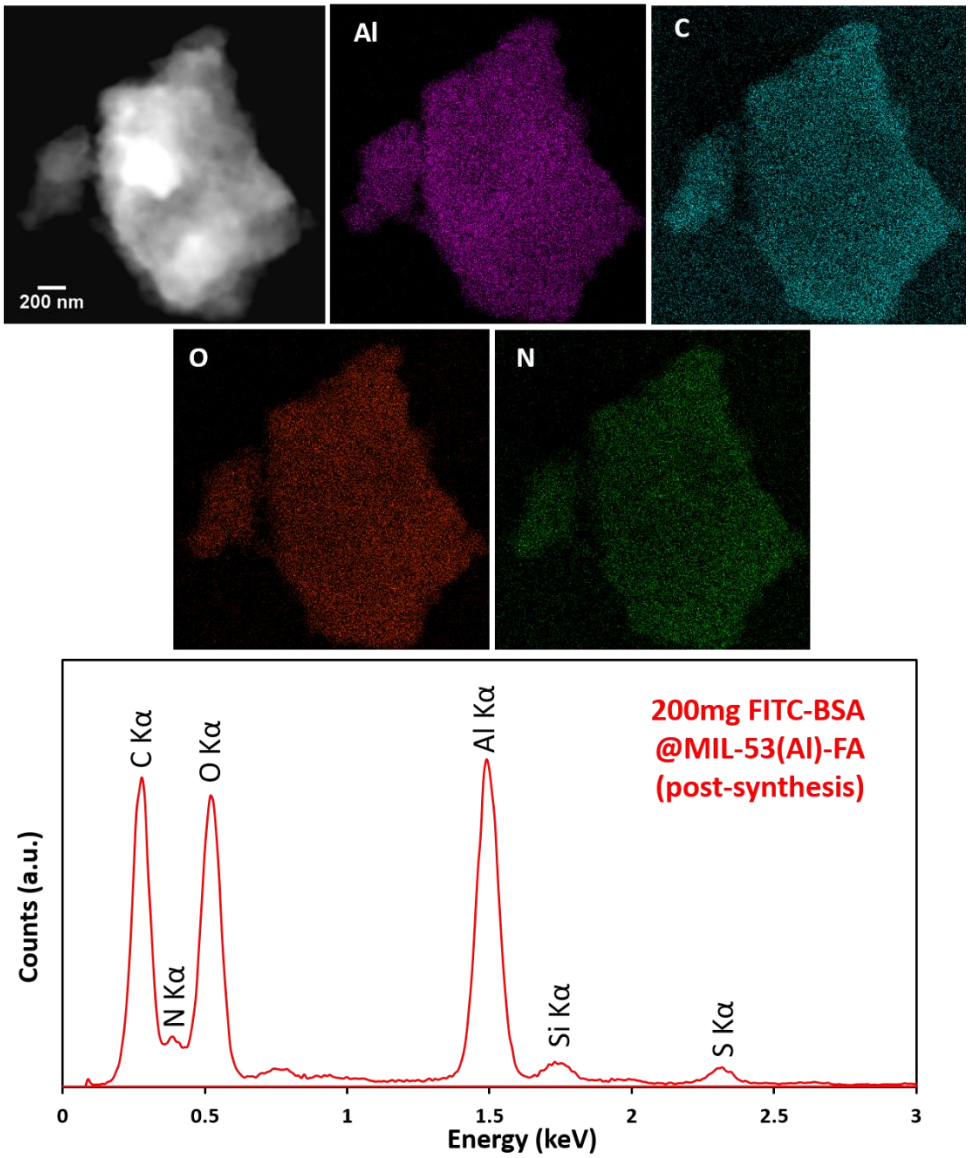

Figure 4-23: STEM-XEDS elemental mapping of 200mg BSA@MIL-53(Al)-FA (post-synthesis) acquired using energy windows related respectively to Al-Kα (magenta area), C-Kα (cyan area), O-Kα (red area) and N-Kα (green area) lines. Elemental maps are not quantitative.

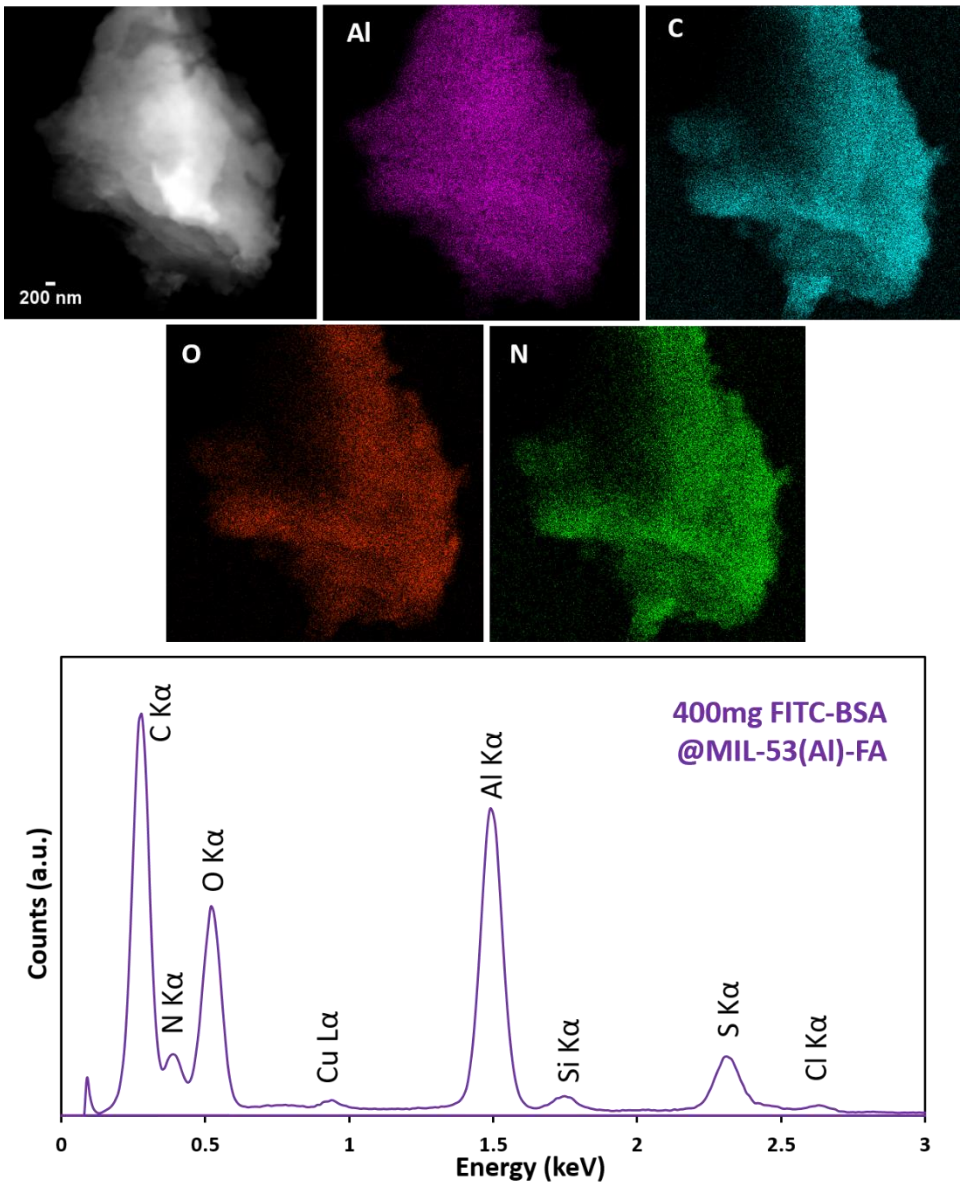

Figure 4-24: STEM-XEDS elemental mapping of 400mg BSA@MIL-53(Al)-FA acquired using energy windows related respectively to Al-Kα (magenta area), C-Kα (cyan area), O-Kα (red area) and N-Kα (green area) lines. Elemental maps are not quantitative.

In order to further investigate the localization of the BSA molecules in the composites and the presence of large interparticle spaces, we employed an in-situ FT-IR analysis upon adsorption of probe molecules. These experiments were performed by Dr. Josefine Schnee and Prof. Marco Daturi, in the Laboratoire de Catalyse & Spectrochimie at the Université de Caen Normandie.

Probe molecules like CO, pyridine and CD_3CN have been extensively used for the investigation of Lewis acid sites (open metal sites) in MOFs, *via in-situ* FT-IR.[2,17–19] This approach was used in this work in order to extract information about the localization of BSA in the composites, the potential pore blockage or the presence of large interparticle spaces, compared to the parent MOF. More precisely, two nitriles of different size were used, deuterated acetonitrile (CD_3CN) (kinetic diameter = 0.38-0.42 nm) and pivalonitrile ($(CH_3)_3CCN$) (kinetic diameter ≥ 0.6 nm).[20] CD_3CN was used instead of CH_3CN, as it gives a less complex spectrum, in which the *ν*(CN) frequency is not perturbed by the Fermi resonance.[19] The nitriles probes interact with the Lewis acid sites of the MOF through the electron lone pair of the nitrogen atom. Thus, after their coordination to the electron acceptor open metal sites of the MOF, a *ν*(CN) stretching mode can be observed on the FT-IR spectrum of the MOF. By comparing the area of this IR band in the spectra of MIL-53(Al)-FA and its composites with BSA, it may be possible to extract information about the external surface of the materials, as well as their porosity.[2,19]

Prior to the adsorption of the probe molecules, the samples were heated at 150 °C under secondary vacuum (10^{-6} Torr), overnight to evacuate physisorbed water. Except the free BSA which was deposited on a silicon wafer, all samples were pressed into a self-supported disc (2 cm^2 area, 10 mg cm^{-2}), resulting in pellets. These were placed into a homemade IR cell equipped with KBr windows and a heating system. In the case of free BSA, a homogeneous deposition was not possible and so it was not analyzed. The preparation of the pellet of the 200 mg BSA@MIL-53(Al)-FA (post-synthesis) composite was also complicated, as the material presented an extra hardness, possibly due to the large amount of BSA at its external surface. The signal of this sample was very weak and not exploitable. Thus, only the results of MIL-53(Al)-FA and its composites with BSA, prepared with the *in-situ* method are given below.

As seen in Figure 4-25(a) and Table 4-3, in the case of the smallest probe molecule CD_3CN, the area of the IR absorption band associated to the characteristic *ν*(CN) (~2320 cm^{-1})[2] decreases with increasing concentrations of immobilized BSA. Due to the incompatibility of BSA dimensions (140 × 40 × 40 Å)[21] and the pore dimensions of MIL-53(Al)-FA (5.7 × 6.0 Å), the presence of BSA inside the pores is excluded. The decreased area of *ν*(CN) could be attributed to the blockage of some pores by BSA molecules that are located at the surface of the MOF particles, reducing the accessibility to the Lewis acid sites. The composite with 200 mg BSA shows a small decrease of this band compared to that of the composite with 50 mg BSA, which is also consistent with the similar BET surface areas shown above. However, the composite with 400 mg BSA shows an important decrease in the area of the *ν*(CN) band, which is also in agreement with the lower surface area of this sample. When the larger probe molecule $(CH_3)_3CCN$ was used, the observed area of the *ν*(CN) band at ~2300 cm^{-1} increased importantly

in the presence of 50 and 200 mg BSA, compared to that observed for MIL-53(Al)-FA and to a lesser extent to that observed in the presence of 400 mg BSA (Figure 4-25(b)). The diffusion of a larger probe molecule seems thus to be favored in the presence of BSA, which could possibly indicate that the BSA is not immobilized exclusively at the external surface of the material, as if it was the case the diffusion of larger probe molecule would not be favored. The presence of BSA may have induced large interparticle spaces, as the $(CH_3)_3CCN$ is too large to diffuse inside the pores of MIL-53(Al)-FA but small enough to diffuse through the composites. Taking into consideration the low area of the IR band of the composite with 400 mg, it could be assumed that when very high amounts of BSA are used, the amount of BSA at the surface increases and BSA may induce diffusion issues that minimize the access to the open-metal sites.

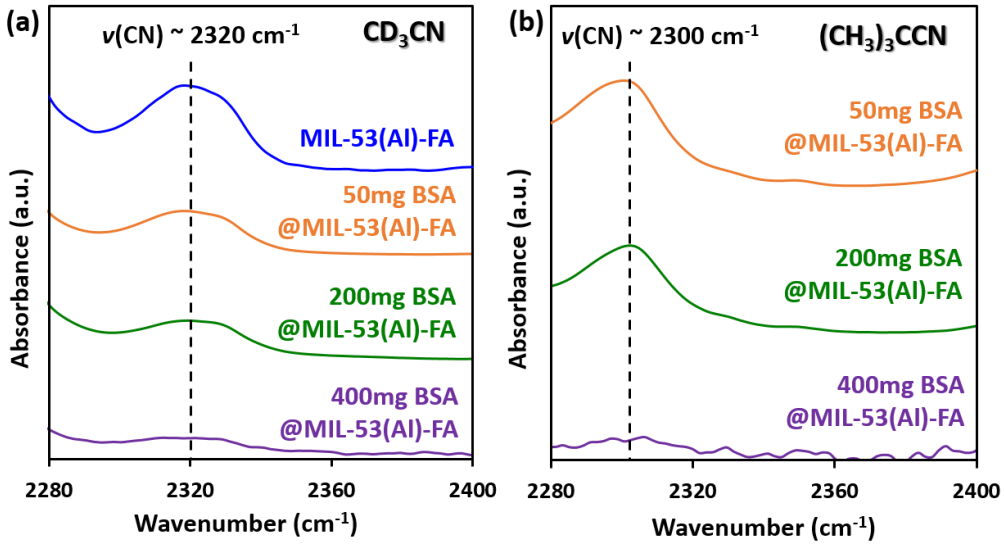

Figure 4-25: Absorbance IR spectra of MIL-53(Al)-FA (blue), 50mg BSA@MIL-53(Al)-FA (orange), 200mg BSA@MIL-53(Al)-FA (green) and 400mg BSA@MIL-53(Al)-FA (purple) after adsorption of nitriles; (a)CD_3CN and (b) $(CH_3)_3CCN$. The spectra show only the characteristic IR band of the *ν*(CN) vibration due to the chemisorption of the nitriles on the MOFs.

Table 4-3: Area of the IR band characteristic of each adsorbed nitrile in the Lewis sites of MIL-53(Al)-FA

Probe molecule	CD_3CN	$(CH_3)_3CCN$
MIL-53(Al)-FA	4.25	0.25
50 mgBSA@MIL-53(Al)-FA	3.03	1.80
200 mgBSA@MIL-53(Al)-FA	2.90	2.06
400 mgBSA@MIL-53(Al)-FA	1.72	0.67

Attempts to perform mercury porosimetry measurements (in collaboration with Dr. Pascal Yot, ICGM) were also exploited to further characterize these interparticle spaces. However, the mechanical robustness of the composites was not sufficient to allow accurate measurements.

In conclusion, the characterization of the composite samples showed that the crystalline structure of MIL-53(Al)-FA was preserved when synthesized in presence of BSA. High BSA

loadings were achieved, while no phase separation between BSA and MIL-53(Al)-FA were observed, suggesting that BSA was dispersed in the material. An extra mesoporosity was observed for the *in-situ* samples (for 50 and 200 mg of BSA) that may be due to interparticle porosity. This mesoporosity was not observed for the post-synthesis adsorbed BSA, suggesting that the presence of BSA impacts the synthesis of MIL-53(Al)-FA. This might be due to the influence of the BSA surface on the nucleation process of the MOF; however, further studies are required to conclude on the exact mechanisms.

4. Preliminary catalytic results: Immobilization of HRP enzyme

In order to evaluate the effectiveness of MIL-53(Al)-FA as a matrix for the design of a biocatalyst, we proceeded with the immobilization of Horseradish Peroxidase (HRP). HRP was chosen to be immobilized for several reasons. First, HRP is a bulky enzyme (~44 kDa), which means that its 3D confinement inside a MOF material can only by performed with the "*in-situ* synthesis" approach. Second, it is a commercially available enzyme, which allows to perform easily preliminary tests. Third, studying the catalytic activity of immobilized HRP, a typical peroxidase, in reactions similar to the ones described in Chapters 1 & 2 was of interest, and, if promising results were to be obtained, the encapsulation of MP8 could also be envisioned next. Finally, HRP is a relatively stable enzyme that could probably be little affected by the relatively acidic conditions used for the synthesis of MIL-53(Al)-FA.

For the preparation of the biocatalyst, a procedure identical to that used for the BSA composites was followed: 5 mg HRP were dissolved in 10 mL H_2O. 2 mmol of fumaric acid and 6 mmol of NaOH were added to the HRP solution and the mixture was then stirred for 5 min at RT. A solution containing 1 mmol of $Al_2(SO_4)_3 \cdot 18H_2O$ in 10 mL H_2O was prepared and was added to the HRP/fumaric acid/NaOH solution. The mixture was left under stirring at RT for 24 h. This shorter reaction time (24 h instead of 48 h of the original synthesis) was preferred to minimize to presence of HRP in acidic conditions. The immobilized HRP was recovered by centrifugation (10000 rpm, 3 min) and washed six times with water to remove any unreacted precursors and non-entrapped HRP. Finally, it was redispersed in 20 mL water and stored at 4 ^oC until used. As seen in Figure 4-26, the presence of HRP did not influence the crystallization of the MOF The PXRD diagram of the HRP@MIL-53(Al)-FA superimposed with that of the pure MOF. No difference was observed by IR spectroscopy, TG analysis and N_2 porosimetry, between the composites and the MOF (Figure 4-27). Considering the low quantity of the immobilized HRP (~0.01 mg HRP/mg MIL-53(Al)-FA)) this behavior was expected and was also in agreement with the 5 mg FITC-BSA@MIL-53(Al)-FA system.

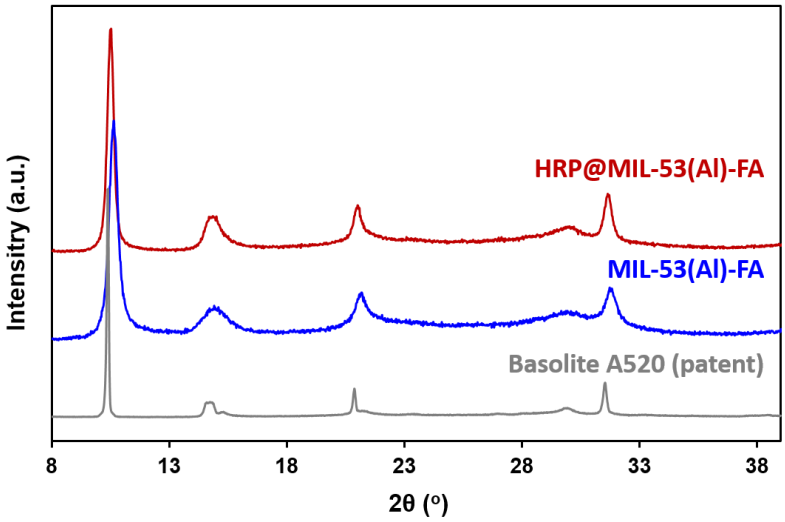

Figure 4-26: Normalized PXRD patterns of Basolite A520 (patent) (grey), MIL-53(Al)-FA (blue) and HRP@MIL-53(Al)-FA (red).

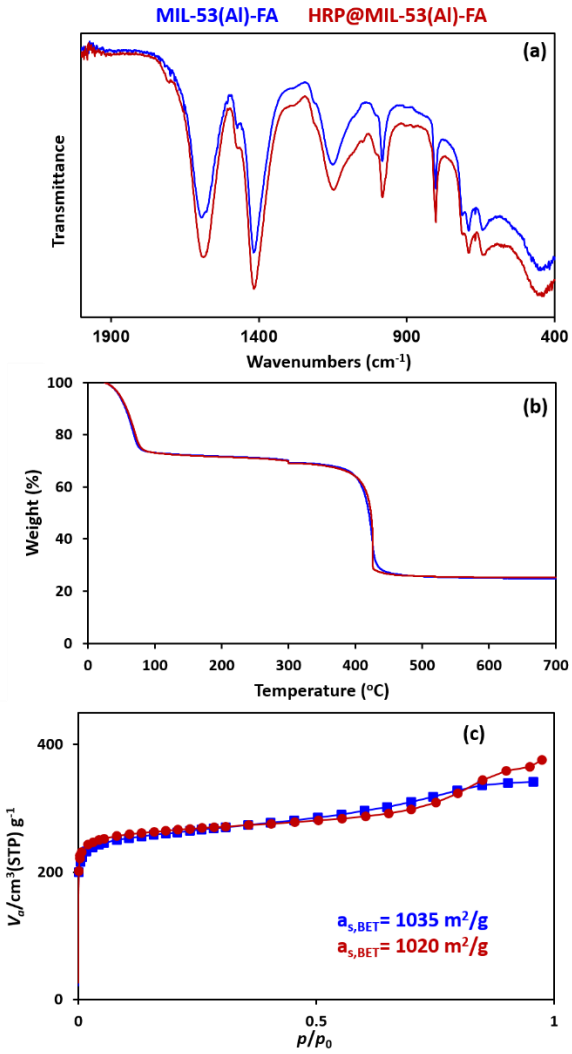

Figure 4-27: (a) FT-IR spectra, (b) TGA curves, under O_2 flow and (c) N_2 adsorption isotherms at 77 K of MIL-53(Al)-FA (blue) and HRP@ MIL-53(Al)-FA (red).

The immobilization efficiency of the MOF was evaluated by analyzing the supernatant of HRP@MIL-53(Al)-FA by UV-vis spectroscopy. As seen in Figure 4-28(a), the supernatant was clear, showing no absorbance at 406 nm (Soret band of HRP, ε_{406} = 1.5 × 10^5 M^{-1} cm^{-1}),[22] therefore indicating that all the HRP was immobilized in the MOF matrix. A more extensive quantification by ICP-OES of the HRP loading should be performed in the future (the ratio between the Fe^{3+} of HRP and the Al^{3+} of MIL-53(Al)-FA should be determined). The catalytic efficiency of HRP@MIL-53(Al)-FA was evaluated by its capacity to oxidize the chromogenic substrate ABTS (2,2'-Azino-bis(3-ethylbenzthiazoline-6-sulfonic acid)) and was compared to that of the free HRP. No catalytic activity was detected when MIL-53(Al)-FA was used. Briefly, 0.55 µM catalyst (free HRP or HRP@MIL-53(Al)-FA) and 10 mM ABTS were added to phosphate buffer (0.01 M) at pH 7 in a total volume of 3 mL. The reactions were initiated by addition 16 µM H_2O_2 and left to react for 30 min, under stirring. At the end of the reaction, the sample containing the immobilized HRP was centrifuged to remove HRP@MIL-53(Al)-FA, as the particles of the MOF could interfere in the UV-vis measurement by causing light scattering. Both reactions were then analyzed by UV-vis spectroscopy. As seen in Figure 4-28(b), HRP@MIL-53(Al) oxidized similar amount of substrate ([$ABTS^{\cdot+}$]= 21.7 µM) with the free HRP ([$ABTS^{\cdot+}$]= 19.6 µM). The concentrations of oxidized ABTS ([$ABTS^{\cdot+}$]) were calculated based on the reported extinction coefficient, ε_{420} = 3.6 × 10^4 M^{-1} cm^{-1}.[23] These first catalytic results are very promising as they show that the activity of HRP was maintained after the *in-situ* immobilization and encourage for further extensive studies of this MOF as immobilization system.

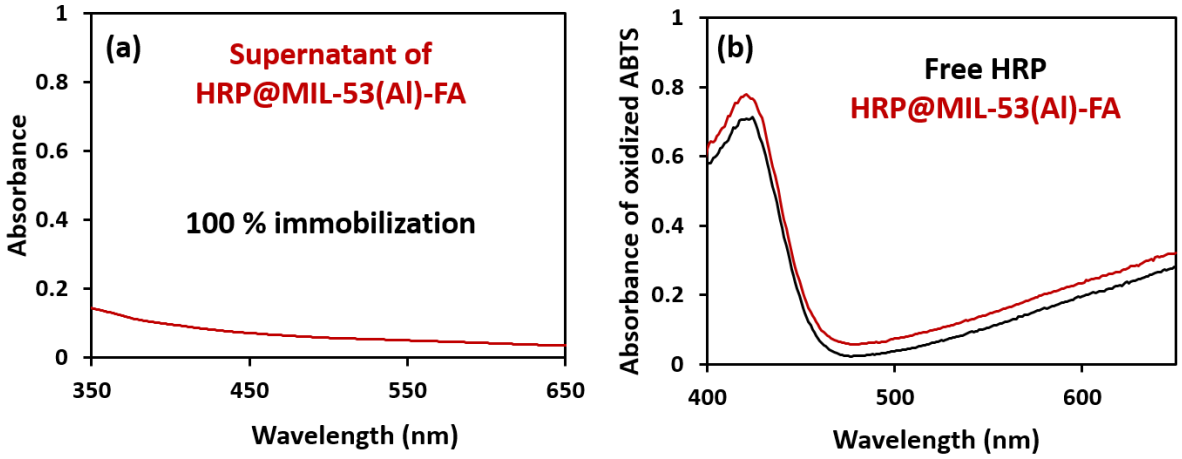

Figure 4-28: (a) UV-vis spectrum of the supernatant of HRP@MIL-53(Al)-FA; (b) UV-vis spectra of oxidized ABTS after 30 min of reaction using 0.55 µM catalyst (free HRP or HRP@MIL-53(Al)-FA), 16 µM H_2O_2 and 10 mM ABTS in phosphate buffer (0.01 M), pH7.

B. Perspectives: Alternative systems

1. Protection of fragile enzymes and shaping of MIL-53(Al)

While the first results concerning the use of MIL-53(Al)-FA as an *in-situ* immobilization matrix for biomolecules are rather promising, the relatively acidic conditions (pH 4) during its

synthesis could be problematic for pH-sensitive enzymes. A direct increase of the pH (during the synthesis) was not compatible with the formation of MIL-53(Al)-FA, as discussed above. It was thus considered important to investigate an alternative approach, in which pH-sensitive enzymes can be protected during the synthesis of the MOF. Inspired by previous systems, where the combination of multiple materials have been used to design biocompatible and stable matrices (*e.g.* silica & alginate),[24] we decided to associate alginate with MIL-53(Al)-FA. Alginate salts have the ability to form hydrogels upon metal exchange with metal cations (typically Ca^{2+}). The metal cation is coordinated to the carbonyl and hydroxyl groups of four α-L-glucuronic acid-monomers, deriving from two different chains of the biopolymer (for more details see chapter 1).[25] Alginate would thus provide a biocompatible environment for fragile enzymes and MIL-53(Al)-FA, a mechanically and chemically stable porous shell that could allow the controlled diffusion of reactants (Figure 4-29). This process has already been reported with HKUST-1/alginate beads that resulted in the homogeneous crystallization of the MOF particles around the alginate core.[26] Nonetheless, this possible core-shell structure of MIL-53(Al)-FA/alginate beads remains to be confirmed experimentally.

Figure 4-29: Schematic illustration of a possible MIL-53(Al)-FA/alginate bead.

The different routes tested for the preparation of MIL-53(Al)-FA/alginate beads are presented in Figure 4-30. The first step of the procedure concerned the preparation of alginate beads. Once the beads were successfully formed two different approaches were investigated for the formation of the MIL-53(Al)-FA/alginate beads: a one-pot route and a layer-by-layer route. The parameters studied for the preparation of MIL-53(Al)-FA/alginate beads are presented in Table 4-4.

Table 4-4: Parameters studied for the preparation of MIL-53(Al)-FA/alginate beads.

Parameters	Tested Conditions	Optimal Conditions
Sodium alginate concentration (w/v %)	3, 5, 10	10
Gelation agents	Ca^{2+}, Ca^{2+}/Al^{3+}, Al^{3+}	Al^{3+}
Gelation agent concentration (M)	0.1, 0.2, 0.3	0.3
Molar ratio metal:ligand:NaOH	1:2:6, 1:2:3	1:2:3
Temperature (°C)	RT, 37	RT
Addition of reactants	One-pot, layer-by layer	layer-by layer

Formation of alginate beads: The dropwise addition of a concentrated aqueous solution of sodium alginate in an aqueous solution containing metal cations allowed the formation of hydrogels, upon exchange of sodium cations with the cations in the solution. Once the alginate beads were successfully formed, they were added to solutions containing the precursors of MIL-53(Al)-FA ($Al_2(SO_4)_3$)·$18H_2O$, fumaric acid/NaOH) for the formation of the MOF around the alginate beads.

For this study, a 10 % w/v sodium alginate aqueous solution was preferred as it resulted in more robust alginate beads. Concerning the choice of the gelation cation, the most commonly used Ca^{2+} was studied, along with a mixture of Ca^{2+}/Al^{3+} and Al^{3+}. Aluminium was chosen as it is a consecutive part of MIL-53(Al)-FA and may interact with the fumaric acid and favor the formation of the MOF around the alginate bead. When $CaCl_2$·$2H_2O$ (0.1 M) was used as a gelation agent, it resulted into robust alginate beads, which however did not allow the formation of MIL-53(Al)-FA around them. A mixture of $CaCl_2$·$2H_2O$ (0.1 M)/ $Al_2(SO_4)_3$·$18H_2O$ (0.2 M) was tested so that the Al^{3+} cations may promote the formation of the MOF, while Ca^{2+} could serve as complexing cation. This procedure resulted in the crystallization of MIL-53(Al)-FA around the beads and it was assumed that Al^{3+} cation was indispensable for the formation of the MOF around the beads. These results encouraged us to test pure Al-Alginate beads. When a solution $Al_2(SO_4)_3$·$18H_2O$ (0.1 M) was used, the beads were successfully formed, but the MOF was not formed around the beads (based on PXRD measurements). Higher concentration of $Al_2(SO_4)_3$·$18H_2O$ solution (0.3 M) were thus tested to increase the amount of Al^{3+} ions so that they could serve both for the gelation of the beads and the formation of the MOF. The increased concentration of Al^{3+} promoted the formation of MIL-53(Al) around the beads and was preferred in order to avoid the unnecessary use of Ca^{2+}.

Formation of MIL-53(Al)-FA/alginate beads: After the successful formation of the Al^{3+}-alginate beads, two different synthetic routes were investigated for the formation of the MOF: a one-pot addition of all reactants (metal cation/ligand/base aqueous solution) and a layer-by-layer addition of reactants (ligand/base solution and then metal cation aqueous solution). While the one-pot route would be ideal due to its simplicity, the MOF was formed mostly in the solution and not around the beads probably due to the fast kinetics of the MIL-53(Al)-FA synthesis in solution, compared to the much slower process required for its formation around the beads. The layer-by-layer approach was successful, resulting in the formation of mechanically stable MIL-53(Al)-FA/alginate beads.

The detailed layer-by-layer preparation of the MIL-53(Al)-FA/alginate beads is presented in Figure 4-30. An aqueous solution of sodium alginate (10 % w/v, 3 mL) was added dropwise to an aqueous solution of $Al_2(SO_4)_3$·$18H_2O$ (0.3 M, 10 mL). After the addition, the beads were left under stirring in the metal cation solution for 1 h. Then the solution was removed, the beads were washed three times with water and transferred into an aqueous solution (10 mL) containing fumaric acid (0.2 M) and NaOH (0.3 M) and left under stirring for 30 min. When compared to the original synthesis of the MOF, the concentration of NaOH was reduced from 0.6 to 0.3 M, as the very basic conditions of the solution (with 0.6 M NaOH, pH 12), resulted

in the dissolution of the alginate beads. After 30 min, the beads were washed with water and transferred into an aqueous solution of $Al_2(SO_4)_3 \cdot 18H_2O$ (0.1 M, 10 mL) for 30 min. This procedure was repeated once more and finally the beads were kept overnight under stirring in the metal cation solution. At the end of the layer-by-layer procedure, the beads were washed and stored in water, while some of them were dried at 100 °C for 2 h for further characterization.

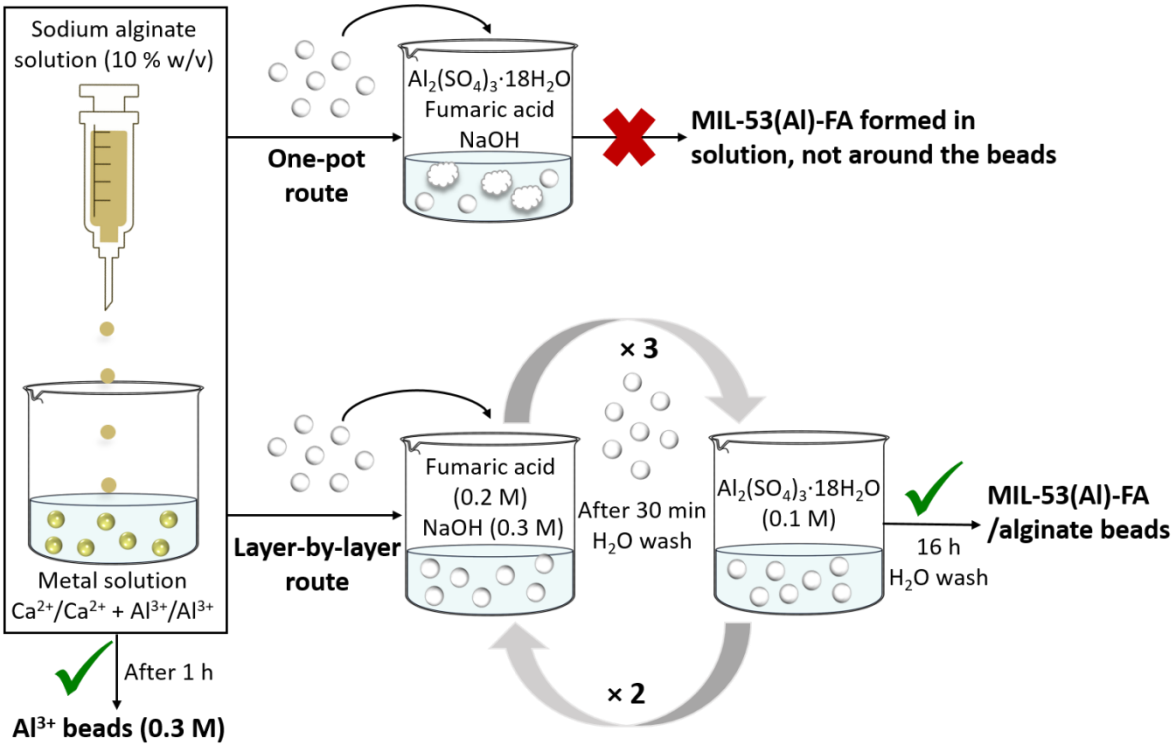

Figure 4-30: Schematic illustration for the preparation of MIL-53(Al)-FA/alginate beads.

Although, this synthetic procedure can be considered as being relatively time-consuming, each step was found to be crucial for the crystallization of the MOF. Moreover, this layer-by layer approach may allow to finely control the thickness of the MOF layer, which may not be the case with an one-pot approach. Finally, the different metal cation and ligand solutions that were used in the process can be recycled and reused for the whole procedure, thus minimizing the cost of preparation. Besides, the shaping of the MIL-53(Al)-FA into beads can be of interest for different applications. As observed in Figure 4-31, the MIL-53(Al)-FA/alginate beads are white (the original alginate beads were brownish), as a result of the formation of the MOF shell at their surface, with a homogenous size and a diameter of about 3 mm. The beads were stable in water for more than three months, as no change in their shape was observed. However, an extensive mechanical and chemical stability study must be performed in the future, especially to investigate whether the MOF is only present as a shell on the outside of the bead or if it is also present within the alginate bead.

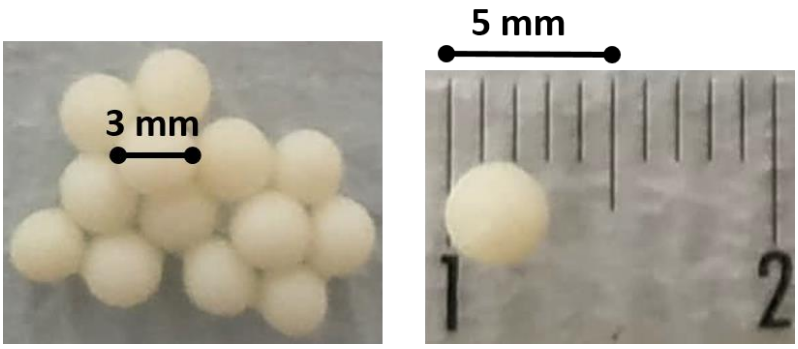

Figure 4-31: Pictures of the MIL-53(Al)-FA/alginate beads.

The PXRD diagram of the beads is show in Figure 4-32. The beads show the characteristic Bragg peaks of MIL-53(Al)-FA at 10.5, 15 and 21°. However, they show a reduced crystallinity when compared to that of the pure MIL-53(Al)-FA, which could be assigned to the presence of a high amount of the amorphous alginate hydrogel, in the former case. The FT-IR spectrum of the beads is shown in Figure 4-33. The very weak band at 1700 cm^{-1} is assigned to traces of unreacted fumaric acid in the beads. The asymmetric (1600 cm^{-1}) and symmetric (1430 cm^{-1}) stretching modes of the carboxylates of the MIL-53(Al)-FA are overlapping with those of sodium alginate. The band at 1030 cm^{-1} is assigned to the ν(C-O-C) stretching mode of the six-membered ring of alginate (1020 cm^{-1} is sodium alginate).[27]

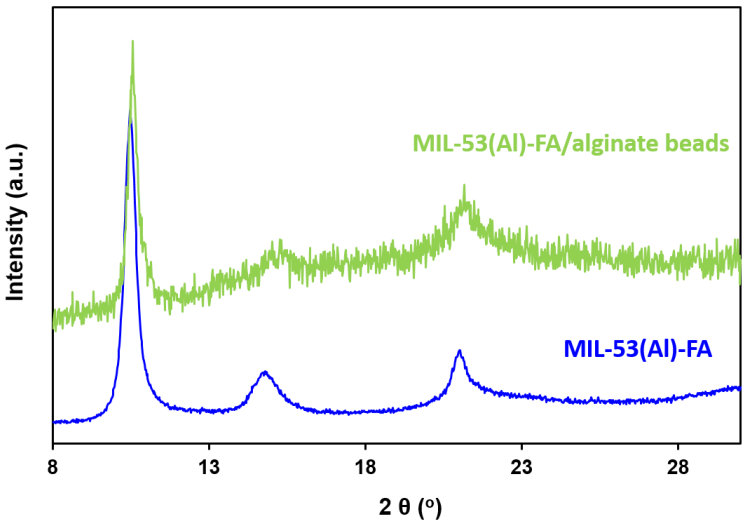

Figure 4-32: Normalized PXRD diagrams of MIL-53(Al)-FA (blue) and MIL-53(Al)-FA/alginate beads (green).

The beads were also characterized by N_2 porosimetry (Figure 4-34). Prior to the measurements, the beads were grinded and activated at 150 °C under vacuum. As expected the beads were almost non-porous ($a_{s,BET}$= 83 m^2/g), due to the large amount of the non-porous alginate network. The surface area of the beads were calculated without taking into account the mass of alginate, as the chemical composition of the beads has not been investigated yet. The large amount of alginate can also be confirmed by the color change of the grinded beads after thermal treatment (inset in Figure 4-34).

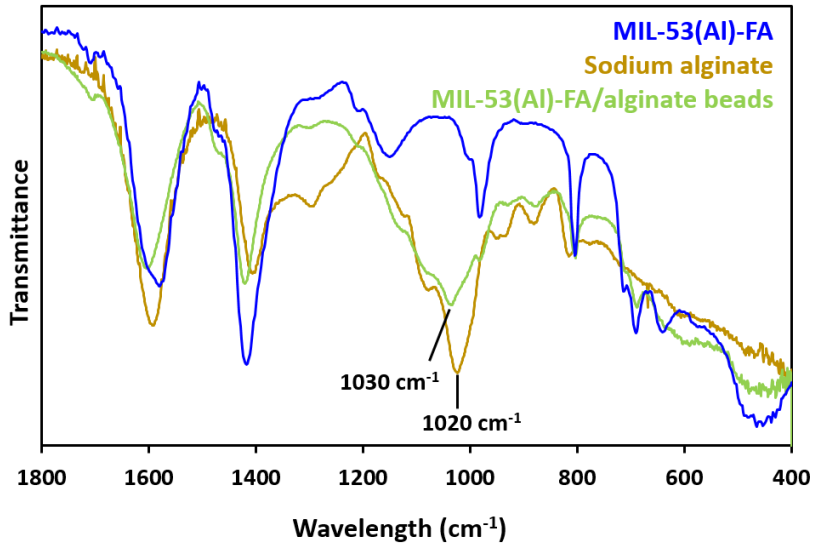

Figure 4-33: FT-IR spectra of MIL-53(Al)-FA (blue), sodium alginate (brown) and MIL-53(Al)-FA/alginate beads (green).

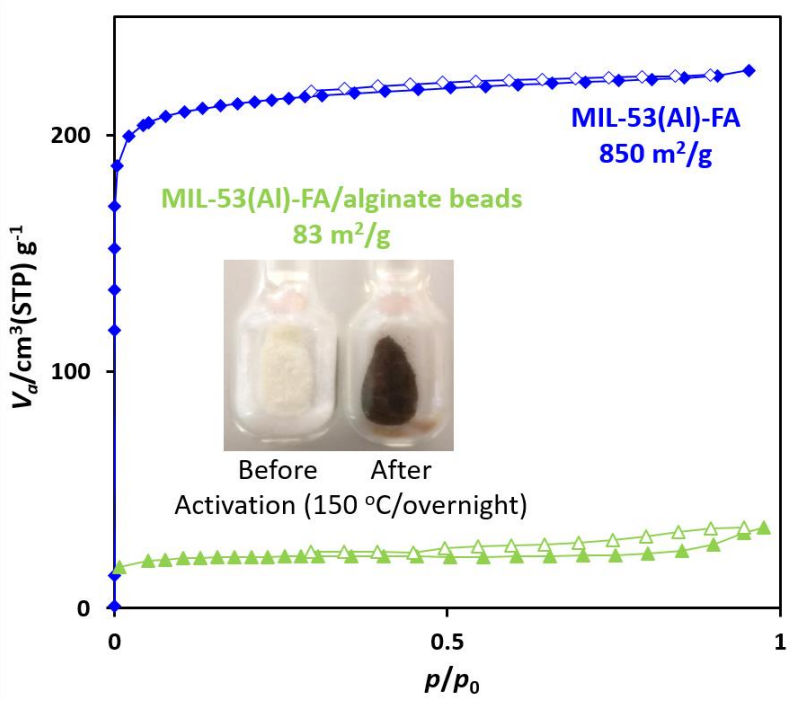

Figure 4-34: N_2 sorption isotherms of MIL-53(Al)-FA (blue diamonds) and MIL-53(Al)-FA/alginate beads (green triangles), measured at 77 K. Filled symbols correspond to the adsorption process and unfilled symbols to the desorption process. Sample activation: 150 °C for 16 h, under secondary vacuum. Inset: image of crushed MIL-53(Al)-FA/alginate beads before and after activation.

The next step of this work would be the full characterization of the beads (chemical composition, TG analysis, morphological characteristics *via* SEM, TEM, thickness of the MOF layer, *etc.*). Finally, the entrapment of enzymes in the alginate hydrogel will be performed, prior to the formation of the MIL-53(Al)-FA/alginate, in order to evaluate the protective effect of this system.

2. MIL-100(Fe)

The other candidate selected for the "*in-situ* synthesis" approach was MIL-100(Fe).[28] This MOF results from the connection of trimesic acid and μ_3-oxo trimers of Fe^{3+}, leading to a mesoporous structure with MTN-type topology (Figure 4-35).[28] MIL-100(Fe) presents two kinds of cavities with different diameters (24 and 29 Å), interconnected *via* microporous windows (5.5 and 8.6 Å) and it shows a maximum specific surface area of ~ 2000 m^2/g.[28] It has been one of the most studied MOFs for biological applications[29,30] and more recently for the surface adsorption of enzymes,[31,32] thanks to its stability, bio-compatibility (non-toxic components) and bio-degradability. Those same reasons render MIL-100(Fe) suitable for the *in-situ* entrapment of enzymes. Moreover, by comparison with the microporous MIL-53(Al)-FA, its mesoporosity would be an added benefit, as it would enhance the diffusion of substrates to the catalytic center of the entrapped enzymes. Another important characteristic of MIL-100(Fe) is its peroxidase-like activity that could be potentially coupled with enzymes, to obtain enhanced biocatalysts.[31]

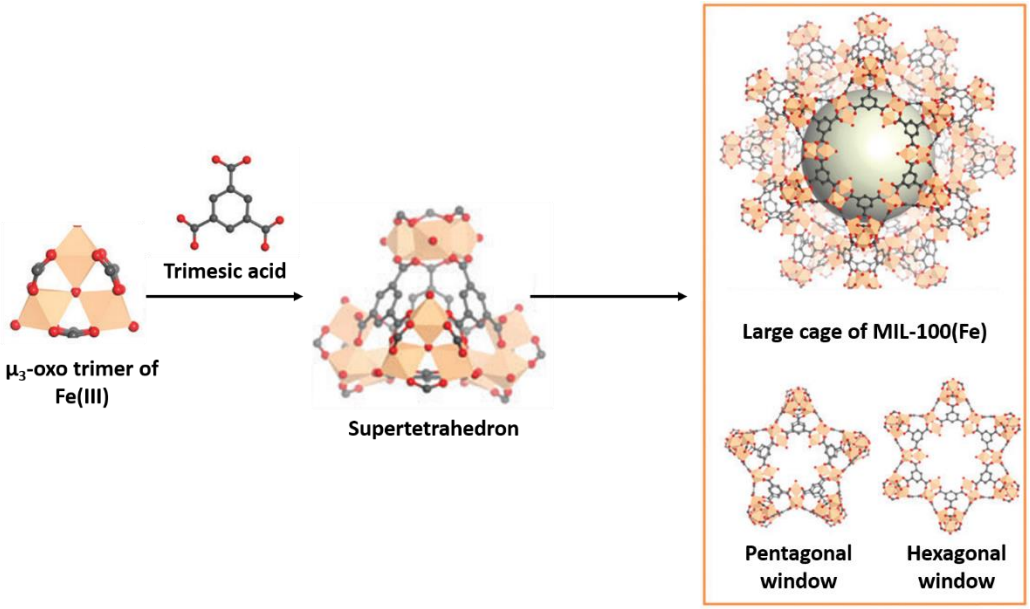

Figure 4-35: Schematic illustration of the construction of MIL-100(Fe). Adapted from[31]

Monik Panchal, Dr. Farid Nouar and Dr. Christian Serre had already performed the synthesis optimization of MIL-100 (Fe) in water, at room temperature at the Institut Lavoisier de Versailles. The synthesis of MIL-100(Fe) in water, at room temperature is part of a submitted patent, thus the specific synthetic procedure is not described. Their synthetic conditions were slightly adjusted for the in-situ immobilization of enzymes.

For reasons similar to those described above for MIL-53(Al)-FA, BSA was used as a model protein. Various quantities of protein (5, 10 and 15 mg) were dissolved in water and mixed with the precursors of MIL-100(Fe) (Fe^{3+} cations and trimesic acid). The reactions kept under stirring for 72 h, at RT. The samples were then recovered by centrifugation (15 min, 14500

rpm) and washed six time with water. A part of the samples was dried at 100 °C overnight, for further characterization while the rest were stored in water.

As can be seen from the Figure 4-36, the PXRD diagrams of MIL-100(Fe) with BSA, superimposed well with that of the calculated pattern, indicating the formation of MIL-100(Fe). However, the BSA@MIL-100(Fe) composites showed a poor crystallinity that might be due to the low solubility of trimesic acid in water (2.6 g/L at 25 °C) that did not facilitate the crystallization of the MOF particles. N_2 sorption measurements should be performed in the future to validate the formation of MIL-100(Fe) and exclude the possibility of forming the semi-amorphous Fe-BTC phase (Basolite F300).

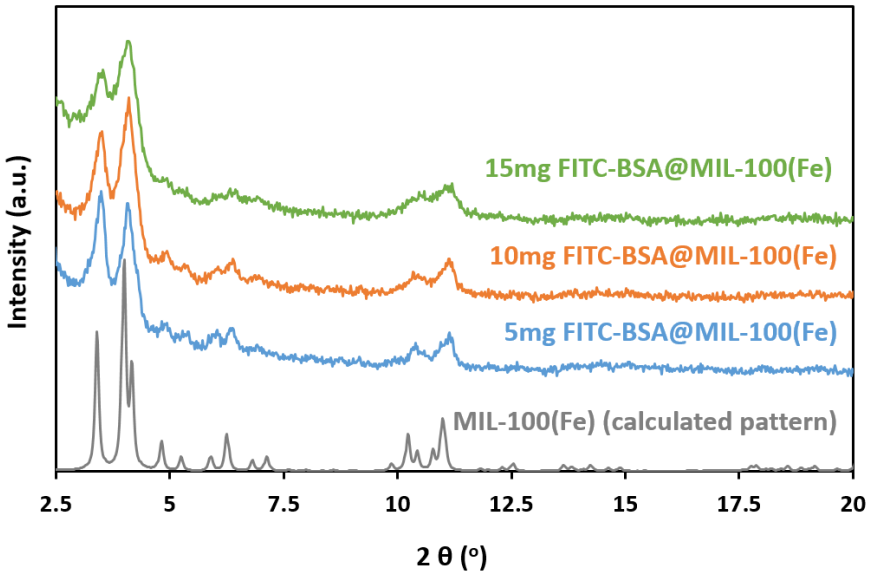

Figure 4-36: Normalized PXRD patterns of 5mg FITC-BSA@MIL-100(Fe) (blue), 10mg FITC-BSA@MIL-100(Fe) (orange), 15mg FITC-BSA@MIL-100(Fe) (green) and the calculated pattern of MIL-100(Fe) (black).

From the FT-IR spectra of the composites (Figure 4-37), we can observe a band around 1550 cm^{-1} that may correspond to the amide II vibration of the immobilized BSA. The amide I & III bands (1639 and 1390 cm^{-1}, respectively) could not be observed as they overlap with the asymmetric and symmetric stretching modes of the carboxylates of MIL-100(Fe) (1631 and 1380 cm^{-1}, respectively)

The TGA curves of the MIL-100(Fe) composites are shown in Figure 4-38. As expected, since similar amounts of protein were used, the three products displayed similar thermal profiles and close to that of MIL-100(Fe). Nonetheless, with increasing amounts of BSA, a small decrease of the decomposition temperature is observed, which may indicate that the structure of MIL-100(Fe) is more affected than MIL-53(Al)-FA in the presence of small amounts of biomolecules.

The extensive study of MIL-100(Fe) as immobilization matrix could not be completed during this PhD work, but the first result seem promising and encourage for the investigating this MOF as enzymatic support.

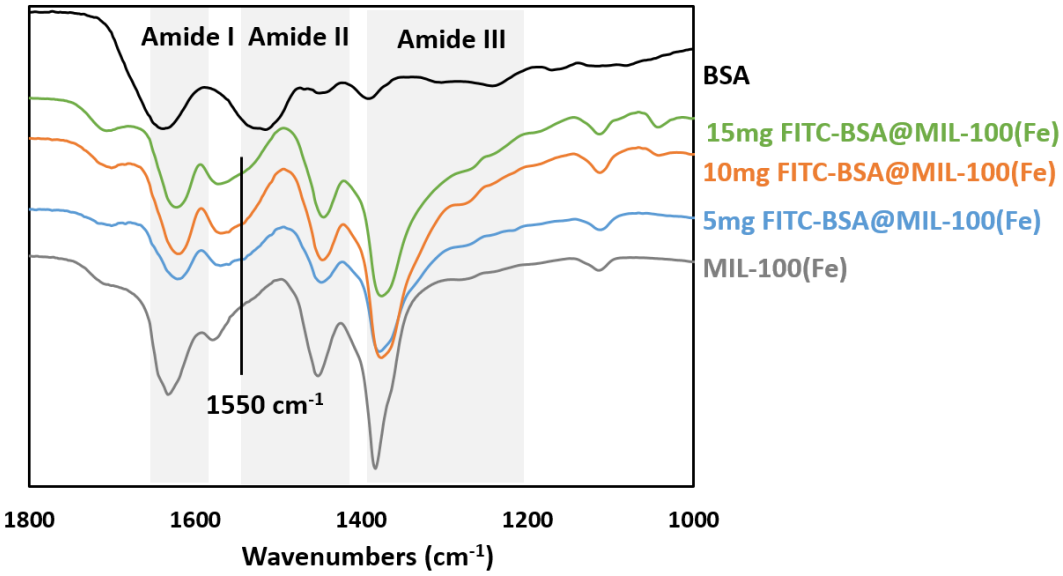

Figure 4-37: FI-IR spectra of MIL-100(Fe) (grey) 5mg FITC-BSA@MIL-100(Fe) (blue), 10mg FITC-BSA@MIL-100(Fe) (orange), 15mg FITC-BSA@MIL-100(Fe) (green) and BSA (black).

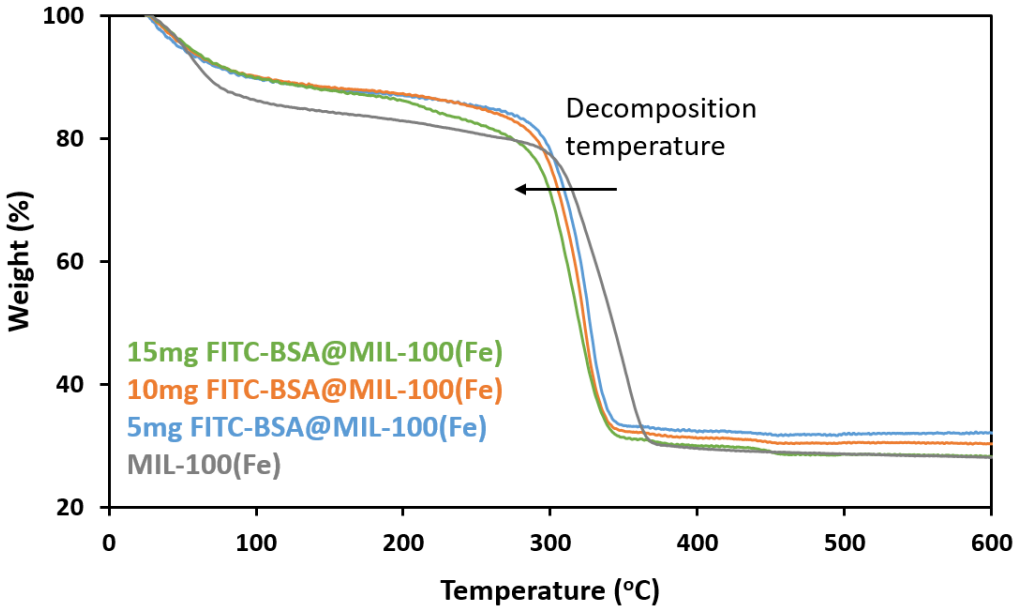

Figure 4-38: TGA of MIL-100(Fe) (grey) 5mg FITC-BSA@MIL-100(Fe) (blue), 10mg FITC-BSA@MIL-100(Fe) (orange) and 15mg FITC-BSA@MIL-100(Fe) (green), performed under O_2 flow.

C. Conclusions

This chapter was focused on the investigation of MOFs that can be used for the immobilization of enzymes *via* the *in-situ* synthesis approach to result in their 3D confinement inside the porous structure of MOFs. Two different MOFs were selected, the microporous, hydrophilic MIL-53(Al)-FA and the mesoporous, amphiphilic and catalytically active MIL-100(Fe). The selection of both MOFs was based on their high chemical stability, the non-toxicity of reactants used for their synthesis and the possibility to synthesize them in water at RT and in the presence of enzymes.

Prior to using MIL-53(Al)-FA for the *in-situ* immobilization, an extensive synthesis optimization was performed that resulted in two different routes to obtain this MOF, in water at room temperature. While $Al_2(SO_4)_3{\cdot}18H_2O$ gives higher reaction yields, the alternative synthesis with the $NaAlO_2$ precursor is of interest as no additives are required, which can be advantageous for scale up applications. Moreover, $NaAlO_2$ is a very cheap aluminum precursor (5 kg, 132 €, Sigma-Aldrich) which is also important for large-scale syntheses. The increase of the reaction time (over 48 h) could eventually result in higher yields. MIL-53(Al)-FA ($Al_2(SO_4)_3{\cdot}18H_2O$) was then synthesized in the presence of high amounts of the BSA protein, entrapping almost the totality of the protein used. The different BSA@MIL-53(Al)-FA composites were characterized by various techniques (PXRD, FT-IR, TGA) that confirmed both the preservation of the MIL-53(Al)-FA structure and the presence of BSA molecules. Moreover, the proteins may have induced the formation of large interparticle spaces in the in the MIL-53(Al)-FA composites, as revealed by N_2 porosimetry, TEM and *in-situ* FT-IR adsorption studies. A preliminary catalytic study with the immobilized Horseradish Peroxidase in MIL-53(Al)-FA, revealed that the enzyme preserved its activity after immobilization.

An alternative immobilization approach was investigated through the formation of MIL-53(Al)-FA/alginate beads for the entrapment of fragile enzymes that may be harmed by the acidic conditions of the MIL-53(Al)-FA synthesis.

The synthesis optimization of MIL-100(Fe) in water at RT had already been performed from colleagues at ILV/IMAP and was used during this work for the entrapment of BSA. The protein molecules did not influence the synthesis of the MOF and they were successfully immobilized in the porous matrix. This study is at a very preliminary step, but the advantages of using MIL-100(Fe) as a host matrix (chemical stability, biocompatibility, mesoporosity, peroxidase-like activity…) are encouraging for an extensive study of this system.

D. References

(1) Gaab, M.; Trukhan, N.; Maurer, S.; Gummaraju, R.; Müller, U. The Progression of Al-Based Metal-Organic Frameworks – From Academic Research to Industrial Production and Applications. *Microporous and Mesoporous Materials* **2012**, *157*, 131–136. https://doi.org/10.1016/j.micromeso.2011.08.016.

(2) Alvarez, E.; Guillou, N.; Martineau, C.; Bueken, B.; Van de Voorde, B.; Le Guillouzer, C.; Fabry, P.; Nouar, F.; Taulelle, F.; de Vos, D.; et al. The Structure of the Aluminum Fumarate Metal-Organic Framework A520. *Angewandte Chemie International Edition* **2015**, *54* (12), 3664–3668. https://doi.org/10.1002/anie.201410459.

(3) Leung, E.; Müller, U.; Trukhan, N.; Mattenheimer, H.; Cox, G.; Blei, S. Process for Preparing Porous Metal-Organic Frameworks Based on Aluminium Fuamrate. *EP Patentanmeldung 10183283.0* **2010**.

(4) Loiseau, T.; Volkringer, C.; Haouas, M.; Taulelle, F.; Férey, G. Crystal Chemistry of Aluminium Carboxylates: From Molecular Species towards Porous Infinite Three-Dimensional Networks. *Comptes Rendus Chimie* **2015**, *18* (12), 1350–1369. https://doi.org/10.1016/j.crci.2015.08.006.

(5) Merino, E.; Harvey, C.; Murray, H. H. Aqueous-Chemical Control of the Tetrahedral-Aluminum Content of Quartz, Halloysite, and Other Low-Temperature Silicates. *Clays and Clay Minerals* **1989**, *37* (2), 135–142. https://doi.org/10.1346/CCMN.1989.0370204.

(6) Liang, K.; Ricco, R.; Doherty, C. M.; Styles, M. J.; Bell, S.; Kirby, N.; Mudie, S.; Haylock, D.; Hill, A. J.; Doonan, C. J.; et al. Biomimetic Mineralization of Metal-Organic Frameworks as Protective Coatings for Biomacromolecules. *Nature Communications* **2015**, *6*, 7240. https://doi.org/10.1038/ncomms8240.

(7) Liang, W.; Ricco, R.; Maddigan, N. K.; Dickinson, R. P.; Xu, H.; Li, Q.; Sumby, C. J.; Bell, S. G.; Falcaro, P.; Doonan, C. J. Control of Structure Topology and Spatial Distribution of Biomacromolecules in Protein@ZIF-8 Biocomposites. *Chemistry of Materials* **2018**, *30* (3), 1069–1077. https://doi.org/10.1021/acs.chemmater.7b04977.

(8) Maddigan, N. K.; Tarzia, A.; Huang, D. M.; Sumby, C. J.; Bell, S. G.; Falcaro, P.; Doonan, C. J. Protein Surface Functionalisation as a General Strategy for Facilitating Biomimetic Mineralisation of ZIF-8. *Chem. Sci.* **2018**, *9*, 4217–4223. https://doi.org/10.1039/C8SC00825F.

(9) Li, S.; Dharmarwardana, M.; Welch, R. P.; Benjamin, C. E.; Shamir, A. M.; Nielsen, S. O.; Gassensmith, J. J. Investigation of Controlled Growth of Metal–Organic Frameworks on Anisotropic Virus Particles. *ACS Applied Materials & Interfaces* **2018**, *10* (21), 18161–18169. https://doi.org/10.1021/acsami.8b01369.

(10) Gascón, V.; Carucci, C.; Jiménez, M. B.; Blanco, R. M.; Sánchez-Sánchez, M.; Magner, E. Rapid In Situ Immobilization of Enzymes in Metal-Organic Framework Supports under Mild Conditions. *ChemCatChem* **2017**, *9* (7), 1182–1186. https://doi.org/10.1002/cctc.201601342.

(11) Wu, X.; Ge, J.; Yang, C.; Hou, M.; Liu, Z. Facile Synthesis of Multiple Enzyme-Containing Metal–Organic Frameworks in a Biomolecule-Friendly Environment. *Chem. Commun.* **2015**, *51* (69), 13408–13411. https://doi.org/10.1039/C5CC05136C.

(12) Barth, A. Infrared Spectroscopy of Proteins. *Biochimica et Biophysica Acta (BBA) - Bioenergetics* **2007**, *1767* (9), 1073–1101. https://doi.org/10.1016/j.bbabio.2007.06.004.

(13) Kong, J.; Yu, S. Fourier Transform Infrared Spectroscopic Analysis of Protein Secondary Structures. *Acta Biochimica et Biophysica Sinica* **2007**, *39* (8), 549–559. https://doi.org/10.1111/j.1745-7270.2007.00320.x.

(14) Sing, K. S. W.; Williams, R. T. Physisorption Hysteresis Loops and the Characterization of Nanoporous Materials. *Adsorption Science & Technology* **2004**, *22* (10), 773–782. https://doi.org/10.1260/0263617053499032.

(15) Cai, G.; Jiang, H.-L. A Modulator-Induced Defect-Formation Strategy to Hierarchically Porous Metal-Organic Frameworks with High Stability. *Angewandte Chemie International Edition* **2017**, *56* (2), 563–567. https://doi.org/10.1002/anie.201610914.

(16) Hao, L.; Li, X.; Hurlock, M. J.; Tu, X.; Zhang, Q. Hierarchically Porous UiO-66: Facile Synthesis, Characterization and Application. *Chemical Communications* **2018**, *54*, 11817–11820. https://doi.org/10.1039/C8CC05895D.

(17) Hu, Z.; Zhao, D. Metal–Organic Frameworks with Lewis Acidity: Synthesis, Characterization, and Catalytic Applications. *CrystEngComm* **2017**, *19* (29), 4066–4081. https://doi.org/10.1039/C6CE02660E.

(18) Hwang, Y. K.; Hong, D.-Y.; Chang, J.-S.; Jhung, S. H.; Seo, Y.-K.; Kim, J.; Vimont, A.; Daturi, M.; Serre, C.; Férey, G. Amine Grafting on Coordinatively Unsaturated Metal Centers of MOFs: Consequences for Catalysis and Metal Encapsulation. *Angewandte Chemie* **2008**, *120* (22), 4212–4216. https://doi.org/10.1002/ange.200705998.

(19) Volkringer, C.; Leclerc, H.; Lavalley, J.-C.; Loiseau, T.; Férey, G.; Daturi, M.; Vimont, A. Infrared Spectroscopy Investigation of the Acid Sites in the Metal–Organic Framework Aluminum Trimesate MIL-100(Al). *The Journal of Physical Chemistry C* **2012**, *116* (9), 5710–5719. https://doi.org/10.1021/jp210671t.

(20) Hadjiivanov, K. Identification and Characterization of Surface Hydroxyl Groups by Infrared Spectroscopy. In *Advances in Catalysis*; Burlington: Academic Press: Norman, Oklahoma, USA, 2014; Vol. 57, pp 99–318.

(21) Wright, A. K.; Thompson, M. R. Hydrodynamic Structure of Bovine Serum Albumin Determined by Transient Electric Birefringence. *Biophysical Journal* **1975**, *15* (2), 137–141. https://doi.org/10.1016/S0006-3495(75)85797-3.

(22) Goral, V.; Ryabov, A. Reactivity of the Horseradish Peroxidase Compounds I and II toward Organometallic Substrates. A Stopped-Flow Kinetic Study of Oxidation of Ferrocenes. *IUBMB Life* **1998**, *45* (1), 61–71. https://doi.org/10.1080/15216549800202432.

(23) Kenzom, T.; Srivastava, P.; Mishra, S. Structural Insights into 2,2'-Azino-Bis(3-Ethylbenzothiazoline-6-Sulfonic Acid) (ABTS)-Mediated Degradation of Reactive Blue 21 by Engineered Cyathus Bulleri Laccase and Characterization of Degradation Products. *Applied and Environmental Microbiology* **2014**, *80* (24), 7484–7495. https://doi.org/10.1128/AEM.02665-14.

(24) Coradin, T.; Nassif, N.; Livage, J. Silica–Alginate Composites for Microencapsulation. *Applied Microbiology and Biotechnology* **2003**, *61* (5–6), 429–434. https://doi.org/10.1007/s00253-003-1308-5.

(25) ErtesvÃ¥g, H. Alginate-Modifying Enzymes: Biological Roles and Biotechnological Uses. *Frontiers in Microbiology* **2015**, *6*. https://doi.org/10.3389/fmicb.2015.00523.

(26) Lim, J.; Lee, E. J.; Choi, J. S.; Jeong, N. C. Diffusion Control in the in Situ Synthesis of Iconic Metal–Organic Frameworks within an Ionic Polymer Matrix. *ACS Applied Materials & Interfaces* **2018**, *10* (4), 3793–3800. https://doi.org/10.1021/acsami.7b17662.

(27) Xiao, Q.; Gu, X.; Tan, S. Drying Process of Sodium Alginate Films Studied by Two-Dimensional Correlation ATR-FTIR Spectroscopy. *Food Chemistry* **2014**, *164*, 179–184. https://doi.org/10.1016/j.foodchem.2014.05.044.

(28) Férey, G.; Serre, C.; Mellot-Draznieks, C.; Millange, F.; Surblé, S.; Dutour, J.; Margiolaki, I. A Hybrid Solid with Giant Pores Prepared by a Combination of Targeted Chemistry, Simulation, and Powder Diffraction. *Angewandte Chemie International Edition* **2004**, *43* (46), 6296–6301. https://doi.org/10.1002/anie.200460592.

(29) Horcajada, P.; Gref, R.; Baati, T.; Allan, P. K.; Maurin, G.; Couvreur, P.; Férey, G.; Morris, R. E.; Serre, C. Metal–Organic Frameworks in Biomedicine. *Chemical Reviews* **2012**, *112* (2), 1232–1268. https://doi.org/10.1021/cr200256v.

(30) Sene, S.; Marcos-Almaraz, M. T.; Menguy, N.; Scola, J.; Volatron, J.; Rouland, R.; Grenèche, J.-M.; Miraux, S.; Menet, C.; Guillou, N.; et al. Maghemite-NanoMIL-100(Fe) Bimodal Nanovector as a Platform for Image-Guided Therapy. *Chem* **2017**, *3* (2), 303–322. https://doi.org/10.1016/j.chempr.2017.06.007.

(31) Patra, S.; Hidalgo Crespo, T.; Permyakova, A.; Sicard, C.; Serre, C.; Chaussé, A.; Steunou, N.; Legrand, L. Design of Metal Organic Framework–Enzyme Based Bioelectrodes as a Novel and Highly Sensitive Biosensing Platform. *J. Mater. Chem. B* **2015**, *3* (46), 8983–8992. https://doi.org/10.1039/C5TB01412C.

(32) Patra, S.; Sene, S.; Mousty, C.; Serre, C.; Chaussé, A.; Legrand, L.; Steunou, N. Design of Laccase–Metal Organic Framework-Based Bioelectrodes for Biocatalytic Oxygen Reduction Reaction. *ACS Applied Materials & Interfaces* **2016**, *8* (31), 20012–20022. https://doi.org/10.1021/acsami.6b05289.

Conclusions & Perspectives

Conclusions & Perspectives

While enzymes are very efficient biocatalysts, their practical use is limited due to their fragile nature and the difficulty to recover and reuse them. This work was mostly focused on microperoxidase 8, a small enzyme that combines the activity of both peroxidases and monooxygenases (typically that of Cytochrome P450s). MP8 presents several limitations in solution that hinder its practical use (easy deactivation and poor selectivity). These disadvantages were addressed through its immobilization in MOF solid matrices.

Among the different methods used to immobilize enzymes, the approaches that consist in a three-dimensional confinement inside a porous matrix (cage inclusion and entrapment) and that may provide a protective microenvironment for MP8 were preferred. MOF materials were preferred to traditional inorganic or organic materials because they combine hybrid crystalline structures, with a uniform porosity and high surface areas. Their organic-inorganic nature can minimize enzyme leaching, while their high and uniform porosity can provide a stabilizing and protective environment for enzymes, while favoring reactants diffusion.

The first part of the thesis investigated the immobilization of MP8 *via* the cage inclusion approach (*i.e*. inclusion of the bio-entity inside the porosity of preformed chemically stable mesoporous MOFs). This approach could be applied thanks to the small molecular size of MP8. Two mesoporous MOFs were selected for this study based on their compatible pore dimensions with the size of MP8 and their reported water stability, which is essential for biocatalytic applications. An optimization of the synthesis of PCN-333(Al) was realized since the reported synthetic procedure was not reproducible. However, after a careful reevaluation of its water stability, PCN-333(Al) was not found suitable for the immobilization of MP8. Therefore, only the ultra-stable mesoporous MIL-101(Cr) was used as an immobilization matrix for MP8. The immobilized enzyme showed an enhanced stability under acidic conditions (pH 5) and in the presence of oxidizing agents (H_2O_2), which confirmed the protective effect of the 3D framework. MP8@nanoMIL-101 could be recycled several times and showed a stable activity under storage for several weeks. Finally, the selective adsorption of dye molecules by MIL-101(Cr) induced an enhanced selective biodegradation of the harmful methyl orange by the immobilized MP8, through a charge-based pre-concentration mechanism.

In a second part, the ligand functionalization of MIL-101(Cr) and its influence on the encapsulation and on the catalytic activity of MP8 was studied. For the functionalization of the framework, a direct approach was preferred to a post-synthetic functionalization, due to its higher simplicity and reproducibility. Two functionalized ligands were selected, 2-aminoterephthalic acid and 2-sulfoterephthalic acid that led to the synthesis of respective MIL-101(Cr)-NH_2 and MIL-101(Cr)-SO_3H. These MOFs possessed different polarity and acidity, as well as a different particles surface charge. The functionalized MOFs resulted in MP8 loadings higher than that in the bare MOF, possibly because of additional specific interactions (H-bonding, additional electrostatic interactions *etc*…) that stabilized some enzyme molecules

at the external surface of the MOFs. The catalytic activity the immobilized MP8 was evaluated through the oxidation of a typical chromogenic substrate (ABTS) by H_2O_2 and through a more challenging catalytic reaction, the oxidation of thioanisole derivatives bearing electron donating, EDG (-CH_3, -OCH_3) or electron withdrawing, EWG (-NO_2) groups by H_2O_2. MP8@MIL-101(Cr) and MP8@MIL-101(Cr)-NH_2 showed similar activities, presumably because of the similar microenvironment around MP8 in their structures in terms of surface charge and acidity. MP8@MIL-101(Cr)-SO_3H showed a poor activity probably because its high acidity caused the cleavage of the Fe-histidine18 bond, which is essential for the activity of MP8. Similarly to free MP8, the immobilized enzymes were more reactive when sulfides bearing EDG groups were used.

In a similar approach, the metal functionalization of MIL-101(Cr) was investigated. The goal was to substitute a few Cr(III) centers of the Secondary Building Unit by Fe(III) ions to obtain a stable mesoporous structure that would be catalytically active (as Lewis acid catalyst and/or peroxidase-like catalyst). Two MOFs with different Cr(III)/Fe(III) ratios, MIL-101(Cr/Fe) (4:1) and MIL-101(Cr/Fe) (5.9:1) were obtained. Both MOFs showed a good chemical stability and were found to catalyze the Prins reaction and the ring opening of epoxides.

The last part of the thesis was focused on the immobilization of enzymes following the entrapment approach (*i.e.* formation of the immobilization matrix in the presence of the bio-entities). Two MOFs were selected, namely MIL-53(Al)-FA and MIL-100(Fe) according to their high chemical stability and their synthesis that required non-toxic reactants. Concerning MIL-53(Al)-FA, an extensive synthesis optimization was performed in order to obtain this MOF in water at room temperature. MIL-53(Al)-FA was then synthesized in the presence of high amounts of a model protein, Bovine Serum Albumin (BSA), giving rise to composites with immobilization rates close to 100 %. The presence of BSA in the composites and the preservation of the MOF structure were confirmed with various techniques (PXRD, FT-IR, TGA, NMR, fluorescence confocal microscopy, TEM-XEDS). Furthermore, based on N_2 porosimetry and *in-situ FT-IR* adsorption studies, an extra mesoporority was evidenced. The protein molecules may have induced the formation of large interparticle spaces in the composites that could be due to the aggregation of small nanoparticles of MIL-53-FA. A preliminary catalytic study with horseradish peroxidase immobilized in MIL-53(Al)-FA revealed that the enzyme preserved its activity after immobilization. An alternative immobilization approach was investigated through the formation of MIL-53(Al)-FA/alginate beads for the entrapment of pH-sensitive enzymes that may be harmed by the acidic conditions of the MIL-53(Al)-FA synthesis. Concerning MIL-100(Fe), the BSA molecules did not influence its synthesis and they were successfully immobilized in the porous matrix. Thus, the first preliminary results are encouraging for an extensive study of this system.

While the cage inclusion of MP8 was thoroughly studied during the course of the thesis, some further work is needed to fully complete the study of the *in-situ* systems.

The *in-situ* formation of MIL-53(Al)-FA in the presence of BSA resulted in the entrapment of high amounts of biomolecules. The characterization of the composites by confocal microscopy using a fluorescent biomolecule (FITC-BSA) suggested that the presence of the biomolecules influences the morphology of the resulting particles. It is possible that the BSA molecules induce the nucleation of the MOF; however, this phenomenon is not yet understood. The investigation of the role of BSA could give useful information for the nucleation and growth of MIL-53(Al) and the possibility to control the morphology of the MOF, by tuning the nature of the biomolecule. *In-situ* liquid cell TEM may be a useful tool to follow the growth mechanism of MIL-53(Al)-FA directly in the reaction mixture, in presence of biomolecules. This technique has been successfully used to monitor the formation of gold nanoparticles and it has also been reported for the direct observation of MOF materials, like UiO-66. The second synthetic procedure, using $NaAlO_2$ as precursor in presence of BSA should also be investigated. Finally, we should proceed with an extensive investigation on the catalytic activity of enzyme@MIL-53(Al)-FA bio-hybrids.

A thorough investigation of the *in-situ* synthesis of MIL-100(Fe) in presence of enzymes must also be performed.

Concerning the MIL-53(Al)-FA/alginate beads material, an extensive investigation on its structure must be performed. Microscopy techniques, coupled with spectroscopy mapping (*e.g.* TEM/micro-IR and/or TEM/micro-Raman) may be used to investigate the micro-structure of the beads and the localization of the MOF particles. A next step would be the immobilization of pH-sensitive enzymes into the beads and the investigation of the protective effect of the matrix. A comparison with the immobilized enzyme in a MIL-53(Al)-FA matrix should be performed to evaluate the extent of protection by the alginate biopolymer. Finally, the stability and recyclability of the beads along with the possible leaching of the enzyme must be evaluated. The removal of alginate (*via* EDTA, citrate) after the immobilization of the enzyme should also be considered in order to limit the diffusion barriers of the system, along with decreasing the size of the beads, which could also improve the diffusion of substrates to the enzyme. Considering the microporosity of MIL-53(Al)-FA shell, the variety of substrates that can be used may be limited. Thus, the formation of MIL-100(Fe)/alginate beads would also be of interest in order to allow the diffusion of larger molecules through the mesopores of MIL-100(Fe).

Another aspect that we have started studying in this work consists in combining the catalytic properties of the MOF with those of the enzyme, in order to perform cascade –or tandem-reactions. Both MIL-101(Cr/Fe) products synthesized during this work showed good water stability and Lewis acid catalytic activity (Prins reactions and ring opening of epoxides). It would thus be of interest to combine the Lewis acid activity of theses MOFs with the catalytic activity of MP8. While, the ring opening of epoxides catalyzed by MIL-101(Cr/Fe) requires elevated temperatures (~ 50 ^{o}C) and the use of MeOH, MP8 (due to its simple structure) may be robust enough to preserve its enzymatic activity. Thus, a catalytic system able to perform cascade reactions could be designed by associating MP8 immobilized in MIL-101(Cr/Fe) that

could catalyze the epoxidation of olefins, with MIL-101(Cr/Fe) that could then catalyze the ring opening of the formed epoxides, thus mimicking microsomal epoxide hydrolases. Alternatively, a tandem reaction could be designed using the peroxidase-like activity of MIL-101(Cr/Fe)s in combination with glucose oxidase immobilized at the external surface of MIL-101(Cr/Fe), that would produce the hydrogen peroxide substrate of the peroxidase reaction.

Similarly, MIL-100(Fe) combines chemically stability, bio-compatibility and catalytic activity, which could also be coupled with enzymes for tandem reactions.

While very promising results were obtained in this work and in the literature, the use of MOFs for the immobilization of enzymes is a new research field and remains relatively unknown and unexplored. Many limitations need to be overcome, which leaves plenty of room for future studies. The cage inclusion of enzymes using MOF materials has been shown to adequately promote the design of stable and active immobilized biocatalysts. However, this approach is limited to a few small enzymes and to mesoporous MOFs with high water stability. There is thus a need to expand the number of possible MOF-enzymes. As discussed in chapter 1 the chemical stability of MOFs is a complex physicochemical phenomenon that depends on multiple parameters (metal cation, ligand, hydrophobicity, porosity…). Nonetheless, the use of the highly inert Cr(III) cation, which shows very low water exchange rate is interesting when high chemically stable and highly porous structures are targeted. The use of tetravalent metal cations (Ti, Zr) could be a more eco-friendly approach to design chemically stable mesoporous MOFs. The synthesis of extended organic ligands can allow the increase to some extent of the pore dimensions of MOFs, but as already discussed, very long organic ligands require complicated, time-consuming and sometimes toxic organic syntheses. Moreover, the use of extended ligands often results in unstable MOF structures. Thus, in order to enable a universal use of MOFs for the cage inclusion of enzymes, *via* a sustainable synthetic process, other approaches must be envisioned. The partial dissolution of the MOF matrix, either *via* the introduction of labile to hydrolysis ligands or by a chemical treatment could promote the formation of large cavities, able to host large enzymes. The key issue will be to control the localization of such defects in the structure, in order to allow a homogeneous distribution of the enzymes. Another alternative approach could be the formation of ordered mesoporous super-structures, by introducing surfactants during the MOF synthesis. In that way, the material retains all the properties of the parent MOF that makes it promising for enzyme encapsulation (crystallinity, hybrid nature, ordered porosity…), while the formation of large mesopores by the surfactants allows the immobilization of large enzymes. Examples of such structures have already been reported (chapter 1), but to my knowledge their use for the immobilization of enzymes has not been thoroughly studied.

Following the concept of designing MOF-enzyme systems, in which MOFs are active components of the catalytic application, other systems can be targeted. For example, glucose isomerase is used for the conversion of D-glucose to D-fructose for the industrial production of high-fructose corn syrup. The immobilization of glucose isomerase in solid supports has been targeted for years for recycling purposes and stability issues. This enzyme requires

divalent metal ions (*e.g.* Mg^{2+}, Mn^{2+}, Co^{2+}) for both maximal catalytic activity and stability. The immobilization of glucose isomerase in a MOF matrix that is constructed with divalent cations, could eventually promote its activity and stability and enable its reuse. However, the use of divalent cations often results in unstable MOF structures. A way to overcome this limitation could be the synthesis of mixed-valence MOFs that contain divalent cations needed for the catalytic activity and trivalent or tetravalent cations to ensure the stability of the structure. Considering the dimensions of glucose isomerase (~ 176 kDa), the *in-situ* approach should be preferred for its immobilization. Nonetheless, the synthesis of mixed-valent MOFs in presence of enzymes may be a rather complicated process. A solution would thus be the preformation of the mixed-valent secondary building units (SBUs), which could then react with the chosen organic ligands and the enzyme. Examples of such MOFs have already been reported, like MIL-125-(Fe(III)/M(II) (M = Ni, Co, Mg). However, for the *in-situ* approach the choice of the ligand is limited to relatively water-soluble molecules. Thus, one possibility would be the formation of a mixed-valent MIL-100(Fe)/M(II), starting with preformed Fe(III)/M(II) trimeric SBUs.

Annex 1

Catalytic properties of mixed-metal MIL-101(Cr/Fe)

The catalytic tests were performed at the Universitat Politècnica de València in Spain, in the group of Prof. Hermenegildo García by Cristina Vallés, Dr. Andrea Santiago, Dr. Mónica Jiménez-Marques, Prof. Mercedes Álvaro and Prof. Sergio Navalón.

Prior to the utilization of the mixed metal MOFs as potential catalytically active immobilization matrices, it was important to fully evaluate their catalytic activity. First, the ability of MIL-101(Cr/Fe) (4:1) to be used as catalyst was studied using two different types of organic reactions usually catalyzed by a Lewis acid, the Prins coupling reaction and the ring opening reaction. The catalytic activity of MIL-101(Cr) was already studied for such reactions, but relatively low conversions were obtained. Fe-based MOFs showed an enhanced activity compared to that of Cr-based MOFs, which was due to the redox properties of trivalent iron species that played a significant role in activating the reactants, as already demonstrated for Friedel-Crafts reactions catalyzed by MIL-100(Fe).[1] It was thus believed that the mixed metal MIL-101(Cr/Fe) (4:1) would show a higher activity than both MIL-101(Cr) and the unstable MIL-101(Fe).

Before starting the experiments, MIL-101(Cr/Fe) (4:1), MIL-101(Fe) and MIL-101(Cr) catalysts were activated at 150 ^{o}C for 16 h, in order to remove solvent molecules and to generate open-metal sites (OMSs) in the inorganic clusters. For each test, 10 mg of catalyst were used. For the Prins reaction, β-pinene (1 mmol) and formaldehyde (1 mmol) were dissolved in 2.5 mL acetonitrile and the solution was mixed with the activated catalyst at 80 ^{o}C. For the ring opening reaction, styrene oxide (1 mmol) was dissolved in 2.5 mL methanol and mixed with the activated catalyst. The reactions were stirred and aliquots were taken at various reaction times.

Figure 1 shows the first results obtained for the Prins reaction. In the presence of MIL-101(Cr/Fe) (4:1), a maximum conversion of 70.3 % was reached after 24 h of reaction, whereas only 53.0 % conversion was observed with MIL-101(Fe). The higher activity of the mixed-metal MOF than that of its Fe analog was attributed to the higher stability of its framework. As revealed by the PXRD analysis of the catalysts after the reaction, MIL-101(Fe) had been totally converted into the more dense and stable phase MIL-88B, while no changes were observed for MIL-101(Cr/Fe) (4:1) (Figure 3). The conversion of the mesoporous MIL-101(Fe) into the microporous MIL-88B(Fe) may explain the apparent lower activity of the MOF, as the diffusion of reactants would be limited in the later MOF. The reported conversion of MIL-101(Cr) for the Prins reaction was around 30 %, which is in agreement with the lower Lewis acid activity of Cr-based MOFs.[2]

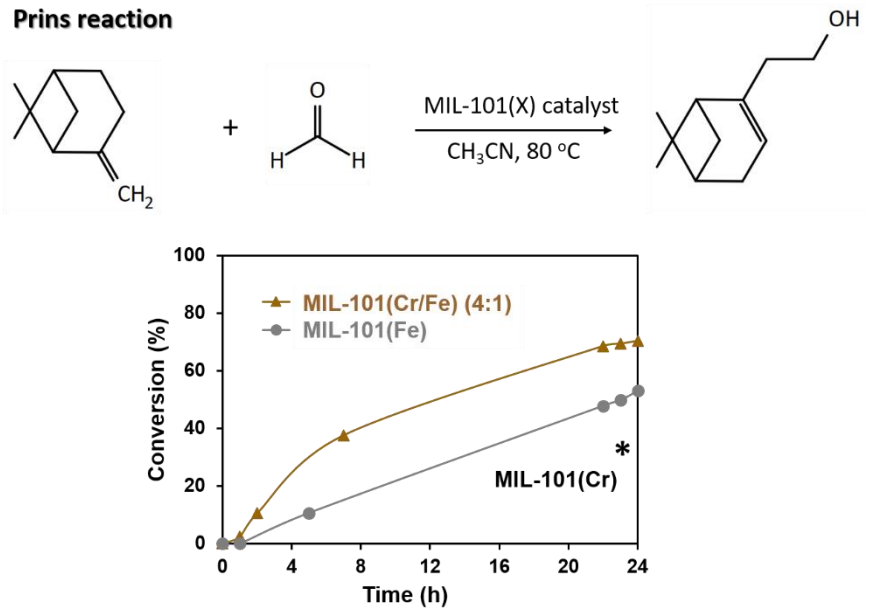

Figure 1: Top: schematic illustration of the Prins coupling reaction of β-pyrene and formaldehyde, catalyzed by MIL-101(X) materials at 80 °C; Bottom: time-conversion plot for the Prins coupling catalyzed by MIL-101(Cr/Fe) (4:1) (brown triangles), MIL-101(Fe) (grey circles) and the reported value for MIL-101(Cr) (black asterisk).[2]

The results for the catalysis of the ring opening reaction are shown in Figure 2. In this case, similar conversion was observed both with MIL-101(Cr/Fe) and MIL-101(Fe) as catalysts after 24 h of reaction (43.9 % and 38.3 %, respectively). The slightly higher activity of the mixed metal MOF was again attributed to the instability of MIL-101(Fe) under the reaction conditions that resulted in its transformation into MIL-88B (Figure 3). MIL-101(Cr) was much less active, leading to a conversion of 12 %.

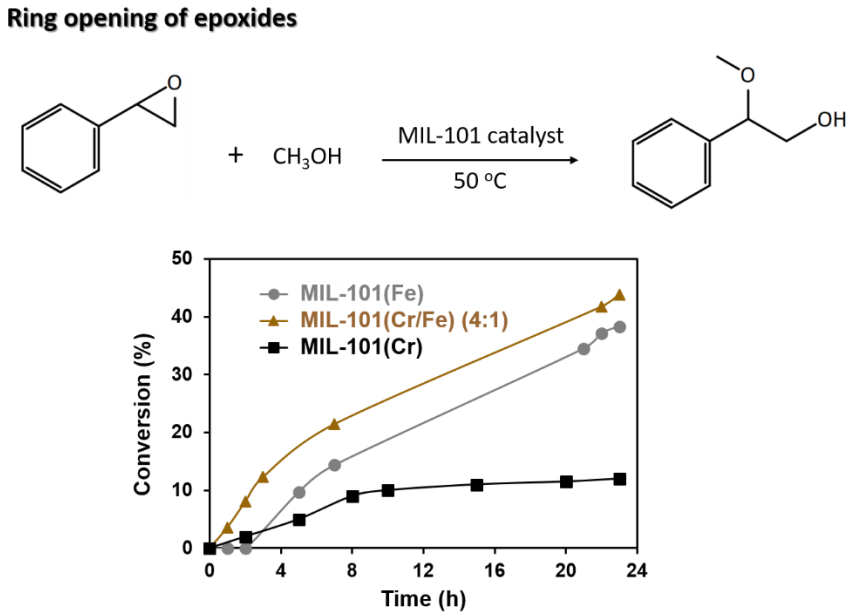

Figure 2: On top, schematic illustration of the ring opening reaction of epoxide by methanol, catalyzed by MIL-101(X) materials at 50 °C; On bottom, time-conversion plot for ring opening catalyzed by MIL-101(Cr/Fe) (4:1) (brown triangles), MIL-101(Fe) (grey circles) and the reported values for MIL-101(Cr) (black squares).[2]

These first catalytic results thus appeared to be promising, which encourage for a more extensive study of the activity of MIL-101(Cr/Fe) (4:1) and also MIL-101(Cr/Fe) (5.9:1). Currently the catalytic activity of both MOFs is tested in Lewis acid catalyzed reactions, with a more extensive study on the stability of the catalysts (leaching of metal ions) and on their potential reusability. A comparison with more stable Fe-MOFs (like MIL-88B) is as well investigated. Once the catalytic activity of the mixed-metal MOFs will have fully been evaluated, they will be eventually studied as host matrices for enzymes.

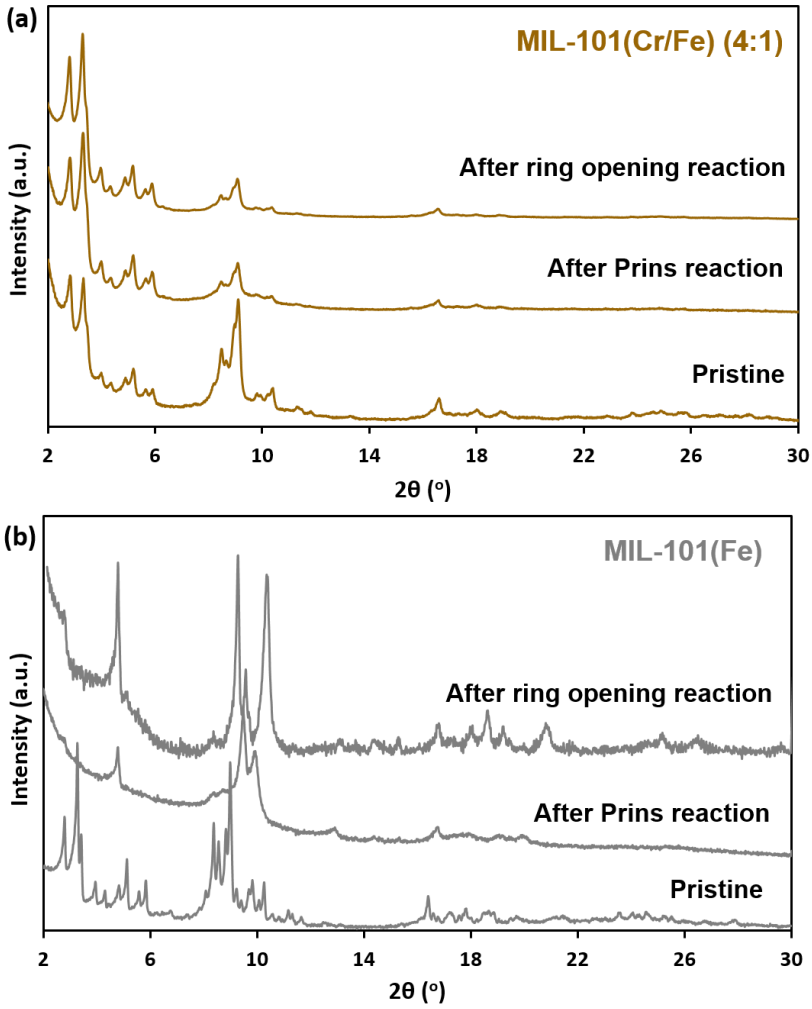

Figure 3: Normalized PXRD diagrams of (a) MIL-101(Cr/Fe) (4:1) and (b) MIL-101(Fe) before and after catalysis.

References

(1) Horcajada, P.; Surblé, S.; Serre, C.; Hong, D.-Y.; Seo, Y.-K.; Chang, J.-S.; Grenèche, J.-M.; Margiolaki, I.; Férey, G. Synthesis and Catalytic Properties of MIL-100(Fe), an Iron(III) Carboxylate with Large Pores. *Chem. Commun.* **2007**, No. 27, 2820–2822.

(2) Santiago-Portillo, A.; Navalón, S.; Concepción, P.; Álvaro, M.; García, H. Influence of Terephthalic Acid Substituents on the Catalytic Activity of MIL-101(Cr) in Three Lewis Acid Catalyzed Reactions. *ChemCatChem* **2017**, *9* (13), 2506–2511.

Annex 2

Solid-state NMR of MIL-53(Al)-FA and its composites with BSA

The solid-state NMR study was performed by Dr. Charlotte Martineau-Corcos at the Institut Lavoisier de Versailles.

The two MIL-53(Al)-FA products obtained at room temperature, in water ($Al_2(SO_4)_3 \cdot 18H_2O$ and $NaAlO_2$) and the composites of MIL-53(Al)-FA ($Al_2(SO_4)_3 \cdot 18H_2O$) with BSA were analyzed by solid-state NMR spectroscopy to gain insights about their structure.

^{27}Al nuclear magnetic resonance spectroscopy was used to confirm the formation of MIL-53(Al)-FA, in water, at room temperature. Since ^{27}Al is a quadrupolar nucleus (I= 5/2 > 1/2), the nucleus interacts both with the external magnetic field and the electric filed gradient that is generated by its surrounding environment.[1,2] This usually gives rise to broadened and overlapping NMR resonances that are composed of a central transition (+1/2 ↔ -1/2), surrounded by satellite transitions (spinning sidebands). The chemical shift range of ^{27}Al is relatively wide (~ -100 - 300 ppm) with the reference $Al(H_2O_6)^{3+}$ at 0 ppm.[1,2] It can give information about the coordination number of aluminium, with the general trend showing that the aluminium cations in octahedral environment usually show high field resonances, compared to tetrahedral of five-coordinated aluminum atoms. The chemical shift is mainly influenced by the electronegativity of the ligand and the more the aluminium is coordinated with donor ligands (*e.g.* O-, S-, -N-, P-) the stronger the shielding around the Al-center.[1,2] In Al-based MOFs, the aluminium atom is always in octahedral environment. However, depending on the synthetic conditions (ligands, temperature, solvent, pressure, reaction time *etc.*) different aluminium clusters (secondary building units, SBU) can be formed. For more details on SBUs, see chapter 1. The ^{27}Al spectrum is representative of a specific SBU. The shape of the spectrum is yet importantly influenced by the hydration state of the MOF and the degree of crystallinity.[1,2]

Figure 1 shows the ^{27}Al MAS NMR spectrum of MIL-53(Al)-FA ($Al_2(SO_4)_3 \cdot 18H_2O$), compared with that of Basolite A520 (patent)[3,4] and MIL-53(Al)-FA obtained with the reported optimized hydrothermal synthesis.[4] All three spectra have similar line shapes and chemical shifts, characteristic of carboxylate-coordinated aluminium octahedra (AlO_6), sharing opposite corners (Figure 2).[4,5] It thus confirms the formation of MIL-53(Al)-FA in water, at room temperature. As already demonstrated by the PXRD analysis, MIL-53(Al)-FA ($Al_2(SO_4)_3 \cdot 18H_2O$) shows a lesser extend of crystallinity compared to the patent synthesis,[3] while the optimized hydrothermal synthesis[4] forms better crystallized particles compared to the two former samples. This is also confirmed, through the broadening of right part of the ^{27}Al NMR resonance that follows the order of crystallinity MIL-53(Al)-FA (hydrothermal) > Basolite A520 (patent) > MIL-53(Al)-FA ($Al_2(SO_4)_3 \cdot 18H_2O$). Moreover, the spectrum of MIL-53(Al)-FA ($Al_2(SO_4)_3 \cdot 18H_2O$) shows a broadening on the left part (denoted with *) that can be attributed to small traces of amorphous Al oxide/hydroxide.[4]

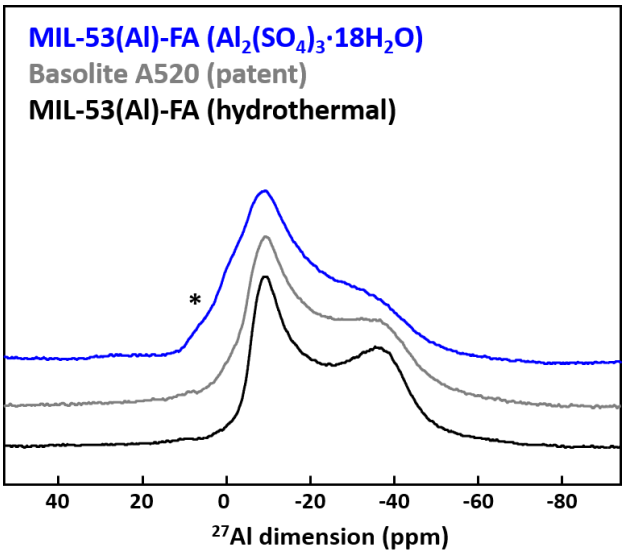

Figure 1: ^{27}Al MAS NMR spectra of MIL-53(Al)-FA ($Al_2(SO_4)_3 \cdot 18H_2O$) (blue), Basolite A520 (patent) (grey) and MIL-53(Al)-FA (hydrothermal) (black). All samples were dried at 100 °C overnight prior to the NMR measurement. Stars indicate the presence of aluminum oxide.

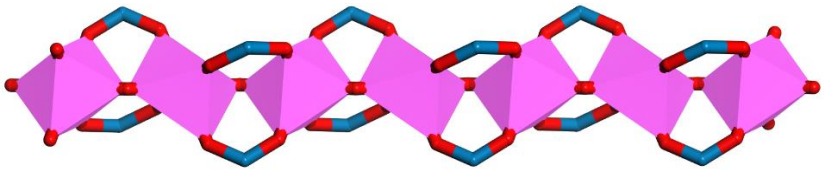

Figure 2: The SBU of MIL-53(Al)-FA (or Basolite A520) 1D chain of AlO_6 octahedra, sharing opposite corners.

The ^{27}Al MAS NMR of MIL-53(Al)-FA ($NaAlO_2$) is almost identical to the one of MIL-53(Al)-FA ($Al_2(SO_4)_3 \cdot 18H_2O$) thus, confirming the synthesis of the MOF, by both synthetic roots (Figure 3). Moreover, both products showed the same amounts of Al oxide/hydroxide impurity in their structure. This is not in accordance with the TG analysis showed in chapter 4, which highlights the important standard error of TGA. The difference on the right part of the spectra is attributed to the different levels of hydration of the samples. The signals denoted with * are attributed to spinning sidebands.

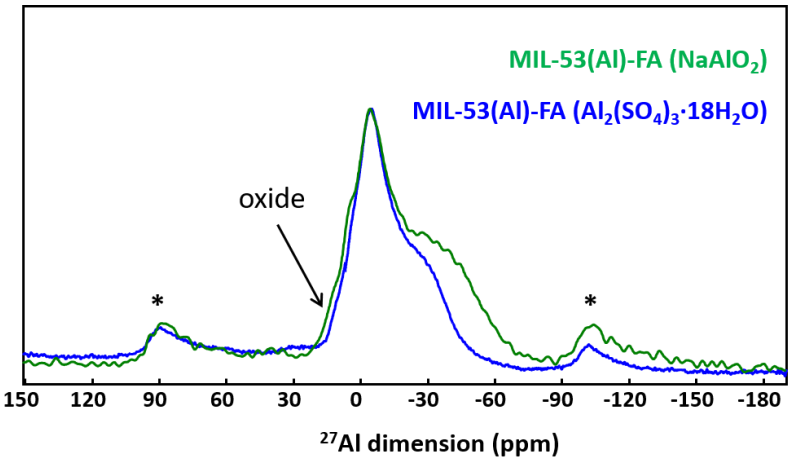

Figure 3: ^{27}Al MAS NMR spectra of MIL-53(Al)-FA ($Al_2(SO_4)_3 \cdot 18H_2O$) (blue) and MIL-53(Al)-FA ($NaAlO_2$) (green). Stars indicate the position of the spinning sidebands.

The presence of BSA during the synthesis of MIL-53(Al)-FA did not seem to affect the crystal structure of the MOF. The ^{27}Al MAS spectra of the composites with BSA are identical to the parent MOF, showing the same line shape, chemical shift and degree of signal broadening (Figure 4).

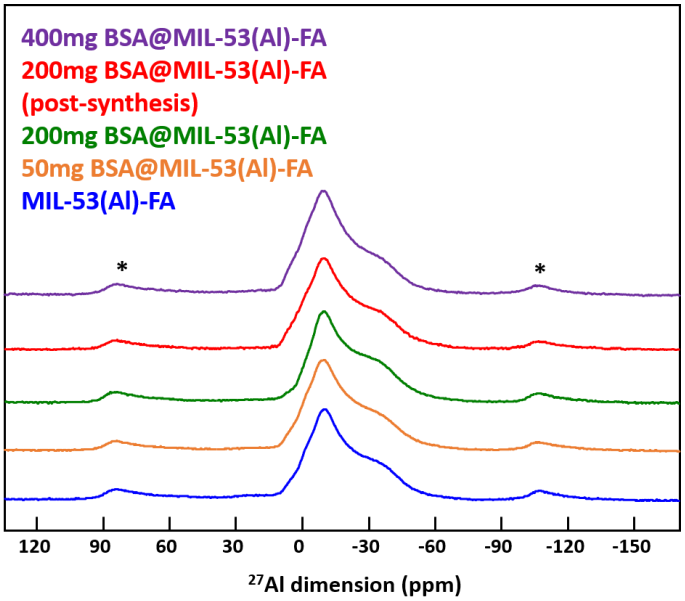

Figure 4: ^{27}Al MAS NMR spectra of MIL-53(Al)-FA (blue), 50mg BSA@MIL-53(Al)-FA (orange), 200mg BSA@MIL-53(Al)-FA (green), 200mg BSA@MIL-53(Al)-FA (post-synthesis) (red) and 400mg BSA@MIL-53(Al)-FA (purple). All samples were dried at 100 °C overnight prior to the NMR measurement. Stars indicate the position of the spinning sidebands.

MIL-53(Al)-FA and its composites with BSA were also analysed by solid-state ^{13}C NMR spectroscopy. The ^{13}C MAS NMR spectrum of MIL-53(Al)-FA exhibits two signals at δ ~ 138 and 170 ppm (Figure 5). The high-field signal can be attributed to the two carbon atoms of the double bond (a) and the low-field signal to the two carboxyl carbon atoms (b). The small signal at δ ~ 172 may be due defects or disorder in the crystal structure of the MOF. The two principal signals are broader compared to those of Basolite A520, due to the lower crystallinity of the sample.

Figure 6 shows the ^{13}C MAS NMR spectra of BSA, MIL-53(Al)-FA and its composites with BSA. BSA exhibits a broad high-field signal between 10-70 ppm that can be attributed to the overlapping of resonances of α-carbons and aliphatic carbons.[6–8] The small signal at δ ~ 130 ppm may be due to the aromatic carbons, while the low-field signal at ~180 ppm can be attributed to the carbonyl carbons of the peptide bonds. [6–8] The composites of MIL-53(Al)-FA with important amounts of BSA (200 mg, 400 mg *in-situ* and 200 mg post-synthesis) exhibited similar ^{13}C resonances with BSA, which is consistent with the presence of the biomolecules in the crystal structure of the MOF. The similar line shape and chemical shift of the BSA signals in the composites, compared to the free biomolecule may indicate that the BSA remained intact after immobilization The BSA incorporation had no effect on the ^{13}C NMR line shape of the MOF.

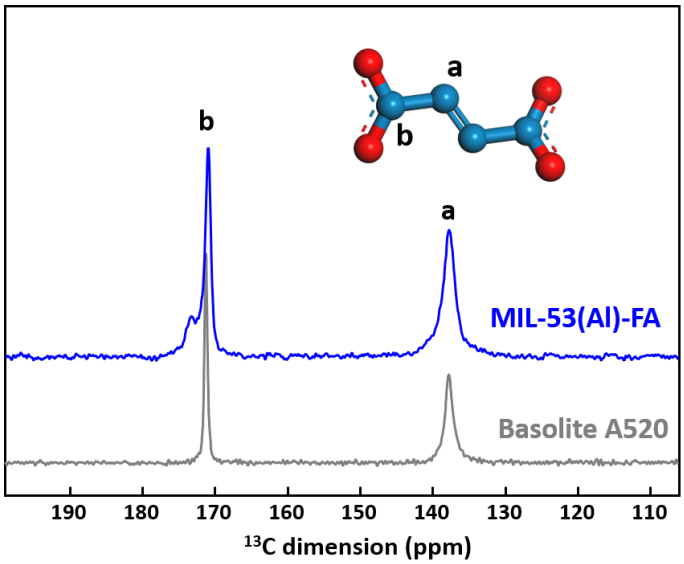

Figure 5: ^{13}C MAS NMR spectra of MIL-53(Al)-FA (blue) and Basolite A520 (grey). Samples were dried at 100 °C overnight prior to the NMR measurement. Stars indicate the presence of an aluminum oxide.

The solid-state NMR analysis confirmed the formation of MIL-53(Al)-FA in water, at room temperature ($Al_2(SO_4)_3 \cdot 18H_2O$ and $NaAlO_2$). The broadened line shape of the ^{27}Al resonances are in agreement with the lower crystallinity of the samples, observed by the PXRD analysis. ^{13}C NMR confirmed the presence of BSA in the composite of MIL-53 (Al)-FA, without however giving any further information about specific interactions of BSA with the MOF structure. The MIL-53(Al)-FA structure was not influenced by the presence of BSA, based on ^{27}Al and ^{13}C NMR.

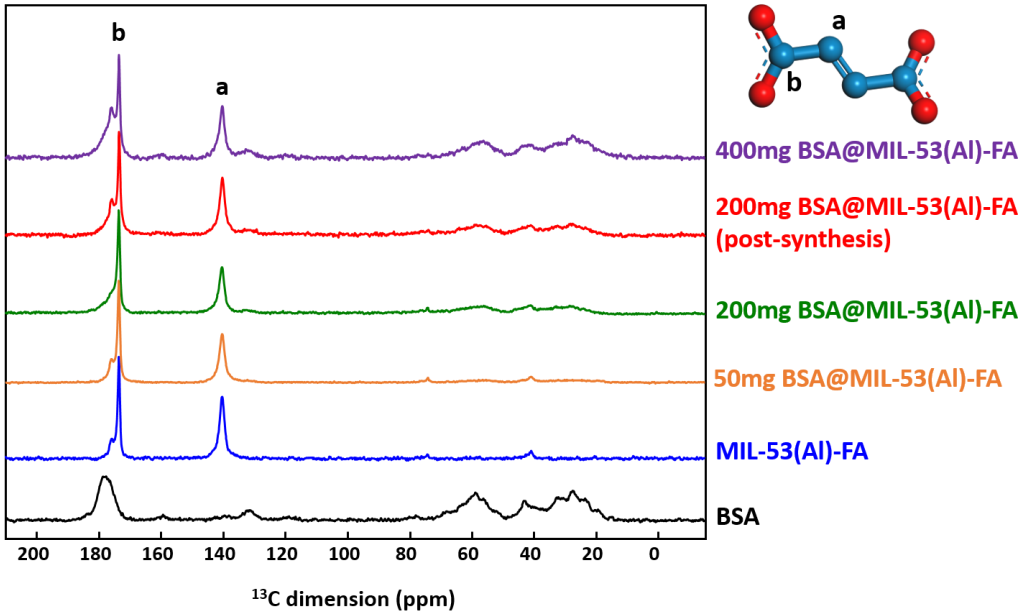

Figure 6: ^{13}C MAS NMR spectra of BSA (black), MIL-53(Al)-FA (blue), 50mg BSA@MIL-53(Al)-FA (orange), 200mg BSA@MIL-53(Al)-FA (green), 200mg BSA@MIL-53(Al)-FA (post-synthesis) (red) and 400mg BSA@MIL-53(Al)-FA (purple). All samples were dried at 100 °C overnight prior to the NMR measurement.

References

(1) Martineau, C.; Taulelle, F.; Haouas, M. The Use of 27 Al NMR to Study Aluminum Compounds: A Survey of the Last 25 Years. In *PATAI'S Chemistry of Functional Groups*; Rappoport, Z., Ed.; John Wiley & Sons, Ltd: Chichester, UK, 2016; pp 1–51.

(2) Haouas, M.; Taulelle, F.; Martineau, C. Recent Advances in Application of 27 Al NMR Spectroscopy to Materials Science. *Progress in Nuclear Magnetic Resonance Spectroscopy* **2016**, *94–95*, 11–36.

(3) Leung, E.; Müller, U.; Trukhan, N.; Mattenheimer, H.; Cox, G.; Blei, S. Process for Preparing Porous Metal-Organic Frameworks Based on Aluminium Fuamrate. *EP Patentanmeldung 10183283.0* **2010**.

(4) Alvarez, E.; Guillou, N.; Martineau, C.; Bueken, B.; Van de Voorde, B.; Le Guillouzer, C.; Fabry, P.; Nouar, F.; Taulelle, F.; de Vos, D.; et al. The Structure of the Aluminum Fumarate Metal-Organic Framework A520. *Angewandte Chemie International Edition* **2015**, *54* (12), 3664–3668.

(5) Loiseau, T.; Serre, C.; Huguenard, C.; Fink, G.; Taulelle, F.; Henry, M.; Bataille, T.; Férey, G. A Rationale for the Large Breathing of the Porous Aluminum Terephthalate (MIL-53) Upon Hydration. *Chemistry - A European Journal* **2004**, *10* (6), 1373–1382.

(6) Gregory, R. B.; Gangoda, M.; Gilpin, R. K.; Su, W. The Influence of Hydration on the Conformation of Bovine Serum Albumin Studied by Solid-State 13 C-NMR Spectroscopy. *Biopolymers* **1993**, *33* (12), 1871–1876.

(7) Ravera, E.; Corzilius, B.; Michaelis, V. K.; Luchinat, C.; Griffin, R. G.; Bertini, I. DNP-Enhanced MAS NMR of Bovine Serum Albumin Sediments and Solutions. *The Journal of Physical Chemistry B* **2014**, *118* (11), 2957–2965.

(8) Wang, Y.; Griffin, P.; Jin, K.; Fogel, M. L.; Steele, A.; Cody, G. D. Tracing H Isotope Effects in the Dynamic Metabolic Network Using Multi-Nuclear (1H, 2H and 13C) Solid State NMR and GC–MS. *Organic Geochemistry* **2013**, *57*, 84–94.

Titre : Elaboration de nouvelles matrices d'immobilisation enzymatique à base de Metal-Organic Frameworks pour la dégradation catalytique de polluants environnementaux

Mots clés : MOFs, enzyme, immobilisation, bio-catalyse, environement

Résumé : Les enzymes sont des biocatalyseurs de plus en plus utilisés pour la transformation de molécules organiques (chimie fine, bioconversions, dépollution, chimie du pétrole) car elles possèdent de très bonnes sélectivité et réactivité, générant rapidement de larges quantités de produit. Cependant, la fragilité des enzymes, notamment en solution, limite souvent leur utilisation. Il est donc crucial de les immobiliser et de les stabiliser dans des supports adaptés. Une grande variété de matrices d'immobilisation (organiques ou inorganiques) a déjà étudiée, mais aucune ne satisfait pleinement aux critères nécessaires pour le développement de bio-réacteurs (accessibilité au site actif de l'enzyme, relargage de l'enzyme, diffusion des réactifs, recyclabilité, stabilité..). En outre, la majorité de ces matrices présente une porosité désordonnée, inadaptée pour une immobilisation homogène. L'utilisation de matériaux hybrides, cristallins et poreux de type Metal-Organic Frameworks (MOFs) a été récemment proposée comme alternative avec des applications en biocatalyse et en biodétection.
Le travail de cette thèse a consisté à associer des matériaux de type Metal-Organic Frameworks à une mini-enzyme, la microperoxidase 8 (MP8), afin d'obtenir des matériaux multifonctionnels. Dans une première partie, le MOF mésoporeux, MIL-101(Cr), a été utilisé pour encapsuler la MP8, ce qui a conduit à une amélioration de son activité catalytique dans des conditions qui ne sont pas adéquates pour l'activité enzymatique (conditions acides, forte concentration en H_2O_2), démontrant ainsi le rôle protecteur du MOF vis-à-vis de l'enzyme. De plus, il a été possible de recycler le biocatalyseur. Cette approche a également permis d'améliorer considérablement la sélectivité de la MP8 pour la dégradation d'un colorant organique toxique négativement chargé, le méthyl orange, grâce à son adsorption sélective par interaction électrostatique avec les particules de MIL-101(Cr). La seconde partie a été consacrée à l'utilisation de matériaux MIL-101(Cr) fonctionnalisés. Tout d'abord, l'influence de la fonctionnalisation du ligand (avec un groupement $–NH_2$ ou $–SO_3H$) sur l'encapsulation de la MP8 ainsi que sur son activité catalytique pour des réactions de sulfoxydation a été étudiée. Il a été montré que l'activité catalytique et la réactivité de la MP8 sont affectées par le microenvironnement spécifique des pores du MOF, notamment pour des réactions de sulfoxydation mettant en jeu des dérivés thioanisole. Ensuite, un MOF à métal mixte (MIL-101(Cr/Fe)) choisi pour ses propriétés catalytiques stables, a été synthétisé et caractérisé. Enfin, la dernière partie de cette thèse a été consacrée à la synthèse in-situ d'un MOF (le microporeux MIL-53(Al)-FA) en présence de biomolécules (BSA) dans des conditions compatibles avec la préservation de la structure protéique (en solution aqueuse à température ambiante). Les matériaux hybrides obtenus ont été caractérisés en couplant de nombreuses techniques. Cette méthode d'encapsulation a conduit à des taux d'immobilisation extrêmement élevés. Une étude préliminaire a été initiée avec l'enzyme, Horseradish Peroxidase , qui conserve son activité catalytique après immobilisation.

Title : Elaboration of novel enzymatic immobilization matrices, based on Metal-Organic Frameworks for the catalytic degradation of environmental pollutants

Keywords : MOFs, enzyme, immobilization, bio-catalysis, enviroment

Abstract : The use of enzymes in biocatalytic processes has been a challenging goal over the years. While enzymes present exceptional catalytic properties, their fragility hinders their industrial application. Their stabilization and protection are therefore of paramount importance. This can be effectively addressed through their immobilization within host solid matrices. Traditional materials (silica, clays, polymers, biopolymers, porous carbons…) have been widely studied as supports. Their pure organic or inorganic nature often requires a compromise between affinity with enzymes and robustness of the matrix. Besides, most of them have non-ordered porosity, with non-homogenous pore size distributions, unsuitable for homogeneous immobilization. Metal-Organic Frameworks (MOFs) have been recently introduced as alternative supports, thanks to their hybrid nature and their crystalline and highly porous structures.
The aim of this PhD was to combine Metal-Organic Frameworks (highly porous and chemically stable polycarboxylate MOFs) and a mini-enzyme, microperoxidase 8 (MP8) to obtain multifunctional biocatalysts. In a first part, the mesoporous MIL-101(Cr) was used as a host matrix to encapsulate MP8. The encapsulation led to an increased catalytic activity under conditions (acidic conditions, high concentration of H_2O_2) detrimental to the catalytic activity of MP8, thereby demonstrating the protecting effect of MIL-101(Cr) matrix. The biocatalyst was also efficiently recycled. The selectivity of MP8 for the degradation of the harmful negatively charged organic dye methyl orange was also enhanced, thanks to the charged-based selective adsorption of the dye in MIL-101(Cr) porosity. A second part of the work was devoted to the use of functionalized MIL-101(Cr) analogs. First, functionalized ligands (bearing $–NH_2$ and $–SO_3H$ groups) were used, and their influence on MP8 encapsulation was evaluated. The catalytic activity toward sulfoxidation reactions was also studied. The successful encapsulation of MP8 was strongly dependent on charge matching between the enzyme and the MOFs particles, while its catalytic activity was affected by the specific microenvironment of the pores. The MOF frameworks also modified the reactivity of MP8 toward different thioanisole derivatives. Then, a mixed metal MOF (MIL-101(Cr/Fe)), selected for its stable catalytic properties, was synthesized and characterized. Finally, the last part was devoted to the in-situ synthesis of MOFs (microporous MIL-53(Al)-FA) in presence of biomolecules (BSA) under compatible conditions with the preservation of the protein's quaternary structure (aqueous media and room temperature). The resulting hybrid materials were thoroughly characterized and presented high loadings of BSA. A preliminarily study was performed with the enzyme, Horseradish Peroxidase, which retained its catalytic activity after immobilization.